Thermal evolution of binary aqueous alkali silicates : properties of solutions, xerogels and coatings

Hamza Mohsin

INSTITUT POLYTECHNIQUE DE PARIS

ÉCOLE POLYTECHNIQUE

IP PARIS

NNT : 2022IPPAX003

Thèse de doctorat

Thermal evolution of binary aqueous alkali silicates: Properties of solutions, xerogels and coatings

Thèse de doctorat de l'Institut Polytechnique de Paris
préparée à l'École Polytechnique

École doctorale n°626 de L'Institut Polytechnique de Paris (ED IP Paris)
Spécialité de doctorat : Chimie

Thèse présentée et soutenue à Palaiseau, le 28 Janvier 2022, par

Hamza Mohsin

Composition du Jury :

Philippe Barboux Professeur, Chimie Paristech, Université PSL	(IRCP – UMR 8247)	Président
Sylvie Rossignol Professeure, Université de Limoges	(IRCER – UMR 7315)	Rapporteure
Nadia Pellerin Maitre de Conférence, Université d'Orléans	(CEMHTI – UPR 3079)	Rapporteure
Cédric Boissiere Directeur de Recherche, Sorbonne Université	(LCMCP – UMR 7574)	Examinateur
Michael Toplis Directeur de Recherche, OMP Toulouse	(IRAP – UMR 5277)	Examinateur
Ekaterina Burov Ingénieure de Recherche, SGR Paris	(SVI – UMR 125)	Examinatrice
Thierry Gacoin Professeur, Ecole Polytechnique, IP Paris	(LPMC – UMR 7643)	Directeur de thèse
Emmanuelle Gouillart Directrice Scientifique, SGR Paris		Directrice de thèse

There is no knowledge and science like pondering and thought; and there is no prosperity and advancement like knowledge and science

Acknowledgements

Words and complements are never enough to acknowledge someone's support in one's struggle towards knowledge and wisdom as it is a path that can rarely be traversed all alone. *'As you start to walk on the way, the way appears'* says Rumi making quite precisely a point. The beginning of this PhD journey was possible thanks to Saint-Gobain Research Paris's trust in me despite coming from a slightly different scientific background and expertise not directly related to the subject. It was not an undemanding task, initially, as my job was not only to take care of the scientific details involved, but also to confront the diverse thought processes of my supervisors. But credit is due to their ever-available time, kindness and supportive attitude for enabling me to improve on my shortcomings and, of course, to efficiently move towards the attainment of the set objectives.

A genuine 'Merci Beaucoup !' to my thesis directors, Emmanuelle Gouillart and Thierry Gacoin, as well as all other supervisors – Ekaterina Burov, Lucie Devys, Sébastien Maron and Isabelle Maurin, for always being there to guide me through this rightly-called challenging and interesting phase of scientific career, which wasn't difficult but tricky. I cannot, honestly, thank you enough, Emmanuelle and Thierry, for the improvement I see in myself as a scientist today. Your tips and tricks on continuous improvement, Emmanuelle, and your scientifically challenging attitude, Thierry, inculcated in me the seeds to improve and transform my attitude towards quality science. I have learnt a lot from our meetings and discussions (both individual and collective) on the various aspects of the thesis among many other things and don't really recall a time where I had to wait and wait for a rendez-vous. I can go on and on how supportive the two of you have been but there's also Katia, who has played a pivotal role in this project. Though together we did a lot of Raman analyses, difficult, tricky and sometimes non-conclusive, it was more your openness and readiness to discuss on all the different aspects of the thesis and the extremely valuable input I got from your side every time we had a chat, that helped us progress.

A bit different was your way of working and thinking, Lucie, and I learnt quite a bit about the way people really approach things in R&D. I appreciate you for being there in the meetings we had despite your tight schedule, and am grateful for all the interesting insights you brought and the helping hand you lent for experimentations within SGR. Sébastien, I can't acknowledge you enough since we had a more informal interaction and a kind of friendship. Firstly, thank you for all the NMR experiments we did together that served as a very crucial part of the work. Secondly, merci pour les échanges scientifique et non scientifique en français. That made my PhD life much easier and I would also like to appreciate you truly for your gentle nature. That leaves me with you, Isabelle, to thank for the support in the first year of my thesis. It was crucial, and without your help I wouldn't have been more efficient in my experimental approach. Thank you for getting me on track in the initial days, taking care of even the very minute details.

Next, I would like to acknowledge the support of the two host organizations, Saint-Gobain Research Paris and LPMC, Ecole Polytechnique, in terms of the availability of the major resources including expertise and equipment for carrying out the research work. Thanks to Jérémie Teisseire, Marine Brunet, François Compoint and Maxence Wilmet from the RFL group, SGR Paris for the

valuable scientific input on and off the meetings and for seriously following-up on the thesis every now and then. Interacting with you added a new dimension to the work and has allowed me to think more from a purely R&D perspective. I am extremely grateful to Dejan Skrelic from SVI, SGR Paris for providing his absolute help with all the Raman measurements (ex-situ and in-situ) and the corresponding analysis we did together. Thanks is also due to Hervé Montigaud from SVI for the help he has rendered throughout the thesis especially with SIMS measurements in the beginning, and Thierry Cretin for running the SIMS analysis as well as making sure we were able to find the right parameters. I acknowledge the support of Emmanuel Garre from SVI who helped me a lot with the necessary chemical lab trainings and the day-to-day experimental necessities. I also appreciate Sirine Ben Khemis from SVI for the Ta-coated glass samples I used for the Raman analysis on coatings. Further, thanks to others from SGR Paris including Johnny Vallon for Na-silicate glass samples, Jean-Patrick Cochard for thermal analysis discussions, Alexandre Blanchet for Hot-stage microscopy measurements, Estelle Rondet and Nathalie Ferruaud for TGA and DSC measurements, Anaïs Dalencourt for the trainings in the RFL chemistry lab, Ludivine Jego for thickness measurements on dektak and Lionel Homo for the SEM training.

On the side of LPMC, Ecole Polytechnique, I duly acknowledge Sandrine Tusseau-Nenez for the training and support on XRD measurements as well as the development of the deconvolution method that helped us advance on the critical understanding of things, Mélanie Poggi for TGA and SEM trainings, Lucio Martinelli and Fabian Cadiz for the trainings on Raman spectroscopy, Catherine Henry de Villeneuve for FT-IR training and François Ozanam for the support, Khalid Lahlil for the hydrophobic and moisture experimental trials and Rabei Mohammedi for the absolute help in all the experimental and chemical lab-related necessities.

Most of the equipment used was available within the two setups except for the High Field and CP MAS NMR experiments for which appreciation is due to Grégory Tricot (UMR8516 LASIR, Université de Lille) for helping us with the understanding of some critical details. Acknowledgement is also due to Cédric Boissiere (LCMCP, Sorbonne Université) and Michael J. Toplis (IRAP, Université de Toulouse) for the extremely useful suggestions during the mid-thesis defense. Furthermore, I'd also like to thank Santiago Alvarez for the nice work we did during his M2 internship that brought new avenues and did help advance the subject.

Apart from all the scientific involvement, I am very glad to have spent these 3 years or so at SVI, SGR Paris and LPMC, Ecole Polytechnique. Both the labs had an amazing on and off work atmosphere and I cannot thank my colleagues enough for the wonderful time we spent together. Most importantly, le fait que je parle français aujourd'hui c'est grâce à toi Capucine Cleret de Langavant, merci pour ton soutien pendant ma thèse. I am grateful to you as well, my dear friend and colleague Jeongmo Kim, for all the nice moments in and outside the lab.

Lastly, I would like to whole-heartedly appreciate my family, especially my mom and dad, for the unwavering support, prayers and belief in whatever I've wanted to choose for myself including this PhD; something that has truly allowed me to pursue my journey towards achieving long-term life goals.

Abstract

The thermal behavior of industrially valuable aqueous alkali silicates is of particular interest especially in fire-resistant applications owing to their intumescent nature. It has been investigated for Na, K and Li-silicates of two different molar ratios to better understand the macroscopic and microscopic structural evolution in terms of foaming and network condensation. A quantitative experimental strategy involving a combination of tools (TGA, ^{29}Si NMR spectroscopy, XRD) has been utilized to probe the state of the network on thermal evolution starting mainly from 'xerogels'. Heating alkali silicates leads to structural changes due to the evolution of water where the quantity of leftover water (network silanols or solvating water) in the xerogel, when observed from TGA, obeys an Arrhenian evolution for Na-silicates with an activation energy of 30 kJ.mol^{-1} below 400°C, consistent with the geochemistry literature. In contrast, multiple activation energies are displayed by K and Li-silicates due to crystallization.

Foaming is observed at temperatures above 150°C in Na and K-silicates mainly due to the condensation of silanols and subsequent removal of solvating water molecules with dependence upon the composition and heating rate. Increasing the alkali concentration, for instance Na, results in a larger quantity of water retained in the xerogel, which correlates with a lower softening temperature of the material and is, macroscopically, related to a higher foaming of the silicate. K-silicate solutions foam extensively at a heating rate of 10°C/min, however, suppression of foaming is a consequence of crystallization on heating at either lower rate (especially for lower K content) or pre-drying at 150°C. A combined effect of phase separation and crystallization is responsible for no foaming observed in Li-silicate solutions and xerogels, irrespective of the heating rate, resulting from a relatively less mobile nature of the network due to limited quantity of silanols and alkali ions. High temperature measurements in the case of Na-silicates suggest the systems to exhibit a xerogel-to-glass evolution at 400°C above which a behavior similar to conventional glasses is observed until 1100°C when seen under a Hot-stage Microscope. Finally, homogeneous and thick silicate gradient coatings (of the order of microns) developed from these solutions show a critical thickness for: foaming in Na-silicates, crystallization and foaming in K-silicates depending upon the composition, or cracking in Li-silicates. Furthermore, the addition of foreign entities like ethylene glycol and tetramethylammonium silicate limits foaming in the case of Na-silicates. Such a study has allowed to have a better in-depth understanding of the thermal behavior of alkali silicates for addressing the issues being faced in the industrial sector.

Résumé

Les silicates alcalins aqueux sont des matériaux bon marchés, stables et respectueux de l'environnement avec un potentiel dans un certain nombre d'applications industrielles, dont les verres résistants au feu, les cartons et les peintures. La nature intumescente de ces matériaux est d'un intérêt pratique pour des applications devant résister au feu. Ce comportement a été étudié pour les silicates de sodium, potassium ou lithium (avec deux rapports molaires M_2O/SiO_2). Les évolutions structurelles macro- et microscopiques en termes de moussage et de condensation du réseau ont été étudiées avec la température. Les solutions de silicates initiales sont séchées à 150°C pour obtenir des xérogels, dans lesquels l'eau est censée être éliminée. Pour sonder l'état du réseau en fonction de la température, une combinaison d'outils a été utilisée. À l'échelle microscopique, la spectroscopie RMN en phases liquide et solide a permis la quantification des unités structurelles Q^n. La RMN à l'état solide associée à la spectroscopie Raman permet de caractériser l'arrangement structurel local, en particulier dans les silicates de sodium. Des analyses quantitatives par DRX ont aidé à évaluer la cristallisation et l'impact correspondant sur le moussage des silicates de potassium et de lithium.

Le chauffage des silicates alcalins à plus de 500 °C conduit à des changements structuraux. Le matériau se déshydrate par condensation des silanols ou évaporation des molécules d'eau de solvatation. La perte de masse associée est quantifiée par ATG et obéit à une évolution de type Arrhénien. Pour les silicates de sodium l'énergie d'activation unique est conforme à la littérature (30 kJ/mol en dessous de 400 °C). Une approche quantitative combinatoire impliquant des données d'ATG et de RMN suggère que l'existence de cette énergie d'activation unique est une conséquence d'un équilibre entre la condensation des silanols et la présence d'eau de solvatation. A contrario, les multiples énergies d'activation pour les silicates de potassium et de lithium sont observées et expliquées par la cristallisation ou séparation de phase. Un moussage est observé à des températures supérieures à 150 °C en raison principalement de la condensation des silanols et de l'élimination subséquente des molécules d'eau solvatées. Cette température dépend de la composition, du type d'alcalin et de la vitesse de chauffage. L'augmentation de la concentration en alcalin, par exemple en sodium, entraîne une rétention d'eau plus importante dans le xérogel. Cette rétention est corrélée à une température de ramollissement inférieure du matériau et est, macroscopiquement, liée à un moussage plus élevé du silicate.

Les solutions de silicate de potassium moussent abondamment pour une rampe de température de 10 °C/min. Ce moussage peut néanmoins être supprimé par la cristallisation qui intervient soit à une vitesse plus faible de chauffage (en particulier pour une teneur en potassium plus faible), soit lors d'un pré-séchage à 150 °C. Un effet combiné de séparation de phases et de cristallisation est responsable de l'absence de moussage observée dans les solutions de silicate de lithium et les xérogels, quelle que soit la vitesse de chauffage. Ce qui s'explique par une mobilité réduite du réseau en raison de la quantité limitée des silanols et d'ions alcalins. Des observations au microscope optique équipé d'une platine chauffante sur les silicates de sodium suggèrent que les systèmes présentent une évolution du xérogel vers le verre à 400 °C. Au-dessus de cette

température, un comportement similaire aux verres (préparés par la voie conventionnelle de fusion et de trempe) est observé suggérant des variations de viscosité similaires.

Enfin, des revêtements de silicate homogènes et épais (de l'ordre du micron) développés à partir de ces solutions aqueuses sont étudiés. Ils présentent une épaisseur critique pour (i) le moussage dans les silicates de sodium, (ii) la cristallisation et le moussage dans les silicates de potassium selon la composition, ou (iii) le craquage dans les silicates de lithium. L'existence de cette épaisseur critique est attribuée à la distribution et à la longueur de diffusion des molécules d'eau s'échappant des systèmes. En outre, l'ajout d'entités étrangères telles que l'éthylène glycol et le silicate de tétraméthylammonium a permis de supprimer le moussage dans les silicates de sodium. En bilan, cette étude a permis d'avoir une meilleure compréhension du comportement thermique des silicates alcalins aqueux pour répondre aux problématiques rencontrées dans le secteur industriel.

Table of Contents

Aqueous alkali silicates: Industrially crucial, fundamentally less understood

Industrial context

Aqueous alkali silicates have garnered quite an extensive industrial attraction over the decades particularly due to their ability of withstanding elevated temperatures – a source of fire-protection[1,2] in several construction materials including fire-resistant glasses. Furthermore, the capacity of such silicate materials to act as strong binders (especially in geopolymers[3–6] and coatings[7–9]) makes them a potential candidate for a low-cost, stable and green (environmentally friendly) alternative to several organic systems as they are not derived from oil. Furthermore, they don't emit any volatile organic compounds potentially reducing the associated health hazards. Vetrotech, Saint-Gobain's Contraflam fire-resistant glass systems rely on the intumescent nature of environmentally friendly, transparent and UV-stable alkali silicate mixtures that allow for compartmentalization in the case of a fire break out providing with a 30-45 min safety window. Their utilization for other products including paints, where gluing/binding or mechanical flexibilities are of interest, has also been researched.

Figure I: Saint-Gobain products based on aqueous silicates.

Intumescent/Foaming properties of aqueous alkali silicates are of particular interest, with the corresponding behavior being a consequence of endothermic removal of water on contacting fire resulting in a rigid foam that is thermally insulating. However, limitations on the availability of a solid in-depth understanding on the way these silicates behave thermally has led to their sluggish improvement that has hindered, over the years, their true potential for industrial systems. Thus, a fundamental understanding for a better structural analysis in terms of thermal evolution of aqueous alkali silicates has to be established to allow for new avenues that are expected to aid in further exploitation of their properties.

Motivations & objectives

Alkali silicates, despite being quite advantageous industrially, pose issues arising from the fact that they are less stable as compared to pure SiO_2. Thermally-induced intumescence (shown in **Figure II**(b)) is not well understood fundamentally apart from it being unnecessary in applications involving the use of alkali silicates as binders in paints or other coating-related prospects. The

comprehension on rheological properties of these systems is not well-established either owing to the diffusion-related concerns of species, for instance, protons or alkali ions. Cracking, imparted by mechanical fragility of the alkali silicate network, is generally observed in thicker coatings (**Figure II**(d)) and is linked to the generation of strains due to condensation reactions during the coating processing (especially on drying). Furthermore, diffusion of alkali ions leads to the formation of surface carbonates[10,11] (see **Figure II**(e) and (f)) when these silicates are deposited as thin films or thick coatings impacting directly the mechanical properties of the network, rendering it brittle.

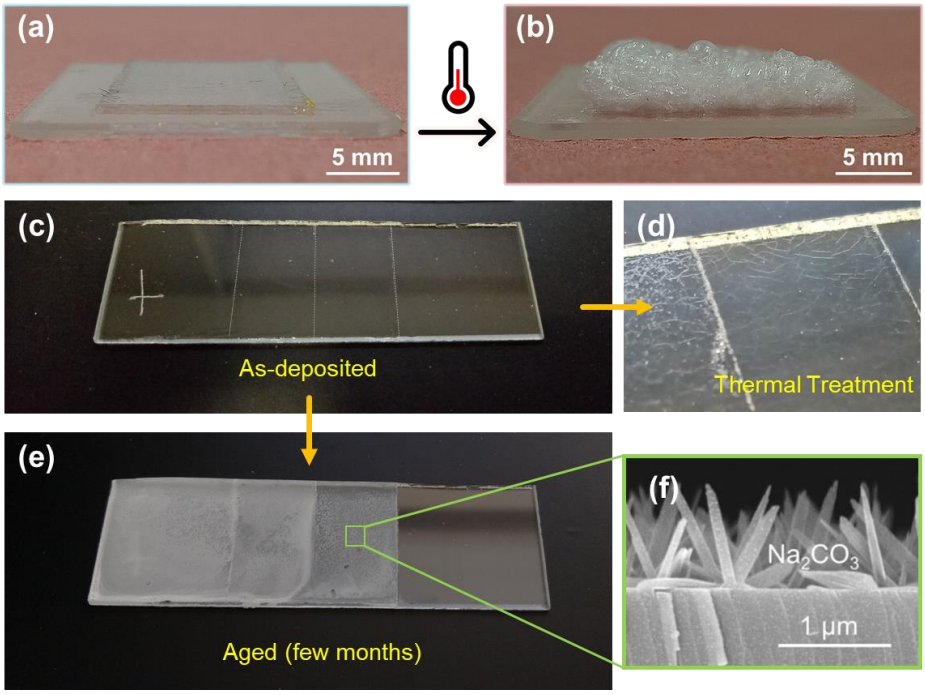

Figure II*:* Na-silicate coatings on glass: thick coating (a) before and (b) after thermal treatment, step coating with variable thickness (c) as-deposited on glass showing cracking after thermal treatment (d) and (e, f[11]) surface carbonation on ageing the as-deposited sample.

Macroscopic thermal behavior of these silicates has a direct link to the changes in structural properties at the microscopic scale, that are not clearly understood and there remains a need to create a link between the real-time performance of the materials and the underlying phenomenon. An in-depth understanding of fundamental properties is, therefore, of interest to follow the structural evolution with temperature in terms of water removal, condensation of silanols and its link to volumetric structural expansion related to foaming, xerogel-to-glass transition and crystallization. Such an investigation is expected to aid in the improvement of existing systems.

Application-related challenges are mainly linked to the rheological properties of the coatings as determined by alkali and water content as well as mass diffusion phenomena (surface carbonation and exchanges with the substrate). One difficulty when trying to understand these phenomena is that the composition of aqueous alkali silicates evolves with temperature or ageing as water is being removed from the material, due to the possibilities of crystallization, or diffusion of the alkali ions. A major goal is, therefore, to try to probe the macroscopic state of aqueous alkali silicates as

a function of temperature (and time if relevant), and then their structure as a more refined measure, in order to understand if it is possible to use the vast literature on alkali silicates (with a small water content) prepared from the traditional melt and quench preparation method and studied in particular in the geochemistry community. A comparative analysis is important to fundamentally understand the thermal evolution of alkali silicates based on the type of alkali ion and the corresponding variations in composition. Thermal treatments are of interest because of the utilization of alkali silicates in fire-retardant applications. And, secondly, due to the fact that industrial glasses are tempered at temperatures approaching 650°C for the processing of functional layers. Furthermore, such coatings tend to crack resulting in inhomogeneous and poor-quality systems that has limited their use for some potential products.

In order to address the limitations of aqueous alkali silicates keeping in view the industrial relevance, this thesis aims at their fundamental understanding upon thermal evolution by:

- Development of a characterization strategy and precise protocols to be able to efficiently study the macroscopic and microscopic structural properties.
- Linking the chemical composition of alkali silicates with thermal history i.e. qualitative and quantitative investigation as a function of temperature for an in-depth analysis of foaming phenomenon.
- Investigating the structure in terms of aqueous preparation method and thermal treatment as well as comparison with glasses produced by industrial melt and quench process, for probing the possibility of having systems (e.g. functional coatings) with glass-like properties through sol-gel processing.
- Development of thick (≥ 30 µm), homogeneous and high-quality inorganic coatings without any cracks followed by the investigation of their thermal behavior and possibilities of limiting/controlling foaming.

The preceding work (at LPMC in collaboration with SGR Paris) related to this subject focused more on the diffusion-related aspects of thin films (few 100s of nm) that were relatively homogeneous and crack-free.[11] Different compositions of Na, K and Li-silicate films were prepared and analyzed for structural changes at room temperature and 450°C showing a densification of the silica network on annealing due to condensation.[11] Surface carbonation was observed on ageing for Na and K-based coatings while Li-silicate films were relatively stable. However, for a comprehensive understanding of the structural properties in thin films or thicker coatings, a fundamental comprehension of the thermal behavior of solutions or pre-dried powders is necessary at first.

Outline of the thesis

This work showcases the fundamental understanding of aqueous alkali silicates in solutions, powders and coatings. A combination of characterization tools has been used to probe the state of alkali silicate network in starting solutions and pre-dried powders (obtained by pre-drying solutions) on thermal evolution. A link between macroscopic and microscopic structural evolution has been established by comparing the behavior of different alkali silicates and compositions. Thermal properties of thick and homogeneous coatings obtained from the various aqueous alkali silicates have also been investigated.

The thesis is structured into the following 5 Chapters:

Chapter 1 gives a literature overview of the various binary alkali silicates including soluble silicates, xerogels, glasses and the corresponding crystalline compounds. Their preparation methods and the various properties especially those concerning the structure are discussed along with the different techniques generally used for their characterization.

Chapter 2 discusses the **experimental methodology** followed. Starting materials and their preparation methods are listed followed by the discussion on the developed 'characterization strategy' involving a combination of several tools for investigating the structural properties.

Chapter 3 gives a detailed analysis on the 'thermal behavior of aqueous alkali silicates' starting from the structural properties in solutions. Macroscopic and microscopic structural evolution of pre-dried powders, in terms of the evolution of proton-related species and alkali ions, is then discussed where Na, K and Li-silicates of two different molar ratios each are compared quantitatively in terms of their network-related properties below 450°C. Impact of water release, crystallization and phase separation on the corresponding thermal evolution is presented in detail. In-situ evolution of pre-dried pellets above 450°C has also been discussed.

Chapter 4 is dedicated more to the macroscopic structural changes of solutions and pre-dried powders in terms of foaming i.e. volumetric changes observed visually. A comparison on thermal evolution is also drawn for the thick and homogeneous coatings developed from the various alkali silicate solutions along with some possibilities of limiting the extent of foaming.

Chapter 5 concludes globally the main outcomes of the work followed by the possibilities of the various future directions for further structural investigation mainly in coatings.

Chapter 1.

Binary alkali silicates: An overview

Glass has been an integral part of our lives since centuries with modern applications ranging from glasses for drinking, building windows, lenses, biomedical implants, optical fibers to aircraft windshields. The main structural component of glass is the network former which in most cases is silica (SiO_2), with compositions that correspond to roughly a third of the earth's crust by weight, and is arranged in the form of corner/edge sharing tetrahedrons. Both crystalline and amorphous forms of SiO_2 are possible depending upon the cooling rate once molten SiO_2 is cooled down.[12] Foreign elements such as alkali ions (sodium Na, potassium K, lithium Li) can be added that act as network modifiers and change the properties of the network.[13–16] Aqueous solutions with similar structural arrangements are also possible and have been termed as water-soluble or aqueous alkali silicates.

1.1. Aqueous alkali silicates

Large amount of alkali ions leads to soluble silicates commonly referred to as 'water glass', a term coined by Johann Nepomuk von Fuchs while investigating their industrial production around the 1820s. Solid glassy materials with various multiscale structures can be produced through drying of these aqueous solutions and represent a silicate network as shown in **Figure 1.1** with the structure depending upon the amount of alkali ions and water.[17–20]

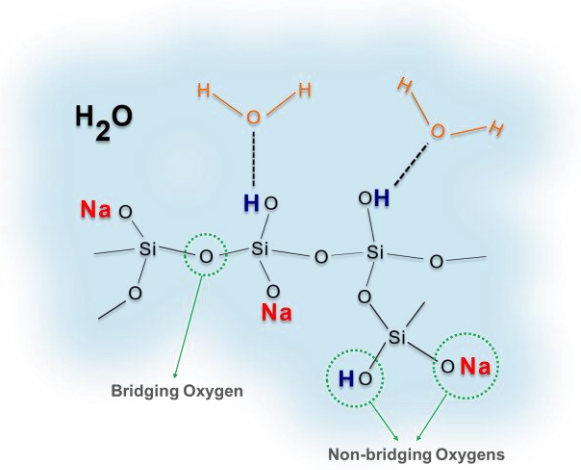

Figure 1.1: Schematic illustration of the network structure in aqueous alkali silicates.

These commercially available (or lab-prepared) solutions are generally defined in terms of their molar ratio M_2O/SiO_2 (or sometimes weight ratio for practical purposes) where M represents the alkali ion (Na, K, Li) in the network. They are composed of SiO_2 tetrahedrons linking up to make long chains with the network comprising of bridging oxygens (BOs) and non-bridging oxygens

(NBOs) depending upon the connectivity. BOs are the oxygens that are further connected to nearby Si atoms while those linked to alkali ions or protons are referred to as NBOs. Proton-related species in the solution are available as free water, network silanols and solvating water (molecules H-bonded to silanols or alkali ions).[21] The nature of alkali ion and the corresponding composition including the concentration of alkali, silica and water has a direct influence on the overall properties of the network including solubility, viscosity, glass transition temperature (T_g) and diffusion behavior.

1.1.1. Preparation

Soluble silicates were prepared formally and have been in use ever since the mid-late 1900s. Several refinements in the conventional production route of these aqueous silicates, involving the reaction of carbonate or sulfate-based precursors with sand above 1300°C, have been made over the years.[22] Modern routes for obtaining these silicates utilize similar methods with possibilities of their commercial as well as lab-scale preparation.

1.1.1.1. Commercial

Current commercial production of aqueous alkali silicates is based on melting[22–26] or hydrothermal process[22,25,26] shown schematically in **Figure 1.2**. The raw materials used in the process include sand (pure silica-Quartz or other sources), alkali carbonates (Na_2CO_3, K_2CO_3, Li_2CO_3), alkali hydroxides (NaOH, KOH, LiOH) and water. SiO_2 and alkali carbonates are the ingredients for production through the melting/solving process while hydroxides are reacted with SiO_2 when employing the hydrothermal route.

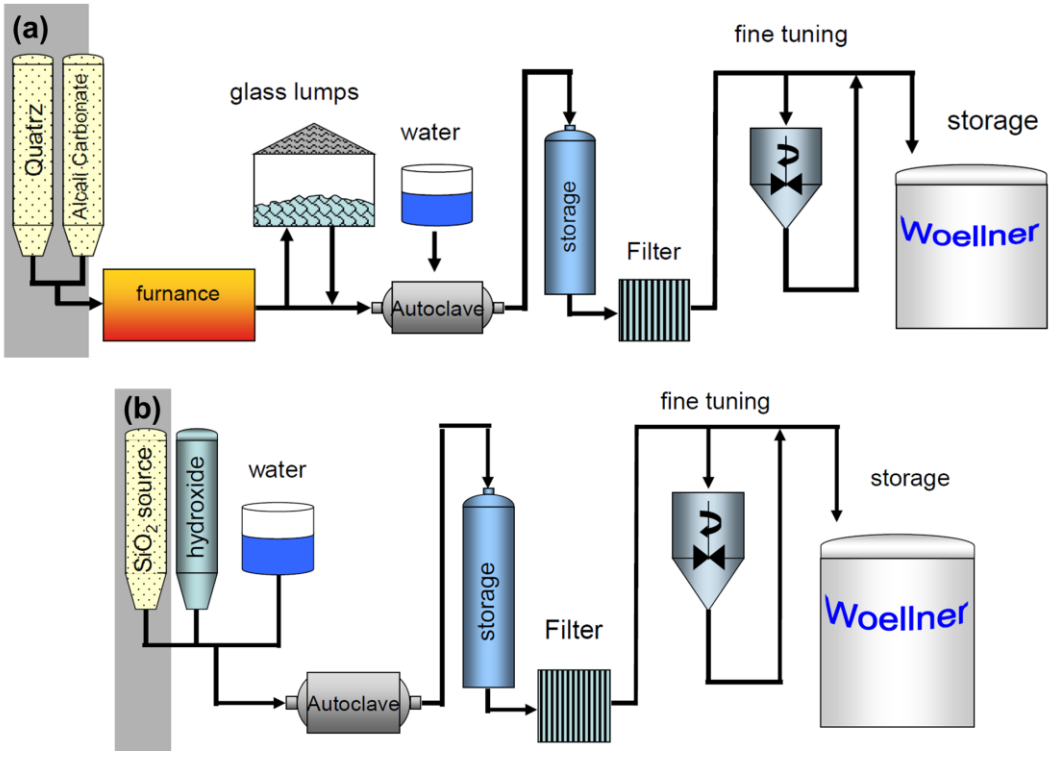

Figure 1.2: Schematic illustration of (a) melting and (b) hydrothermal process for the commercial production of aqueous alkali silicates (reproduced from Woellner group's document available online[25]).

The initial step in the production of alkali silicates through the melting process is the direct fusion of Quartz with the corresponding alkali carbonate at temperatures above 1300°C followed by cooling and crushing to obtain glass lumps (**Figure 1.2**(a)) according to eq. 1.1 as:

$$M_2CO_3 + xSiO_2 \rightarrow M_2O.xSiO_2 + CO_2 \quad (1.1)$$

$$2MOH + xSiO_2 \rightarrow M_2O.xSiO_2 + H_2O \quad (1.2)$$

where 'M' corresponds to the alkali ion while 'x' indicates the SiO_2/M_2O molar ratio. The glass lumps' composition is non-stoichiometric and depends upon the ratio of starting constituents. These lumps or stones are then dissolved in hot water under pressure in an autoclave to obtain a solution that is then filtered to remove turbidity and non-reacted/dissolved glass constituents.

Hydrothermal process involves a reaction between the reactive SiO_2 source (sand) and alkali hydroxide solution, represented by the eq. 1.2, to obtain alkali silicates followed by dissolution in water and subsequent filtering as shown in **Figure 1.2**(b). The commercially produced aqueous silicates are available in various compositions, which can be used directly for lab-scale manipulation of molar ratios or prepared through solution-based routes.

1.1.1.2. Lab-scale

Solutions of varying compositions of Na, K and Li silicates can be prepared by addition of known quantities of corresponding alkali hydroxide pellets[6] or solutions[18,27,28] and SiO_2 amorphous fumes[6] or colloidal solutions[27] into the commercially available aqueous alkali silicates depending upon the target molar ratio. Furthermore, mixing directly known quantities of alkali hydroxide with SiO_2 (colloidal,[20,28–30] gel,[18,31] amorphous fumed[18,32–34] or crystallized[35]) and water (if required) results in the formation of aqueous silicates rather easily at the lab-scale with properties similar to commercially available compositions.

1.1.2. Properties

The concentration of constituents i.e. alkali and SiO_2 is directly related to the relevant properties of soluble silicates. For practical purposes, solutions are generally prepared in particular molar ratio (M_2O/SiO_2) ranges that correspond to the stability regime of aqueous solutions depending upon the alkali type. Commercial solutions from Woellner are available in the ranges shown in **Table 1.1**. while higher molar ratio values approaching 1.4 for Na[17] and 2.2 for K-silicate[36] solutions have also been reported. Alkalinity, buffering ability, solubility, bound moisture, drying time and reactivity decrease on lowering the molar ratio while an inverse behavior is observed for other properties including dried strength, viscosity and chemical resistance.[23,25,26]

Table 1.1: Molar ratio range for the various aqueous alkali silicates currently produced by Woellner[25] and the corresponding conversion factor for weight ratio.[8,23,25]

Soluble Silicate	Molar Ratio (M_2O/SiO_2)	Conversion factor (Molar Ratio/Weight Ratio)
Na-silicate	0.24 – 0.59	1.031
K-silicate	0.25 – 1	1.568
Li-silicate	0.2 – 0.4	0.497

1.1.2.1. Viscosity

From an application point of view, the usefulness of soluble silicates is strongly dependent upon the viscosity of these solutions with, for instance, a lower viscosity being preferred in cases where adhesive action is required. Changes in viscosity of the silicate solutions are associated with the variations in molar ratio as well as the solid content.[37] Viscosity, in general, tends to increase with an increase in the amount of SiO_2 in the system for the molar ratio range given in **Table 1.1**. Moreover, as a function of alkali concentration and above the molar ratio ranges shown, a steeper increase in viscosity is seen for the solutions with relatively higher content of SiO_2 with an even increased viscosity as a function of solid content.[23,37,38] Viscosity variations in K-silicates are more abrupt as compared to their Na-silicate counterparts with K-silicates showing higher viscosities for similar molar ratios[26,37] and thus are utilized accordingly for industrial purposes.

Viscosity is directly related to the ability of the network to form bonds with foreign species, a property useful for adhesive applications, with lower viscosity allowing for an increased reactivity.[23,25] It has also been seen, especially in the case of Na-silicates, that there exists a break point in the viscous behavior of molar ratios approaching 0.25 above which a slight loss of water may result in a steep increase in the viscosity values generating a semi-solid behavior.[8,37] This break point is shown in **Figure 1.3** with the effect being more pronounced on increasing SiO_2 concentration (**Figure 1.3**(a)).

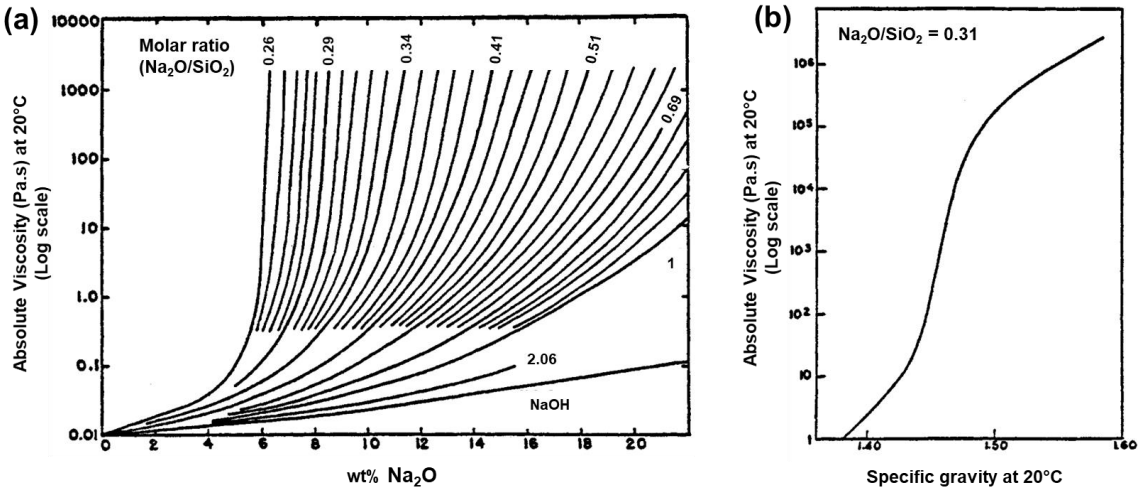

Figure 1.3: Viscosity of (a) sodium silicate solutions as a function of concentration and molar ratio, and (b) the molar ratio Na_2O/SiO_2=0.31 at 20°C as a function of concentration.[37]

For instance, **Figure 1.3**(b) shows the viscosity break point for the molar ratio Na_2O/SiO_2=0.31 whereby removal of around 2% water increases the viscosity to 11.1 Pa.s.[37] A slight further removal of water above this point results in an exponential increase in viscosity up to the specific gravity (density of Na-silicate/density of water) value of 1.48 (or 1.4 wt% Na_2O) with further viscosity increase inducing gel-like properties.[37] This results in the loss of the tackiness of the solutions. Hence, changes in viscosity of the solutions on changing the composition tend to impact their stability in terms of the ability of the solutions to gel or phase separate.

1.1.2.2. Stability

The stability of soluble silicates in terms of molar ratio (M_2O/SiO_2) is dependent upon the solution properties with respect to the SiO_2 constituents in the form of particles. Size of colloidal particles (few nm) does not depend on the type of cation and increases on increasing the SiO_2 content with linear relation in the molar ratio ranges shown in **Table 1.1**, while below such values the increase is less steep.[27,39] The monomer (isolated SiO_2 tetrahedrons) concentration increases rapidly on going from molar ratio of 0.25 to higher values while it remains relatively constant below this range. Gelling of the solutions is observed for Na and K-silicates[27] below the molar ratio range shown here. The instability of solutions at higher SiO_2 concentrations leads to phase separation, gelation or turbidity in Na-silicates. This is due to the changes associated with network condensation when properties were investigated using a combination of Fourier-Transform Infrared (FTIR) spectroscopy, Small Angle X-Ray Scattering (SAXS) and Dynamic Light Scattering (DLS) measurements.[39] Monomeric species are in abundance in the lower SiO_2 content solutions with a rapid increase in the polymerization of the network (within the stability molar ratio regime) associated to condensation of these monomeric species as shown schematically in **Figure 1.4**(a). Above a molar ratio of 0.25 (in **Figure 1.4**(a)), less monomeric species are available as compared to clusters of condensed particles. Higher SiO_2 content systems tend to be unstable due to the formation of large sized spheres, as a result of condensation of clusters, that can agglomerate resulting in gelation of the solution.

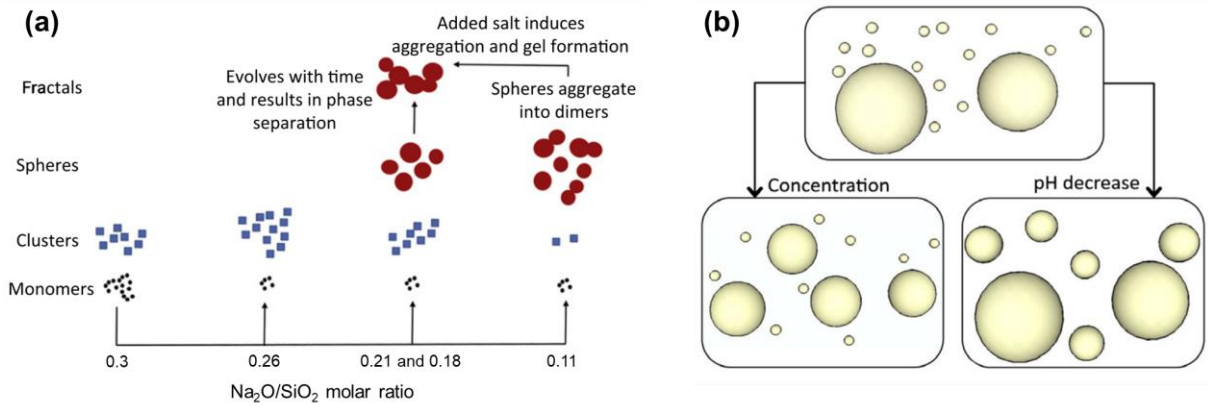

Figure 1.4: Schematic illustration of (a) main constituents[39] of Na-silicate solutions and (b) the corresponding gelation observed as a consequence of increased SiO_2 concentration and decreased pH.[40]

Gelation behavior in alkali silicates was also studied by manipulating the concentration as well as pH of the solutions.[18,40,41] Lowering pH and increasing SiO_2 concentration in Na-silicates tends to shift the viscosity towards higher values with Newtonian behavior observed for lower concentration and higher pH while shear thickening at highest concentration and lowest pH at higher shear rates.[40] Increasing concentration or lowering the pH (typically <11.2 or even 10)[26] tends to shift the system towards a gel-like state. As a function of increasing SiO_2, a greater number of smaller particles (with an increased surface area) are formed from the larger ones while condensation of smaller particles leads to larger particles on decreasing pH as indicated in **Figure 1.4**(b). Thus, changing the molar ratio tends to impact the solution properties both in terms of the physical changes observed as well as the structural changes at the microscopic scale.

1.1.2.3. Structural variations upon changing composition

The structural organization of aqueous alkali silicates has been investigated by a number of different techniques to probe the properties of the network. FTIR spectroscopy has provided a more qualitative measure of the distribution of the silicate structure as shown in **Figure 1.5**.[42] Bands, corresponding to various structural building blocks, are generally observed in the range 700-1250 cm^{-1},[6,42] with the stretching vibration of Si-O-Si appearing in 900-1250 cm^{-1} range. Increasing the quantity of SiO_2 i.e. reducing the molar ratio leads to a more condensed network with the intensity of the band moving towards higher wavenumber.[6,17,30,39,42] Such measurements have allowed to get a more general information on the structure and are not very quantitative.

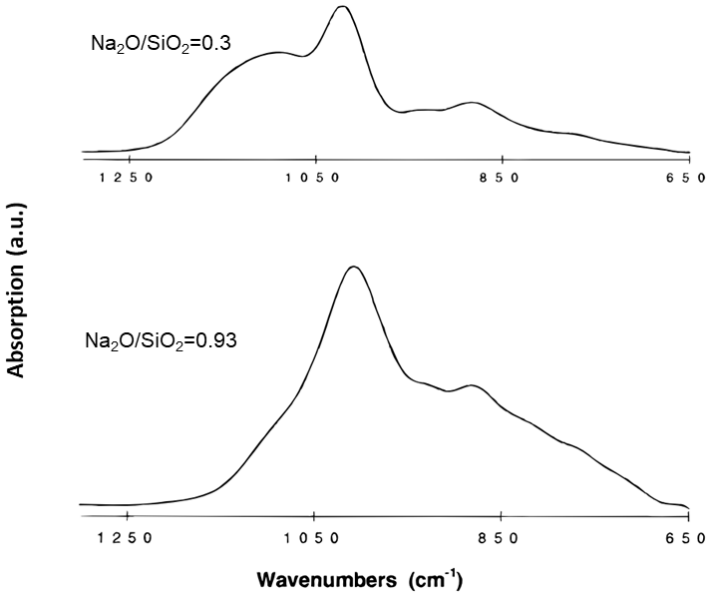

Figure 1.5: Impact of changing the Na_2O/SiO_2 molar ratio on the structure of sodium silicate solutions determined through FTIR spectroscopy.[42]

Quantitative analysis of the network in aqueous alkali silicates has been studied in-depth through liquid-state ^{29}Si Nuclear Magnetic Resonance (NMR) spectroscopy measurements.[17,18,20,28,31–34,43,44] It has been found that changing the quantity of constituents causes variations in the relevant structural properties of soluble silicates which are generally characterized for their structure in terms of Q^n units that serve as the building blocks of the network. A schematic illustration of the Q^n units is shown in **Figure 1.6**(a) and (b). 'Q' represents the silicon atom of a tetrahedron while 'n' indicates the number of corresponding BOs. Q^0 indicates an isolated tetrahedra also referred to as a monomer. If one of the oxygen atoms of the tetrahedron is further connected to silicon atom of another tetrahedron, the linkage is referred to as Q^1. Similarly, Q^2, Q^3 and Q^4 units indicate the subsequent connectivity of 2, 3 and 4 oxygen atoms, respectively. NMR has been employed to study the distribution of these Q^n units. One such example is shown in **Figure 1.6**(c), (d) and (e) for Na-silicates solutions[18] indicating the distribution of Q^n units corresponding to specific chemical shift values. These peaks can be integrated for the area to obtain the exact amount of each specie giving a plausible quantitative information relevant to the network.

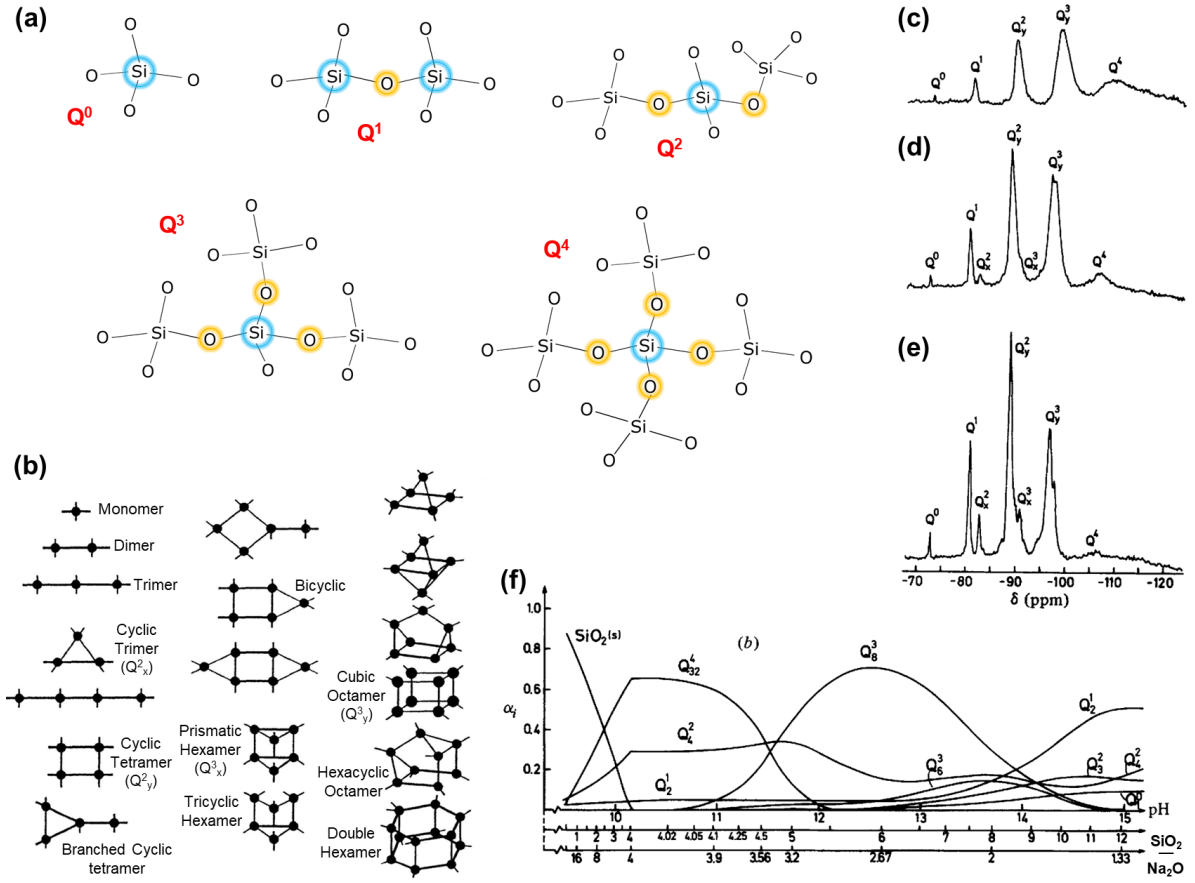

Figure 1.6: Schematic illustration of the various (a) commonly observed Q^n unit forms from ^{29}Si NMR and (b) the different organizations possible, (c), (d) & (e) the corresponding spectrum for molar ratio Na_2O/SiO_2 of 0.29, 0.36 and 0.44, respectively (Q^2_y also represents middle groups while Q^3_y indicates branching groups of the chain), and (f) the variation of Q^n units as a function of pH and molar ratio reproduced from Svensson et al.[18]

The broadness in each peak is indicative of the various arrangements possible with 4 for Q^1, 10 for Q^2, 20 for Q^3 and 35 for Q^4, respectively, along with the existence of different cyclic or branched species (as shown in **Figure 1.6**(b)) at similar chemical shift values making it difficult to resolve the complete distribution[44] at lower field e.g. 8.4 T. Increasing the amount of alkali ion in the network tends to shift the spectrum towards lower Q^n units indicating depolymerization of the structure,[17,18,34,42,44] irrespective of the type of alkali silicate, as shown in **Figure 1.6**(c), (d), (e) and (f) for Na-silicates. A similar trend is observed on dilution or increasing pH.[18,42] Moreover, gelation was observed for solutions approaching Na_2O/SiO_2 molar ratios of 0.25 on increasing SiO_2 content[18] due to increases in viscosity suggesting a direct relation between the distribution of the network structure to the properties observed.

For instance, binding strength is higher for lower molar ratios (more depolymerized state), as that allows for more bonding options (in the form of siloxane bonds) to the incoming mineral fillers[17,18,28] when these silicates are used as binders in some applications. The quantitative measure of the polymeric state of a solution,[28] representative of its activity in terms of binding, is:

$$S = \frac{\rho c_{SiO_2}}{10 M_{SiO_2}} \sum_{n=0}^{4} (4-n) c_{Q^n} \qquad (1.3)$$

where '*S*' represents the total concentration (mol/L) of SiO^-M^+ and SiOH, 'ρ' is the solution density, '*c*' the concentration in wt%, '*M*' the molar mass of SiO_2 and '*n*' the number of BOs. A higher value of '*S*' would suggest a lower connectivity of the solution and, therefore, a higher binding activity.

Apart from FTIR and NMR techniques, Raman spectroscopy has also been utilized[17,29,45,46] to study the structure and, hence, the properties of soluble silicates but provides a more qualitative assessment, in terms of the evolution of Q^n units, in general. Various bands are seen in the spectrum (as shown in **Figure 1.7**) with that corresponding to alkali network modifiers ($-M^+-O^-$) centered at 340-360 cm^{-1}, the range 400-700 cm^{-1} represents the Si-O-Si scattering while the distribution of Q^n units lies in the Raman shift range 800-1300 cm^{-1}. Increasing the SiO_2 content in the silicate[17,29,46] or reducing the pH of solutions[29] tends to shift the Q^n band towards higher Raman shift values suggesting the network to be proceeding towards a more polymerized state while an inverse behavior is observed on increasing the alkali content with the corresponding band at 340-360 cm^{-1} increasing in contribution.[17,46]

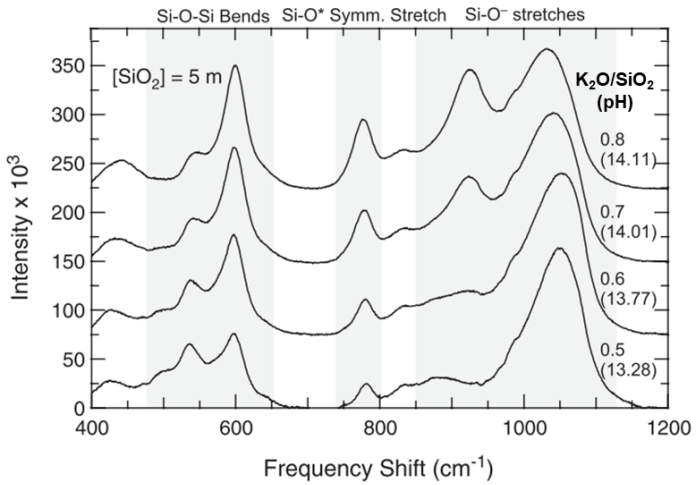

Figure 1.7: Evolution of the structure of K-silicate solution as a function of molar ratio (and pH) observed through Raman spectroscopy.[29]

Raman spectroscopic data, although being qualitative, can also provide a quantitative measure of the state of the network when correlated with the Q^n units obtained from NMR spectroscopy. For instance, deconvolution of the Q^n band gives information on the structural variations in terms of each individual Q^n unit or the area under the peak for $-M^+-O^-$ when correlated with NMR Q^n units suggests a decreased network connectivity on increasing the concentration of alkali in the silicate.[17]

The structural investigation of aqueous silicates provides a plausible information on the way these systems are expected to behave practically. Physical properties change as a function of the structural variations that can be tuned by changing the molar ratio of aqueous silicates and characterized to probe the state of the silicate for imparting the relevant properties important in industrial systems.

1.1.3. Applications

Aqueous alkali silicates present a cheap, stable, high temperature resistant and green class of materials with a number of applications relevant for various industrial sectors with the main contribution being towards construction-related needs. Intumescent property of alkali silicates has garnered quite an extensive research and industrial attraction over the decades particularly due to their ability of withstanding elevated temperatures – a source of fire-protection[1,2,47,48] in several construction materials including fire-resistant glasses. They have been quite extensively studied for applications in geopolymers,[3,4,6,36,49] refractory cements[26] and coatings[7–9,26] mainly because of their binding ability. Moreover, these systems have also been researched for applications involving coatings with tunable optical properties.[11,50] Furthermore, their useful properties are also being utilized in detergents, water treatment, textiles and petroleum processing.[26]

1.2. Xerogels

Drying at ambient/higher temperatures or thermally treating aqueous alkali silicates removes water from the system turning the material into a solid called 'xerogel', from the Greek word 'xeros' meaning dry. This leads to changes in the structural organization of the material.[51–53] In order to relate the network reorganization to accommodate the loss of water from the system, an understanding of how the sol-gel reaction proceeds in the case of silica is thus necessary.

1.2.1. Sol-gel chemistry of silica

Monosilicic acid – $Si(OH)_4$, the chemical source of silica, is soluble in water at SiO_2 concentrations below 100 ppm. Above 100-200 ppm, the monomer tends to polymerize to form higher molecular weight species as a consequence of condensation.[54] A schematic illustration of the process proposed by Iler[54] is shown in **Figure 1.8**(a). Dimers, trimers or even cyclic species are formed to which further addition of monomers may take place. This leads to the formation of particles that tend to grow in size due to a reduced quantity of terminal SiOH groups with the core of the particles being anhydrous. These particles serve as nuclei and may grow further due to Ostwald ripening whereby smaller particles, having a high surface charge density, merge with the larger ones resulting in an increase in the size of particles along with a reduction in total quantity.

Growth of particles into sols or three-dimensional gel networks is dependent mainly upon the pH and is influenced also by the addition of salts (e.g. NaCl, HCl). At high pH values (7-10), in the absence of salt, silica particles are negatively charged and repel each other so the particle growth occurs without aggregation (**Figure 1.8**(b)) and continues until the size is 5-10 nm after which the growth is slower. However, adding some salt reduces the charge repulsion by neutralization of the particles leading to aggregation and gelation. The rate of polymerization and depolymerization is slower at lower pH (<7) limiting the particle growth once the size reaches 2-4 nm. Furthermore, the ionic charge on silica particles is low at low pH values that may lead to aggregation and gel formation.

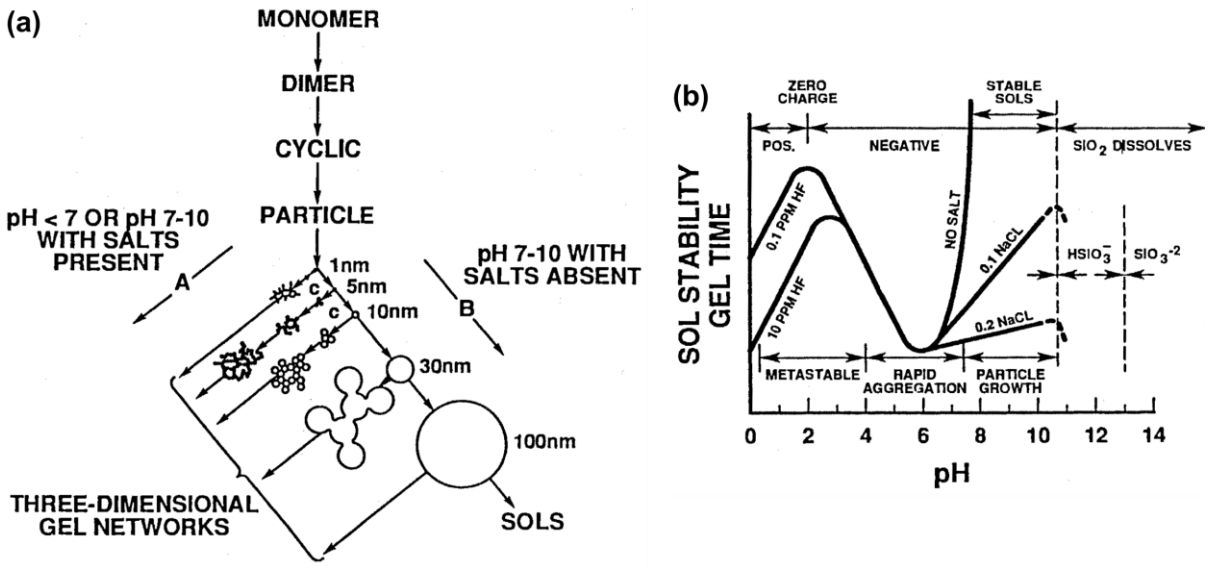

Figure 1.8: (a) Polymerization behavior in aqueous silica showing the impact of pH and salts on the network organization (basic conditions (B) let particles in sol grow in size with decrease in numbers while acidic conditions (A) cause aggregation of particles into three-dimensional gel networks) and (b) effect of pH on the gelling of silica sols. (Both the figures are reproduced from literature[54,55])

1.2.1.1. Dependence on pH

The polymerization process is divided into three pH ranges i.e. pH<2, pH=2-7 and pH>7. pH=2 represents the point of zero charge where the total net charge on the particles' surface is zero while the isoelectric point is also in the pH range 1-3. Polymerization is a consequence of the catalytic activity of H^+ (or F^- from HF) at pH<2 and OH^- at pH>2. In the pH range 2-7, the gel times reduce and condensation is proportional to the concentration of OH^- governed by the following reactions:

$$\equiv Si - OH + OH^- \rightarrow \equiv Si - O^- + H_2O \quad (1.4)$$

$$\equiv Si - O^- + OH - Si \equiv \rightarrow \equiv Si - O - Si \equiv + OH^- \quad (1.5)$$

Polymerization is a consequence of intermediate ionization of silanol groups to $\equiv SiO^-$ (eq. 1.4) that react with a non-ionized silanol leading to condensation (eq. 1.5). Condensation thus occurs between a more condensed species and a less condensed one suggesting the rate of dimers' formation to be low as at lower pH values, $Si(OH)_4$ is ionized to a small degree. If dimer is a stronger acid (i.e. greater number of siloxane linkages of Si than silanols) than monomer, the following reaction leads to a trimer:

$$(OH)_3SiOSi(OH)_2O^- + (OH)_4Si \rightarrow (OH)_3SiOSi(OH)_2OSi(OH)_3 + OH^- \quad (1.6)$$

Dimers, once formed, react with monomer to form trimers that in turn may react with another monomeric unit to result in a tetramer (schematic illustration of the species is shown in **Figure 1.9**(a)). Furthermore, cyclic species tend to form owing to the fact that SiOH end groups of linear polymers have close enough proximity for condensation to occur. As the cyclic species dominate, further condensation of silanol groups leads to three-dimensional species in the form of a particle with anhydrous core and surface silanols as shown by the model in **Figure 1.9**(b).[54] Further growth of the particles continues with monomers or oligomers reacting with the surface silanols until

most of the oligomers are consumed at which point the particles start to grow at the expense of smaller particles while decreasing in number at the same time. Addition of an acid would tend to reduce the possibilities of dissolution of the particles by limiting the depolymerization reaction i.e. preventing siloxane bonds from being hydrolyzed once they are formed. The particles, which are 2-4 nm in size at this point due to limited solubility of silica at lower pH values, may coalesce to form siloxane linkages through the interaction of ionized groups and neutral silanols at the particle's surface shown schematically in **Figure 1.9**(c). This type of agglomeration or coalescence would then continue until a larger three-dimensional gel-like network is formed.

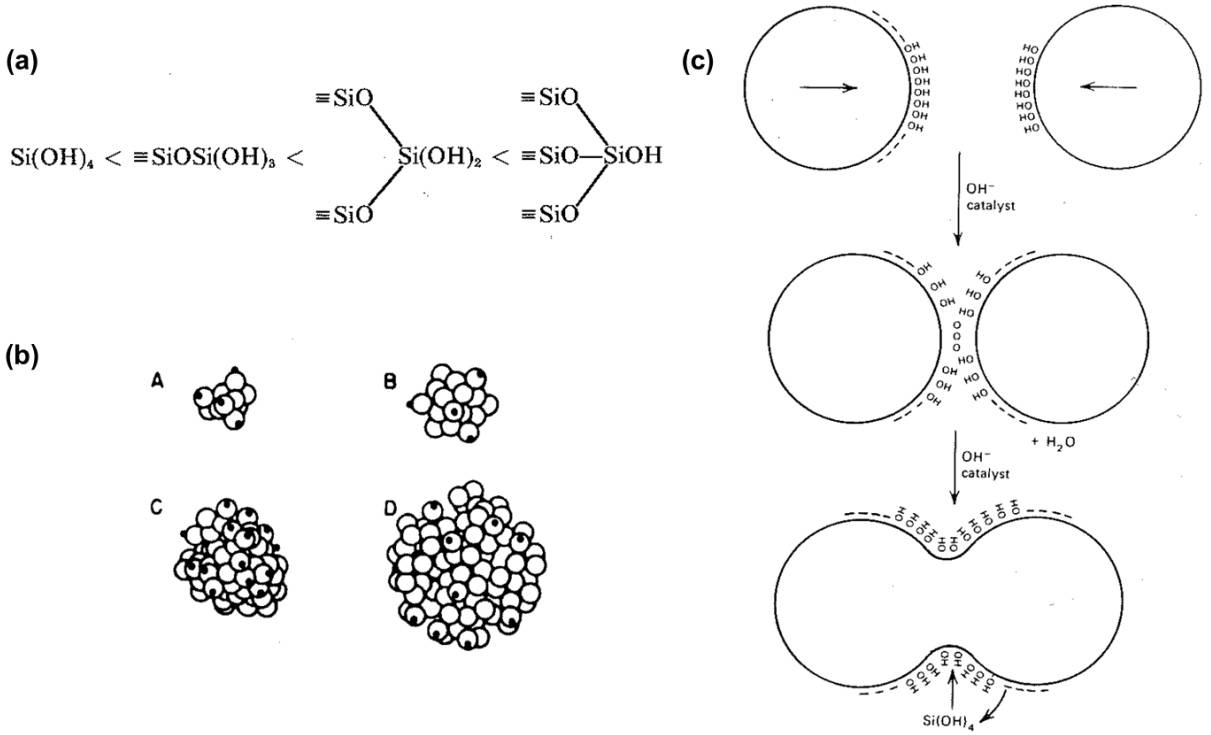

Figure 1.9: Schematic illustration of (a) the various linkages present in the solution, (b) A-cyclic trisilicic acid, B-cubic octasilicic acid and C, D-corresponding theoretical colloidal particles formed with open circles representing oxygen atoms while black dots indicating surface hydrogens, and (c) Aggregation resulting in bond formation between silicate particles.[54]

Above the pH value of 7, ionization of the polymer species is very high and that leads to a rapid reduction in the number of monomers or oligomers. Coalescence or aggregation of particles is not observed due to their repelling nature induced by surface charges. Thus, the polymerization reaction involves only an increase in the size of particles along with a reduction in their quantity with monomers depositing on the surface of particles. At pH approaching 12 and above, most of the silanols are available as deprotonated species with cyclic trimers and tetramers being the building blocks of the network suggesting the dissolution of silica as silicate.

1.2.2. Alkali silicate xerogels

The starting aqueous alkali silicates are synonymous to colloidal dispersions of amorphous silica,[27,40,52,56] referred to as alkali silicate sols[22,56] and can be aggregated in the size range 30-100 nm[56] (or approaching even 1300 nm when dried)[57] along with the availability of smaller 1-5 nm particles,[22] depending highly upon the molar ratio used, with pH values above 10 in general. The

colloidal dispersions are stabilized by a double layer comprising of negatively charged SiOH groups that are covered by hydrated alkali ions e.g. Na^+. Reducing the molar ratio of the silicate i.e. increasing SiO_2 content, tends to increase the size of the polysilicate species in the solution impacting directly the structural arrangement and distribution.

1.2.2.1. Drying of aqueous solutions

On drying, structural modifications are induced in aqueous silicates to the extent that the volume of interstitial solution (i.e. voids between particles) is reduced until aggregates are in proximity resulting in the formation of new connections and a rigid structure.[52] Drying kinetics are influenced by the way water is released from the system. During the drying process of porous gels, a constant water loss is observed initially when surface water is removed followed by a decay in the rate of this evaporation once the evaporation front moves towards the inside of the material.[55] The rate of mass loss during drying may be given by Hertz-Knudsen equation[58] as:

$$\frac{\mathrm{d}m}{\mathrm{d}t} = (p_v - p_p)\sqrt{\frac{m_{molecule}}{2\pi k_b T}} \qquad (1.7)$$

where 'm' is the mass of drying body, 't' the time, 'p_v' the vapor pressure of liquid, 'p_p' the partial pressure of evaporating molecule in gas phase, '$m_{molecule}$' the mass of evaporating molecule, 'k_b' the Boltzmann constant and 'T' the absolute temperature. Eq. 1.7 suggests that the mass loss would stop once the vapor pressure of the drying liquid becomes equivalent to the vapor pressure of water in the gas phase i.e. $\Delta p = (p_v - p_p)$ becomes zero.

Na-silicate solutions, when dried at 80°C for longer durations approaching 50 days, tend to show the mass loss behavior shown in **Figure 1.10**(a)[57] with a constant weight observed for longer drying times indicating a thermodynamic equilibrium between the vapor pressure of atmospheric water and dried sodium silicate. Water content decreases with increasing drying temperature, and decreasing molar ratio i.e. increasing SiO_2.[57] At the structural scale, an initial rearrangement of interstitial species (attributed to Na^+, OH^-, H_2O distributed randomly) has been suggested to occur around 60-80°C as shown in **Figure 1.10**(b) where the entities organize themselves towards more energetically favorable sites.[51] Drying may also lead to the formation of larger particles approaching sizes of 1300 nm due to aggregation.[57] The manner in which these changes take place is quite related to the way the sol-gel reaction proceeds in the case of silica and has in fact been called as a sol-colloid glass transition or a sol-gel transition due to the aggregates forming a random closed packing, solidifying the sol into a dense gel by reducing the distance between the colloids.[52] The structure of the material is believed to proceed from a sol to that of a particulate with further drying inducing a finer structure.

If the dried water glass microstructure is assumed to be composed of random close packing of particles, capillary forces can be calculated considering that capillaries represent voids (with sizes in the range 0.7-10 nm) between the particles saturated with solution.[57] On drying, deformation of the particles is suggested to be induced as a consequence of aggregation as shown schematically in **Figure 1.10**(c). The volume of the solid is reduced due to the capillary pressures

imposed whereby their values exceed those of the stresses required to generate plastic deformation.[57] Once dried at relatively higher temperatures (approaching 130°C), structural changes are induced at the network scale[51–53] due to reorganization and condensation leading to the formation of a xerogel, modifying the degree of polymerization of the system in the process. Condensation occurs when adjacent terminal silanol groups interact resulting in the formation of siloxane bonds, and the process continues as enough water is available to catalyze further reactions (**Figure 1.10**(d) and (e)).[51]

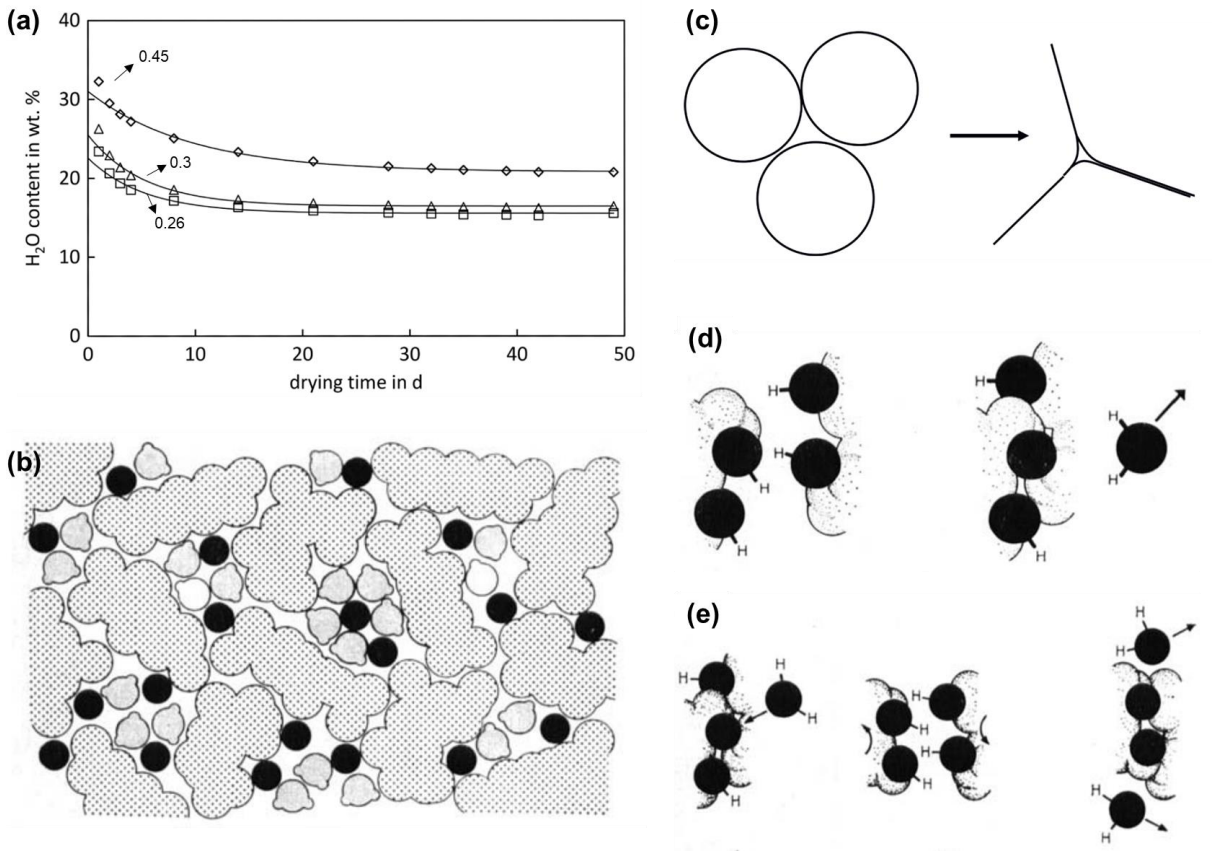

Figure 1.10: (a) Water content in sodium silicates with M_2O/SiO_2=0.45, 0.3 and 0.26 as a function of drying time (in days) at 80°C,[57] and schematic illustration of structural variations on drying of sodium silicates: (b) gently dried material with silicate ions shown in lightly stippled units of various shapes, sodium ions in back, hydroxyl groups containing one and water molecules two lobes, respectively,[51] (c) aggregation of particles leading to neck formation due to plastic deformation,[57] (d) reaction between silanol groups to form siloxane bond,[51] and (e) mechanism for water to act as a catalyst.[51] Note that black circles in (d) and (e) represent oxygen atoms.

1.2.2.2. Foaming and xerogel-to-glass transition

Dried sodium silicates with water content less than 45% have been suggested to have a transparent and amorphous aspect, comparable to vitreous materials.[59] Heating Na-silicates (pre-dried at <100°C for varying amount of time and up to even 64 days) to temperatures approaching 300°C under hydrothermal conditions leads to the release of water inducing physical changes to the aspect of the material[59] with water-related species being removed as free water, solvating water molecules and silanols.[53] At temperatures approaching 150-180°C (corresponds to a step in Differential Scanning Calorimetry – DSC measurements), foaming[53,59–61] is observed as shown in **Figure 1.11**(a) and (b) due to rapid dehydration of the system. This coincides with a DSC peak corresponding to glass transition at which a solid-liquid transformation takes place.[59]

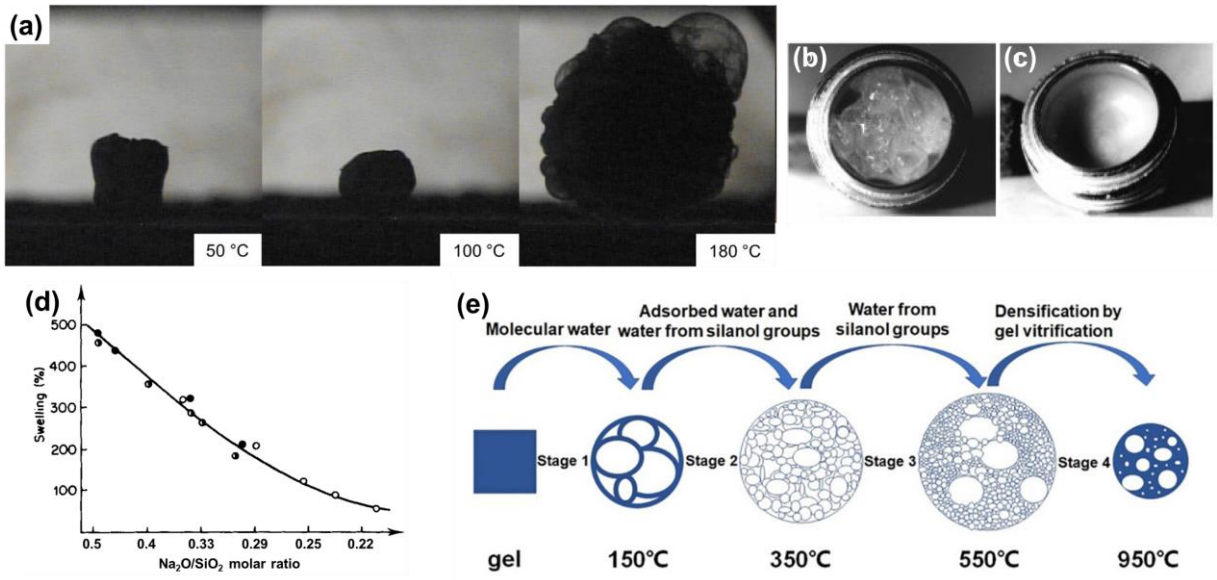

Figure 1.11: (a) In-situ Hot-Stage Microscopy images of dried Na-silicate (Na_2O/SiO_2=0.29) heated up to 180°C,[61] hydrous sodium silicate heated to (b) 175°C & (c) 300°C at 10°C/min,[59] (d) swelling observed in boards based on Na-silicates as a function of molar ratio[1] and (e) schematic illustration of foaming in K-silicates.[53]

The Hot-stage Microscopy images shown in **Figure 1.11**(a) suggest that the dried Na-silicate pellet composed of free water, solvating water and silanols shrinks around 100°C[61] due to the fact that the system is losing free water and undergoing structural modifications shown in **Figure 1.10**(c–e). Volumetric expansion of the material or foaming occurs due to pressure imposed by the release of solvating water and silanols at temperatures approaching 180°C.[61] The extent of this expansion is linked directly to the composition or molar ratio of the silicate with an increased expansion exhibited on increasing molar ratio as shown for Na-silicates in **Figure 1.11**(d). Once all the water is removed from the system as a consequence of this transition, the material goes back to behave as a solid with a curved and cracked surface observed at and above 300°C (**Figure 1.11**(c)). A schematic illustration of this foaming process has also been proposed for K-silicate gels, as shown in **Figure 1.11**(e), to be a consequence of the gradual release of various water-related species.[53] Free water is removed up to 150°C that leads to a little volumetric expansion followed by the subsequent release of adsorbed water and water from the condensation of silanols increasing further the size of foam until all the silanols are released leaving behind a vitrified product.[53]

The T_g of these silicate xerogels, a consequence of the rapid release of water when the system foams, appears to be quite low when compared with those of silicate glasses that approach temperatures reaching 500°C or higher. **Figure 1.12** gives a comparison of the T_g of hydrous sodium silicates with varying amount of water content (on pre-drying at lower temperatures) and a corresponding glass composition (<0.1 mass% water) prepared by the conventional melt and quench route.[59] It can be seen that, indeed, reducing the water content in the silicate tends to shift the T_g towards higher temperatures until at some point, the values overlap with that of the conventional glass once most of the water is removed from the system.

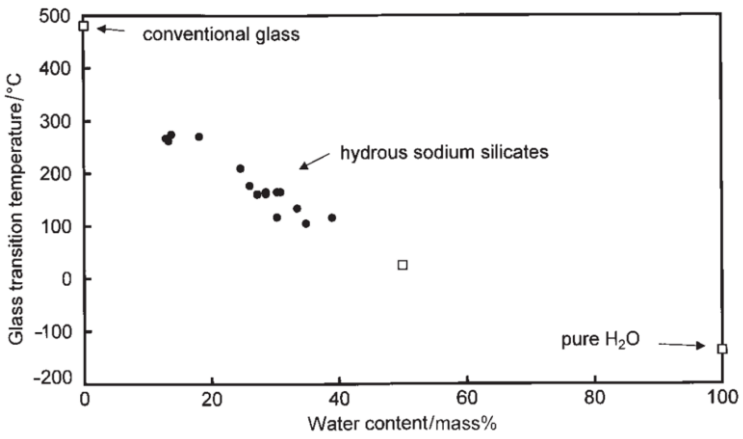

Figure 1.12: Glass transition temperatures (obtained from DSC measurements) of the $Na_2O_3 \cdot 3.3SiO_2 - H_2O$ system as a function of water content after drying,[59] the pure H_2O point is the reported T_g of water.[62]

Thus, the silicate xerogels obtained by drying aqueous solutions exhibit structural changes on thermal evolution; macroscopically in terms of foaming and microscopically in terms of network organization. Once the rapid dehydration (or foaming) temperature range is crossed, further microstructural changes are expected to be induced in the system. This happens due to the removal of left-over water until the material begins to exhibit glass-like behavior suggesting a xerogel-to-glass transition on thermal treatment of aqueous silicates. The microscopic state of the material appears to have similar structural organization as that observed in corresponding glasses for which water content is negligible. Structural properties of glasses are strongly dependent upon the starting composition and generally don't change much below the T_g, however, the behavior may be dependent upon the preparation route as discussed in the upcoming section.

1.3. Silicate glasses

Glasses are in general defined as supercooled liquids or solids that lack periodicity in the structure unlike that observed in crystals. Silica-based glasses have been quite extensively studied and represent the most widely used class. Silica may exist in different forms depending upon the temperature range as shown in **Figure 1.13**(a) with tridymite, cristobalite and quartz being the crystalline phases comprising of α and β polymorphs that represent low temperature inversions.[13] SiO_2 is in molten form above 1710°C, and if cooled rapidly forms the corresponding glass phase that has a metastable or frozen structure of the melt.

Temperature at which thermodynamic properties of a glass-forming liquid change abruptly is referred to as the glass transition temperature (T_g) as shown in **Figure 1.13**(b) and is the point where the material becomes a solid due to an increase in viscosity. The structural rearrangements tend to be rapid in a liquid while their frozen nature in a glassy solid makes them relatively slow. The rate at which liquid is cooled down impacts the value of T_g (or fictive temperature T_f) with faster cooling rates resulting in higher values.[63,64] Crystallization appears once the system is cooled down slowly or set at values above the T_g for longer durations. Once in-between the melting point (T_M) and T_g, the system is referred to as a supercooled liquid. T_g can be detected by a jump in the

specific heat (C_p) measurements in DSC (**Figure 1.13**(c)), also called as the calorimetric T_g, when a glass is heated to higher temperatures.[63]

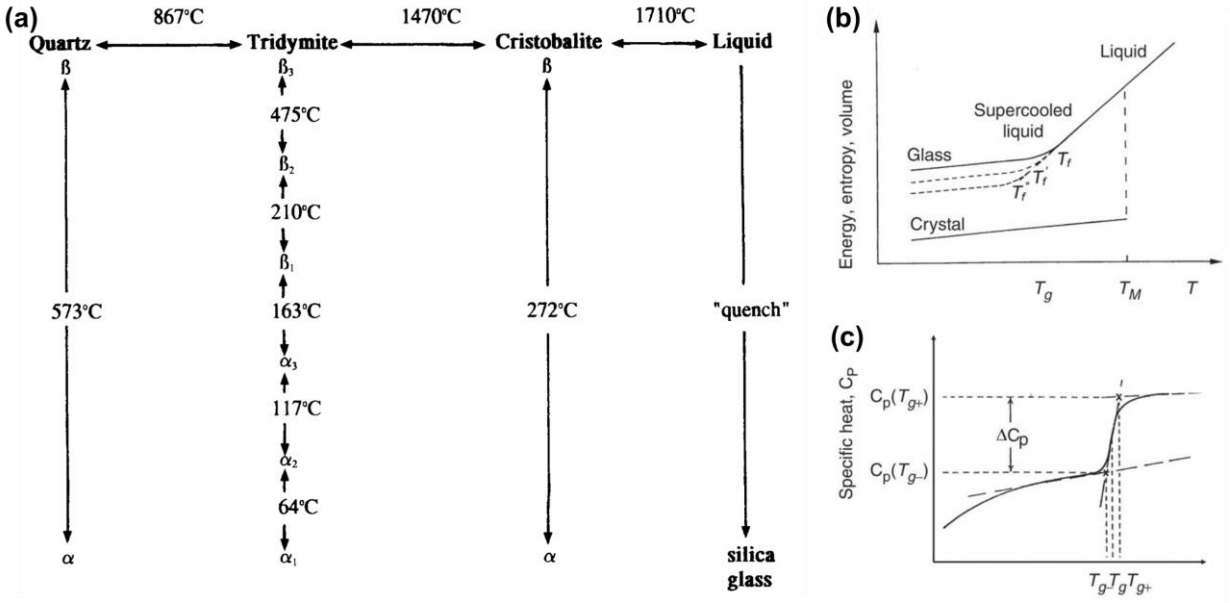

Figure 1.13: (a) Stable phases observed for silica,[13] (b) thermodynamic properties as a function of temperature and the corresponding forms,[63] and (c) variation of heat capacity (C_p) with temperature on heating a glass showing T_g.[63]

The resulting network organization of the crystals is periodic with corner-sharing SiO_2 tetrahedrons arranged as shown by the 2D schematic illustration for quartz in **Figure 1.14**(a).[12] Since glass is amorphous, the tetrahedrons arrange themselves randomly without any plausible long-range order indicative of a continuous random network (CRN) shown in **Figure 1.14**(b).[12] Adding a network modifier, i.e. Na_2O, K_2O or Li_2O, tends to disrupt the connectivity of the network resulting in the formation of NBOs (**Figure 1.14**(c)) with one alkali ion contributing to one NBO by occupying the empty spaces in the network. The resulting structure is composed of channels created by the addition of alkali ions shown schematically in **Figure 1.14**(d) and called as the modified random network (MRN)[65] since the position of alkali is not random as in early models.

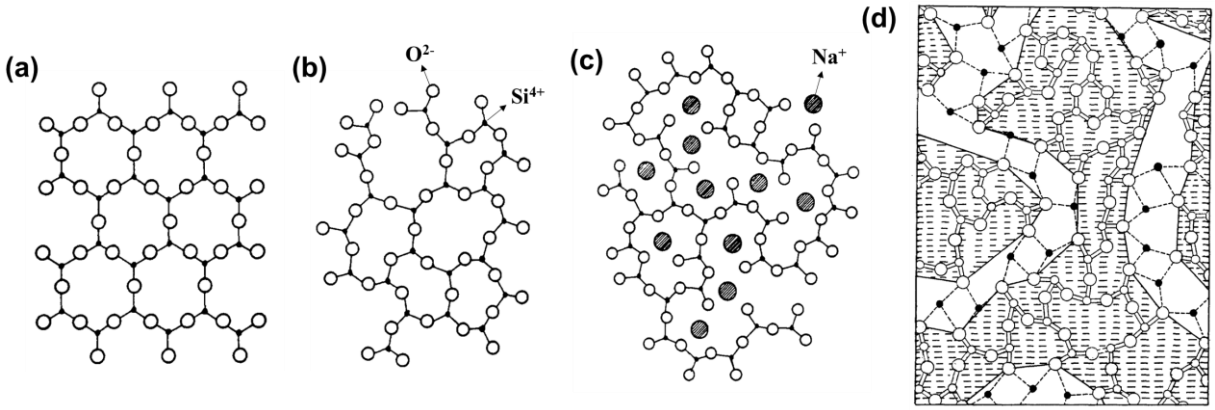

Figure 1.14: Schematic illustration of the network arrangement in (a) crystalline silica, (b) silica glass with a continuous random network (CRN)[12,13] and (c) & (d) sodium silicate glass with a modified random network (MRN).[12,13,65] Black dots in (a), (b) and (c) represent Si atoms while O is represented by open circles. In (d), big open circles correspond to O atoms, small open circles to Si atoms while bold black circles to Na atoms.

1.3.1. Preparation

Silicate glasses have been prepared quite extensively at the industrial and lab scale utilizing the conventional melt and quench route. However, the possibilities of obtaining glasses starting from a solution at room temperature have also been widely reported as efficient methods of silicate glass production. **Figure 1.15** shows the various steps involved in both the processes.[66]

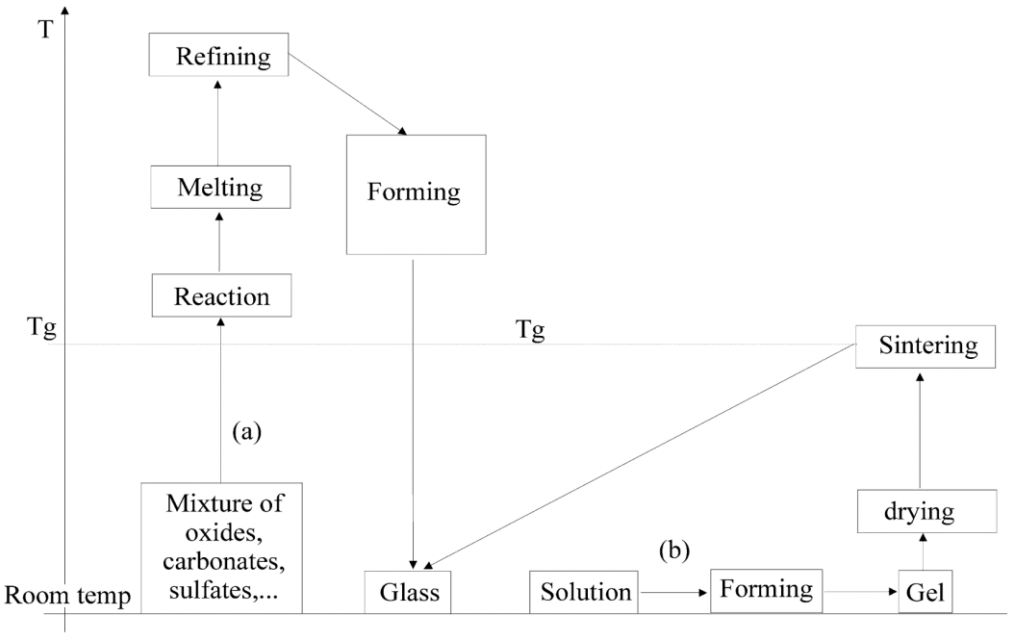

Figure 1.15: (a) Conventional melt & quench and (b) sol-gel route for glass preparation.[66]

1.3.1.1. Conventional

The conventional method of making alkali silicate glasses involves melting of the precursors (SiO_2 source, and alkali carbonates) followed by rapid quenching to room temperature[14,15,67–70] according to the scheme (a) in **Figure 1.15**. The precursors are heated to temperatures above 1000°C in general, or above the liquidus temperature, in a ceramic[71] or platinum crucible with the reaction taking place above the T_g of the material following the eq 1.1. Refining of the melt is done to make it more homogeneous and remove bubbles of either trapped air, nitrogen or decomposition products of raw materials like CO_2. If large enough, the bubbles rise to the surface and can be removed easily. Adding fining agents like arsenic, antimony oxides or sodium sulfate (mostly used today) tend to change the oxidation state of the melt resulting in the collapse of smaller bubbles inside the melt.[71] Once refined, forming into the desired shapes takes place that may include fiber drawing, casting, blowing or pressing etc. followed by cooling to ambient. The obtained glass may also be tempered/annealed above the T_g to relieve the stresses generated during quenching.

1.3.1.2. Sol-gel

Sol-gel route of glass production involves thermal treatment of the starting raw solution that contains precursors for obtaining the gel to be converted into glass (**Figure 1.15**(b)). One way is to heat the soluble alkali silicates obtained through the colloidal silica production route until molten, followed by quenching to obtain glass. Another method involves a chemical reaction leading to

hydrolysis and polycondensation of metal alkoxide chemical compounds[72–74] that results in a gel of high purity on drying. The corresponding reactions involved (hydrolysis in eq. 1.8, 1.10 and polycondensation in eq. 1.9) when using tetramethoxysilane ($Si(OCH_3)_4$) and sodium methylate ($NaOCH_3$) as precursors[73,74] are:

$$Si(OCH_3)_4 + 4H_2O \rightarrow Si(OH)_4 + 4CH_3OH \quad (1.8)$$

$$\equiv Si - OH + OH - Si \equiv \rightarrow \equiv Si - O - Si \equiv + OH^- \quad (1.9)$$

$$NaOCH_3 + H_2O \equiv \rightarrow Na^+ + OH^- + CH_3OH \quad (1.10)$$

$$\equiv Si - O - Si \equiv + Na^+ + OH^- \rightarrow \equiv Si - O^-Na^+ + \equiv Si - OH \quad (1.11)$$

Drying the gel (at ambient for months[75] or at higher temperatures e.g. 250°C[72,75]) leads to the removal of water from the system resulting in a xerogel that is dense but relatively porous as compared to glass and has a similar short-range order.[66,72] CH_3OH evaporates rather rapidly at room temperature as it has a high vapor pressure.[74] Heating a xerogel to the viscous sintering regime (approaching >500°C) leads to densification resulting in a solid similar to glass.

1.3.2. Structural properties

The properties of binary alkali silicate glasses have been quite extensively studied in terms of the impact on the material based on changes in composition and type of alkali. Such changes lead to variations in the structure of the material that has been researched using a number of different techniques. It has been found that increasing the alkali concentration in the glass tends to reduce the T_g (calculated from DSC measurements) irrespective of the type of alkali ion, though some dependence of this behavior is linked to phase separation as shown in **Figure 1.16**(a).[15] T_g values remain constant until 33% Li_2O and 20% Na_2O content in Li and Na-silicate glasses due to the fact that these compositions correspond to the phase separation dome in the phase diagrams,[76] above which a decrease in T_g is seen as a function of alkali concentration.

A more structural analysis of alkali silicate glasses is given by Raman spectroscopy[14,77–80] that is considered as one of the go-to tools for the characterization of glasses in general. Such measurements give information on the type of network organization in terms of both the silica network and Q^n units as given in **Figure 1.16**(b) and (c). The spectrum consists of several bands with two of them being the main contributors i.e. the stretching vibrational modes of Si-O-Si and Q^n units. Pure silica has major characteristic bands around 400 cm^{-1} corresponding to stretching while 800 cm^{-1} representative of bending vibrational modes of the network.[14] Adding network modifiers tends to disrupt this organization resulting in further contributions mainly in the Q^n range centered around 1100 cm^{-1}. The characteristic silica bands (440 cm^{-1} and 800 cm^{-1}) decrease in intensity on increasing alkali content.[14] This is shown in **Figure 1.16**(b) and (c) where an increased concentration of alkali ions leads to changes in the lower frequency range as well as an increased contribution for the Q^n units irrespective of the alkali type. An increase in bands between 500-600 cm^{-1} is observed along with a shift in band position near 500 cm^{-1} to higher frequency on increasing alkali content.[14,78,81]

Li-containing glasses exhibit a behavior slightly different than that observed for Na and K-silicates, with bands centered around 500 cm^{-1} and 600 cm^{-1} decreasing in intensity up to 15% Li_2O

content in glass and contain a broad feature of these bands instead of being distinct bands. Silica features decrease progressively in the order Li<Na<K, band width is increasingly broadened in the order K<Na<Li and intensity of the 950 cm^{-1} band increase in the order K<Na<Li.[14,77] All this indicates a more disordered structure, in terms of bond lengths and bond angles for Li-silicate glasses and a more ordered structure for K-silicates with Na-silicates showing an intermediate behavior.[77] With increasing order, the fluctuations in bond angles and distortions of the tetrahedra are reduced. Li tends to cluster in some regions within the glass leaving the other regions relatively less altered in terms of the silica glass structure. This regional clustering is indicative of phase separation.[14]

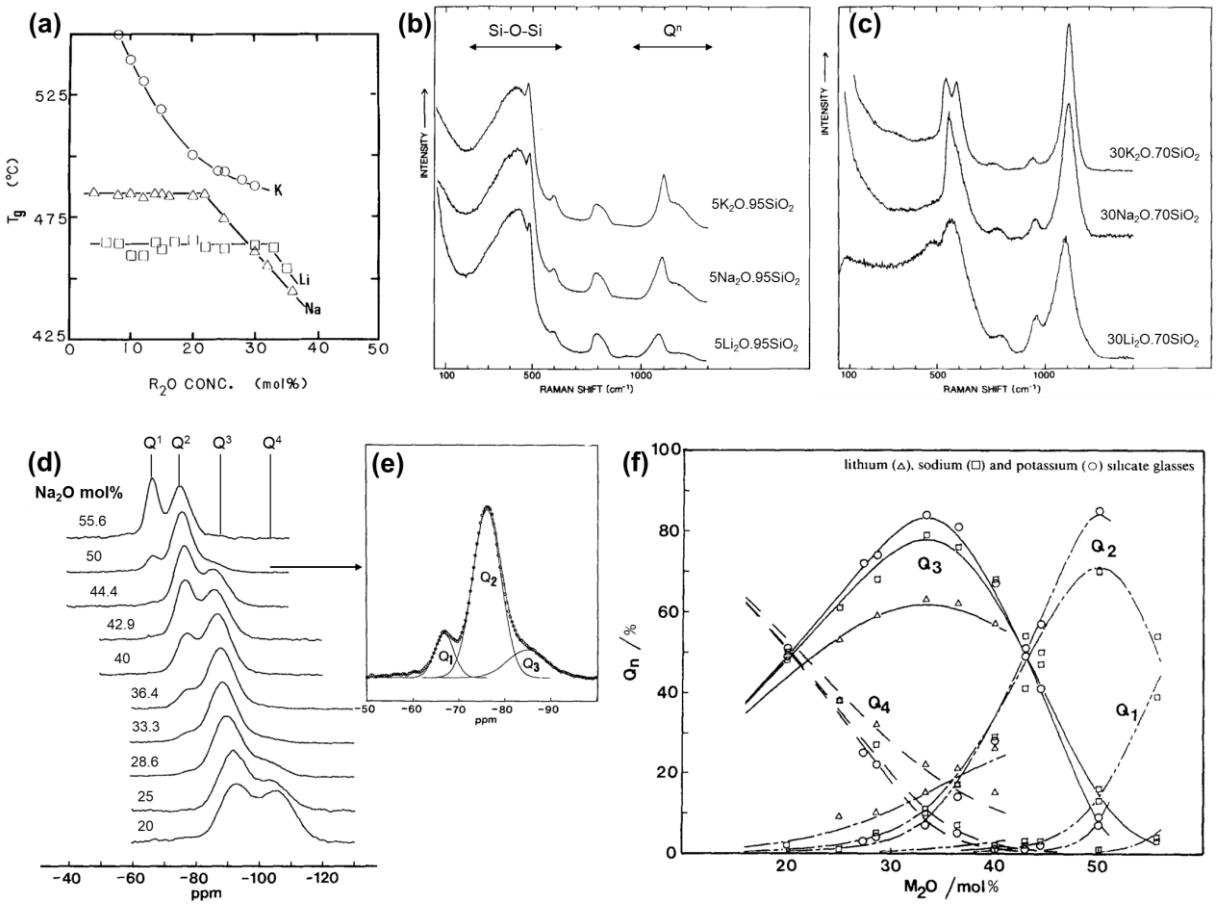

Figure 1.16: Properties of alkali silicate glasses: (a) variation of T_g with increasing concentration of alkali oxide,[15] Raman spectra[14] for (b) 5% and (c) 30% alkali oxide, solid-state ^{29}Si NMR spectra at 4.7 T[69] (d) on increasing Na_2O content in the glass and (e) the deconvolution of the metasilicate composition, and (f) comparison of the evolution of NMR Q^n units as a function of increasing alkali oxide concentration.[69]

The structure of silicate glasses also shows marked differences in the Q^n band range as a function of increasing alkali content with an increase in intensity in the range 850-1250 cm^{-1}.[14,77,78,81] These Q^n species in glasses have been proposed to follow a disproportionation reaction, especially in disilicate systems, given as:

$$2Q^n \rightleftharpoons Q^{n-1} + Q^{n+1} \qquad (n = 1, 2, 3) \tag{1.12}$$

Investigation of the Q^n bands has led to their deconvolution revealing information related to the distribution of individual units.[67,78,80,81] Quantitative analysis from Raman spectroscopy suggests

an increase in lower Q^n units on increasing alkali concentration.[78,81] The impact of temperature on the evolution of bands was also investigated[78,80,81] suggesting an increase in the intensity of Q^n bands (Q^2 and Q^4) with increasing temperature linked to the changes associated with structural reorganization above the T_g in accordance with the equilibrium proposed in the reaction given by eq. 1.12.

An exact quantitative measure of the structural organization, mainly in terms of the Q^n units, has been widely discussed from solid-state ^{29}Si NMR spectroscopic measurements.[69,70,82,83] Wider distribution of atomic arrangements around the silicon atom results in a broader linewidth of the NMR spectrum obtained as shown in **Figure 1.16**(d) and (e) with the possibility to deconvolute the bands into individual components. Increasing the concentration of alkali in the system tends to shift the distribution towards less negative chemical shifts i.e. towards an organization with higher quantity of lower Q^n units[69,83] suggesting a reduction in shielding of ^{29}Si nuclei.[69,70] **Figure 1.16**(f) gives a comparison on the evolution of Q^n units for Na, K and Li-silicate glasses on increasing the alkali concentration. The general evolution is similar for all the systems with the amount of Q^3 up to 40% alkali oxide content being higher in the order K>Na>Li.[69] Increasing the size of the cation (Li^+<Na^+<K^+) tends to shift the equilibrium in eq. 1.12 towards the left suggesting more Q^3 presence in the system. Furthermore, it is suggested that Li_2O addition into Li-silicate glasses may not really indicate that all the Li is distributed over the network rather some quantity may stay as isolated Li_2O due to a higher energetic stability as a consequence of a more covalent character of Li-O as compared to Na-O and K-O bonds.[69]

The structural properties in binary silicate glasses are thus influenced strongly by the presence of the various alkali ions that tend to impact the network organization of the systems. Glasses, in general, are composed of negligible quantity of water that may be present in various forms. However, properties do change once the amount of water in system is increased influencing directly the physical behavior of the systems.

1.3.2.1. Hydrated silicate glasses

Water tends to change the composition of silicate glasses, in the sense that a ternary system is then established. Water bearing glasses can be achieved either by heating the crushed glass in an autoclave in the presence of water[84,85] or sealed Pt crucible for 5-24 h under pressure and hydrothermal conditions[86–89] until water diffuses homogeneously in the form of solvating water molecules (solvating silanols or alkali ions) or isolated silanols.[84,86,90]

Adding water tends to change the network organization of the glass structure inducing depolymerization of the network.[86,91] The impact of added water content on Na tetrasilicate glass is shown by the solid-state ^{29}Si NMR spectra in **Figure 1.17**(a) and (b). Increasing the water content from 2.6 wt% to 10 wt% tends to increase the amount of Q^2 and Q^3 at the expense of Q^4 following the reaction in eq. 1.13 leading to the generation of silanols.[91]

$$\equiv Si - O - Si \equiv + H_2O \rightarrow \equiv Si - OH + OH - Si \equiv \qquad (1.13)$$

Figure 1.17(c) shows the global variation of NBOs/Si as a function of increasing alkali amount in hydrated Na-silicate glasses.[86] Assuming that all the introduced water is a part of the network as silanols, the total NBOs/Si show a linear increasing behavior indicated by the upper solid line in **Figure 1.17**(c). The actual points obtained from NMR measurements (indicated by black points in **Figure 1.17**(c)) suggest that protons are, indeed, not only as silanols but also as solvating water molecules.[86] At very high sodium content, the dissolved water does not impart depolymerization and the structure is similar to anhydrous Na-silicate glass.[86,91] At lower Na concentrations, however, H exists mostly in the form of SiOH. Thus, a more quantitative information on the various arrangements possible for water-related species and their corresponding concentration gives a better insight into the exact structural changes imparted on addition of water or increasing Na content in already hydrated Na-silicate glasses.

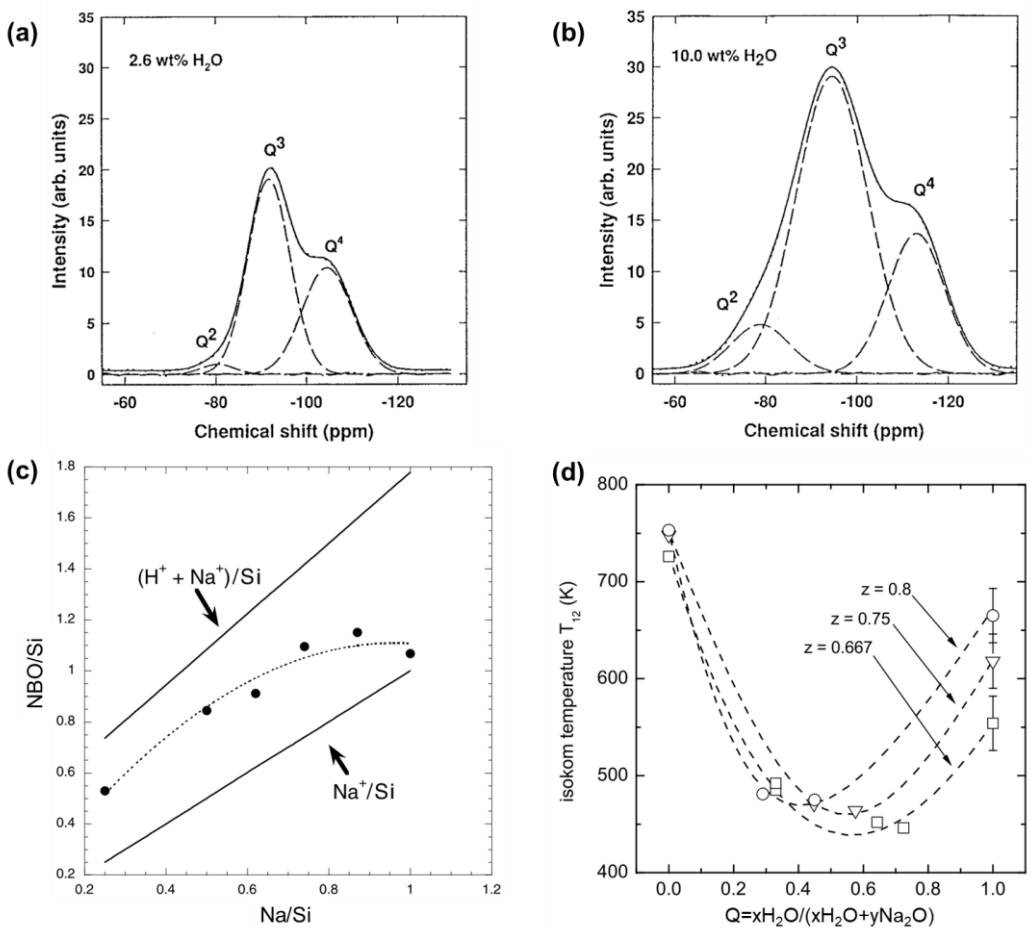

Figure 1.17: (a) & (b) Solid-state ^{29}Si NMR spectrum for Na tetrasilicate glass with 2.6 wt% and 10 wt% H_2O, respectively,[91] (c) total NBOs/Si including Na and H ions as a function of increasing Na content in the glass[86] and (d) variation of T_g as function of water content in Na-silicate glasses (note that the lines are guide for the eyes and x, y and z indicate the mole fraction of H_2O, Na_2O and SiO_2 representing disilicate (z=0.667), trisilicate (z=0.75) and tetrasilicate compositions (z=0.8)).[87]

Thermally treating hydrated Na-silicate glasses results in the loss of water as indicated by weight loss measurements obtained through Thermogravimetric Analysis (TGA).[89] Further investigation suggests that an increased water content in silicate glasses tends to reduce the T_g[87,89] to values as low as 175°C as shown by the **Figure 1.17**(d). Such low values of T_g are attributed to the existence of a mixed alkali effect on addition of water, with more OH reducing the mobility of Na. Addition

of water increases the global mobility and reduces the viscosity of the network leading to a reduction in T_g.[87]

This kind of a behavior suggests a strong correlation between aqueous alkali silicates and their glass counterparts with a conversion of such solutions into actual glassy materials on thermal treatment (at relatively lower temperatures i.e. the T_g would be expected to be reduced)[59] once water is lost from the system. Furthermore, the structural properties of silicate glasses tend to be dependent not only on the water content but also the actual composition of the material in terms of alkali or silica concentration, impacting directly the physical properties showing further similarities among glasses prepared by the melt and quench route and soluble silicates. The structural changes induced in glasses in terms of variations in T_g or the degree of polymerization on added water content or increasing alkali concentration are not the only expected phenomena. Rather crystallization may occur depending upon the conditions and has been observed for a number of silicate glass compositions.

1.4. Crystalline silicate compounds

Thermal treatments of a glass to an annealing temperature above its T_g (or holding above T_g) and below T_M for some time during cooling results in crystallization[71,92,93] inducing changes in glass properties like viscosity and coefficient of thermal expansion. Growth of crystals within the glass tends to change its optical properties such as transparency. Depending upon the application, crystallization may or may not be required. For instance, optical fibers need transparency to ensure long distance transmission and thus crystallization is undesirable. However, for applications involving the use of glasses as refractories, insulators or where mechanical strength is crucial, glass-ceramics play a crucial role. Such materials are obtained by inducing crystallization on special heat treatments of some specific glass compositions (especially Li-based silicates)[94–97] in order to obtain a uniform dispersion of crystals.

1.4.1. Mechanism of crystallization

Crystallization follows a mechanism of nucleation and growth of crystals. Nucleation involves the rearrangement of amorphous matrix molecules to become part of the nucleating crystalline phase. The steady-state nucleation rate 'I' for homogeneous crystal nucleation[71] is given as:

$$I = B\, exp\left(\frac{-Q + W^*}{kT}\right) \tag{1.14}$$

where 'B' is a constant, 'Q' the activation energy for molecular transport in the matrix phase, 'k' the Boltzmann's constant, 'T' the temperature and 'W^*' the work of critical nucleus formation as:

$$W^* = \frac{-16\pi\gamma^3}{3(\Delta G_v)^2} \tag{1.15}$$

where 'γ' is the interfacial energy between matrix phase and nucleus, 'ΔG_v' the thermodynamic force per unit volume for transformation from matrix to the critical nucleus, whose radius 'r^*' is:

$$r^* = \frac{2\gamma}{\Delta G_v} \tag{1.16}$$

Heterogeneous nucleation is quite common in glasses and may be a consequence of foreign particles, bubbles, surfaces or defects acting as catalysts.[71] Surface nucleation is observed due to dust particles or some alkali impurities like Na or Ca adhering to the melt during cooling. Furthermore, addition of foreign elements like metals (Au, Ag, Pt, Pd, Cu) or non-metals (TiO_2, P_2O_5, ZrO_2) can result in the nucleation of uniform crystallization in glasses.[71] Glasses containing nucleating agents generally follow a two-step heat treatment process. Heating just above the T_g causes nucleation also referred to as the 'nucleation treatment' followed by heating to higher temperatures for crystallization. Phase separation has also been reported to be a driving force for crystallization (especially in Li-silicates) [71,98,99] as the role of the catalyst may be played by the boundary between the phases i.e. direct heterogeneous crystal nucleation may occur at the interface.[98,99] It is also possible that the crystalline phase may have the same composition as that of the matrix or dispersed phase, or there might be precipitation from one of the phases.[98,99]

Growth of the crystals occurs in three ways once the nuclei is formed and the size is above the critical radius of nucleation ($r > r^*$), where accidental attachments and detachments from the nuclei surface take place.[98] Normal growth (on an atomically unsmooth surface) involves the movement of the nuclei-matrix interface along its normal whereby the motion is provided by accidental attachments of the structural units to growing crystal's surface. In the case of stepwise growth (on an atomically smooth surface), emergence of screw dislocations or a layer due to attachment of several structural units leads to a tangential motion of the interface over the surface. Lastly, the growth through surface nucleation mechanism is related to the formation of 2D nuclei that lead to the generation of steps on the crystal surface resulting in the formation of new mononuclear layers.

1.4.2. Structural evolution towards crystallinity

1.4.2.1. Silicate glasses

Crystallization in alkali silicate glasses suggests that anhydrous (M_2SiO_3 – metasilicate, $M_2Si_2O_5$ – disilicate) and their hydrous crystalline counterparts are possible depending upon the starting composition and temperature of thermal treatment.[22] Anhydrous crystalline phases appear on annealing glasses above the T_g. The size of critical nucleus 'r^*' was calculated for binary alkali silicate glasses and found to be dependent on the starting composition (smaller nuclei with increasing alkali content), the type of alkali ion (larger nuclei for larger alkali) and the annealing temperature (larger size at higher temperatures).[100] Nuclei with sizes of 12.5-14.8 Å closer to the disilicate composition while 8.9-10.6 Å for monosilicate composition have been reported for binary Na-silicates.[100] Similarly, for Li-silicate systems, the disilicate composition has a critical nucleus in the size range 6-9 Å as compared to 4-5.3 Å for the metasilicate glasses.[100]

It has been suggested that increasing the heating rate increases crystallization temperature in Li-silicate based glasses (with T_g approaching 475°C) along with a similar increase on increasing the SiO_2 content in the system as observed from DSC measurements.[95] When samples are heated all the way up to 900°C,[95,96] crystalline Li_2SiO_3 is observed at 750°C with needle-like features while $Li_2Si_2SO_5$ appears in abundance at 900°C with crystals having a granular shape, suggesting the formation of a glass-ceramic.[95] Similar behavior has been seen on heating Li-silicate binary glasses

around 450°C for longer durations indicating the formation of both meta and disilicate crystalline phases concurrently with the metasilicate crystalline phase in abundance up to 10 h due to its ease of formation when the system phase separates.[93] On heating for 120 h, the number of metasilicate crystals decreases with none being seen for longer durations and the disilicate phase then dominates as indicated by the X-ray Diffraction (XRD) measurements shown in **Figure 1.18**(a).[93]

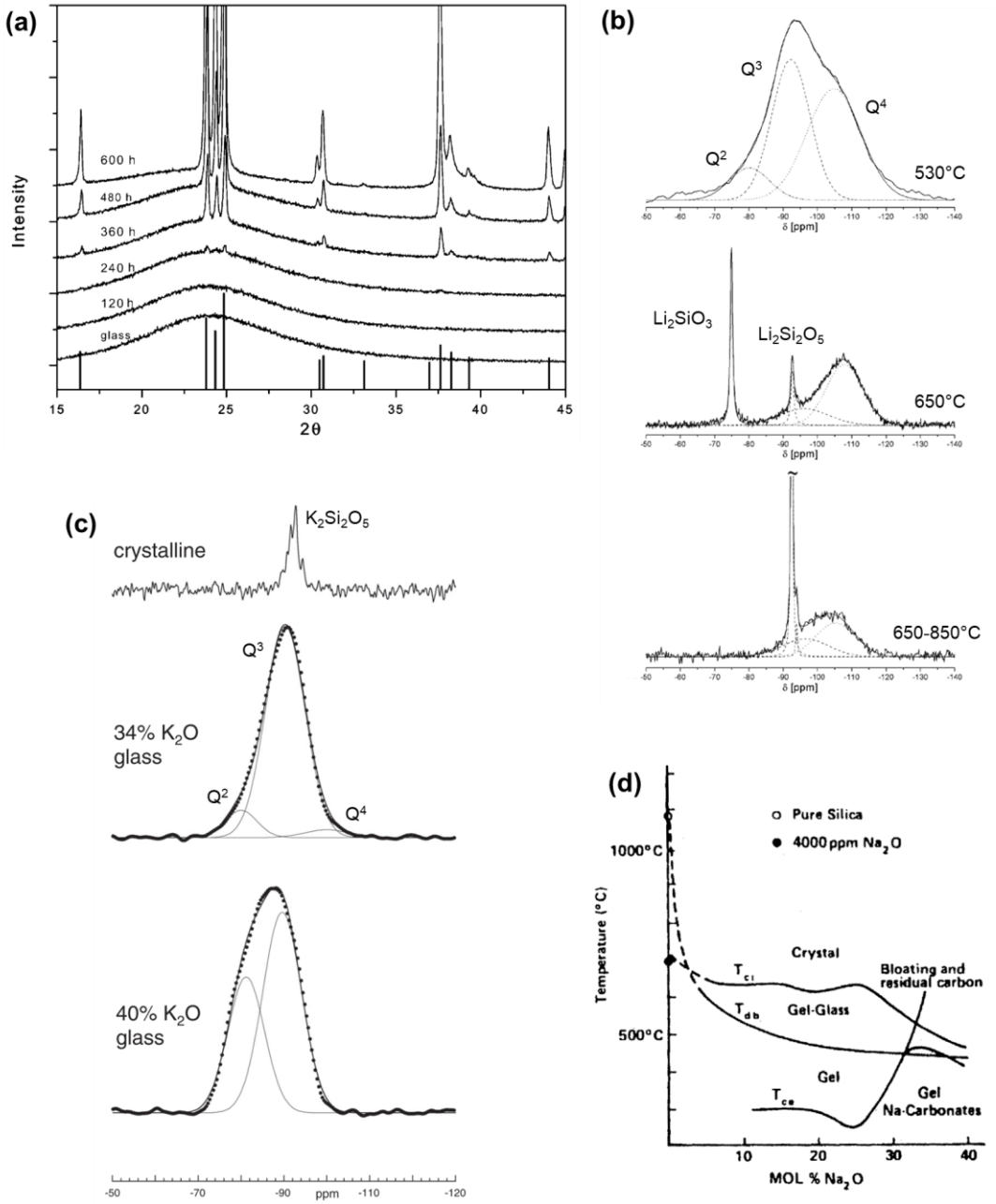

Figure 1.18: (a) XRD diffractograms of binary 34.6 mol% Li_2O silicate glass heated at 454°C for 120-600 h with the vertical lines corresponding to $Li_2Si_2O_5$ crystalline phase,[93] solid-state ^{29}Si NMR at 7 T for (b) 28 wt% Li_2O based glass on annealing at 530°C, with glass-ceramic formed at 650°C and 850°C[94] & 14.1 T for (c) K-silicate glasses and crystalline $K_2Si_2O_5$,[92] and (d) gel-processing diagram for Na_2O-SiO_2 system with T_{ce}=carbonate elimination, T_{db}=beginning of densification and T_{cl}=start of crystallization.[101]

Li-silicate based glass of the composition (28% Li_2O – 66.9% SiO_2 and traces of Al_2O_3, K_2O, P_2O_5) presents a strong response for the Q^3 and Q^4 species at 530°C when the structure is observed

through solid-state ^{29}Si NMR spectroscopy as shown in **Figure 1.18**(b).[94] Increasing the annealing temperature to 650°C results in crystallization with metasilicate Q^2 being the abundant crystalline phase (24%) as compared to 10% Q^3 disilicate. This temperature evolution follows the disproportionation reaction shown in eq. 1.12 suggesting the conversion of glassy Q^3 into crystalline Q^2 and glassy Q^4. Increasing the temperature further to 850°C results in the diminishing of metasilicate altogether with around 63% contribution from the disilicate Q^3 component indicating the conversion of crystalline Q^2 and glassy Q^4 into crystalline Q^3. It must be noted that phase separation occurs, prior to the formation of metasilicate, even below 650°C but is not detected due to the features being nanoscale and thus contributing to the broadness in the spectrum observed at 530°C.[94]

In the case of binary K-silicate glasses, characterization by ^{17}O NMR indicates the existence of a broader, lower frequency peak corresponding to BO while a narrower, higher frequency peak to NBO.[92] Narrower and sharper peaks are observed in the case of crystalline $K_2Si_2O_5$ (obtained by heating 33% K_2O glass to 755°C for 24 h) system suggesting a more ordered structure as compared to glasses. ^{29}Si NMR data, shown in **Figure 1.18**(c) also confirms that the amorphous structure observed in glasses with a broader distribution of signal tends to become relatively narrow for the Q^3 $K_2Si_2O_5$ crystalline phase observed at 755°C with the disappearance of Q^2 and Q^4 contribution as that seen for the 34% K_2O glass.[92]

Unidirectional crystallinity (by generating a heat gradient) is also possible in binary 40% K_2O glass heated to temperatures approaching 950°C, with the formation of $K_2Si_2O_5$ phase confirmed by XRD measurements, though the rapid conversion of crystalline phase into hydrated form makes characterization a bit problematic.[102] Further quantification of the crystalline components in phosphate-based systems has been reported[103] where deconvoluting the peaks observed in XRD diffractogram using the Rietveld refinement approach has aided to classify the systems in which multiple crystalline phases may coexist along with some amorphous character.

Binary Na-silicate glasses also show crystallization once the melt and quench glass samples are heat treated to temperatures above the T_g.[104,105] A two-step heat treatment – nucleation at 400-500°C for varying amount of time followed by development (where the growth rate is much higher than the nucleation temperature) at 590°C for 4 min – of 46, 48.1 and 50 mol% Na_2O glass resulted in the formation of Na_2SiO_3 crystals, confirmed by XRD measurements, with maximum rate of metasilicate crystals being observed at 460°C.[104] Moreover, the rate at which the nuclei achieve a critical radius for growth was calculated to be rather fast or instant especially for the 46 mol% Na_2O glass.[104] In-situ ^{29}Si NMR study on 40 mol% Na_2O – 60 mol% SiO_2 glass has also revealed the appearance of crystalline phases corresponding to both Q^2 metasilicate and Q^3 disilicate composition at temperatures approaching 600°C with distinct amorphous bands coalescing within 200°C of the T_g of such glasses.[105]

Hence, crystallization appears to be a common phenomenon in binary alkali silicate glass systems linked to a gradual nucleation and growth of meta and disilicate crystals with Li and Na-based glasses being the most widely researched. The usual characterization techniques used for

structural evaluation of glasses (like NMR and XRD) are generally enough for detecting crystallization events. Such a behavior should also be expected for glassy compositions prepared from sol-gel based routes as well as aqueous silicates indicating similarities among the different systems.

1.4.2.2. Gels and aqueous silicates

Crystallization is also observable in the case of binary alkali-silicate gels depending upon the composition.[101,106–108] **Figure 1.18**(d) shows a gel-processing diagram for Na_2O-SiO_2 system[101] indicating the possibility of crystallization once the binary Na-silicate composition is heated above the densification temperature range, though crystallization precedes densification at very low Na_2O concentrations. Li-silicate gels of varying compositions were obtained through the sol-gel route by drying the parent mixture at 30-70°C for 7 days followed by melting in steps all the way up to 1450°C to obtain glass.[108] The two-step heat treatment involved nucleation in the 400-500°C range followed by growth at 600°C for 10 min. XRD measurements indicate the presence of crystalline Li-disilicate up to 33 mol% Li_2O while metasilicate is observed above 40.7 mol% Li_2O.[108] The sol-gel method leads to glasses with a homogeneous spatial arrangement of crystals. Meta and disilicate crystallization from the Li-silicate gel compositions has also been reported on direct heating of gels to temperatures approaching 500°C and beyond[107] suggesting a reasonable tendency of gels to crystallize in a manner similar to glasses. Furthermore, a combination of DSC, XRD and ^{29}Si NMR has also helped in the evaluation of the crystallization behavior in Li-silicate gels with the formation of both meta and disilicate phases depending upon the heating rate employed.[106]

Soluble alkali silicates also undergo structural changes on thermal treatments with crystallization appearing in some cases with the phases being the same as those observed in glasses produced by conventional melt and quench route as well as sol-gel methods. For instance, sodium silicate water glass with a molar ratio Na_2O/SiO_2=0.33 dried at ambient conditions for 5 h followed by heating to 850°C with a dwell time of 24 h resulted in crystallization.[109] Crystalline $Na_2Si_2O_5$ began to appear around 400°C with increasing intensity of the XRD peaks up to 550°C where phase separation of the crystalline components takes place between the disilicate and cristobalite phase.[109] The disilicate disappears at 750°C with the formation of $Na_6Si_8O_{19}$ phase while a glassy behavior prevails around 850°C.[109] Disilicate crystalline phases have also been seen in the case of aqueous K and Li silicates when the systems were heated to 500°C[47] with K-silicate showing the tendency to form hydrated disilicate.

1.5. Summary – Missing links and scientific questions

Structural properties of binary soluble silicates, xerogels, glasses and the corresponding crystalline compounds have been quite extensively studied. In the case of soluble silicates, there exists a tendency to have a glass-like behavior depending upon the thermal history. Aqueous alkali silicates have emerged as an industrially important class of materials with their thermal behavior being of particular interest due to their intumescent nature. They foam, i.e. expand volumetrically, on contacting fire as a consequence of the release of water from the system that imparts structural

changes at the microscopic scale. Microscopic properties, at the scale of the network, have been studied through a number of techniques sometimes utilizing a combinatory approach (resorting to qualitative as well as quantitative methods) for addressing network-related queries in both glasses and alkali silicate solutions.

The structural properties have generally been fundamentally and thoroughly investigated below 150°C in the case of aqueous silicates and above 400/500°C in the case of glasses. Some mechanisms have been proposed that add to the understanding of the densification of xerogels or pre-dried aqueous silicates before foaming starts but an in-depth understanding on how the structure is evolving microscopically (using quantitative approaches) and the corresponding impact on the foaming behavior has not been clearly elaborated. Furthermore, the impact of water evolution in the system on the T_g of silicates is not evident and the crystallization behavior of aqueous alkali silicates is not well understood either, and it is not clear how the systems would behave if crystallization or phase separation is observed below 400°C. Thus, it is necessary to find solutions to the missing links by establishing a thorough qualitative and quantitative understanding of the macroscopic and microscopic thermal evolution of aqueous alkali silicates to be able to predict their properties as a function of composition as well as the type of alkali.

Specifically, this manuscript addresses the thermal behavior of aqueous Na, K and Li-silicates of two different molar ratios by utilizing the experimental methodology devised. Structural properties in terms of microscopic network organization and foaming have been investigated both qualitatively and quantitatively. Such an in-depth investigation has allowed to address several scientific questions: How does the composition (solid and water content) and structure (structure of the silicate network, nature of amorphous or crystalline phases) of alkali silicates evolve with temperature below 400/450°C? Is there a difference in the thermal evolution of solutions/ xerogels based on the alkali cations such as Na, K and Li? Do any of these systems exhibit a T_g? Furthermore, we would like to relate this microscopic thermal evolution to the macroscopic behavior in terms of foaming. We have addressed this question for two different kinds of geometries corresponding to different industrial applications: bulk geometry, related more to the geometry of intumescent materials, and liquid films, corresponding to the case where alkali silicates are used as coatings.

Chapter 2.

Experimental methodology

2.1. Starting materials & preparation methods

Aqueous alkali silicates based on Na, K and Li were thermally treated to various temperatures to study their structural properties depending upon the starting state of these materials. The details on the various samples used for the investigation of their thermal behavior are given explicitly in the forthcoming sub-sections.

2.1.1. Solutions and Glasses

Commercially available and lab prepared alkali silicate solutions as well as reference Na-silicate glasses obtained by the industrial melt & quench route (at SGR Paris) were used as the starting materials. They have been defined in terms of their **Molar Ratio** as **$nM_2O/nSiO_2$** (where M corresponds to the type of alkali ion i.e., Na, K or Li). Note that all the alkali silicate systems would, from now on, be denoted by their molar ratio throughout the manuscript. Solutions (and Na-silicate glasses) with two different molar ratios were used in all the cases and the respective composition of each system is given in **Table 2.1**. Na-silicate extra pure solution (Na_2O/SiO_2=0.29) was purchased from Sigma-Aldrich, Na-silicate crystal 0095 solution (Na_2O/SiO_2=0.5) from PQ Corporation, K-silicate K 35 T (K_2O/SiO_2=0.29) and K-silicate Geosil 14517 (K_2O/SiO_2=0.59) solutions from Woellner while Lithium polysilicate solution (Li_2O/SiO_2=0.2), Ludox AS-30 colloidal silica (30 wt% suspension in H_2O), Lithium hydroxide monohydrate (≥98%) and TetramethylAmmonium silicate (TMAS) from Sigma-Aldrich. Ethylene glycol (pure) was procured from Carlo Alba, Sodium hydroxide solution (cNaOH=1 mol/L) from Merck and pellets from Fluka whereas sodium carbonate powder (anhydrous ≥ 99.5%) was purchased from VWR Chemicals BDH.

Table 2.1: Composition (in wt%) of the starting alkali silicate solutions and Na-silicate glasses.

Alkali Silicate	M_2O (wt%)	SiO_2 (wt%)	H_2O (wt%)	Molar Ratio ($nM_2O/nSiO_2$)	Preparation
Na	8.25	27.75	64	0.29	Commercial
	13.75	27.25	59	0.5	Commercial
Na (Glass)	23	77	-	0.29	Melt & Quench
	33	67	-	0.5	Melt & Quench
K	11	24	65	0.29	Commercial
	17	23	60	0.5	K-Silicate 0.59 + Ludox AS-30
Li	1.8	18.2	80	0.2	Commercial
	2.6	17.8	79.6	0.29	Li-silicate 0.2 + LiOH powder
	3.4	17.3	79.3	0.4	Li-silicate 0.2 + LiOH powder

K-silicate (K_2O/SiO_2=0.5) solution was prepared by mixing known amount of Ludox AS-30 in K-silicate Geosil 14517 (K_2O/SiO_2=0.59) with constant stirring until the solution becomes transparent. Li-silicate solutions (Li_2O/SiO_2=0.29 and 0.4) were prepared by adding known quantity of Lithium hydroxide monohydrate powder into Lithium polysilicate solution (Li_2O/SiO_2=0.2) with constant stirring at 60°C until the solutions become transparent. Note that the molar ratio of 0.4 represents the upper limit of stability for Li-silicate solutions.

Tests were also made to check the effect of preparation route on the stability and structure of the starting Na-silicate solutions. For this purpose, known amount of NaOH solution/pellet was added into the commercial Na-silicate 0.29 solution to obtain a molar ratio of 0.5. Furthermore, Ludox AS-30 was mixed with Na-silicate 0.5 solution to check for the possibility of tuning the molar ratio i.e. achieving a lower molar ratio value of 0.33.

Mixing of alkali silicates and the addition of foreign entities to the commercial Na-silicate solutions was also investigated. Li-silicate 0.2 solution was mixed with Na-silicate solutions as well as known quantities of TMAS and ethylene glycol solutions were also added into the pure Na-silicate solutions. Details of the respective compositions are given with the results (**Chapter 4**).

Thermal treatments on the solutions were generally carried out at 150°C, 275°C, 350°C, 400°C and 450°C at a heating ramp of 5°C/min. Some heating experiments were performed at 300°C especially those for K-silicate solutions. The impact of varying heating rate from 1 to 5 to 10°C/min was also investigated for all the silicates by heating in a rate-controlled oven at 250°C for 30 min.

2.1.2. Powders

Alkali silicate dried powders were prepared by heating the initial solutions in an oven at 150°C for 17 h to remove maximum amount of free water and limit the extent of foaming while performing further analyses. A porcelain crucible was used as the jar for solutions. For our investigations, powders were also obtained by thermally treating the solutions at 275°C, 350°C, 400°C and 450°C at a heating rate of 5°C/min for 2 h each. Obtained powders or reference glasses were grinded and stored in sealed glass vials. Grinding of powders obtained from the solutions was achieved using a mortar and pestle while a planetary ball mill (Fritsch Pulverisette 6 operated at 400 rpm for 10 min with 10 repetitions) was used for grinding the Na-silicate glass chunks.

Table 2.2: Techniques and the corresponding substrates used for the deposition of alkali silicate coatings.

Coating Method	Substrate	Pre-Cleaning
Spin Coating	Silicon wafer (single and double side polished)	Acetone, then ethanol followed by UV-Ozone treatment at 50°C for 15 min (utilizing Novascan PSD-UV – Benchtop UV-Ozone Cleaner)
	Microscopic glass slide	Acetone and ethanol
	Tantalum-coated glass	Ethanol followed by UV-Ozone treatment
Blade/Pool Coating	Microscopic glass slide	Acetone and ethanol
Gradient Bar Coating	Planiclear glass plate (Saint-Gobain)	Rubbing with Cerox (20% in H_2O) followed by rinsing with distilled water

2.1.3. Coatings

Properties and thermal evolution of thin films and thick coatings obtained by depositing raw aqueous alkali silicates were also investigated. **Table 2.2** lists the different coating techniques and the pre-cleaned substrates used for the deposition of thin and thick alkali silicate coatings.

2.1.3.1. Spin Coating

Thin (250 nm) and homogeneous coatings of diluted pure 1.5 M (in terms of SiO_2 concentration) Na_2O/SiO_2=0.29 and carbonated solutions were spin coated on double side polished silicon wafers (1x1.5 cm) at 2000 rpm for 60 s for infra-red spectroscopic analysis. Pure Na_2O/SiO_2=0.29 and 0.5 solutions were used for obtaining similar thin films on tantalum (Ta)-coated glass substrate followed by heat treatment at different temperatures for Raman spectroscopic measurements. A 20 nm layer of Ta was sputtered on glass using magnetron sputtering. Thin films of Na_2O/SiO_2=0.29 solution on single side polished silicon wafers (1x1.5 cm) were also prepared for secondary ion mass spectroscopy.

Raw concentrated Na-silicate solutions were used as received for the deposition of thicker coatings (on silicon wafer and glass substrates at 2000 rpm for 60 s) i.e. in the range 5-8 µm and were thermally treated at and above 250°C. Some multi-layered coatings (with a pre-drying step of 70°C) were also achieved from both the molar ratios of Na-silicates, however, glass was finally chosen as the substrate for further thick coating experiments as delamination of the layers was observed on ageing of spin coated silicon wafer substrates. Furthermore, thicker coatings of the order of 10s of microns were difficult to be prepared by spin coating route so the process had to be changed.

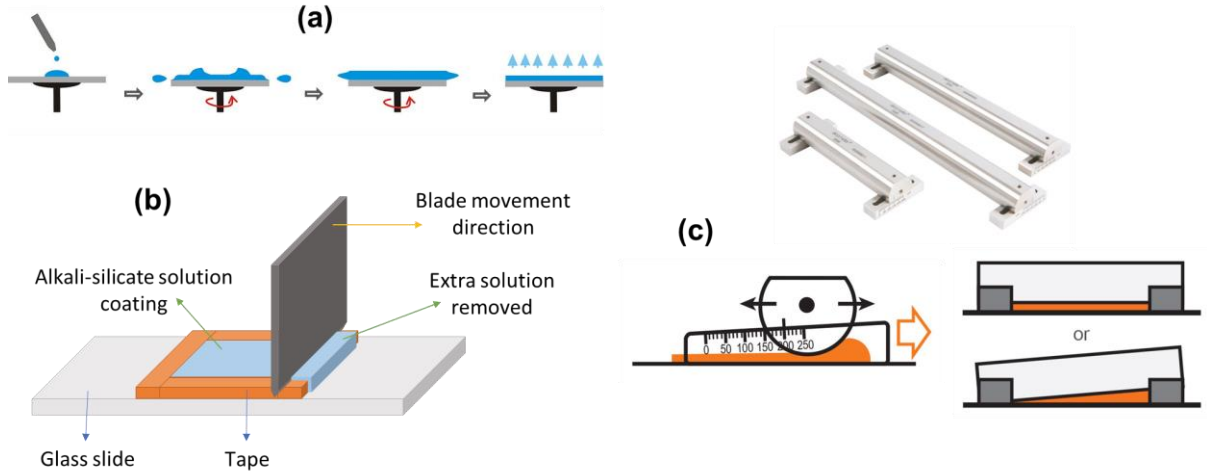

Figure 2.1: Schematic illustration of (a) spin, (b) blade/pool and (c) gradient bar coating (and the corresponding adjustable bars used)[110] process.

2.1.3.2. Blade/Pool Coating

Thicker coatings, in the order of 10s of microns, for all the alkali silicates were achieved using blade/pool coating setup shown in **Figure 2.1**(b). A double-sided tape (with a thickness of 170 µm) was used to create a square/rectangular pool on the substrate to prevent the flow of solution. The extra solution at the top was removed using a blade to achieve a relatively flat surface and the

coating was dried both at ambient as well as 70°C followed by subsequent heating. This setup allows for generating coatings with thickness values reaching 100s of microns retaining the homogeneity depending upon the composition.

2.1.3.3. Gradient Bar Coating

Coatings with gradient in thickness for the different alkali silicates and molar ratios were deposited using an Elcometer 3530 thickness adjustable bar, 25 cm in length, shown in **Figure 2.1**(c). Pre-cleaned Planiclear glass plates (30x30 cm) were used as the substrates and three gradient coatings were tested by adjusting the bar ends at 10-100, 10-200 and 10-250 µm. Depositions were generally made using Elcometer 4340 Automatic Film Applicator (carriage speed position was set to 3 that allows for the bar movement speed of 20 mm/s). Samples were pre-dried at 70°C for 5 min followed by thermal treatments at 250°C and 450°C. An impact of the heating rate was also investigated by varying from 1 to 5 to 10°C/min in a rate-controlled oven.

2.2. Characterization strategy

Alkali silicate solutions, powders and coatings have all been investigated for their thermal behavior to establish a concrete fundamental understanding of the structural properties at both the macroscopic and microscopic scales. **Figure 2.2** lists the various techniques utilized to create a strategy for being able to efficiently characterize the systems in terms of the different structural properties of interest.

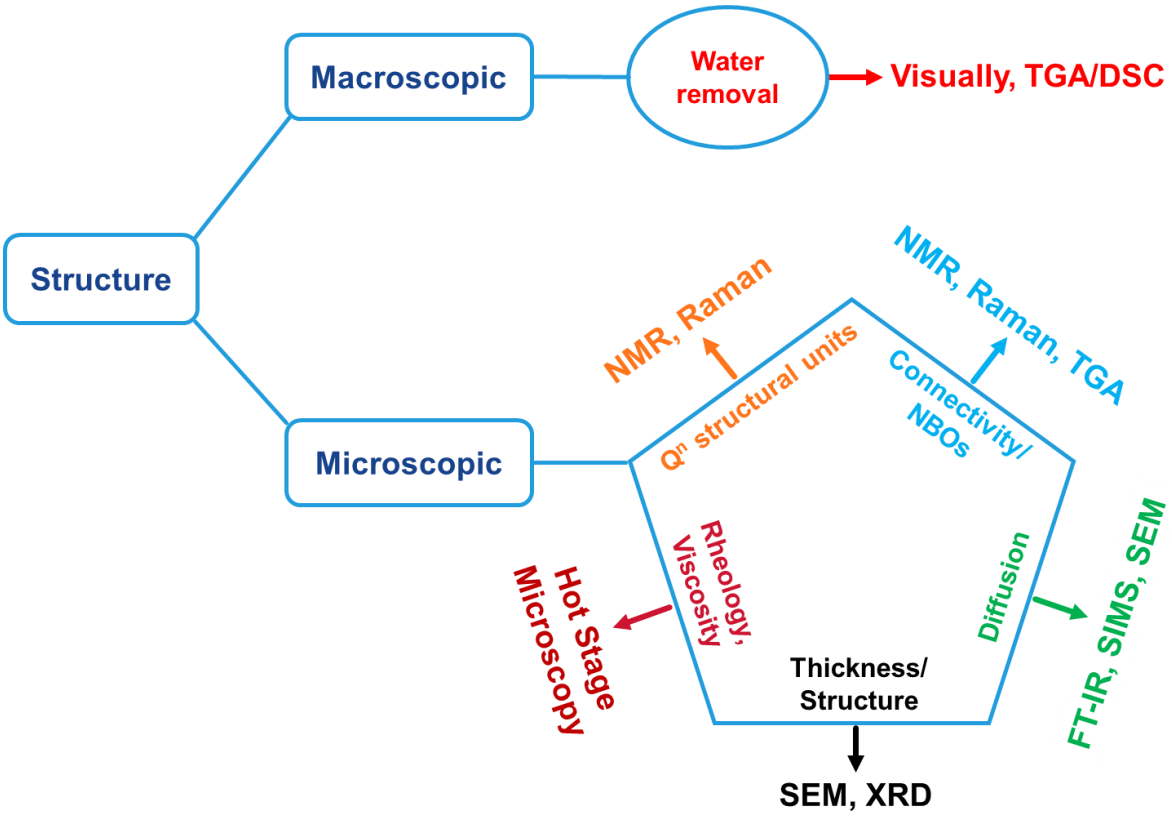

Figure 2.2: Schematic illustration of the characterization methodology followed for extracting the various macro and microscopic structural properties of aqueous alkali silicates at ambient conditions and on thermal treatment.

The developed methodology is based on the expertise and availability of various characterization tools in the laboratories involved in the project. For instance, liquid and solid-state Nuclear Magnetic Resonance (NMR) spectroscopic know-how and equipment at LPMC, Ecole Polytechnique has been used to investigate quantitatively the structural organization of alkali silicates in terms of the silicate network evolution on thermal treatment. Raman spectroscopy, the expertise of which lie at SVI, Saint-Gobain Research Paris, has provided a qualitative information complementary to NMR. A combination of different techniques has thus helped in providing information on the state of alkali silicates.

2.2.1. Macroscopic View

Thermally treating aqueous alkali silicates leads to the removal of water from the system. The global evolution of this water content and the corresponding influence of macroscopic structural evolution in terms of foaming has been analyzed using visual methods involving real-time observation of solutions and powder pellets. For a more accurate description of this evolution, powders obtained by pre-drying solutions at 150°C, referred throughout the manuscript as 'pre-dried', have been used to follow the behavior from Thermogravimetric Analysis (TGA) in terms of mass loss and Differential Scanning Calorimetry (DSC). It is worth noting here that only pre-dried powders (and not the solutions) were used for TGA/DSC measurements due to the experimental limitations posed by the volumetric expansion of some alkali silicate compositions. Furthermore, the release of water from solutions is too abrupt to disrupt the readings (or damage the equipment as a consequence of splashing) due to blowing away of crucible lid especially in the case of DSC measurements.

2.2.2. Microscopic structural evolution

In order to study the changes at the scale of silicate network configuration, NMR spectroscopy has been utilized to quantify the Q^n structural units (where 'n' corresponds to the number of bridging oxygens or BOs, while non-bridging oxygens are referred to as NBOs) that are expected to change as a function of water/silanols' evolution on thermal treatment. A complementary and more qualitative description of the network has been provided by Raman spectroscopic measurements. Powders obtained by drying the solutions at different temperatures were used for both these techniques.

A further quantitative analysis has been performed by combining TGA mass loss curves with Q^n units obtained from NMR in order to predict accurately the exact evolution of the different proton-related species in the network that gives a more solid understanding on how water or protons are actually leaving the network during the macroscopic foaming phenomenon. Some alkali silicate compositions present crystallization which has also been quantitatively investigated in combination with TGA and NMR data for predicting the changes occurring in the network and the corresponding link to the macroscopic thermal evolution when alkali ions leave the host matrix. Macroscopic changes in the systems are linked to changes in rheology/viscosity once water starts leaving the network and the material starts to approach the T_g. High temperature evolution i.e.

>500°C has been observed on powder pellets under a Hot-stage Microscope that has allowed for the calculation of viscosity curves especially in the case of Na-silicates.

Coatings developed from these aqueous alkali silicates have been investigated for their morphology and thickness using Scanning Electron Microscopy (SEM) while the structure has been identified using X-Ray Diffraction (XRD) and Raman spectroscopy. Diffusion-related properties of thin Na-silicate films, in terms of Na ions, have been explored by combining the carbonation studies performed by Fourier-Transform Infra-Red (FT-IR) spectroscopy with diffusion profiles obtained from Secondary Ion Mass Spectroscopy (SIMS) and carbonates observed under SEM.

2.2.3. Experimental parameters

2.2.3.1. Thermal Analysis

Thermogravimetric Analysis (TGA) was performed using a NETZSCH STA 409 Thermal Analyzer for obtaining mass loss curves up to 1200°C to monitor the evolution of leftover water or silanols with temperature in Na-silicate powders pre-dried at 150°C. An alumina crucible was used as the container and a moisture-free atmosphere was provided by continuously flowing N_2/O_2 gases in nearly equal volume. The measurement was repeated twice. Temperature calibration was performed at heating rates of 5, 10 and 20°C/min from the DTA signal using metal standards with different melting temperatures. Note that the calibration is not accurate at low temperature sweeps when the DTA signal is significantly broadened. Only small quantities of samples could be analyzed for Na and K-silicate, typically 15 mg of the powder pre-dried at 150°C, because of foaming. This led to improper correction of the buoyancy effects in the RT-150°C temperature range. 50 mg powder was used for the analysis of Li-silicate pre-dried systems.

Differential scanning calorimetry (DSC) was utilized for measuring the heat capacity of these silicates on a NETZSCH DSC 404 C under continuous N_2 flow. Typically, 10 mg of pre-dried powders prepared at 150°C were used as the starting material and loaded as-received into a platinum-rhodium crucible without compressing. A heating rate of 10°C/min was employed. For heat capacity measurements, calibration was done by recording a baseline (without the sample) and a reference measurement with Sapphire which gives an energy calibration allowing subsequent calculations to be made using the processing software.

2.2.3.2. Nuclear Magnetic Resonance Spectroscopy

Liquid-state NMR: The structure of Alkali-silicate solutions in terms of Q^n units was analyzed using liquid-state ^{29}Si NMR. Spectra were recorded at 59.63 MHz on a 300 MHz AVANCE II Bruker spectrometer with a BBO probe. A $\pi/2$ pulse was used with a repetition delay optimized at 5 s. 30 vol% heavy water (D_2O) was added to the samples for locking. All ^{29}Si chemical shifts were referenced to tetraethoxysilane (TEOS) as external reference [Chemical shift (Si)=-82 ppm vs TMS]. The contribution of glass tube was corrected by subtracting the spectrum of empty tube from the final spectrum of silicate solutions. The relative proportion of Q^n units was determined by integrating the area under the curve of each peak for an exact quantification of the various species.

Solid-state MAS NMR: The samples treated at different temperatures were analyzed with solid-state magic angle spinning (MAS) NMR experiments. The 1D ^{29}Si NMR spectra were acquired at

71.53 MHz on a Tecmag Apollo360 spectrometer equipped with a 4 mm Bruker probe head operating at a spinning frequency (ν_{rot}) of 15 kHz. The acquisitions were performed with a 3.55 µs pulse length (corresponding to a $\pi/2$ flip angle), 3000 transients and a repetition delay of 20 s. The repetition delay was optimized by going up to 1500 s for Na while 2000 s for Li-silicate but that does not provide higher signal intensity. ^{29}Si chemical shifts were referred to TEOS at -82 ppm. Deconvolution of the ^{29}Si NMR spectra was performed using the Dmfit software[111] with Gaussian fitting function because of the chemical shift distribution of amorphous structures.

For Na-silicates, some measurements were carried out in collaboration with Grégory Tricot (Laboratoire de Spectrochimie Infrarouge et Raman-LASIR, Université de Lille). ^{23}Na and ^{1}H MAS-NMR experiments were recorded at 211.6 and 800 MHz, respectively, on an 18.8 T Bruker spectrometer. All the experiments were performed with a 3.2 mm probe head operating at ν_{rot} of 20 kHz. ^{23}Na MAS-NMR experiments were obtained with a 1 µs pulse length (corresponding to a $\pi/8$ flip angle), 256 transients and an optimized repetition delay of 0.5 s. ^{1}H MAS-NMR spectra were obtained with a 2.7 µs pulse length (corresponding to $\pi/2$ flip angle), 64 transients and an optimized repetition delay of 5 s. The NMR spectra were corrected from the signal coming from the probe. ^{23}Na and ^{1}H chemical shifts were referred to NaCl and TMS solutions at 0 and 0 ppm, respectively. In order to analyze the ^{1}H/^{29}Si and ^{23}Na/^{29}Si interactions, correlation NMR was also applied at 9.4 T with an HXY-4 mm probe head operating at ν_{rot} of 8 kHz. 1D ^{29}Si (^{23}Na) Cross Polarization (CP) NMR technique was used to determine how the Na ions are distributed within the silicate network. The experiment was performed with optimized low radio-frequency fields (around 5-6 kHz for both channels) allowing for an efficient transfer, a contact time of 6 ms and 400 k transients separated by a repetition delay of 0.2 s. 2D ^{29}Si (^{1}H) CP spectra were acquired to trace the Si-OH linkages. The 2k x 10 acquisition points were recorded under rotor-synchronized conditions with ^{1}H and ^{29}Si radiofrequency fields of 50 and 34 kHz and a contact time of 6 ms. Each direct slice was recorded with 512 transients and a repetition delay of 4 s.

2.2.3.3. X-Ray Diffraction

Powder (and some thick coating) XRD experiments were carried out on a high-resolution D8 Advance Bruker AXS (Germany) θ-θ powder diffractometer equipped with the LynxEye XE-T detector (1D mode, maximum detector opening), automatic anti-scatter screen position and a Cu radiation ($K\alpha_1$ = 1.5406 Å and $K\alpha_2$ = 1.5445 Å). Samples were analyzed at room temperature using 2.5° Soller slits and a divergence slit of 0.6° in the 5-70° 2θ range with a step size of 0.025° at 1 s/step. Phase identification was performed with the Bruker AXS DIFFRAC.EVA (V5) software using the PDF2 (release 2004) database. Deconvolution of the XRD diffractograms was carried out on Bruker AXS TOPAS (V6) software. The fundamental parameter approach was used to model the optic contribution and the emission profile of the X-Ray tube was established using LaB_6 NIST standard (Standard Reference Material 660a, cell parameter = 0.41569162 nm – 0.00000097 nm at 22.5 °C). The background was described using a Chebychev polynomial. Since the diffractograms were a combination of amorphous and crystalline characters, split pseudo-voigt (SPV) function was used to define both the amorphous bump (using the single peak method) and crystalline peaks corresponding to the different phases detected. The Crystallographic Information File (.cif) for

each phase was downloaded from the Crystallography Open Database (COD)[112], Inorganic Crystal Structure Database (ICSD) and MaterialsProject.[113] For the Rietveld refinements, cell parameters, microstructure (double-Voigt approach, only crystallite size refined) and preferred orientation (March-Dollase model) were fitted whereas atomic positions and site occupancies were fixed according to the .cif files used.

2.2.3.4. Raman Spectroscopy

Structural changes in terms of densification and polymerization of the Na-silicate network with temperature were studied qualitatively using Raman spectroscopy. The data were acquired on Na-silicate powder pellets (500 mg; 13 mm diameter; load of 2 tons for 60 s by a Specac Manually Operated 15-ton Hydraulic Press) using a Renishaw Qontor Raman Spectrometer equipped with a 532 nm green laser and 50 mW power. A 50X objective lens was utilized for acquiring 992 spectra in the range 300-1300 cm^{-1} with a 90 µm step-size and an exposure time of 20 s. These spectra were averaged using principle component analysis (PCA) for denoising and homogenizing the composition variations from grain to grain over the pellet surface. Spectra were also acquired for Na-silicate thin films deposited on Ta-coated glass substrates using a 100X objective lens. 100 spectra in the extended range 300-4000 cm^{-1} with a 10 µm step-size and an exposure time of 10 s were acquired using 532 nm green laser with a power of 10 mW followed by averaging by PCA.

2.2.3.5. Hot-stage Microscopy

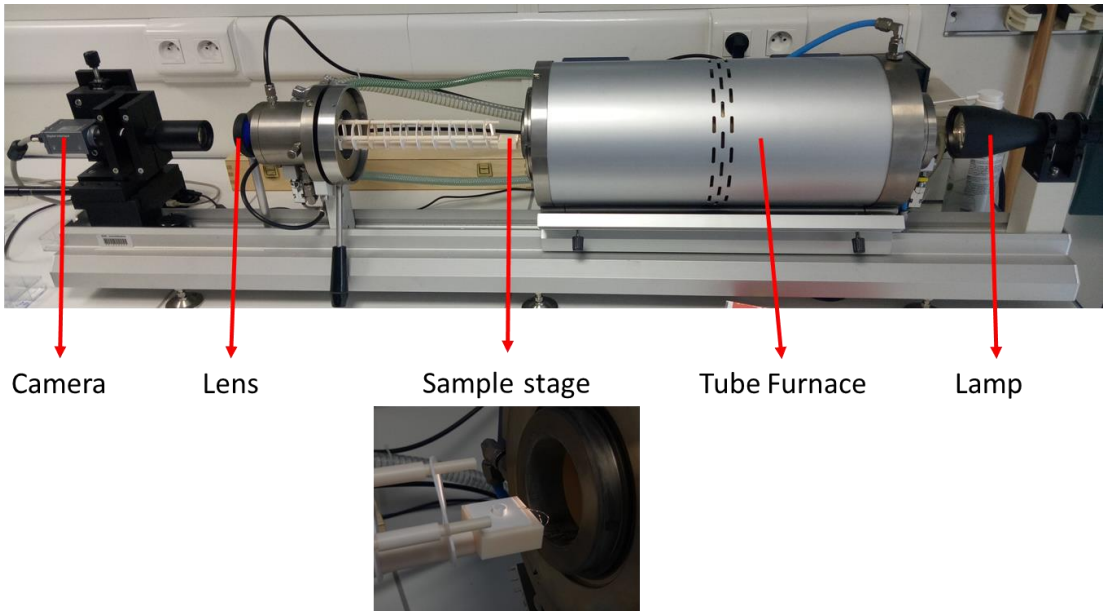

Figure 2.3: Hot-stage Microscope setup used for obtaining image recording of pellets upon thermal treatment.

For precise in-situ monitoring of thermal evolution of pre-dried powder pellets, a LINSEIS in-situ Hot-stage Microscope (see **Figure 2.3**) equipped with a 10X objective was utilized to record a video by capturing several images (1 image/s) on ramping up to 400°C as well as 1200°C (Na-silicate pellets were pre-foamed at 400°C followed by preparation of a pellet out of this powder for heating to 1200°C). 50 and 100 mg pellets with a 5 mm diameter were obtained at a load of 1 ton

for 10 s for the different alkali silicate compositions. Heating ramps of 1, 5 and 10°C/min were investigated for Na-silicates while 10°C/min for K and 5°C/min for Li-silicate powder pellets. Viscosity measurements on Na-silicates and reference glasses were realized by developing models based on pellet shape changes observed above 450°C. These models were obtained by utilizing the viscosity values available in literature models for silicate glass compositions.[114,115]

2.2.3.6. Fourier Transform Infra-Red spectroscopy

Carbonation kinetics of Na-silicate starting solutions and films was followed by utilizing a Bruker Equinox 55 FT-IR spectrometer. Thin films (from as received and carbonated commercial solution) of the order of 250nm were deposited on double-side polished silicon wafer substrate followed by analysis in transmission mode in the range 400-4000 cm^{-1}. A sample holder with a 45° tilt was used for obtaining a spectrum averaged over 200 accumulations under continuous N_2 flow. Measurements were also performed on thick Na-silicate coatings pre-dried at different temperatures to follow the evolution of water.

2.2.3.7. Secondary Electron Microscopy

A Hitachi S-4800 FEG-SEM was employed for cross-sectional and planar views of thin films and thick coatings in secondary electron (SE) mode. Samples were cut to expose the cross-section and a few nm thick Pt layer was sputtered prior to investigation to prevent any charge accumulation on films. Images were recorded at various accelerating voltages and magnifications. Thickness measurements were also carried out on a FEI Quanta 400 SEM mainly for thicker coatings.

2.2.3.8. Secondary Ion Mass Spectroscopy

SIMS analysis was performed by IONTOF TOF.SIMS 5 spectroscope for obtaining diffusion profiles of Na^+ ions present in the thin Na-silicate layer spin coated on silicon wafer substrate. Different sputter sources were used including Cs^+ ion source (2 keV), O_2^+ ion source (20 keV), O_2 cluster source (20 keV) and O_2 cluster source at low temperature (-100°C). A bismuth (Bi) source operated at 30 keV was used for analysis of the sputtered region. O_2 cluster source at low temperature was chosen as the source for future experiments as all other methods resulted in distorted diffusion profiles due to the ions in the films being highly sensitive to the incoming ions. There were issues of charging of the samples that led to ions being pushed inside the films resulting in inhomogeneous profiles.

Chapter 3.

Thermal behavior of aqueous alkali silicates

The structure of aqueous alkali silicates has intrigued much attention due to their important contribution to industrial systems where they are employed in a number of ways with particular interest being in their fire-resistant properties. Literature studies have mainly focused on their structural properties at ambient conditions and do not inform much about their thermal evolution from a more fundamental approach. The structural properties of two different molar ratios of aqueous Na, K and Li-silicate solutions at room temperature as well as on thermal treatment are discussed here in details to draw comparisons among the various alkali silicates. Heating these solutions induces changes at both the macroscopic and microscopic scale due to the removal of water from the system resulting in foaming in some cases. This induces microscopic structural variations that have been studied quantitatively using a combination of characterization tools to predict the actual state of the system and its link to the behavior observed macroscopically. A comparison of the thermal behavior with glasses of similar compositions is also presented. Structural properties of the starting solutions are discussed followed by qualitative and a more quantitative analysis of xerogels in terms of thermal evolution of proton-related species and the corresponding impact on the actual microscopic state of the system below 500°C. Evolution above 500°C in terms of viscosity variations has also been presented using in-situ measurements.

3.1. Structure and reactivity of soluble silicates at room temperature

Aqueous alkali silicates are a mixture of silica network dissolved in water comprising of Q^n structural units (where n=0, 1, 2, 3, 4 corresponds to the number of bridging oxygens referred to as BOs, otherwise non-bridging as NBOs) shown in **Figure 3.1**.

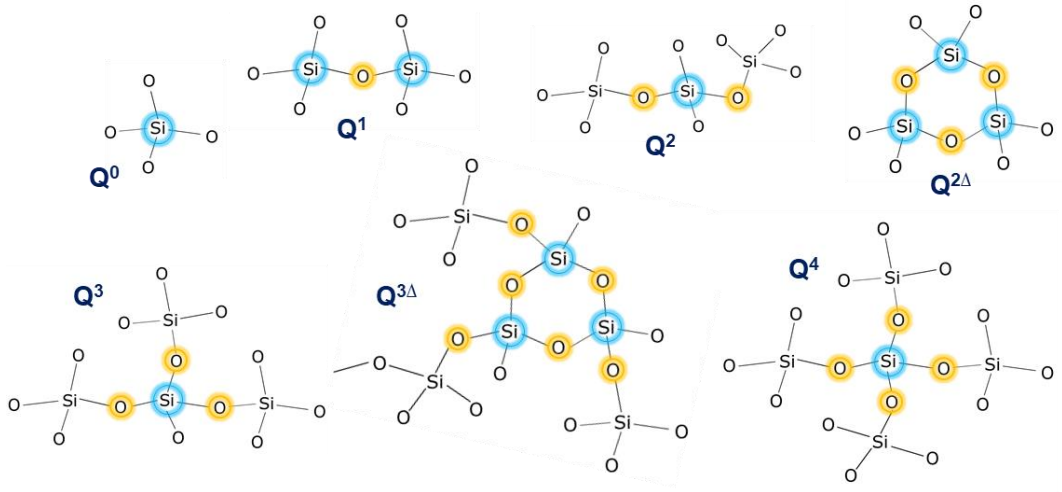

Figure 3.1: Schematic illustration of Q^n species used for defining alkali silicates.

This kind of a classification is generally used for defining the properties of these solutions in terms of the degree of polymerization and is dependent highly on the composition of the systems i.e. alkali and SiO_2 concentration, influencing directly the global changes in viscosity.

3.1.1. Na-silicates

The structure of Na-silicate solutions with two different molar ratios (Na_2O/SiO_2=0.29 and 0.5) has been investigated quantitatively by liquid-state ^{29}Si Nuclear Magnetic Resonance (NMR) spectroscopy. Their spectra exhibit multiple peaks indicative of the coexistence of different Q^n species. The relative proportion of each Q^n unit was determined by taking the integral under each peak and is shown in the corresponding NMR spectrum in **Figure 3.2**. Q^0, Q^1, $Q^{2\Delta}$, Q^2, Q^3 and Q^4 are all present for the solution with lower amount of Na (Na_2O/SiO_2=0.29). Increasing the amount of Na in the solution (Na_2O/SiO_2=0.5) tends to depolymerize the network causing Q^4 to disappear altogether accompanied with a conversion into lower Q^n units. The amount of Q^1, Q^2 and $Q^{2\Delta}$ (cyclic species of Q^2) increases while Q^3 decreases with the appearance of $Q^{3\Delta}$ (branched cyclic species of Q^3) around a chemical shift of -87.4 ppm confirming network depolymerization with the relative positions staying roughly the same for the two molar ratios (cyclic species with different structures have been proposed in the literature for soluble Na-silicates).[18,31,33,34,42]

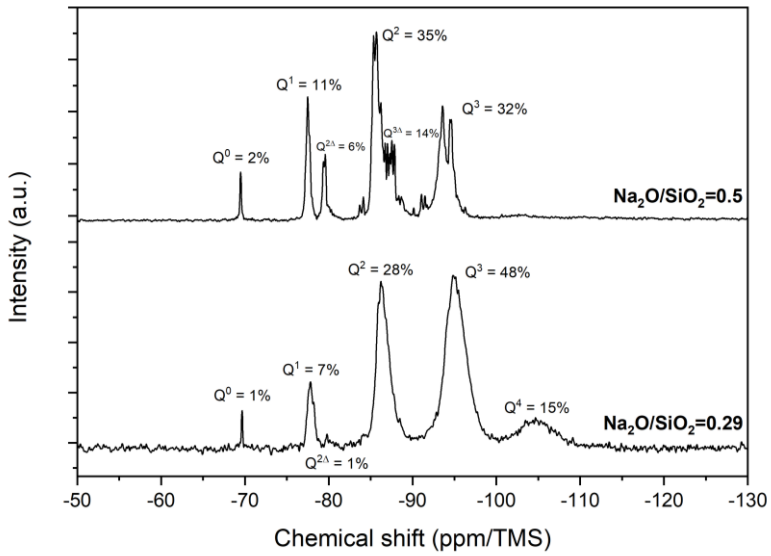

Figure 3.2: Liquid-state ^{29}Si NMR spectrum of Na-silicate solutions with a molar ratio of 0.29 with 27 wt% SiO_2 and 0.5 with 26 wt% SiO_2 detailing the chemical shift (ppm/TMS) and percentage fraction of each Q^n unit for the two molar ratios according to band assignments proposed in literature.[11,18,31–34,42,43,116] Note that a repetition delay of 5 s was chosen as the optimum after performing measurements at 0.5, 1, 5, 10 and 20 s as shown in **Figure A 3.1**.

Lower Na_2O/SiO_2 ratio leads to more condensed species indicating an increased polymerization for which the structure is less defined (i.e. larger distribution of possible structure) leading to broader peaks and less structures in the spectra. This broadness may also be a result of higher viscosity of Na_2O/SiO_2=0.29 solution. Higher amount of Na leads to the splitting of peaks as observed for $Q^{2\Delta}$, Q^2, $Q^{3\Delta}$ and Q^3 in **Figure 3.2** indicating the presence of multiple network configurations upon depolymerization.[17,18,28,42]

The structural dependency on preparation method was also investigated to evidence some possible kinetic effects for reaching a stable structure and it was found that the structure depends on only two parameters i.e. dilution level and molar ratio. We were able to tune continuously the molar ratio of our solutions by adding NaOH or Ludox (colloidal SiO_2) as shown in **Figure 3.3**. The obtained solutions have the same structure as the commercial ones except slight changes due to some differences in dilution level as it tends to depolymerize the network.[42] Thus, it would also be interesting to do the same experiments on solutions with similar dilution levels.

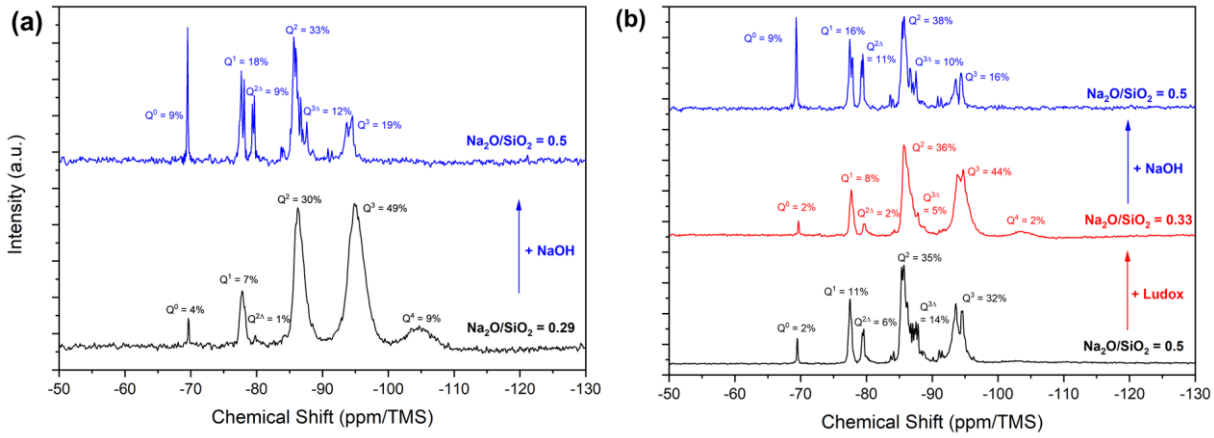

Figure 3.3: Changing the structure by (a) addition of NaOH into Na_2O/SiO_2=0.29 and (b) Ludox followed by NaOH in Na/Si=0.5 solution through Liquid-state ^{29}Si NMR. Black curves represent the as received commercial solutions.

Addition of Ludox into Na_2O/SiO_2=0.5 solution to obtain the molar ratio Na_2O/SiO_2=0.33 changes the structure as can be seen in the red spectrum in **Figure 3.3**(b). Adding NaOH to the same solution changes the molar ratio back to 0.5 but the structure is not exactly the same as the commercial solution because dilution is different. Thus, we are able to produce Na-silicate (or other alkali silicate) solutions of the desired composition by addition of a known amount of Ludox or NaOH. The silicate structure is only dependent on concentration and molar ratio and not on the way it is prepared suggesting the kinetics of the reaction to be rapid.

3.1.2. K and Li-silicates

K and Li-silicate solutions have a structure in terms of the Q^n units as shown by the liquid-state ^{29}Si NMR spectra in **Figure 3.4**. K-silicates are composed of a structure (**Figure 3.4**(a)) quite the same as that observed in Na-silicates.[17,20,28] On increasing the concentration of K in the solution i.e. to achieve a molar ratio of 0.5, network tends to depolymerize resulting in the conversion of higher Q^n units into lower ones. Li-silicates, on the other hand, seem to have a behavior different than that observed in Na and K-silicates.[28] Li_2O/SiO_2=0.29 has a structure in solution similar to Na and K-silicates. However, addition of further Li ions in the solution doesn't seem to strongly impact the network structure[28] as observed for Li_2O/SiO_2=0.4 shown in **Figure 3.4**(b).

Note that Li-silicate solutions were prepared by addition of LiOH powder into Li_2O/SiO_2=0.2 commercial solution. Adding LiOH into Li_2O/SiO_2=0.29 to obtain Li_2O/SiO_2=0.4 changes the network slightly with a reduction in the quantity of Q^3 from 54% to 50% accompanied with an increase in Q^2 from 30% to 35%. The resulting solutions are transparent indicating the added LiOH

to have been dissolved thus suggesting an already saturated network that cannot accommodate more Li ions. Furthermore, LiOH seems to be present as it is and it may or may not be H-bonded to the network, thus, impacting the global thermal evolution of the systems.

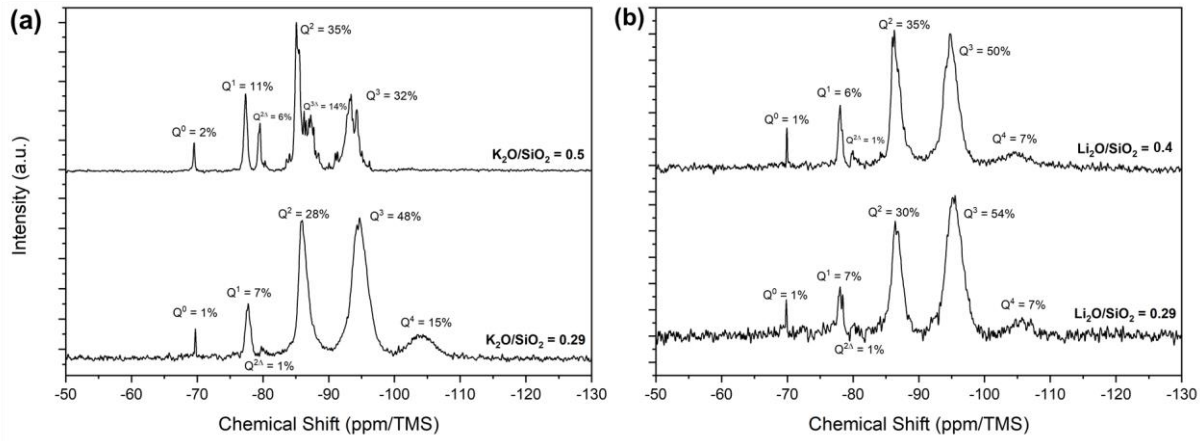

Figure 3.4: Liquid-state ^{29}Si NMR of (a) K and (b) Li-silicate solutions.

Hence, liquid-state ^{29}Si NMR allows to study the structural variations of aqueous alkali silicates. It is possible to tune the molar ratio of these silicates by manipulating the starting composition to obtain the desired structural properties. Increasing the alkali content in the solution tends to depolymerize the network connectivity in both Na and K-silicates while Li-silicates don't show an abrupt change in organization due to a network already saturated with Li ions. Thermal treatments of these solutions are expected to change further the microscopic arrangement as water will be released impacting directly the network polymerization and the macroscopic properties.

3.2. Xerogel formation

The starting aqueous alkali silicate solutions are composed of free water, solvating water (molecules H-bonded to alkali ion or network protons) and silanols[21,117] as shown in **Figure 3.5**.

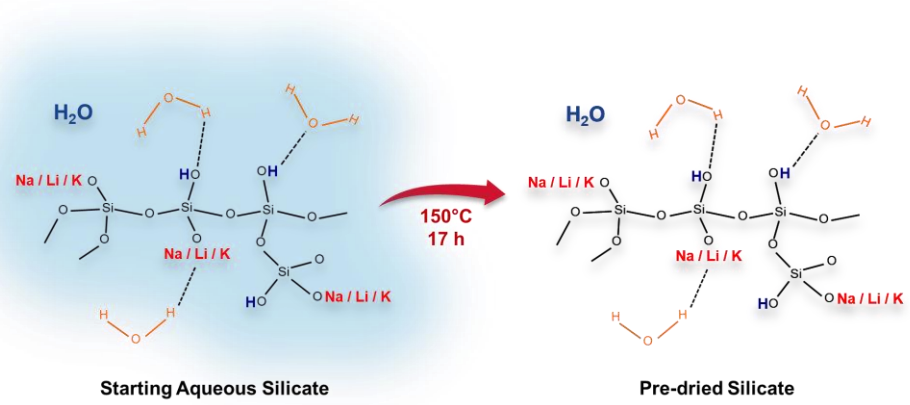

Figure 3.5: Pre-dried silicate obtained by removing free water from raw alkali silicate solutions at 150°C.

In order to investigate the thermal behavior of these silicates keeping in view the experimental limitations posed by the various characterization tools (splashing and foaming-related problems), xerogels were prepared by pre-drying the solutions at 150°C for 17 h to remove maximum amount

of free water from the system. Note that longer durations did not result in further weight loss as evident from isothermal Thermogravimetric (TGA) measurements shown in the appendix (**Figure A 3.2**). These dried but still hydrated powders will be referred to as 'pre-dried' silicates.

The structure of these pre-dried silicates is possible to be observed using solid-state ^{29}Si NMR as shown by the spectra in **Figure 3.6**. Broad bands are observed due to the glassy character of these materials that have been deconvoluted using Gaussian function by Dmfit software[111] to obtain the distribution of individual Q^n units. Since all the free water and a small amount of solvating water is expected to be removed during this pre-drying step, polymerization of the network is achieved when compared to the structure in solutions. The structure of these xerogels is more dominant in terms of the quantity of Q^3 and Q^4 that are much higher than the solutions. Furthermore, depolymerization is observed on increasing the alkali concentration in both Na and K silicates while Li-silicates don't show much difference in the relative distribution of the species. Further details on such solid-state NMR measurements are given in later sections along with the discussion on sharp peaks observed in the case of K-silicates (corresponding to crystallization).

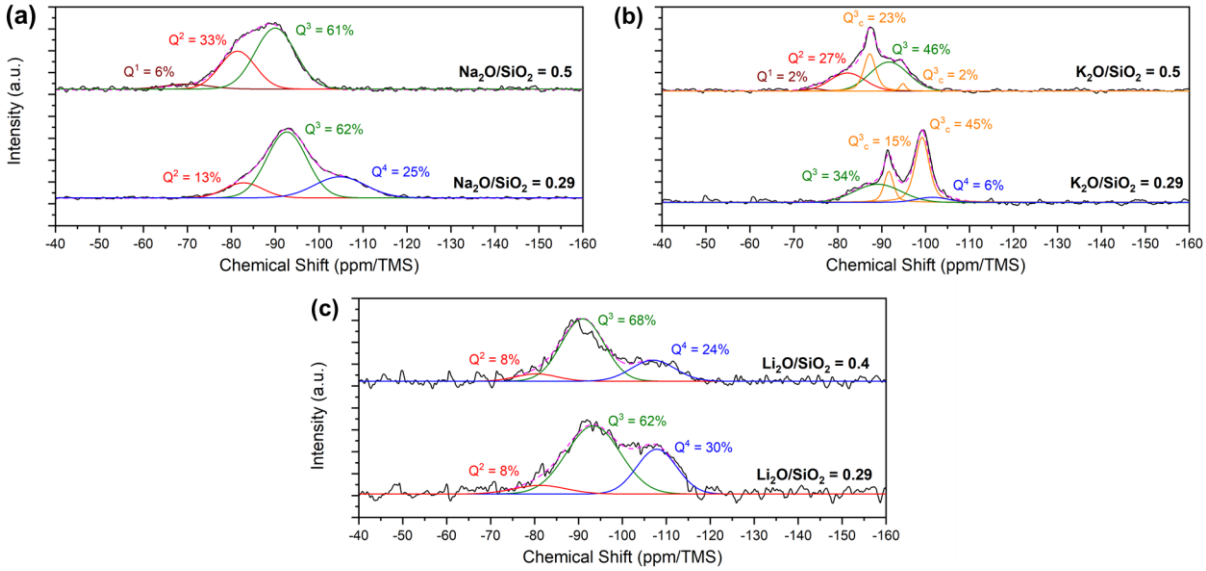

Figure 3.6: Solid-state ^{29}Si NMR at 8.4 T for (a) Na, (b) K and (c) Li-silicate xerogels obtained by pre-drying solutions at 150°C. Note that a drying time of 17 h was used for all the compositions except K_2O/SiO_2=0.5 that was dried for 1 week due to its very hygroscopic nature. Note that all the measurements were performed at repetition delay of 20 s and 3000 scans were acquired after calibrating the parameters (see **Figure A 3.3**).

It must be noted here that these xerogels or pre-dried silicates are the starting point for temperature evolution in order to have a state that is more or less reproducible, keeping in mind also the hygroscopic nature of alkali silicates. Heating these pre-dried systems is expected to induce further changes to the structure of the material, thus, inculcating interest in the fundamental understanding of their thermal behavior.

3.3. Water evolution on thermal treatment

Thermally treating alkali silicates leads to macroscopic and microscopic structural changes due to the release of water from the system. Macroscopically speaking, intumescence/foaming is observed for Na and K-silicates on heating. The material expands volumetrically, depending upon

the starting composition and state of the microscopic network, while Li-silicates don't show any expansion. The macroscopic foaming behavior of the different compositions is discussed in detail in **Chapter 4**. Foaming is related to the release of water from the system and thus necessitates an investigation of the structural evolution of alkali silicates in terms of this water release and its link to the corresponding structural changes observed visually as well as at the scale of the network. Both qualitative and quantitative analysis of the structure is, therefore, important for probing the thermal behavior in terms of water evolution and other relevant phenomenon that may, at the global scale, have an impact on the intumescent nature of the different alkali silicates.

3.3.1. Macroscopic evolution: global water content

Pre-dried alkali silicate powders were subjected to further heating for investigation of properties at both macroscopic (global water evolution) and microscopic (structural) scale. In this section, we describe the macroscopic evolution of these silicate powders and the effect of alkali type and concentration.

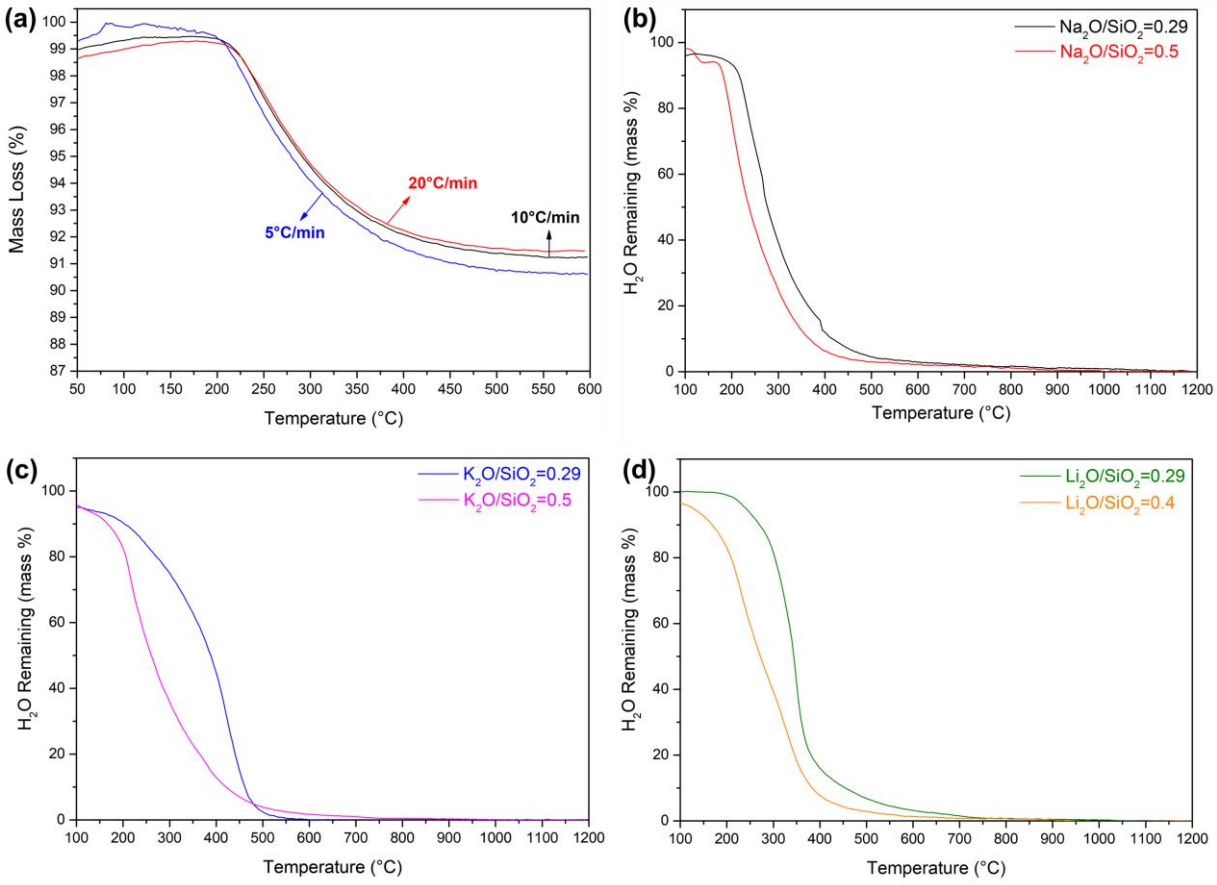

Figure 3.7: TGA mass loss curves (a) at three different heating rates for the Na-silicate powder with a molar ratio of 0.29 prepared at 150°C and at 10°C/min for both molar ratios of (b) Na, (c) K & (d) Li pre-dried silicates.

Thermal evolution of the pre-dried alkali silicates was derived from TGA measurements. Before acquiring data on the respective silicates, Na_2O/SiO_2=0.29 silicate powder was subjected to mass loss measurements at heating ramps of 5, 10 and 20°C/min to determine if the evolution was controlled by kinetic effects (see **Figure 3.7**(a)). The behavior is the same at 10 and 20°C/min ramping rate, with a first plateau up to 150°C because of the removal of almost all the free water

upon drying at this temperature, and then a gradual weight loss above 200°C. The evolution is slightly different at 5°C/min heating rate maybe because of a limitation of initial calibration of the equipment with metal standards. A heating rate of 10°C/min was chosen for further studies as the mass loss seemed to be only temperature dependent, at least for the range of heating rates studied. Furthermore, the impact of pre-drying temperature was also explored but no differences in the thermal behavior were found (see **Figure A 3.4**). Note that the inconsistency in the TGA measurement below 150°C arises from the very small quantities of samples analyzed because of foaming i.e. typically 15 mg of the Na_2O/SiO_2=0.29 powder pre-dried at 150°C. This led to improper correction of the buoyancy effects in the room temperature (RT)-150°C temperature range.

3.3.1.1. Na-silicates

The mass loss curves for the two molar ratios of Na-silicates at a heating rate of 10°C/min are shown in **Figure 3.7**(b) while the percentage of leftover water (calculated by subtracting percentage mass loss at 275, 350, 400, 450, 500, 600 and 1200°C from the overall mass lost in TGA measurements) is plotted as a function of temperature in **Figure 3.8**(a). Note that the step around 400°C for Na_2O/SiO_2=0.29 in **Figure 3.7**(b) and **Figure 3.8**(a) is a consequence of splashing or bubble bursting from the powder and corresponds to a mass loss of 0.4% which is not significant and is, thus, a part of the calculations made here. Dehydration occurs very quickly after heating at temperatures higher than 150°C (pre-drying temperature). Interestingly, DSC curves shown in **Figure 3.8**(b) suggest that the silicates experience a glass transition (T_g) around 210°C for Na_2O/SiO_2=0.29 and 175°C for Na_2O/SiO_2=0.5, in the same range of temperature where dehydration starts. Note that there is an interplay between glass transition and water removal which means that decreasing the water content changes the (supposed) T_g and when the DSC-determined glass transition is reached, water removal increases since the silica network is more mobile and water diffusion is enhanced within the material.

Table 3.1: Comparison of the composition (in wt% and mol%) of Na-silicates before and after pre-drying at 150°C.

Alkali Silicate	Molar Ratio ($nM_2O/nSiO_2$)	Pre-drying	SiO_2 (wt%)	M_2O (wt%)	H_2O (wt%)	SiO_2 (mol%)	M_2O (mol%)	H_2O (mol%)	Molar Ratio (nM_2O/nH_2O)
Na	0.29	None	27.75	8.25	64	11.2	3.2	85.6	0.04
		150°C	69.3	20.7	10	56.5	16.4	27.1	0.61
	0.5	None	27.25	13.75	59	11.5	5.6	82.9	0.07
		150°C	58.7	29.3	12	46.1	22.3	31.6	0.71
K	0.29	None	24	11	65	9.7	2.8	87.5	0.03
		150°C	63.6	29	7.4	59.5	17.4	23.1	0.75
	0.5	None	23	17	60	9.8	4.6	85.6	0.05
		150°C	50.3	37.1	12.6	43.3	20.4	36.3	0.56
Li	0.29	None	17.8	2.6	79.6	6.2	1.8	92	0.02
		150°C	80.2	11.6	8.2	61.4	17.8	20.8	0.85
	0.4	None	17.3	3.4	79.3	6	2.4	91.6	0.03
		150°C	78.1	15.4	6.5	59.8	23.7	16.6	1.43

More overall mass is lost for the silicate with higher Na content in the network indicating a slightly more retention of leftover water in the starting powder prepared at 150°C. Assuming that all water is lost at 1200°C, total water retention is 12% in Na_2O/SiO_2=0.5 and 10% in Na_2O/SiO_2=0.29 starting powder as shown in **Table 3.1**. This slight difference in the amount of water may explain the offset of temperature observed by DSC suggesting a connection between the water content and softening (more mobile network) of the material. Near 150°C, the presence of more retained water when there is higher Na content in the silicate can be attributed to solvating water (linked to silanols or ionic hydration)[21] and a higher number of silanols.

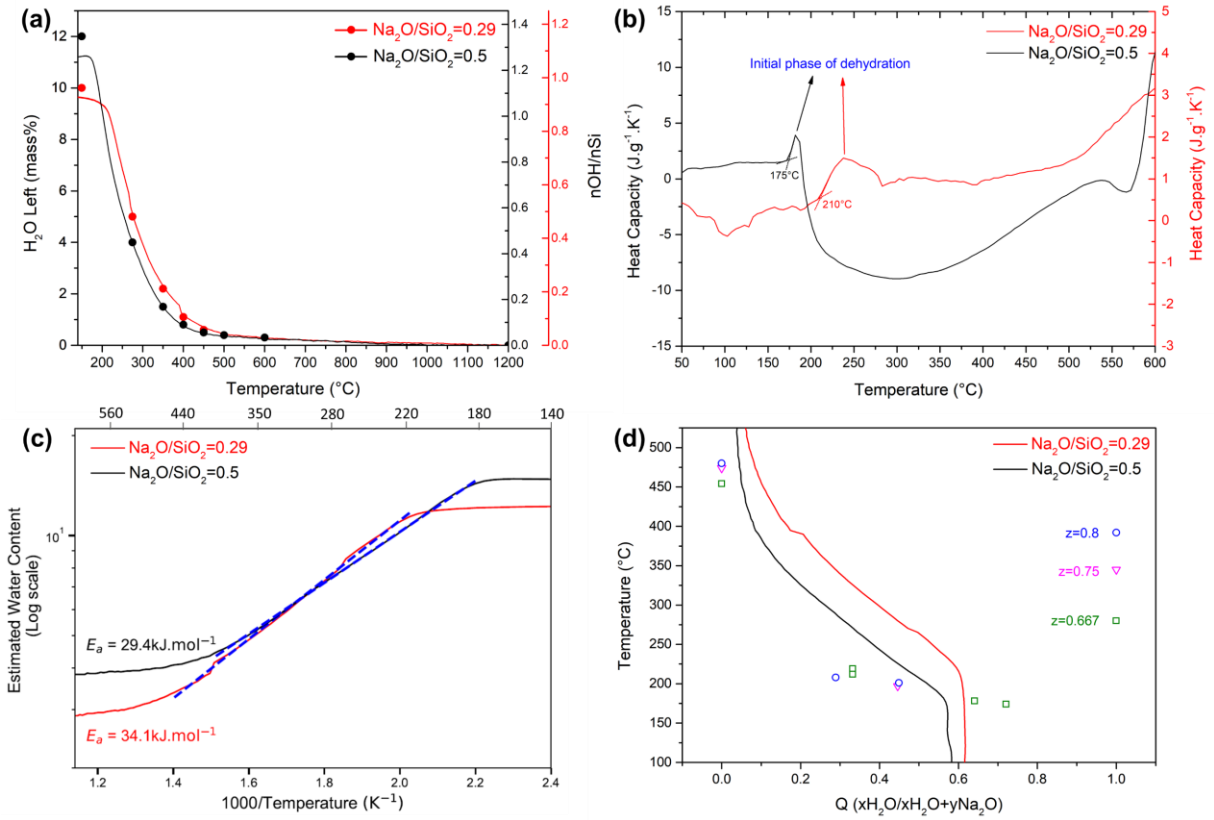

Figure 3.8. (a) Evolution of total water left in the network for the two molar ratios (TGA measurement performed at 10°C/min); note that both y-axes on the right, red corresponding to Na_2O/SiO_2=0.29 and black to Na_2O/SiO_2=0.5, represent nOH/nSi, (b) DSC measurements for heat capacity at 10°C/min also performed on pre-dried powder (the onset of the peaks are identified as a glass transition and match well with the macroscopic foaming temperature), (c) Arrhenian plot of TGA mass loss curves (the fitting temperature range is 220-450°C for Na_2O/SiO_2=0.29 and 180-400°C for Na_2O/SiO_2=0.5, respectively) and (d) comparison of our TGA curves (represented by solid lines) with glass transition temperature reported for hydrated glasses[85,87,89] (Q represents the mole fraction of water while the molar content of SiO_2 (at 150-500°C), represented by z, is in the range 0.56-0.77 moles for Na_2O/SiO_2=0.29 and 0.46-0.66 moles for Na_2O/SiO_2=0.5, respectively, while constant for literature points).

The global evolution behavior of TGA mass loss is almost the same for the two molar ratios although the two curves are just shifted. For a better comparison of the two molar ratios, we plot the leftover water content versus inverse temperature in an Arrhenian diagram in **Figure 3.8**(c). Since TGA data is independent of the ramping speed, we can consider that the Arrhenius law may describe temperature dependence of reaction rates. Considering that all free water has been

removed by the pre-drying step at 150°C, the following possible reactions leading to water release are considered:

$$2SiOH \rightleftharpoons Si - O - Si + H_2O_{atm} \quad (3.1)$$

$$SiO^-H^+ / H_2O_{solv} \ (or\ SiO^- - H_3O^+) \rightleftharpoons SiOH + H_2O_{atm} \quad (3.2)$$

$$SiO^-Na^+ / H_2O_{solv} \rightleftharpoons SiONa + H_2O_{atm} \quad (3.3)$$

where the left-hand side of eq. (3.1, 3.2 and 3.3) represent proton-related species i.e. isolated silanols as well as silanols and Na-linked NBOs solvated by water molecules in the silicate, while the right-hand side indicates water evaporating into the atmosphere on thermal treatment.

As a rough approximation, we consider that reaction 3.1 prevails in the Arrhenius plot since its activation energy is expected to be much higher than the two other reactions associated to the removal of solvated water. The reaction constant (k) of reaction 3.1 can, therefore, be expressed as:

$$k = \frac{p[H_2O]}{c[SiOH]^2} = A\,exp\left(\frac{-E_a}{RT}\right) \quad (3.4)$$

where 'p' is the partial pressure, 'c' the concentration, 'A' the pre-exponential factor, 'E_a' the activation energy, 'R' the gas constant (8.3145 J.mol^{-1}.K^{-1}) and 'T' the temperature in K. Considering that the partial pressure of water is fixed by a large atmospheric reservoir, therefore, making it constant, the E_a is linked to protons as:

$$[SiOH] \sim exp\left(\frac{E_a}{2RT}\right) \quad (3.5)$$

The calculated E_a values in the low temperature range (below 450°C) are 34.1 kJ.mol^{-1} and 29.4 kJ.mol^{-1} for the molar ratio Na_2O/SiO_2=0.29 and Na_2O/SiO_2=0.5, respectively, suggesting same order of magnitude for the two Na-silicates. Such low values of E_a are consistent with literature studies on hydrated Na-based silicate glass melts with values approaching 30 kJ.mol^{-1}.[118,119] Therefore, this suggests that the removal of water is controlled by two simultaneous mechanisms: the removal of solvated water, and the transformation of some hydroxyl groups into solvated water to maintain a ratio corresponding to the equilibrium speciation of water at a given temperature. The latter mechanism also implies that the proton-involving network is relatively mobile.

Regarding the mobility of the network, literature data were obtained from geochemistry studies[85,87,89] on the T_g (corresponding to a viscosity of 10^{12} Pa.s) of hydrated sodium silicate glasses obtained by dissolving water into the melts at high pressure. These values are reported in **Figure 3.8**(d) for different molar ratios along the pure sodium oxide to pure water line. Note that T_g values of these hydrated glasses are much lower than the ones of dry glasses (which would be in the range 500-650°C). Indeed, water decreases the viscosity of silicate melts; one mechanism being the formation of silanols and the depolymerization of the network.[120] We have also included in this figure the TGA curves corresponding to specific water over sodium content at particular

temperature points. Interestingly, the onset of the mass loss corresponds to a temperature just above the literature data for the glass transition, suggesting that water removal is possible only after the network becomes mobile. As the temperature increases, the water content of the material remains high enough so that the glass transition for the obtained composition is lower than the actual temperature, meaning that the network always keeps some mobility. Nevertheless, the difference between the temperature (for a given composition resulting from water loss) and the corresponding T_g is small, suggesting that the system loses water until the viscosity of the system becomes too high. It is possible that in the temperature range of our observations, the composition versus temperature evolution corresponds to an iso-viscosity line with a viscosity close to the one of the glass transition 10^{12} Pa.s.

3.3.1.2. K and Li-silicates

Water content evolution in pre-dried K and Li-silicate powders was also investigated and is shown by the TGA mass loss curves in **Figure 3.7**(c, d) as well as in the **Figure 3.9**(a, b) in terms of leftover water content. Both the Na-silicate compositions (**Figure 3.8**(a)) as well as K_2O/SiO_2=0.5 (**Figure 3.9**(a)) show a rapid and homogeneous release of water while K_2O/SiO_2=0.29 and Li-silicate pre-dried powders tend to evolve in a slightly different manner in the sense that dehydration seems to occur in steps over the temperature interval studied (see **Figure 3.9**(b)).

One commonality among all the systems is that on increasing the alkali concentration, a different offset temperature of mass loss is observed. Higher alkali content silicates tend to start losing water at lower temperatures e.g. K_2O/SiO_2=0.29 sees a gradual drop in the TGA curve around 220°C and the system seems to retain water till higher temperatures while the temperature for the start of dehydration drops to around 190°C for K_2O/SiO_2=0.5 followed by a gradual evolution as observed in Na-silicates. Li-silicates show a similar behavior in terms of the offset in temperature for the start of dehydration with a higher value (200°C) seen for Li_2O/SiO_2=0.29 (the mass loss behavior seems to be slightly different when compared to Na or K silicates). A water retention of 12.6% is observed in K_2O/SiO_2=0.5 while 7.4% in K_2O/SiO_2=0.29 suggesting a behavior similar to that observed in Na-silicates. In contrast, an inverse impact of increasing alkali concentration is observed in Li-silicates i.e. Li_2O/SiO_2=0.29 retains ~8% of water after the pre-drying step while a lower value (6.5%) is observed in Li_2O/SiO_2=0.4.

Na-silicates exhibit a single E_a approaching 30 kJ.mol^{-1}, irrespective of the starting alkali concentration, for the release of water content from the system as discussed previously. K and Li-silicates, on the other hand, tend to show multiple activation energies suggesting a combination of several mechanisms. This can be linked to the macroscopic foaming behavior observed on heating the solutions or pre-dried powders. Na-silicates foam extensively at a heating rate of 5°C/min, Li-silicates don't foam while an intermediate behavior is seen for K-silicates as discussed in **Chapter 4**.

K and Li-silicates have multiple E_a values due to several slopes as shown in **Figure 3.9**(c) and (d), respectively, and hence several mechanisms. The existence of these multiple E_a values happens to be a consequence of microscopic structural changes linked to the release of water and an

underlying phenomenon related to crystallization not at all observed in Na-silicates below 500°C, where the network happens to be mobile enough to let the water molecules escape resulting in extensive foaming.

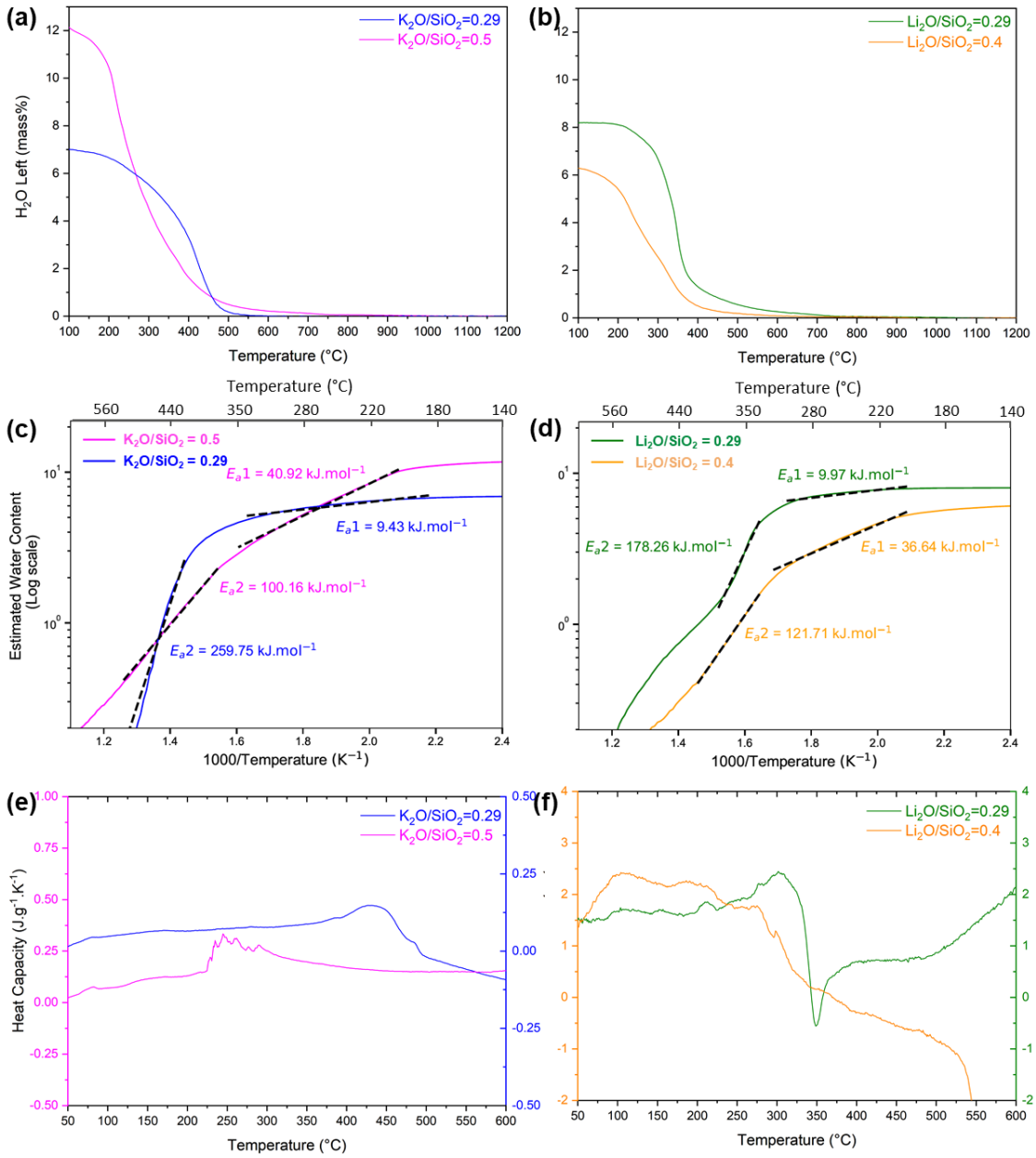

Figure 3.9: TGA mass loss evolution of total water left in the system for two different molar ratios of (a) K-silicate & (b) Li-silicate powders pre-dried at 150°C (all the measurements were acquired at a heating ramp of 10°C/min), activation energy (E_a) obtained from TGA mass loss data indicating (c) Arrhenian behavior for K_2O/SiO_2=0.5 while (c, d) multiple values for K_2O/SiO_2=0.29 & Li-silicate pre-dried powders, and DSC curves at 10°C/min on pre-dried (e) K & (f) Li-silicates showing peaks corresponding to the intrinsic changes.

Changes in the structural properties of aqueous alkali silicates and the link to the stability of different phases could be studied through Phase Diagrams. Ternary phase diagrams were plotted from FactSage[121] (at room temperature and 1 atm) to determine the stable phases in the starting solutions as shown in **Figure 3.10**. All the three silicate systems (Na_2O-SiO_2-H_2O, K_2O-SiO_2-H_2O and Li_2O-SiO_2-H_2O) were simulated through the amorphous phase-related data available in the

FactSage database, however, accurate calculations could not be made for Li-silicates due to unavailability of relevant information. Starting solutions are all in the phase regions termed as 'Liquid + Hydrated Amorphous' (corresponding to the blue dots at arrow tails in **Figure 3.10**) suggesting the existence of an amorphous alkali silicate network dissolved in water. 'Hydrated Amorphous' refers to the amorphous network composed of silanols and solvating water molecules. Blue arrows in **Figure 3.10** serve as a guide for the eyes and point towards a completely dried state once all the proton-related species are removed from the system. However, that does not mean the solutions would pass through the regions indicated in-between as that would be dependent upon the composition of the starting solution, especially, the water content that is expected to change as a function of temperature leading to physical and chemical structural changes.

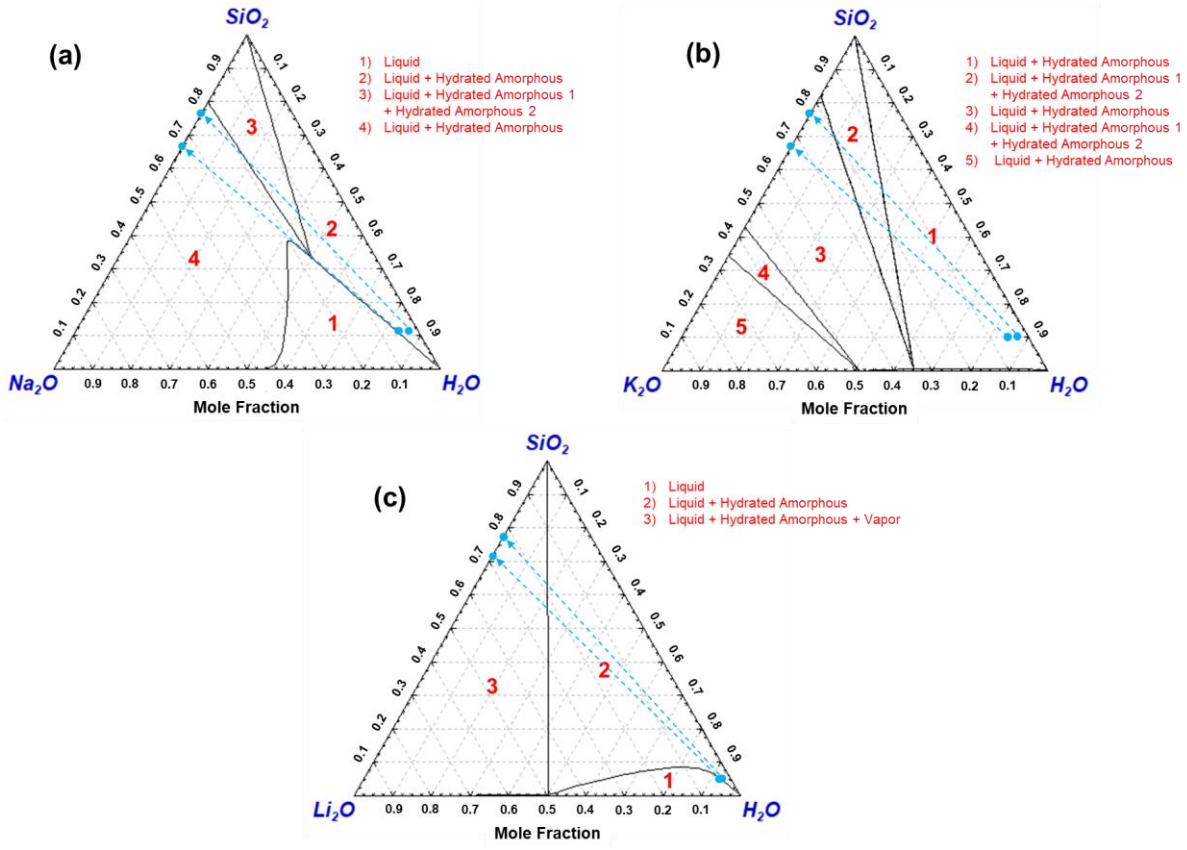

Figure 3.10: Ternary phase diagram at 25°C, 1 atm for (a) Na_2O-SiO_2-H_2O, (b) K_2O-SiO_2-H_2O and (c) Li_2O-SiO_2-H_2O obtained from FactSage. The blue dots are indicative of the starting solutions and the expected composition on complete drying with arrows serving as a guide for the eyes.

The stability regime in the pre-dried state (obtained by drying the solutions at 150°C) is expected to directly influence the thermal behavior. Binary phase diagrams (in terms of total water and total amorphous composition) for Na and K-silicates calculated from FactSage (see **Figure 3.11**) show the temperature range for the existence of different phases upon dehydration. Phases referred to as 'Hydrated Amorphous' are indicative of the amorphous alkali silicate network that is independent of free water but is composed of network silanols and solvating water molecules. 'Vapor' corresponds to the water molecules that are released on thermal treatment while 'Liquid' is representative of free water in the system. Starting solution compositions are shown by the blue

dots while TGA data, at the temperature points studied for quantitative analysis later on, is marked with black points. Note that the black points at 150°C in **Figure 3.11** are the starting points for TGA measurements and represent the water content in the pre-dried silicate powders.

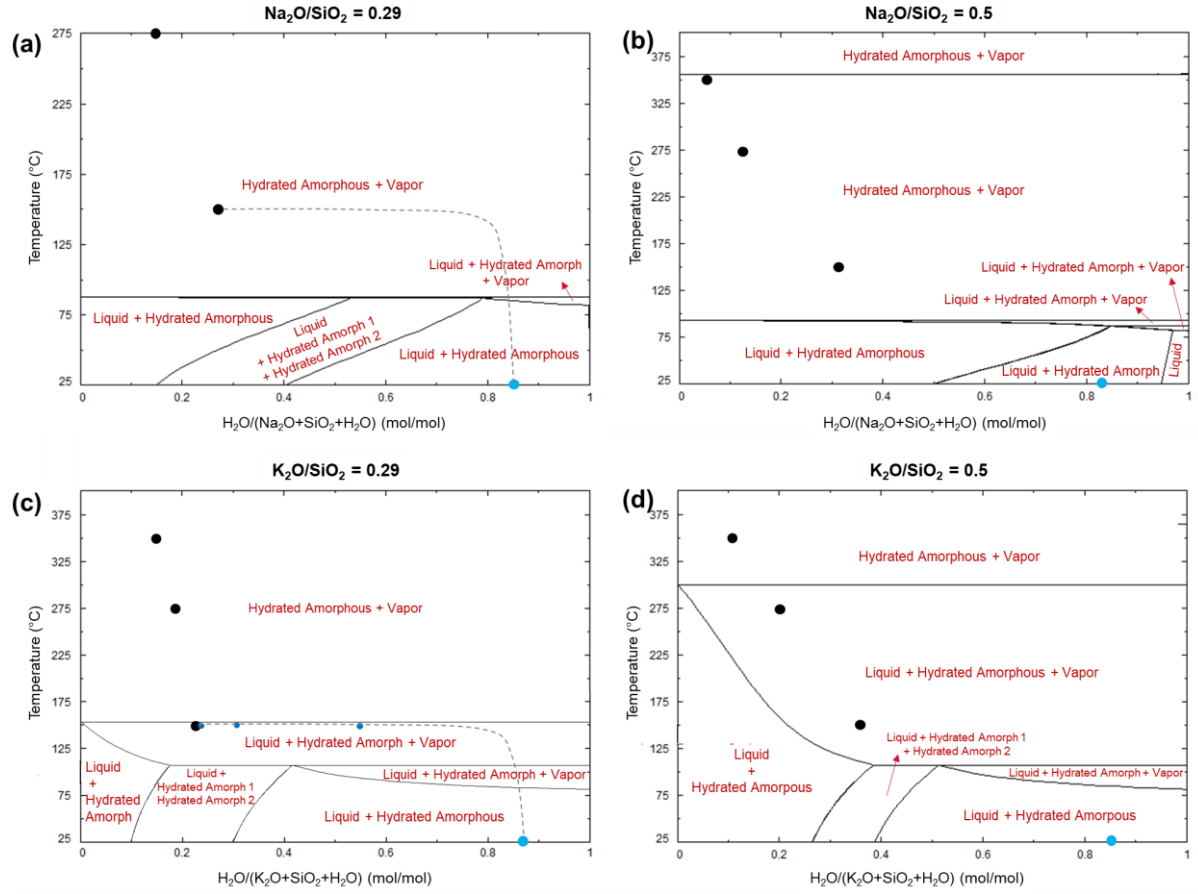

Figure 3.11: Binary phase diagram for (a) Na_2O/SiO_2=0.29, (b) Na_2O/SiO_2=0.5, (c) K_2O/SiO_2=0.29 and (d) K_2O/SiO_2=0.5, obtained from FactSage at 1 atm, indicating the presence of various phases as a function of temperature and mole fraction of H_2O. Light blue points on the diagrams are representative of the starting solutions while black points indicate the TGA evolution of pre-dried powders prepared at 150°C (by drying solutions for 17 h), whereas dashed grey line in (c) is just a rough assumption indicating the loss of water on drying the starting solutions with dark blue points showing the leftover water content after 15 min, 1 h 40 min and 3 h drying at 150°C. Note also that these diagrams were calculated without considering the possibility of crystallization, the corresponding binary diagrams for K-silicates are shown in **Figure A 3.5**.

Evolution of the proton-related species and the extent of foaming observed is expected to be dependent on the stability of different phases in the relevant temperature range. Extensive foaming observed in Na-silicates above 150°C stems from the fact that the system is in the range where the network is in equilibrium with evaporating water as shown by the black points at and above 150°C in **Figure 3.11**(a, b). This means that water can escape rather easily at temperatures as low as around 90°C which is quite close to the boiling point of water. The dehydration in K_2O/SiO_2=0.29 is somewhat similar to Na-silicates above 150°C but the pre-drying step at 150°C, on viewing from the phase diagram in **Figure 3.11**(c), implies the system to be in a state where the thermodynamic stability of free water may be higher than that observed for Na-silicates suggesting it to be more hygroscopic in terms of rheological aspects and thus might influence the foaming behavior. K_2O/SiO_2=0.5 (very hygroscopic), in contrast, has a broad temperature range

100-300°C within which 'Liquid + Hydrated Amorphous + Vapor' co-exist as shown in **Figure 3.11**(d) indicating that the pre-dried powder at 150°C may not be a xerogel, or a dried gel, and the extent of foaming is reduced as compared to Na-silicates due to the relatively stable nature of proton-related species. The system being extremely hygroscopic, thus, is also one of the reasons for the very high amount of retained water in pre-dried K_2O/SiO_2=0.5 i.e. 12.6% as compared to 7.4% observed in K_2O/SiO_2=0.29.

Differences in the foaming/thermal behavior of alkali silicates can further be linked to the network mobility that seems to be limited in the case of K and Li-silicates with the formation of crystallites corresponding to $KHSi_2O_5$ observed in K_2O/SiO_2=0.29[9,21] ($KHSiO_3$ may be observed in K_2O/SiO_2=0.5 depending upon the drying time) while Li_2SiO_3 and $Li_2Si_2O_5$ being the crystalline components in the case of Li-silicates[93,95–98,122,123] explained in detail in the upcoming sections. Furthermore, the Li-silicate compositions studied here lie in the phase separation regime of the binary phase diagram for glasses[93,98,99,124] also suggesting the network to be relatively less mobile due to the formation of a phase with pure SiO_2 network that may well be contributing to the absence of any intumescence.

Globally speaking (and as will be discussed macroscopically in Chapter 4), Na-silicates show extensive foaming, K-silicates may or may not foam depending upon whether the system is crystallized, while Li-silicates do not foam due to the possibilities of phase separation and crystallization. This thermal evolution of alkali silicates is linked to the release of water from the system. TGA evolution suggests the existence of an onset of mass loss in all the alkali silicates with higher alkali content silicate showing a lower onset temperature of mass loss. Na-silicates exhibit a single E_a value approaching 30 kJ.mol^{-1}, irrespective of the Na_2O/SiO_2 molar ratio, linked to the release of solvating water molecules and silanols. Multiple E_a values are observed in the case of K and Li-silicates due to the possibility of having several mechanisms involving crystallization. The ability of a material to release water, crystallize or even phase separate is expected to influence directly the microscopic state of the material in terms of the network organization that would globally impact the foaming-related properties.

These measurements give us a global picture of how water evolves in alkali silicate powders with temperature once the free water has been mostly removed. For a microscopic view of the structure of the material, and in particular the distribution of water between solvated water and silanols, it is important to investigate structural evolution using spectroscopic measurements. And in order to establish the role crystallization plays in reducing or completely suppressing intumescence/foaming, a thorough quantitative structural investigation is required for understanding how the structural mobility may be limited on thermal evolution in the case of K and Li-silicates.

3.3.2. Structural properties

The structure of alkali silicate solutions has been investigated quantitatively by liquid-state NMR as discussed in **section 3.1**. Their spectra exhibit multiple peaks indicative of the coexistence of different Q^n species, where n represents the number of bridging or bonded oxygens (BOs) in the silica network while the other oxygens are referred to as non-bridging or non-bonding oxygens (NBOs).

3.3.2.1. Evolution of structure with temperature

Heating alkali silicate solutions leads to microscopic structural changes along with changes at the macroscopic scale. Evolution of structural properties with temperature was studied on powders by solid-state ^{29}Si MAS-NMR in terms of the evolution of Q^n units (note that the repetition delay is enough to be quantitative as confirmed by measurements shown in **Figure A 3.3** in the appendix). Broad peaks are observed due to the glassy character of the silicates i.e. broad distribution of chemical shifts due to various chemical environments in the structure. These broad bands can be deconvoluted into individual Q^n units by using a Gaussian function through Dmfit software[111] as shown in **Figure 3.12** for Na-silicates. The deconvolution error is estimated to be a few percent for the different units.

(a) Na-silicates

Solid-state ^{29}Si NMR spectra for Na-silicate powders obtained by drying solutions at different temperature is shown in **Figure 3.12**. Q^2, Q^3 and Q^4 are the only species observed for Na_2O/SiO_2=0.29 powders with a variation in the relative proportion of each on increasing temperature. Network polymerization occurs on heating as indicated by the increase of Q^4 along with the decrease of Q^2 as shown in **Figure 3.12**(a). Q^2 vanishes at 400°C while the amount of Q^4 increases from 25% at 150°C to 39% at 400°C indicating an increase in the network connectivity. A similar trend is observed in the system with higher Na content (Na_2O/SiO_2=0.5) as shown in **Figure 3.12**(b). Higher Q^2 fraction is measured for higher Na content in the initial solution due to an already depolymerized network. Q^1, Q^2 and Q^3 units represent the majority species up to 350°C, whereas a small Q^4 contribution (7%) appears at 400°C. Q^1 vanishes at 275°C while a decrease from 33% at 150°C to 9% at 450°C is observed for Q^2 indicating network polymerization. Q^3 is observed to increase until 350°C while the appearance of Q^4 is observed at 400°C. This polymerization of the network is a result of the condensation reaction of silanols present in the network as NBOs. A detailed analysis on the role of free water, solvating water and silanols is given later on.

The structure in terms of the relative fraction of Q^n units of these xerogels after heating to 400°C indicates a structural arrangement very similar to that found in the corresponding glasses prepared by melt and quench process as shown in **Figure 3.12**(c) and (d). The evolution of Q^n fractions with temperature for the two molar ratios and corresponding fraction of Q^n units for glasses is compared in **Figure 3.12**(d). Q^2 and Q^4 follow a similar trend for the two molar ratios while a relatively different behavior is observed for Q^3. The fraction of Q^3 does not change much for Na_2O/SiO_2=0.29 on increasing temperature suggesting it to be relatively independent of the polymerization reaction. For Na_2O/SiO_2=0.5, Q^2 converts into Q^3 until 350°C followed by the

formation of Q^4 at 400°C where the fraction of structural units roughly equates to that of the corresponding glasses for both the molar ratios. Interestingly, for a molar ratio of 0.5, the additional structural disorder associated to the Q^3 dismutation reaction (in our case, $2Q^3 \leftrightarrow Q^2+Q^4$, representing the average structure corresponding exactly to Q^3), is the same for the materials prepared from the solution and from the melt and quench protocol. The fact that the structure of the material is close to the one of the melt's is another hint that the material crosses a glass transition and its silicate network is able to rearrange in order to reach equilibrium.

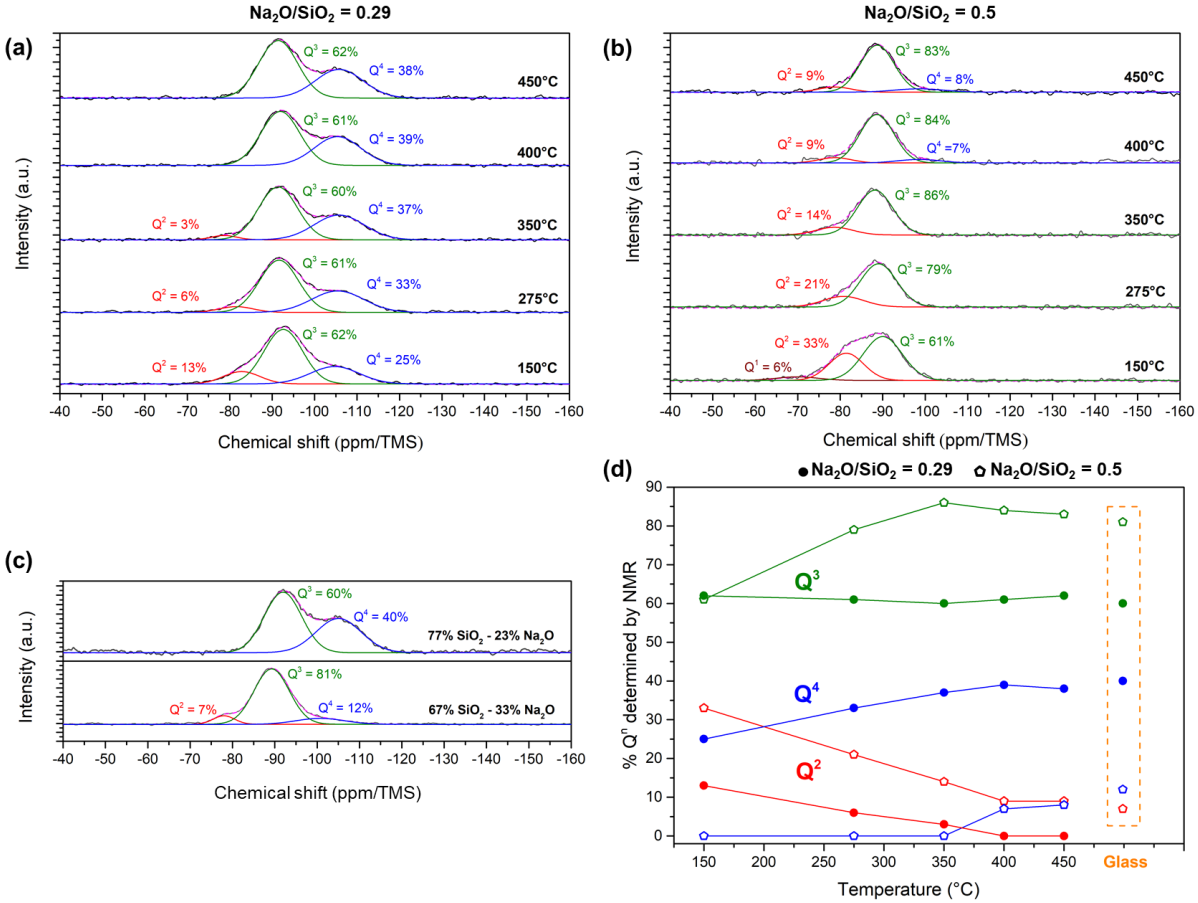

Figure 3.12. Deconvoluted experimental solid-state ^{29}Si MAS-NMR spectra at 8.4 T for Na-silicate powders with a molar ratio (a) Na_2O/SiO_2=0.29 & (b) Na_2O/SiO_2=0.5 and (c) Na-silicate glasses (77% SiO_2 – 23% Na_2O and 67% SiO_2 – 33% Na_2O), together with fitted curves, individual components and their relative fractions, and (d) variation of Q^n fractions with temperature for the two molar ratios (● for Na_2O/SiO_2=0.29 and ✿ for Na_2O/SiO_2=0.5) and points for the corresponding glasses (● for 77% SiO_2 – 23% Na_2O and ✿ for 67% SiO_2 – 33% Na_2O) showing the same fraction of Q^n units at 400/450°C. Deconvolution parameters are given in **Table A 3.1**.

The local structural reorganization of the silicate network can also be determined by Raman spectroscopy which, although being not quantitative, is sensitive to mid-range structural units (e.g. rings) and allows to have a qualitative assessment of the silica network modifications with temperature. **Figure 3.13** shows the Raman response of Na-silicate powder pellets at different temperatures along with the spectrum of glasses corresponding to each molar ratio.

Each spectrum shows two major bands usually observed in sodo-silicates,[14,81,125,126] one corresponding to the bending vibrational mode of Si-O-Si network (centered between 535-550 cm^{-1} for Na_2O/SiO_2=0.29 and 575-590 cm^{-1} for Na_2O/SiO_2=0.5) while the other in the range 825-1250

cm^{-1} is representing the symmetrical stretching vibration of Si-O bonds related to the Q^n units. The small localized contribution centered around 1080 cm^{-1} corresponds to the presence of carbonates that are formed due to high reactivity of Na ions at the surface of the sample. From literature,[126–128] the different Q^n configurations have specific vibrational fingerprints inside the stretching envelope with the contribution of Q^1, Q^2, Q^3 and Q^4 near 850, 920, 1080 and 1140 cm^{-1}, respectively (see **Figure 3.13**). The increase in lower wave number contribution (Q^1, Q^2) with increasing Na content shows the proportion of lower Q^n species to be higher, as observed from the spectra at 150°C and the reference glasses in **Figure 3.13**, due to silica network depolymerization.

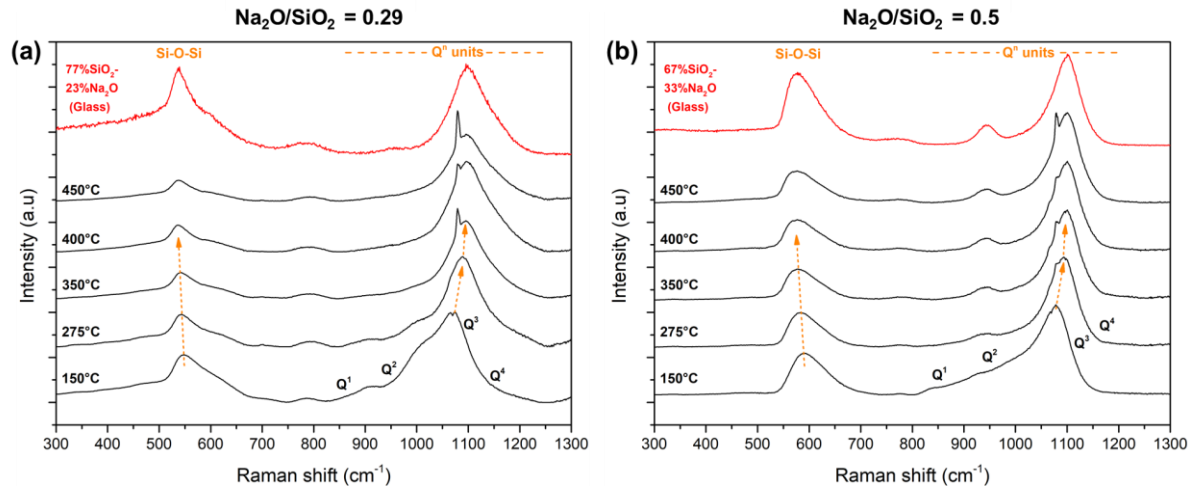

Figure 3.13. Evolution of Raman spectrum (in black) of Na-silicate pellets with temperature for (a) Na_2O/SiO_2=0.29 and (b) Na_2O/SiO_2=0.5. Raman spectra of the corresponding glasses (77% SiO_2 – 23% Na_2O and 67% SiO_2 – 33% Na_2O) are shown by red curves for both the molar ratios. The peak centered at 1080 cm^{-1} (or slight shoulder at 1078 cm^{-1}) is indicative of the presence of carbonates/hydrogen carbonates which are expected to be formed due to the mobility of Na ions and a subsequent reaction with atmospheric CO_2.

The general trend in terms of network polymerization with increasing temperature is the same as observed from ^{29}Si NMR data. A change in the shape of the broad band representing Q^n units is observed for both the molar ratios on going from 150°C to 400°C resulting from the reduction in contribution of lower Q species (Q^1, Q^2) and an increase in the signal from Q^4 indicating a tendency towards more network connectivity on increasing temperature. A slight peak shift is also observed i.e. Q^n band moves from a Raman shift of 1070 cm^{-1} at 150°C to 1097 cm^{-1} at 400°C for Na_2O/SiO_2=0.29 while a shift in position from 1079 cm^{-1} at 150°C to 1100 cm^{-1} at 400°C is observed for Na_2O/SiO_2=0.5, as shown in **Figure 3.13**(a) and (b) respectively.

The intensity of the band centered at lower Raman shift values, attributed to the different Si-O-Si angles or other local configurational variations, is observed to change on changing Na content in the silicate. The different contributions at this band could be due to the existence of different types of bridging oxygens (Q^3-O-Q^3, Q^4-O-Q^4, Q^2-O-Q^3 etc.) or ring configurations.[129,130] Furthermore, network consolidation increases on going from 150°C to 400°C as evident from the left shift in the peak position of Si-O-Si vibration, representative of the variation of Si-O-Si bond angles with temperature. These constraints on bond angles have been reported for Na-silicate glasses[131] where ab-initio calculations showed a variation in the distribution of bond angles on

changing Na content. The spectrum at 400°C for both the molar ratios is very similar to the one obtained for corresponding melt and quench glasses suggesting glass-like structural properties (especially in terms of Q^n units) to have been achieved. Taking the area ratio of the peak at lower Raman shift value to that at higher frequency shows a decreasing trend on increasing temperature indicative of network condensation[132] as shown in **Figure 3.14**. Furthermore, the ratio of peaks is very high for the corresponding reference glasses suggesting the silicate structure for our Na-silicates to be more chain-like than the ring-type observed in glasses. Thus, Raman spectroscopy has provided a complementary understanding of the structural evolution of Na-silicates. At 400°C, the short-range structure (Q^n units) of the xerogel is very close to the one of a melt and quench glass, but at a longer range (at the scale of silica rings), the structure is different, in particular it is less dense.

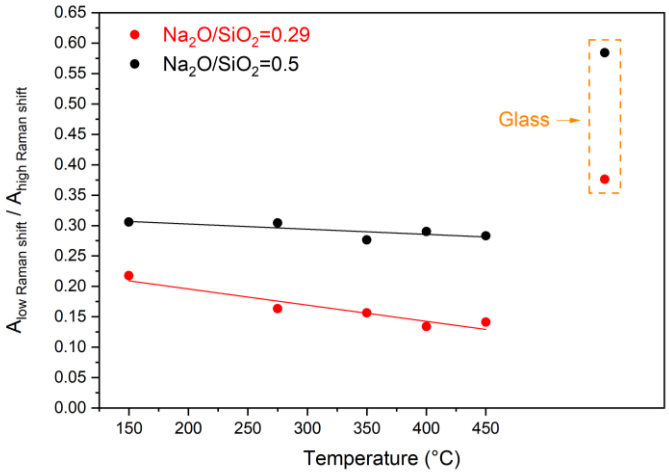

Figure 3.14: Area ratio of Raman peak at lower frequency to higher frequency for Na-silicates and the corresponding reference glass compositions.

The microscopic structural information obtained through solid-state ^{29}Si NMR and Raman spectroscopy suggests an increased polymerization of the Na-silicate network due to condensation of silanols. A xerogel-to-glass conversion is observed at 400/450°C in terms of the Q^n units once the material crosses the foaming regime.

Structural changes at the microscopic scale are also linked to and influenced by the existence and distribution of Na ions and protons in the structure as well as the presence of solvating water. Therefore, it is important to understand the interaction and evolution of these species with the silicate network. Further details of each of these species are discussed in the upcoming sub-sections.

Na distribution within the silicate network

The nature, distribution and specific connectivity of Na in the network was determined by performing ^{23}Na and ^{23}Na/^{29}Si NMR on Na_2O/SiO_2=0.29 powders and 77% SiO_2 – 23% Na_2O reference glass (measurements were performed by Grégory Tricot at LASIR-Université de Lille; 18.8 T field was used for ^{23}Na, 9.4 T for ^{23}Na/^{29}Si). The corresponding spectra are shown in **Figure 3.15**(a). A peak centered at a chemical shift of -2.5 ppm is observed in the ^{23}Na MAS-NMR experiments for the silicate powders at each temperature and glass indicating the environment of

Na to be the same in all the cases. Furthermore, a slight shoulder centered at 10 ppm can also be seen for each temperature and this corresponds to the presence of carbonates. Also, we did not find a signature of NaOH (generally a sharp intense signal close to 0 ppm), meaning that all sodium ions belong to the silicate network. Information about the distribution was given by the 1D Cross-Polarization (CP) NMR spectrum between ^{29}Si and ^{23}Na (**Figure 3.15**(b)). This spectrum shows only the signature of silicate species experiencing a very close spatial proximity to Na ions. In other words, the spectrum in **Figure 3.15**(b) shows the silicate units involved in Si-O^{-} $^{+}$Na linkages. Therefore, the presence of Q^3, Q^2 and Q^1 signals in the CP spectrum indicates that Na ions are homogeneously distributed within the silicate network. This suggests that Na is connected to both Q^2 and Q^3 for Na_2O/SiO_2=0.29 and Q^1, Q^2 and Q^3 for Na_2O/SiO_2=0.5, respectively.

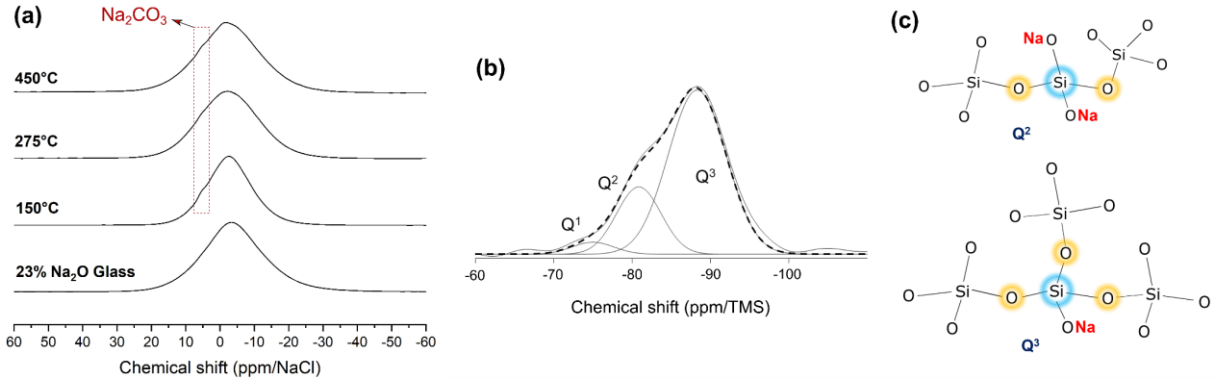

Figure 3.15. Solid-state (a) ^{23}Na NMR spectra at 18.8 T for Na-silicate powder with Na_2O/SiO_2=0.29 and the corresponding glass, (b) ^{29}Si (^{23}Na) Cross-Polarization (CP) NMR spectrum at 9.4 T for the powder with Na_2O/SiO_2=0.5 at 150°C and (c) the corresponding connectivity of Na in the network for Na_2O/SiO_2=0.29.

Evolution of water/silanols

Apart from the structural/network changes in terms of Q^n units, another important aspect to be considered is the evolution of solvating water and silanols. After the removal of free water around the boiling temperature, the network is mainly composed of solvating water (water molecules H-bonded to the network or due to some dipole-dipole interactions) and silanols. **Figure 3.16**(a) shows the ^{1}H NMR spectra for Na_2O/SiO_2=0.29 powders and 77% SiO_2 – 23% Na_2O reference glass. Multiple bands can be seen in all the spectra, especially for the Na-silicate powder at 150°C and 275°C indicating the presence of multiple proton-related species. The band in the range of chemical shift 3-8 ppm, in case of silica, corresponds to silanols[133–135] with possible multiple configurations as well as adsorbed or solvating water molecules.[134,136,137] Hydrous Na-silicate glasses have been reported to have a characteristic connectivity of proton-related species in the network[86,138–140] very similar to the one shown in **Figure 3.16**(a) and (d). Isolated silanols and those solvated by water molecules appear to be centered around 3.9 ppm and 5.7 ppm, respectively. The origin of the band from 8 to 17 ppm is representative of water molecules solvating Na ions (or NaOH) and long-range SiOH-O^{-} H-bonding. Long range H-bonding has been proposed to be a consequence of inter-lamellar interaction, especially in the case of Kanemite ($NaHSi_2O_5.3H_2O$) where the structure is composed of consecutive sheets of SiO_2 tetrahedra arranged in the form of rings.[141,142] This might be representative of inter-silanol interaction in our case as we do not expect our Na-silicates to be composed of a lamellar arrangement.

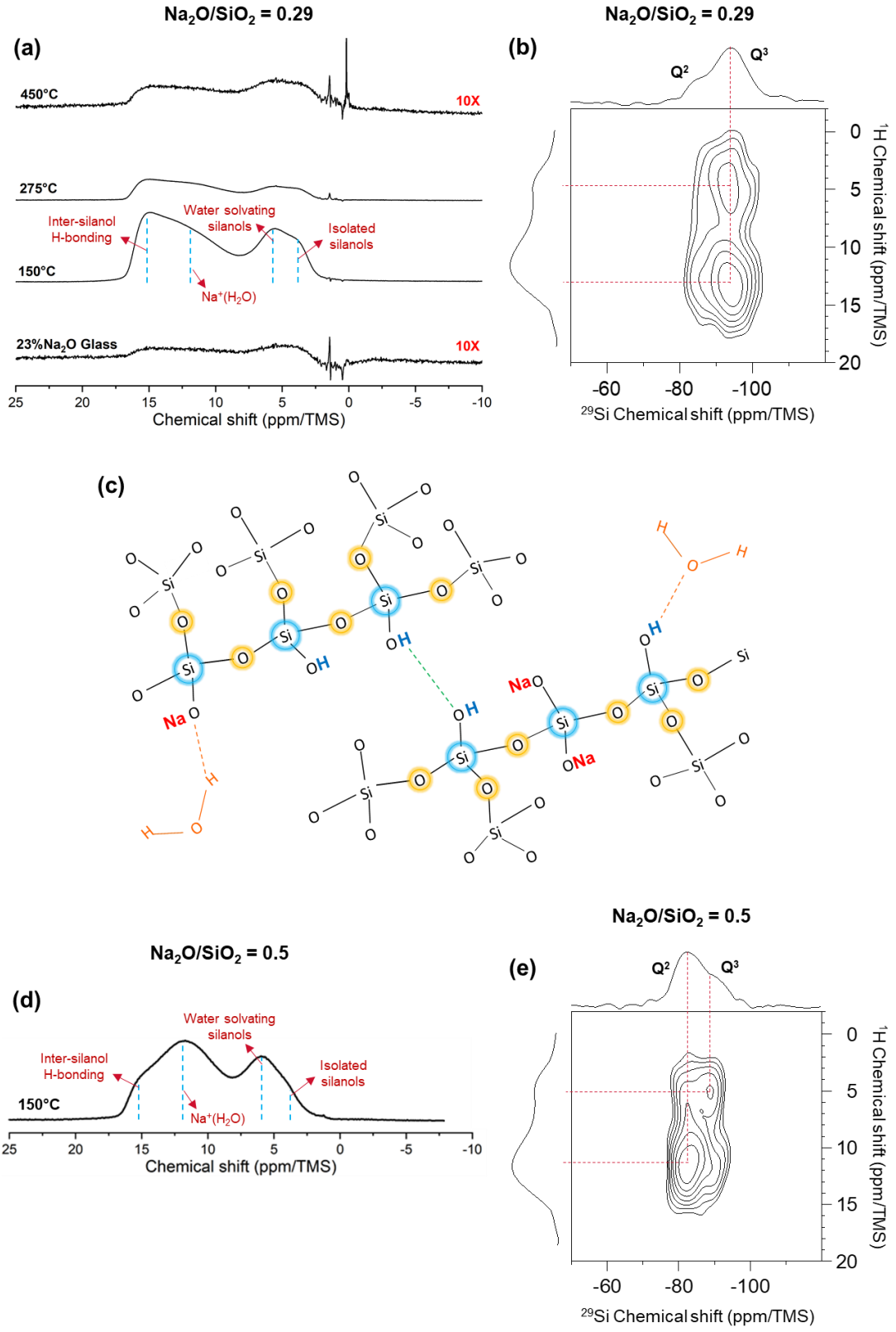

Figure 3.16. Solid-state (a) ^{1}H NMR spectra at 18.8 T for Na-silicate (Na_2O/SiO_2=0.29) powder and the corresponding reference glass (band assignment according to literature[86,139,140]), (b) 2D ^{29}Si (^{1}H) CP-HETCOR NMR spectrum at 9.4 T for the powder with Na_2O/SiO_2=0.29 at 150°C, (c) connectivity of H in the network for Na_2O/SiO_2=0.29 at 150°C, (d) Solid-state ^{1}H NMR spectra at 18.8 T for Na_2O/SiO_2=0.5 powder at 150°C and the corresponding (d) 2D ^{29}Si (^{1}H) CP-HETCOR NMR spectrum at 9.4 T. The peaks between 0-2 ppm in (a) correspond to signal of the probe.

The detected species in our case are linked to mainly Q^3 as shown by the 2D ^{29}Si (^1H) CP-HETCOR NMR spectrum for Na_2O/SiO_2=0.29 in **Figure 3.16**(b) suggesting the structure to be composed of silanols and solvating water, with some inter-silanol H-bonding (see **Figure 3.16**(c)). The fraction of each proton-related specie is reduced on thermal evolution until a proportion quite similar to the reference glass is obtained. Thus, the initial hypothesis that the silicate is converting into hydrated metastable melts (in terms of structural properties) seems to be further cemented with the removal of solvating water and silanols, and the connectivity of protons to the network.

^1H NMR spectrum for Na_2O/SiO_2=0.5 in **Figure 3.16**(d) shows the existence of isolated silanols, solvating water molecules and inter-silanol interaction as that observed in Na_2O/SiO_2=0.29, however, the quantities of each specie tend to vary slightly as a function of Na concentration with an increase in the relative proportion of solvating water molecules as well as silanols observed for Na_2O/SiO_2=0.5. 2D ^{29}Si (^1H) CP-HETCOR NMR spectrum of Na_2O/SiO_2=0.5 at 150°C shown in **Figure 3.16**(e) indicates the presence of both Q^2 and Q^3 connectivity for silanols. This may be indicative of the fact that the amount of silanols is higher when the concentration of Na is increased leading to a lower softening temperature and higher volumetric expansion in terms of foaming. Thus, a chain-like structural arrangement is also predictable for Na_2O/SiO_2=0.5 that is expected to evolve as a function of temperature and have an impact on the thermal behavior.

Figure 3.17 shows the overall schematic illustration of the existence of solvating water and silanols in terms of the variation of NBOs with temperature for Na_2O/SiO_2=0.29. The red curve represents potentially available network modifiers obtained from the same TGA data shown in **Figure 3.8**(a), assuming that all the proton-related species as well as alkali ions in the system are a part of the actual network, and calculated from eq. 3.6 as:

$$\frac{Network\ Modifiers}{Si} = \frac{nNa}{nSi} + \frac{nOH}{nSi} \tag{3.6}$$

where 'n' represents the number of moles.

The black curve in **Figure 3.17** represents NBOs calculated from the NMR data shown in **Figure 3.12**(a) using the eq. 3.7 given as:

$$\frac{NBOs}{Tetrahedra} = 4Q^0 + 3Q^1 + 2Q^2 + Q^3 \tag{3.7}$$

where Q^0 is multiplied by a factor of 4 because it has four NBOs per tetrahedron, Q^1 has three and so on. The relative amount of Na as NBOs is shown in blue and remains constant with temperature[143] (assuming that all Na ions are acting as network modifiers). For Na_2O/SiO_2=0.29, using the NMR results that all the protons in silanol units are linked to Q^3, eq. (3.7) implies that 45% of Na ions are connected to Q^2 and 55% to Q^3 (i.e. 48% Q^3 sites are occupied by protons and the remaining 52% by Na).[144–147]

Initial silicate solution at room temperature is composed of free water, solvating water and silanols that act as NBOs as shown by the region 'a' in **Figure 3.17**. Region 'b' represents the difference between TGA and NMR NBOs and corresponds to solvating water that is still present

(though in very small amount) at 400°C. Silanols in the network are represented by the region 'c' which is the difference in NMR and Na as NBOs. Their amount is less than half of the solvating water at 150°C but the ratio between silanols and solvating water increases with temperature, consistent with results on the speciation of water obtained in the geochemistry community.[118,119] Fully condensed state is shown by the region 'd' where there are no more solvating water molecules or silanols in the network and all the NBOs correspond to the presence of Na linked to Q^3 unit only.

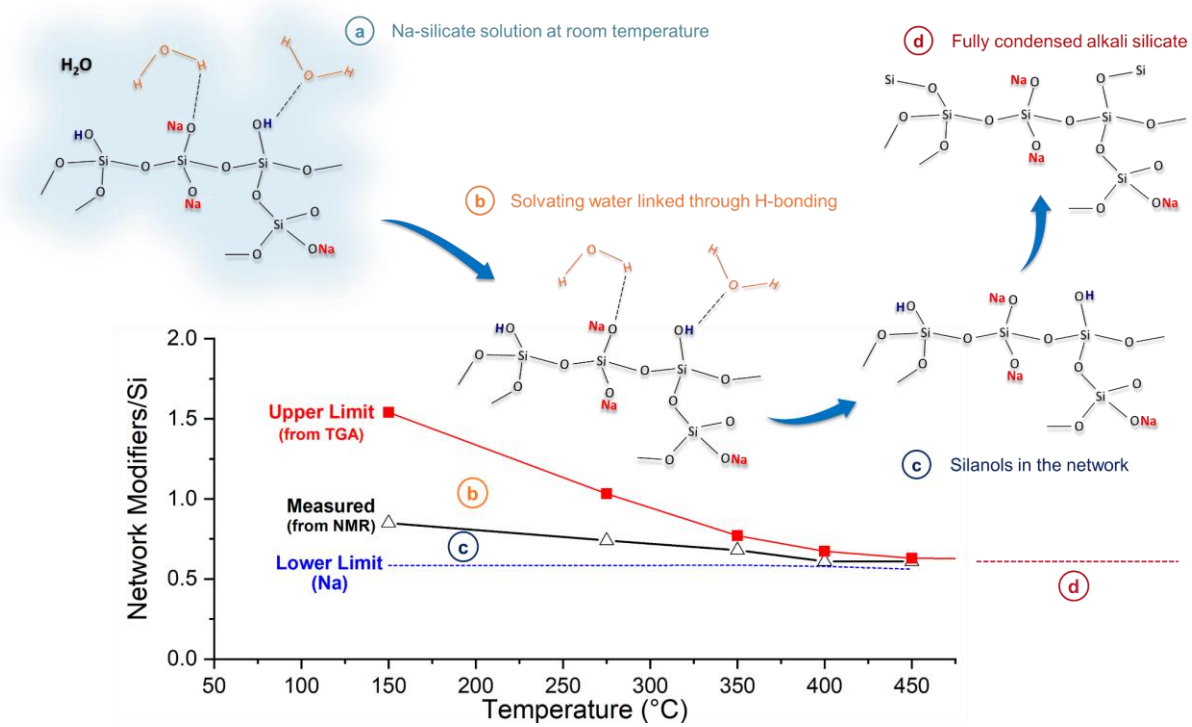

Figure 3.17. Total Network Modifiers/Si from both (■) TGA and (△) solid-state ^{29}Si NMR spectra of Na-silicate (Na_2O/SiO_2=0.29) powder with region 'b' corresponding to the amount of adsorbed/solvating water linked to the network, 'c' corresponding to the relative proportion of OH as NBO and 'd' referring to a completely condensed state at temperatures well above 800°C.

Interestingly, there seems to be some kind of a proportionality between Si-OH and solvating H_2O molecules suggesting a possible existence of an equilibrium between the two species that is proposed to be a consequence of the following reaction:

$$2SiOH \rightleftharpoons SiOSi + H_2O_{solv/ads} \rightleftharpoons Si - O - Si + H_2O_{atm} \quad (3.8)$$

The existence of such an equilibrium indicates that silanols, after all, may not be resulting in the direct evaporation of water on condensation rather they seem to be converting into water molecules that tend to behave as solvating species followed by their release into the atmosphere. Thus, the existence of a single E_a for Na-silicates (as discussed in section **3.3.1.1**) appears to be a consequence of this equilibrium.

The molar ratio Na_2O/SiO_2 is expected to directly influence the amount of silanols in the network. Higher Na concentration in the network has been found to result in higher amount of silanols as NBOs.[148] This suggests the network to possess more H as NBOs for Na_2O/SiO_2=0.5 as

also evident from the comparison shown in **Figure 3.16**(a) and (d) and **Figure 3.18**. The correlation between the concentration of sodium ions and silanol units suggests an equilibrium between sodium and protons in network-modifier sites of the silicate network. The trend is same for both the molar ratios with the existence of all the regions mentioned in **Figure 3.17**, the only major difference being the amount of Na in the initial silicate. Na and H ions acting as network modifiers or NBOs are influencing the overall structural properties. The amount of calculated NBOs is less for the Na_2O/SiO_2=0.29 silicate due to the structure being in a more condensed state than Na_2O/SiO_2=0.5.

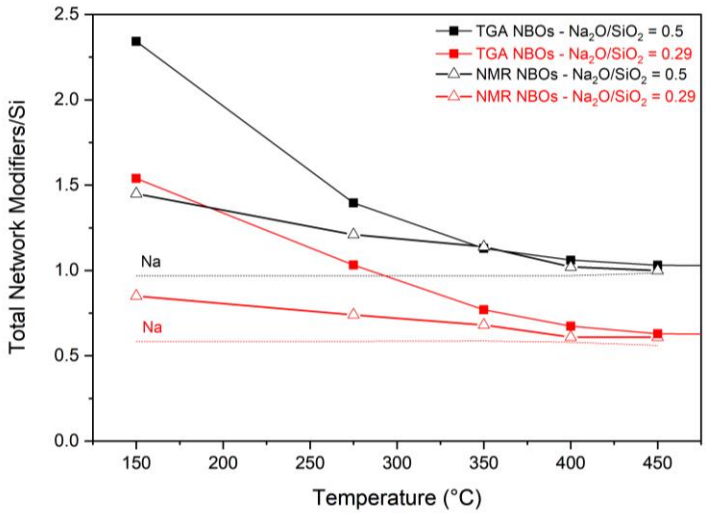

Figure 3.18: Total Network Modifiers/Si for the two Na-silicate molar ratios with the corresponding amount of Na in the network for each represented by the dotted line.

The removal of solvating water and silanols has a direct influence not only on the degree of densification or polymerization but also the extent of volumetric expansion of Na-silicates observed visually upon foaming. Though the structural properties start corresponding to glasses at around 400°C where most of the solvating water and silanols have been removed, experimental evaluation (grinding using mortar and pestle) suggests the existence of a much softer material as compared to glass, probably because of the presence of protons as network modifiers when compared to the dry glass. Apart from the evolution of Q^n units and NBOs, revisiting the macroscopic evolution of Na-silicates from a visual perspective is, therefore, also necessary to understand how the material might behave in different industrial applications especially those related to fire retardance. Hence, the next chapter (**Chapter 4**) is devoted to a detailed description of what happens macroscopically upon heating a liquid droplet or a pre-dried powder.

In general, extensive foaming has been observed for Na-silicates due to the rapid dehydration behavior and the corresponding aforementioned structural changes. It has been shown that, indeed, silanols are responsible for the volumetric expansion of the material. The existence of a single E_a for Na-silicates is due to the equilibrium evolution between silanols and solvating water molecules. This suggests condensation to be the main mechanism on thermal treatment and the driving force for foaming, hinting towards a mobile enough microscopic network of the material. Changing the molar ratio i.e. increasing the concentration of Na in the system allows

for a higher volumetric expansion due to a reduced T_g and increased mobility which are also a consequence of an enhanced quantity of silanols.

Changes to the microscopic network are induced on changing the concentration of Na-silicate as well as the thermal history. Furthermore, not only is the molar ratio expected to induce structural changes, but also the type of alkali silicate may impact the thermal behavior. Changing the type of alkali ion may influence directly the microscopic state of the network impacting strongly the thermal evolution. TGA measurements on K and Li-silicates shown in **Figure 3.9** show the existence of multiple E_a values. This might be attributed to structural modifications different than those observed in Na-silicates, and is discussed in details in the upcoming section in terms of the microscopic structural changes on thermal evolution of K and Li-silicates. An in-depth quantitative analysis is presented along with a comparison for the evolution of various species for all the alkali silicates studied.

(b) K and Li-silicates

The network organization in K and Li-silicates is also expected to change as a consequence of changing water content that is expected to give a concrete information on the link between the state of the network and macroscopic evolution in terms of foaming behavior. **Figure 3.19** shows the behavior of K-silicates in terms of the Q^n units calculated from Solid-state ^{29}Si NMR. As in Na-silicates, broad bands can be seen due to the glassy nature of the samples, which have to be deconvoluted to extract quantitative information on the relative distribution of various species. These broad bands indicate the presence of broad peaks representative of the amorphous content as well as sharp peaks shown in orange (see **Figure 3.19**(a, b)) resulting from the fact that the samples have crystallized. For both the K-silicate molar ratios, the system globally tends to move towards a more polymerized state evident from the fact that the fraction of Q^4 in the system increases with temperature.

At 150°C (pre-dried powder obtained through a drying step of 17 h), K_2O/SiO_2=0.29 is already crystallized evident from the appearance of two crystalline polymorphs of $KHSi_2O_5$, namely, monoclinic denoted by Q^3_{cM} with a fraction of 45% while orthorhombic by Q^3_{cO} contributing 15% to the total sum. On increasing the temperature, a variation in the contribution of these polymorphs is observed i.e. the orthorhombic crystalline phase increases while monoclinic reduces and melting of the crystalline phases is seen at 450°C where the crystalline peaks are no more visible (also confirmed from XRD discussed later in **Figure 3.21**(a)) . Globally, Q^3 tends to reduce while Q^4 increases suggesting network polymerization as a function of temperature.

K_2O/SiO_2=0.5 shows a tendency towards network polymerization as a function of thermal treatment and a behavior quite similar to that observed for Na-silicates. Crystallization is not observed at 150°C for a 17 h-long drying step, however, the powder doesn't really seem to be a xerogel due to the extremely hygroscopic nature as also evident from the phase diagram in **Figure 3.11**(d). The solid-state ^{29}Si NMR for this powder is shown in **Figure A 3.6**(a) that indicates the presence of all the Q^n units due to the hygroscopic nature as well as issues with the rotation inside the rotor used for NMR measurements. Thus, the solution was pre-dried at 150°C for 1 week,

whereby, it presented crystallization with the formation of orthorhombic $KHSiO_3$ crystalline phase contributing 23% to the total fraction of Q^n units (**Figure A 3.6**(b)). Globally, the quantity of Q^3 increases from 46% to ~90% at the expense of the condensation seen for Q^2 units on increasing temperature up to 450°C where 8% of Q^4 is also observed as shown in **Figure 3.19**(b) and (c).

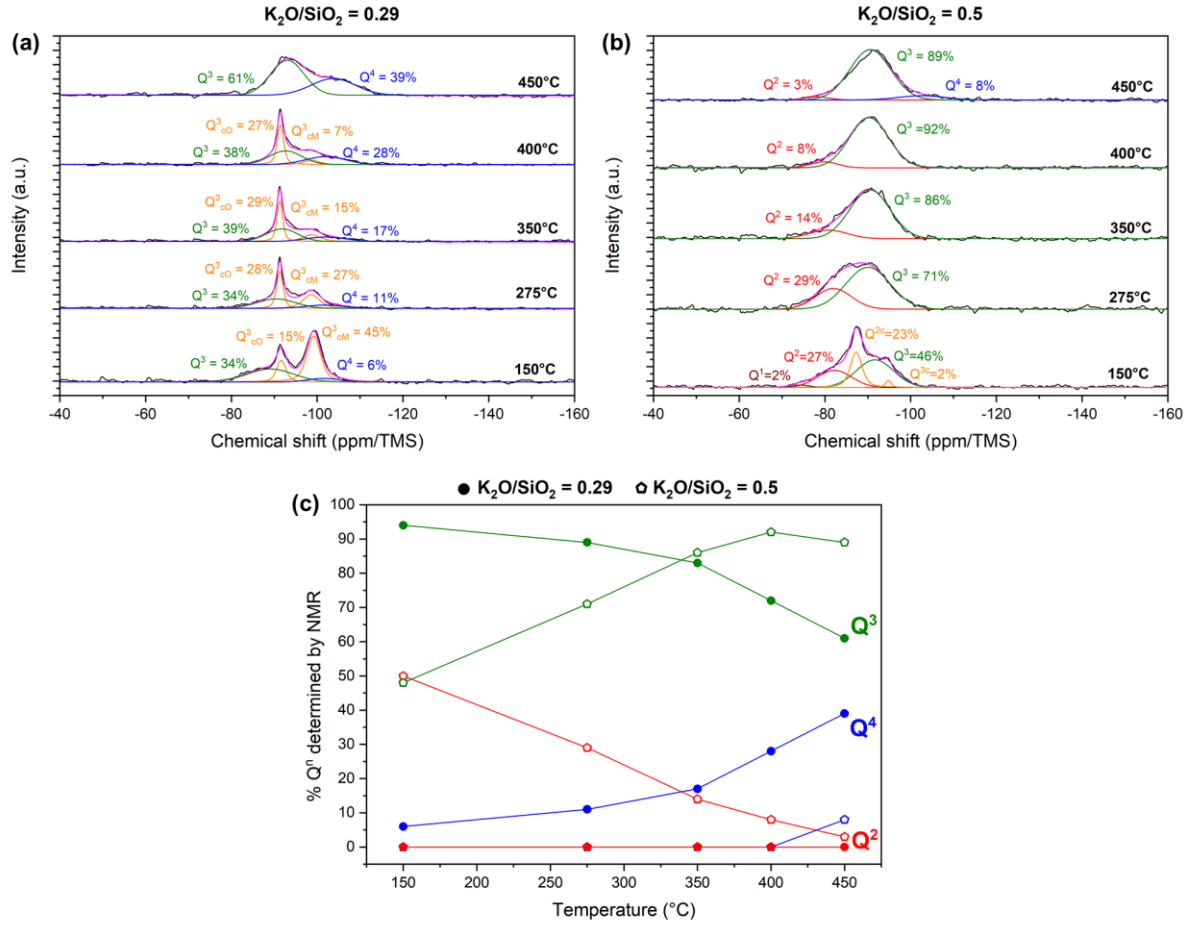

Figure 3.19: Evolution of Q^n units for (a) K_2O/SiO_2=0.29 & (b) K_2O/SiO_2=0.5 powders dried at different temperatures determined from ^{29}Si solid-state NMR spectroscopy at 8.4 T (note that the sharp deconvoluted peaks in orange in (a) represent crystalline phases i.e. Q^3_{cO} for orthorhombic $KHSi_2O_5$ and Q^3_{cM} for monoclinic $KHSi_2O_5$ while those in (b) at 150°C correspond to $KHSiO_3$ as given in **Figure A 3.6**) and (c) comparison of Q^n units evolution for the two molar ratios of K-silicates with '●' representing the molar ratio of 0.29 while '✿' for K_2O/SiO_2=0.5, respectively.[149] Deconvolution parameters are given in **Table A 3.1** in appendix.

Li-silicates show a completely amorphous behavior at 150°C (**Figure 3.20**) with a similar distribution of Q^n units for both the molar ratios suggesting the network to have not changed much on increasing the concentration of Li. Crystalline peaks appear at 275°C and above (as shown later in **Figure 3.21**(b) and (c)) – Q^2_c representing Li_2SiO_3 while Q^3_c indicating the presence of $Li_2Si_2O_5$ observed also in binary Li-silicate glasses with the same composition.[94] Crystallization of the system increases as a function of temperature for both the molar ratios suggesting the existence of the disproportionation reaction: $2Q^3(glassy) \leftrightarrow Q^2(crystalline) + Q^4(glassy)$. Globally, as observed in case of Na and K-silicates, the system tends to evolve towards a more condensed state with Q^4 approaching 60% contribution until 350°C (in both cases) above which it does not change much for Li_2O/SiO_2=0.4. Melting of the crystalline phase is observed for Li_2O/SiO_2=0.4 at 450°C, reducing the Q^4 contribution to 25%, similar to what has been reported for glasses at very

high temperatures (800°C)[94] suggesting a behavior relatively similar to binary glasses, though not a lot of information is available on such glass systems with added water content. A comparison on the evolution of Q^n units for Li-silicates is given in **Figure 3.20**.

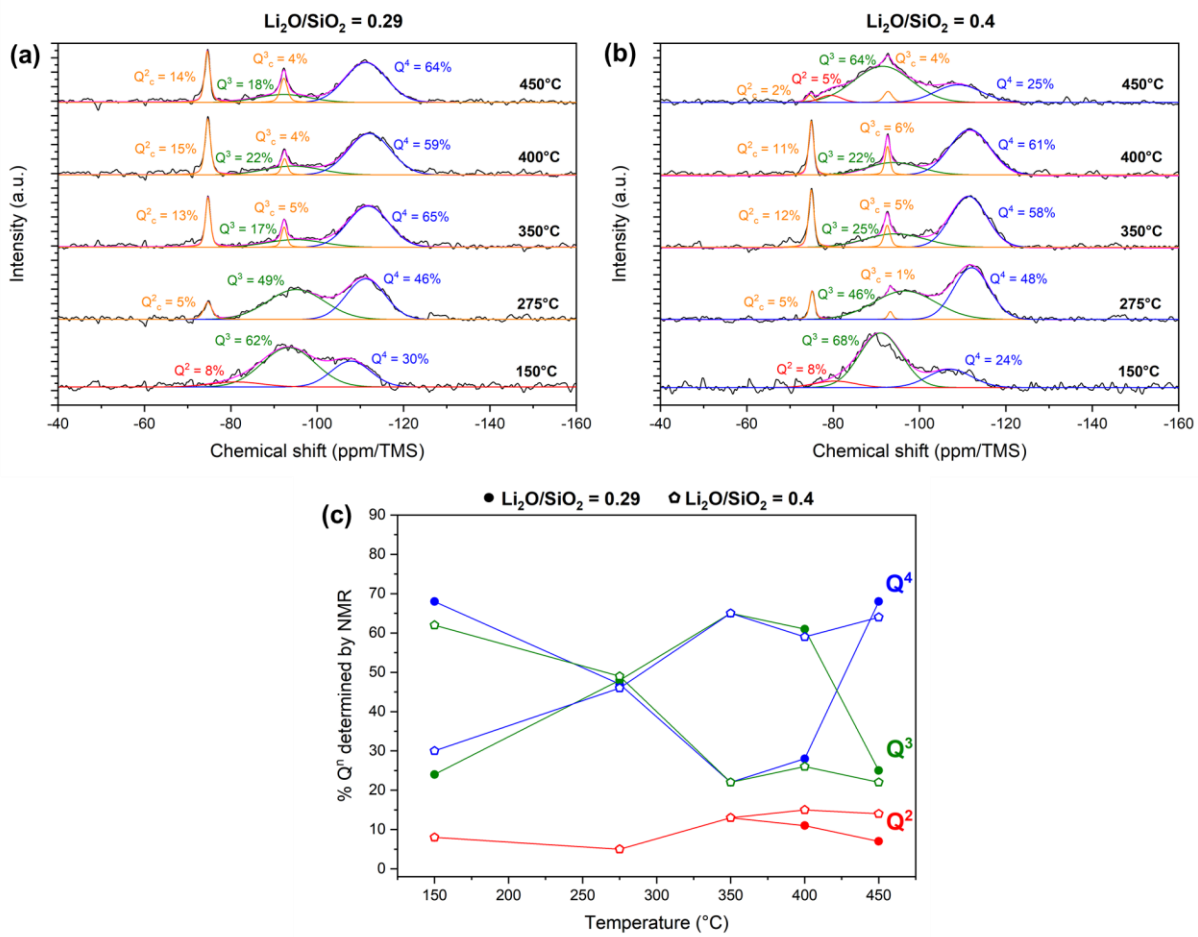

Figure 3.20: Evolution of Q^n units for (a) Li_2O/SiO_2=0.29 & (b) Li_2O/SiO_2=0.4 powders dried at different temperatures determined from ^{29}Si solid-state NMR spectroscopy at 8.4 T (note that the sharp deconvoluted peaks in orange represent crystalline phases i.e. Q^2_c for orthorhombic Li_2SiO_3 and Q^3_c for orthorhombic $Li_2Si_2O_5$ phase in Li-silicates) and (c) comparison of Q^n units evolution for the two molar ratios of Li-silicates with '●' representing the molar ratio of 0.29 while '✿' for Li_2O/SiO_2=0.4, respectively. Deconvolution parameters are given in **Table A 3.1** in appendix

In essence, Na, K and Li-silicates all tend to show structural changes on thermal treatments. Polymerization of the network is observed in all the cases as a consequence of condensation of silanols. However, the existence of crystallization in both K and Li-silicates does also seem to influence the microstructure of the systems, rendering the network relatively less mobile and impacting the way the silicates behave macroscopically in terms of intumescence. ^{29}Si solid-state NMR has, thus, given us a more in-depth information on how the network is behaving in terms of its mobility suggesting a relatively rigid and polymerized network depending upon the composition. Further quantification is, however, required to probe the state of the K and Li-silicates' network in terms of both the evolution of proton-related species and the exact impact of crystallization for being able to compare the foaming behavior with Na-silicates.

Crystallization behavior

To further investigate the crystallization behavior of K and Li-silicates for establishing a quantitative understanding, diffractograms were obtained from powder XRD measurements shown in **Figure 3.21**. The patterns for K_2O/SiO_2=0.29 suggest the existence of a combination of amorphous and crystalline character as represented in **Figure 3.21**(a) and also evident from the ^{29}Si NMR discussed previously. Two different polymorphs exist i.e. monoclinic and orthorhombic $KHSi_2O_5$.[9,21] The XRD patterns have been deconvoluted (using Rietveld refinement approach) to extract quantitative information on the exact amount of crystalline and amorphous phases that has been further utilized to probe the quantity of alkali in the amorphous and crystalline phases, respectively. The degree of crystallinity (DOC)[150] given as:

$$DOC = \frac{Crystalline\ (wt\%)}{Amorphous\ (wt\%)\ +\ Crystalline\ (wt\%)} \tag{3.9}$$

remains roughly 60% at 150°C and 275°C for K_2O/SiO_2=0.29 while an increase to 80% is observed at 350°C and 400°C. This behavior seems to be consistent with the plots in **Figure 3.9**(c) where the values of E_a tend to change above 330°C suggesting a direct link between the crystallization behavior and mass loss evolution. Details of the fitting parameters and the relative quantities of the crystalline and amorphous phases are given in **Table A 3.2**.

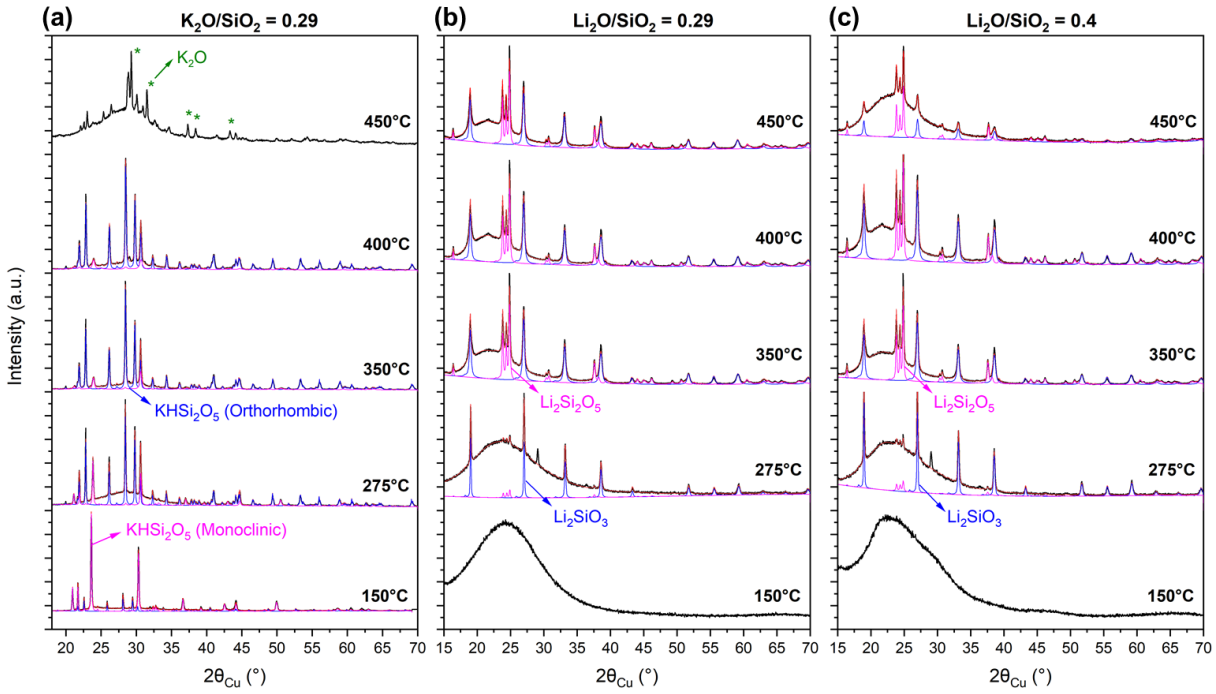

Figure 3.21: XRD data showing a combination of amorphous and crystalline phases in (a) K_2O/SiO_2=0.29 with two polymorphs of $KHSi_2O_5$ and (b) Li_2O/SiO_2=0.29 & (c) Li_2O/SiO_2=0.4 indicating the presence of crystalline orthorhombic Li_2SiO_3 and $Li_2Si_2O_5$. Deconvolution of the peaks allows for quantification of the different phases/species through Rietveld refinement method. Detailed parameters of this quantification are listed in **Table A 3.2** and **Table A 3.3**.

The contribution from monoclinic $KHSi_2O_5$ decreases as a function of temperature while the orthorhombic phase increases until partial melting of the crystalline phases along with the appearance of crystalline K_2O is observed at 450°C. Quantification hasn't been done for the

powder at 450°C due to a lack of availability of the crystallographic information file for various phases present at that particular temperature. K_2O/SiO_2=0.5, in contrast, doesn't readily crystallize at the drying times (at 150°C) used for this study (17 h) rather longer durations tend to favor crystallization with the formation of orthorhombic $KHSiO_3$ phase as shown in **Figure A 3.6**(b).

Li-silicates are amorphous at 150°C and show both crystalline and amorphous character at and above 275°C as shown in **Figure 3.21**(b) and (c) for Li_2O/SiO_2=0.29 and Li_2O/SiO_2=0.4, respectively. Two different crystalline phases, orthorhombic Li_2SiO_3 and $Li_2Si_2O_5$, are observed with a tendency towards increasing disilicate character suggesting the existence of the reaction: $Li_2SiO_3 + SiO_2 \rightarrow Li_2Si_2O_5$. The DOC increases from roughly 8% at 275°C to 50% at 450°C for Li_2O/SiO_2=0.29 while an increase in the crystalline character up to 400°C followed by a decrease due to partial melting of the crystalline phases is observed for Li_2O/SiO_2=0.4 (see **Figure 3.21**(c)). Here again, the fact that DOC remains in the range of 50% from 350°C to 450°C (depending upon the composition), crystallization seems to be directly linked to the existence of multiple and changing E_a values. Therefore, a direct correlation of crystallization seems to be a relatively suppressed macroscopic expansion both in K and Li-silicates (furthermore, phase separation in Li-silicates shouldn't be excluded). Note that the DSC curves shown in **Figure 3.9** are not easily linkable to the crystallization events observed here probably due to limited intensity of the signals in the temperature range of crystallization.

Thus, XRD gives a quantitative measure of the crystallization behavior in K and Li-silicates. These quantified values from the XRD data have allowed to calculate the relative fraction of alkali in the crystalline and amorphous phases at each temperature that may help in predicting the microstructural network evolution on thermal treatment. In order to provide concrete information on the actual evolution of various proton and alkali-related species and their link to the foaming behavior, a combination of TGA, NMR and XRD data has thus been utilized to estimate the quantitative microstructural thermal evolution, in a manner similar to Na-silicates discussed for **Figure 3.17**.

Variation of network modifiers

The starting aqueous alkali silicates, as discussed previously, are composed of large amounts of free water along with solvating water molecules and network silanols. The pre-drying step removes all the free water leaving behind a network containing silanols and H-bonded solvating water. Eq. 3.6 and 3.7 were used to plot the evolution of the various species as Network Modifers/Si for Na-silicates shown in **Figure 3.17**. The same approach has been used here for K and Li-silicates.

From TGA mass loss data (**Figure 3.9**), and assuming that all the proton-related species as well as alkali ions in the system are a part of the actual network, the 'Total Network Modifiers' can be plotted using eq. 3.6 as shown by the red curves in **Figure 3.22** for K-silicates. The concentration of alkali ion, i.e. K, is already known, stays constant[143] and is shown by the blue lines. NMR data provides an exact quantification of the actual number of network modifiers shown in black and computed from eq. 3.7 using the quantification discussed in **Figure 3.19**.

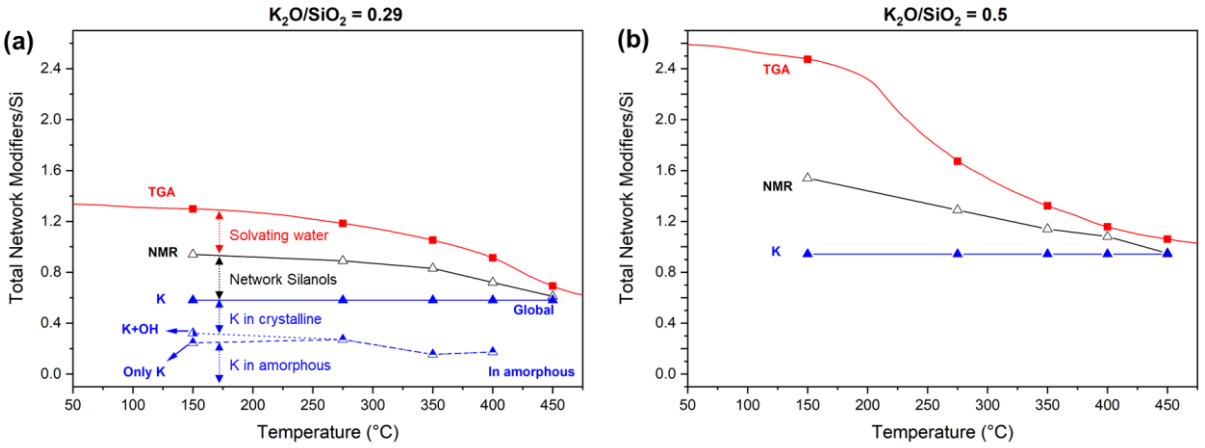

Figure 3.22: Evolution of Total Network Modifiers/Si as a function of temperature for (a) K_2O/SiO_2=0.29 and (b) K_2O/SiO_2=0.5 extracted from a combination of TGA (solid red curve), ^{29}Si solid-state NMR (solid black curve) as well as powder XRD (dotted blue line) data.

Since K_2O/SiO_2=0.29 tends to crystallize on thermal treatment (note that the kinetics of heating may influence the DOC) with the formation of $KHSi_2O_5$ crystallites suggesting that a part of total K ions leaves the amorphous phase, the quantity of alkali in the amorphous and crystalline phases is possible to be plotted from the quantified XRD data shown in **Figure 3.21**. For K_2O/SiO_2=0.29, the dashed blue line (with top filled triangles) in **Figure 3.22**(a) shows the amount of K left in the amorphous phase after the formation of $KHSi_2O_5$ crystallites. The proportion of solvating water is marked with red, network silanols with black while K in crystalline or amorphous phase with blue arrows. It is worth noting that not all the network silanols at 150°C belong to the amorphous phase i.e. only a fraction of the total is linked to the amorphous network while the major chunk represents protons in the crystalline phase. On the contrary, K_2O/SiO_2=0.5 doesn't seem to crystallize (linked to kinetics of drying) as discussed before and, thus, a behavior similar to that for Na-silicates is observed as shown in **Figure 3.22**(b). Note that the system would potentially crystallize on longer drying times, however, that has not been investigated extensively in this work (except for the point at 150°C).

Similar analysis for Li-silicates shown in **Figure 3.23** suggests a slightly different behavior than that observed for Na or K-silicates. The quantity of 'Actual Network Modifiers' from NMR data (given in **Figure 3.20**) seems to cross the dashed blue line, more so for Li_2O/SiO_2=0.4 even at 275°C as compared to the point at 350°C for Li_2O/SiO_2=0.29. This points to the fact that the network may not actually have all the Li as its component, rather some Li may well be in the form of LiOH as also evident from the liquid-state ^{29}Si NMR data in **Figure 3.4**(b) impacting directly the thermal evolution. Furthermore, as discussed for K-silicates, crystallization in Li-silicates resulting in the formation of Li_2SiO_3 and $Li_2Si_2O_5$ leads to the removal of Li ions from the amorphous (network) phase. The dashed blue lines in **Figure 3.23** give the amount of Li remaining in the amorphous phase for both the molar ratios. Amorphous network of Li_2O/SiO_2=0.29 is Li free at 350°C similar to what is seen for Li_2O/SiO_2=0.4 where a minute quantity of Li ions is still intact within the amorphous phase. The increase in the quantity of Li seen for Li_2O/SiO_2=0.4 at 450°C in **Figure 3.23**(b) is a consequence of Q^2 (crystalline) + Q^4 (glassy) ↔ $2Q^3$ (glassy) reaction.

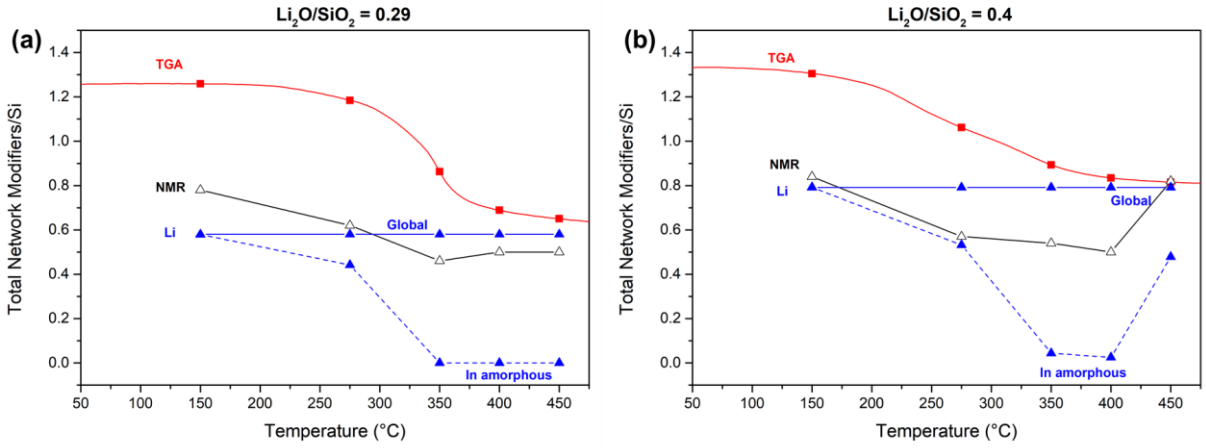

Figure 3.23: Evolution of Total Network Modifiers/Si as a function of temperature for (a) Li_2O/SiO_2=0.29 and (b) Li_2O/SiO_2=0.4 extracted from a combination of TGA (solid red curve), ^{29}Si solid-state NMR (solid black curve) as well as powder XRD (dotted blue line) data.

Hence, the combination of TGA, NMR and XRD data has allowed for following the thermal evolution of K and Li-silicates in terms of quantitative microscopic network-related changes at the scale of NBOs. The mobility of the network appears to be reduced due to crystallization events along with the condensation of silanols. The formation of crystallites causes the alkali ion (and also protons in the case of K-silicates) to leave the amorphous phase rendering the network relatively brittle as compared to Na-silicates where crystallization events don't occur. This is expected to directly influence the macroscopic thermal evolution of the materials. Furthermore, in the case of Li-silicates, presence of LiOH outside the amorphous network is also expected to impact the corresponding mobility. Thus, a quantitative comparison of Na, K and Li silicates is important, and now possible, to distinguish the different compositions at the scale of the actual network in terms of its mobility and the corresponding link to the foaming behavior.

(c) Quantitative comparison of network evolution and the impact on foaming

Figure 3.24 shows the quantitative evolution of the different species present in the system calculated from **Figure 3.18** for Na-silicates, **Figure 3.22** for K-silicates and **Figure 3.23** for Li-silicates to compare the overall evolution and its impact on the structural properties in terms of the alkali silicate composition and type of alkali ion. Evolution of solvating water is shown by green, silanols in the amorphous phase by purple, silanols in the crystalline phase by yellow and the amount of alkali remaining in the amorphous phase by orange bars. The red dotted line indicates the initial quantity of alkali ions in the systems.

Na-silicates

For Na_2O/SiO_2=0.29, as evident from **Figure 3.24**(a), all the silanols are part of the amorphous network and evolve gradually with solvating water molecules as a function of temperature leading to extensive foaming. Similar behavior is observed for Na_2O/SiO_2=0.5 (**Figure 3.24**(b)) with an increased quantity of solvating water molecules and silanols available in pre-dried powder at 150°C resulting in more volumetric expansion than Na_2O/SiO_2=0.29, mainly due to the higher network mobility imparted by the network modifiers either Na ions or protons.

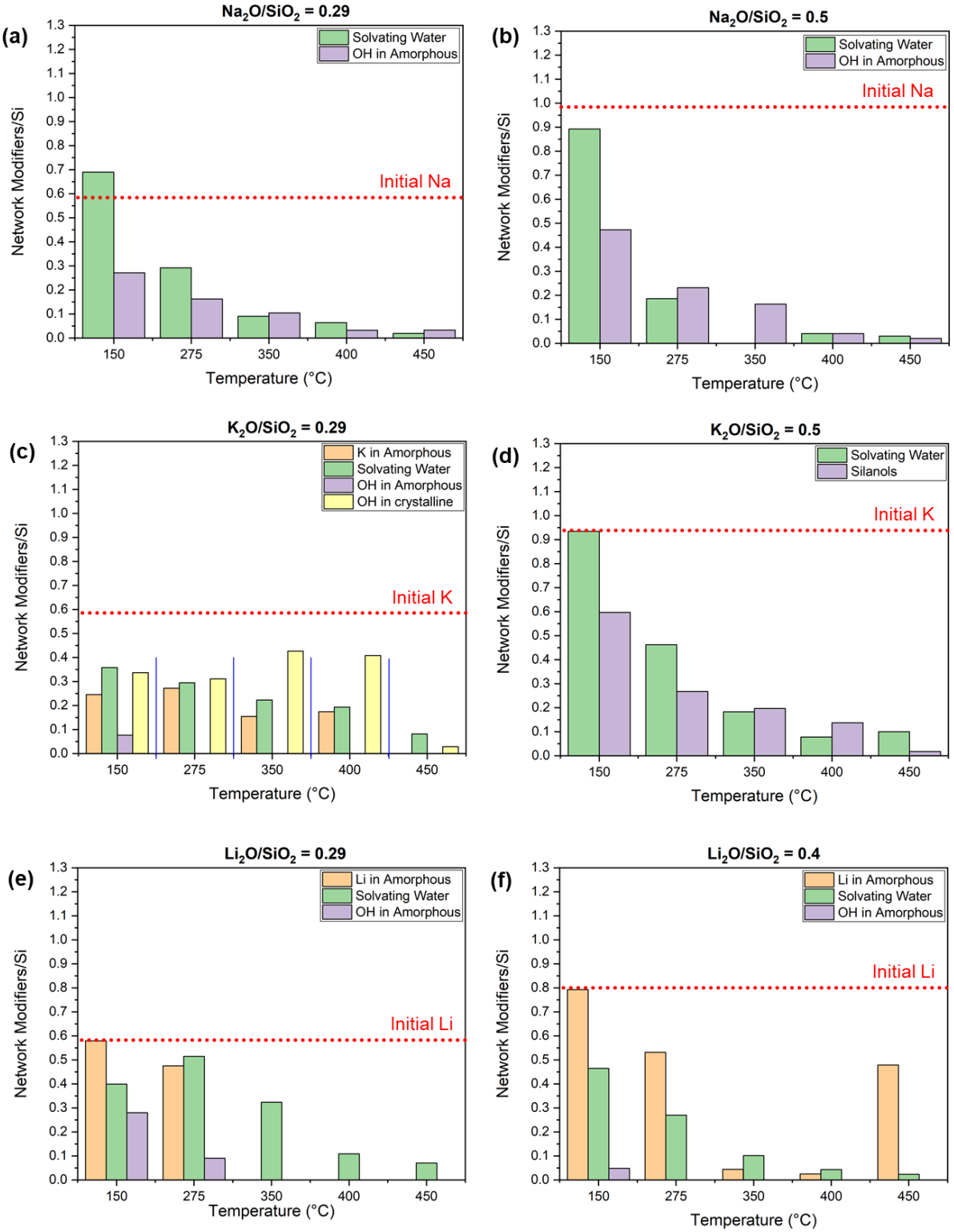

Figure 3.24: Quantitative thermal evolution of different species i.e solvating water, silanols (in amorphous or crystalline phase) and alkali ions for (a, b) Na, (c, d) K and (e, f) Li-silicates extracted from the information given in **Figure 3.18**, **Figure 3.22** and **Figure 3.23**. The dotted line in red is indicative of the initial quantity of alkali ions. Note that Na-silicates and K_2O/SiO_2=0.5 do not exhibit any crystalline behavior and thus the alkali is expected to stay constant in the amorphous phase.

Crystallization or phase separation is not observed in our Na-silicate solutions below 500°C suggesting the network to be indeed relatively mobile enough to allow for extensive foaming. The absence of crystallization or phase separation allows to preserve a silicate network with a

substantial amount of network modifiers up to a rather high temperature (around 450°C), above the apparent T_g (210°C for Na_2O/SiO_2=0.29 and 175°C for Na_2O/SiO_2=0.5), so that the network is mobile enough to ensure foaming while silanols condense thus releasing water.

K and Li-silicates being crystallized show a different behavior for the evolution of the various species as shown in **Figure 3.24**(c–f). It is worth recalling here that Li-silicates don't foam at all while an intermediate behavior (between Na and Li-silicates) is observed for K-silicates (at a heating rate of 5°C/min).

Li-silicates

The mobility of the network is reduced a lot in the case of Li-silicates. This stems from the fact that the starting compositions studied here lie in the phase separation regime (note that the starting solutions become whitish at rather lower temperatures i.e < 150°C) when compared to the reported data for binary Li_2O-SiO_2 glass systems[93,98,124] indicating the formation of a pure SiO_2 phase that is not mobile at all due to the absence of any Li ions or protons in the network.

On thermal treatment of Li-silicates, apart from phase separation, the system tends to crystallize resulting in the loss of Li ions from the amorphous phase. As can be seen from **Figure 3.23**(a) and **Figure 3.24**(e) for Li_2O/SiO_2=0.29, all the Li ions leave the amorphous phase around 350°C rendering the amorphous network brittle. Furthermore, silanols in the amorphous network are also more or less removed at roughly 275°C adding further to the rigidity of the network resulting in a structure that is not mobile enough to expand due to a very viscous nature, thus, suppressing the structure from expanding altogether. Solvating water is, therefore, mainly responsible for the mass loss observed in TGA shown in **Figure 3.9**(b). Moreover, the actual amount of solvating water molecules in Li-silicates, for instance, Li_2O/SiO_2=0.29 shown in **Figure 3.24**(e) could be a combination of solvating water as well as protons in LiOH. Since silanols are all lost below 300°C, solvating water molecules maybe linked to Q^2 and Q^3 crystalline phases as well as LiOH (especially above 275°C) or the LiOH molecules maybe H-bonded to the Q^3 amorphous phase. Li_2O/SiO_2=0.4 shows a similar behavior in terms of the evolution of the different species and thus has a network mobility similar to Li_2O/SiO_2=0.29 resulting in no foaming.

K-silicates

K-silicate compositions, on the other hand, are not in the phase separation regime; however, crystallization does appear on thermal treatment at temperatures as low as 150°C (depending upon the kinetics) as shown in **Figure 3.21**(a), **Figure 3.22**(a) and **Figure 3.24**(c) for K_2O/SiO_2=0.29. It is worth noting here that direct heating of the K-silicate solutions (for instance at 10°C/min or higher) leads to extensive foaming especially for K_2O/SiO_2=0.29 as discussed later in **Chapter 4**. However, drying of the systems at 150°C for a few hours may result in the formation of crystallites suppressing to a large extent the intumescent behavior of K-silicates. For pre-dried crystallized powders, crystalline content represents almost 60 wt% of the total network configuration at 150°C and 275°C while the value goes up to 80% at 350°C and 400°C, however, all the K ions don't leave the amorphous phase at any point allowing for enough network mobility to be retained, although reduced, for the structure to expand as shown in **Figure 3.24**(c). The leftover silanols in the amorphous phase after crystallization are all lost around 275°C while those in the crystalline phase

remain more or less constant up to 400°C whereas solvating water molecules are lost gradually on increasing temperature representative of the mass loss in TGA curves (**Figure 3.9**(a)). It is worth noting here that NMR data doesn't seem to give a precise measure of quantification for crystalline components. For instance, in **Figure 3.22**(a) the NMR NBOs/Si curve tends to reduce as a function of temperature and it might be suggestive of a decrease in the quantity of OH in the crystalline phase which happens to be not true according to the more accurate XRD data. This reduction might arise from the inability of NMR data to show exact quantification of the crystalline phases with respect to the amorphous part (due to the 8.4 T magnetic field strength used that may not be enough to have the best resolution whereas a higher field strength may allow to enhance the sensitivity). It might also be dependent upon the polymorph i.e. determination of orthorhombic $KHSi_2O_5$ may be less accurate as the values reported from XRD data (**Table A 3.2** in appendix) do not correspond well with NMR data. So, the yellow bars representing OH in the crystalline phase in **Figure 3.24**(c) correspond to the values computed from the deconvoluted XRD diffractograms given in **Figure 3.21**(a). Thus, the foaming behavior for pre-dried K_2O/SiO_2=0.29 system tends to be intermediate between Na and Li-silicates mainly due to the existence of enough network mobility at the beginning and throughout. Solvating water molecules appear to be linked to silanols in the amorphous phase (until 150°C), K ions in amorphous Q^3 and crystalline Q^3 phases.

K_2O/SiO_2=0.5, evolution shown in **Figure 3.24**(d), behaves in a manner similar to Na-silicates and a similar extensive foaming behavior may be expected, however, that is not the case as the system tends to be very hygroscopic i.e. water is thermodynamically more stable until 300°C as shown by the phase diagram in **Figure 3.11**(d). Therefore, although the network is mobile as observed for Na-silicates, a behavior intermediate to Li and K-silicates is seen in terms of macroscopic evolution.

Literature report[21] on the thermal evolution of K-silicate solutions suggests the foaming of these systems to be a consequence of the evolution and amount of solvating water molecules. It could partly be true given the fact that silanols tend to convert into solvating water molecules due to the existence of an equilibrium between the two species as has been established for Na silicates, however, a more rigorous quantitative analysis using a combination of different tools (TGA, NMR, XRD) suggests that foaming happens to be a consequence of mainly network mobility and the amount of protons as silanols in the network thus allowing us to clearly distinguish among the various alkali types in terms of their thermal behavior. Moreover, the reported data available in literature concerns more the thick coatings developed from these aqueous solutions for which a global thermal evolution has been presented in **Chapter 4**.

Hence, thermal evolution of aqueous alkali silicates leads to structural changes at the microscopic scale that are directly linked to their macroscopic behavior in terms of foaming. Na-silicates foam because the microscopic network is mobile enough to let that happen as the systems don't crystallize or phase separate. Silanols condense on gradual increase in temperature leading to volumetric expansion of the material. Li-silicates don't foam as the starting compositions lie in the phase separation regime as well as crystallization occurs around 275°C. Furthermore, all the Li ions and silanols leave the amorphous network below 350°C adding further to the reduction in network mobility, thus, preventing volumetric expansion. K-

silicates show an intermediate foaming behavior with K_2O/SiO_2=0.29 crystallizing on pre-drying at 150°C (or heating solutions at slower rates i.e. 1 or 5°C/min as discussed in Chapter 4). The silanols are all lost below 200°C reducing the network mobility and limiting foaming once the system is crystallized. On the other hand, K_2O/SiO_2=0.5 shows reduced foaming due to water being thermodynamically more stable up to 300°C.

The thorough investigation on the evolution of the structural properties thus gives a comprehensive view of how exactly does the network evolve on thermal treatment, that happens to impact directly the macroscopic evolution in terms of foaming behavior, depending upon the composition and type of alkali silicate. The above discussion has been limited to temperatures approaching 450°C where, especially, Na-silicates have indicated a xerogel-to-glass transition in terms of the evolution of Q^n units. The changes in the structural properties over the temperature range studied are in fact linked to the viscosity changes in the system once the quantity of water tends to evolve. Hence, a knowledge of such properties is also important for a complete comprehension of the exact cause of this structural expansion. One step in that direction is to investigate the behavior of these aqueous alkali silicates above 500°C to explore the kind of changes associated with each system in terms of the rheological properties.

Furthermore, foaming is generally not observed for glasses below the T_g and corresponds to structural changes at elevated temperatures due to variations in viscosity. Thus, it is worth investigating the structural variations at temperatures above 450°C once the foaming regime of alkali silicates has been covered, and that necessitates development of a model that can predict viscosity variations.

3.3.3. High temperature evolution

Macroscopic structural changes in terms of foaming and microscopic in terms of network polymerization occur on heat treating aqueous alkali silicates (with Na-silicate showing extensive foaming, K-silicate's behavior depends on crystallization while Li-silicates show negligible expansion) up to 450°C above which further expansion is limited due to a reduced amount of water/silanols in the network. Silicates at this stage may be referred to as 'pre-foamed' i.e. the silicate foamed. This foam can then be crushed and used as the starting material for further analysis. Heating to even higher temperatures after the foaming regime has been crossed is expected to induce further structural changes, and thus inducing interest in understanding rheological issues. The investigation of these changes is important to draw a comparison with the rheological evolution of the melted glass. For this purpose, powder pellets of these alkali silicates (pre-foamed Na and K-silicates while pre-dried Li-silicates) were heated to temperatures reaching 1200°C in an in-situ Hot-stage Microscope for visualizing the macroscopic evolution as well as being able to compute the viscosity by developing theoretical models by defining various temperature points as shown in **Figure 3.25**. Viscosity of glasses has been theoretically calculated by developing models based on Vogel–Fulcher–Tamman's (VFT) equation[151,152] given as:

$$\log \eta = A + \frac{B}{T - T_o} \tag{3.10}$$

where 'η' is the viscosity, 'A', 'B' and 'T_o' are the fitting constants while 'T' represents temperature in K.

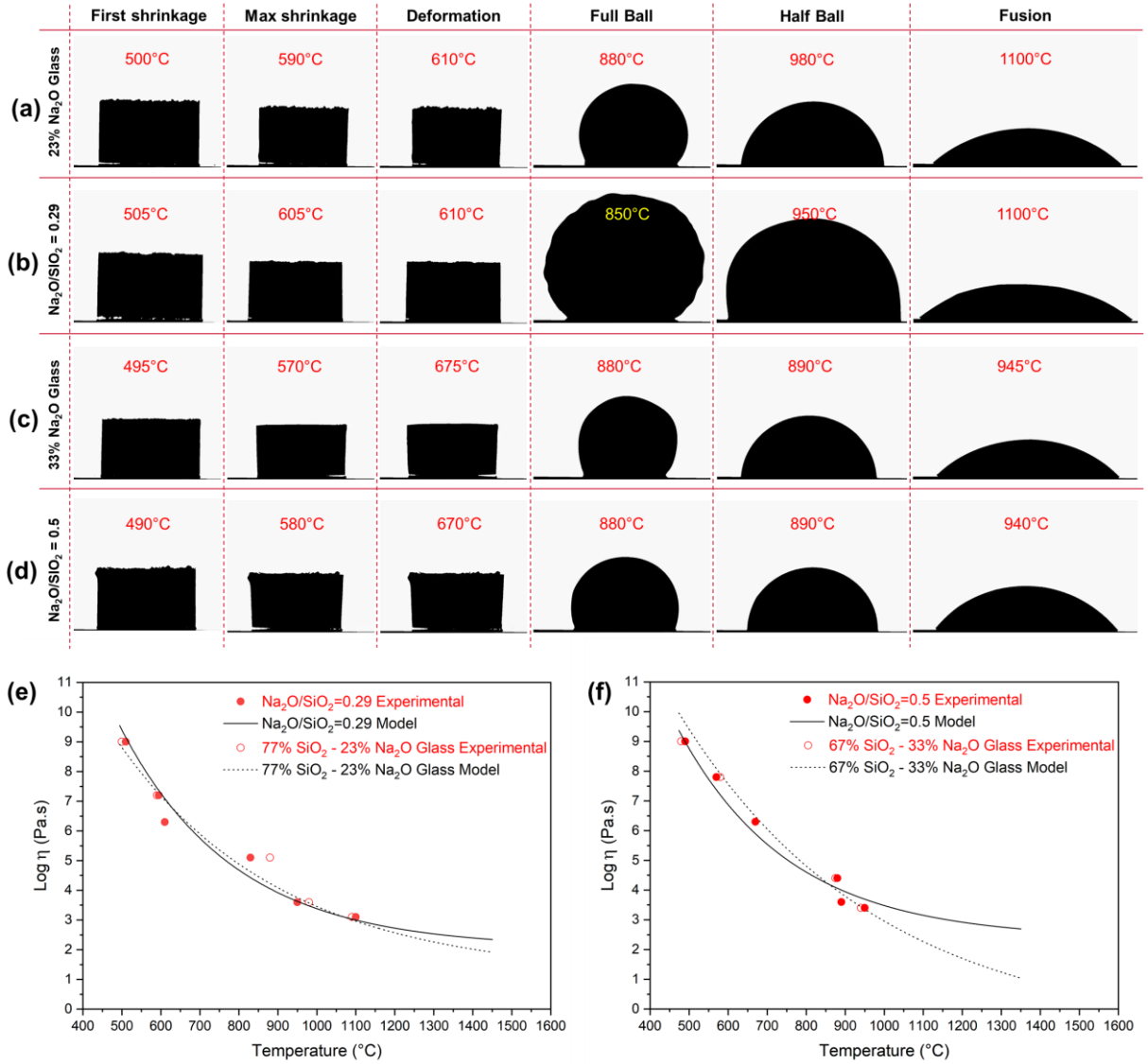

Figure 3.25: Hot-stage Microscopy images of ball-milled (a) 77% SiO_2 – 23% Na_2O reference glass, (b) pre-foamed Na_2O/SiO_2=0.29, (c) 67% SiO_2 – 33% Na_2O reference glass & (d) pre-foamed Na_2O/SiO_2=0.5 pellets heated to 1200°C at a ramp of 5°/min in air, and viscosity variation (based on theoretical model and experimental values) above 450°C for (e) Na_2O/SiO_2=0.29 & corresponding reference glass and (f) Na_2O/SiO_2=0.5 & corresponding reference glass. Model values[114] in (e) and (f) are shown by the lines (where literature VFT parameters have been followed) while symbols indicate experimental values obtained from Hot-stage Microscopy analysis.

Figure 3.25(a-d) show the microscopic images of pre-foamed Na-silicate and reference glass pellets at six distinct points, which represent the general trend of evolution observed. These different points correspond to shape changes on heating: the point of first shrinkage occurs at the instant when pellet starts to sinter (due to porosities in the pellet) followed by a maximum shrinkage point, deformation or softening temperature (pellet shape starts to deform or becomes curved along the corners), full ball temperature, half ball and the fusion point that represents free flow or melting of the pellet. The viscosity of glasses corresponding to these distinct temperatures have been measured experimentally[114] and by theoretical modelling.[153–156] Sintering of the pellets

is dependent upon the particle size,[115,154] which in turn can vary the estimated viscosity of the system. The impact of particle size distribution is assumed to be minimized in our case due to the long and same grinding procedure followed[153] for both glasses and alkali silicate xerogels. Employing Hot-stage Microscopy, each temperature point is extracted from the recorded images and plotted against the corresponding viscosity values to compute the evolution with temperature.

The shape changes observed for Na-silicates and the corresponding dry reference glasses indicate a good agreement between the two, providing evidence to the xerogel-to-glass transition observed for Na-silicates at 400/450°C as discussed previously and shown in **Figure 3.12**. Na_2O/SiO_2=0.5 (**Figure 3.25**(d)) shows the same shape evolution in terms of the extent of 'Full Ball' and 'Half Ball' formation as that observed for 67% SiO_2 – 33% Na_2O reference glass given in **Figure 3.25**(c) while Na_2O/SiO_2=0.29 (**Figure 3.25**(b)) has an expanded 'Full Ball' and 'Half Ball' shape, probably due to the decomposition of any sodium carbonates or the removal of leftover silanols at elevated temperatures, when compared with the shape changes for 77% SiO_2 – 23% Na_2O reference glass **Figure 3.25**(a).

Temperature evolution of viscosity of Na-silicate systems is shown in **Figure 3.25**(e) and (f) for Na_2O/SiO_2=0.29 and Na_2O/SiO_2=0.5, respectively, and an exponentially decreasing trend can be seen which is consistent with literature models. Both the Na-silicates and their corresponding reference glasses show similar experimental and computed values indicating a good agreement between our silicates and reference glasses. This suggests that indeed Na-silicates tend to behave in the same manner as glasses once the initial microstructural conversion is complete at 400/450°C. Viscous sintering tends to occur around viscosity values approaching 10^9 Pa.s for both the molar ratios.

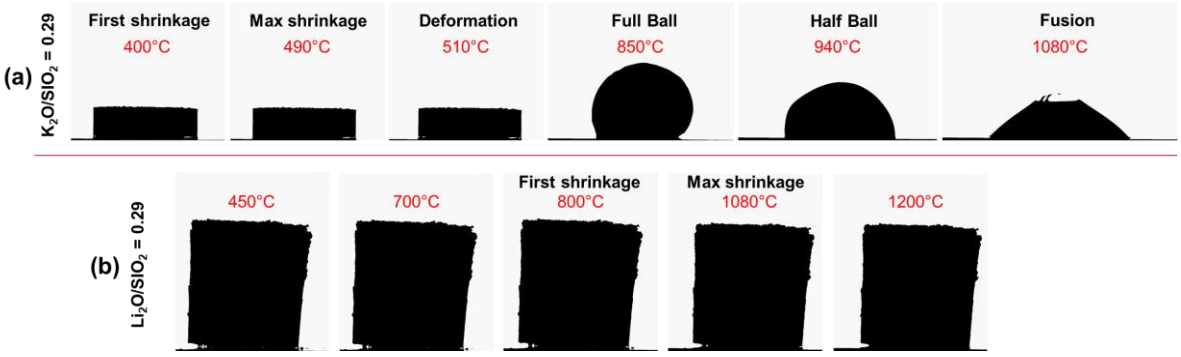

Figure 3.26: Hot-stage Microscopy images of pre-dried (a) K_2O/SiO_2=0.29 and (b) Li_2O/SiO_2=0.29 powder pellets obtained at 5°C/min.

High temperature evolution of K and Li-silicate pellets was also investigated in order to compare the behavior with Na-silicates. **Figure 3.26** shows the changes in shape for K_2O/SiO_2=0.29 and Li_2O/SiO_2=0.29 powder pellets (obtained by pre-drying solutions at 150°C, as negligible foaming is expected). The behavior above 400°C, in terms of shape change on crossing the T_g, for K_2O/SiO_2=0.29 (**Figure 3.26**(a)) appears to be quite similar to Na-silicates with the pellet going through all the steps from initial shrinkage to fusion, the only difference being the temperature of

these various shape changes suggesting a behavior potentially similar to glasses. Li_2O/SiO_2=0.29, in contrast to both Na and K-silicates, appears to be more stable to even higher temperatures. The first shrinkage of the system appearing at 800°C, maximum shrinkage at 1080°C with the absence of fusion (in terms of visual evolution) within the temperature range (up to 1200°C) investigated.

The differences in the behavior observed between Na, K and Li-silicates appears to be directly linked to the rheological properties of the system indicated by the Hot-stage Microscopy images as well as the network evolution investigated using quantitative approach. A link in the thermal evolution observed below 400°C and above has to be, therefore, created to fully understand how the rheological properties of the system, including viscosity, are changing. Viscosity models obtained above 400°C are a step in the right direction to calculate the viscosity changes below 400°C. An extrapolation of this viscosity evolution by introducing more data points is required at this stage to be able to extract an exact T_g for the alkali silicates (especially Na-silicate) as well as the behavior around foaming regime towards a better understanding of the rheological evolution upon thermal treatment.

3.4. Conclusions

Structural properties of aqueous alkali silicates of two different molar ratios (M_2O/SiO_2=0.29 and 0.5 for Na, K while 0.29 and 0.4 for Li-silicate) have been investigated at ambient and on thermal evolution to establish an in-depth fundamental understanding of the structural properties at both macroscopic and microscopic scale. It has been shown that alkali silicate solutions of any desired composition can be prepared by the addition of colloidal SiO_2 and NaOH (for Na-silicates), KOH (for K-silicates) and LiOH for (Li-silicates) provided they are soluble and the molar ratio is low enough. Increasing the amount of alkali ion tends to reduce the degree of polymerization in the network, especially for Na and K-silicates for which a similar liquid-state ^{29}Si NMR response is observed while the network does not change much on going from Li_2O/SiO_2=0.29 to Li_2O/SiO_2=0.4.

Mass loss evolution is dependent upon temperature (mainly for Na-silicates) and alkali content in the silicate. Thermally treating powders (or xerogels) prepared by pre-drying solutions at 150°C suggests the existence of an offset of mass loss with higher alkali content systems showing a lower initial rapid dehydration temperature referred to as the softening point or apparent T_g. For Na-silicates, increasing the Na content tends to reduce the softening temperature (from 210°C for Na_2O/SiO_2=0.29 to 175°C for Na_2O/SiO_2=0.5) along with a higher amount of overall water retention after the initial pre-drying step at 150°C. Such low values of apparent T_g are consistent with the literature on T_g of hydrated glasses suggesting the Na-silicates to retain enough mobility during thermal evolution. A same order of magnitude for mass loss evolution is observed for both the Na-silicate molar ratios with an E_a of 29.4 kJ.mol^{-1} for Na_2O/SiO_2=0.5 as compared to 34.1 kJ.mol^{-1} for Na_2O/SiO_2=0.29.

Heating pre-dried Na-silicate powders tends to increase the degree of polymerization. A xerogel-to-glass evolution in terms of Q^n units at around 400°C is observed for Na-silicates when compared with reference glasses. Complementary information provided by Raman spectroscopy also indicates that the structure condenses and the Raman spectra at 400°C become similar to that of

the corresponding glasses (especially in terms of Q^n units) for both the Na-silicate molar ratios with ring-type structure being more dominant in glasses. Furthermore, high temperature evolution (above 400°C) under the Hot-stage Microscope indicates the pre-foamed Na-silicate powder pellets to have the same macroscopic behavior as the melt & quench reference glasses. An exponentially decreasing trend and similar values of viscosity are observed for both the Na-silicate molar ratios and glasses suggesting, indeed, the existence of a xerogel-to-glass conversion of silicates prepared from solutions.

Further structural investigation below 400°C indicates that Na ions are connected to both Q^2 and Q^3 silicon sites for Na_2O/SiO_2=0.29 suggesting a completely random distribution, while all protons are connected to Q^3 (both Q^2 and Q^3 connectivity is observed in case of Na_2O/SiO_2=0.5) i.e. no free water is present at 150°C. Initial solutions are composed of free water, solvating water and silanols which tend to evolve depending upon the heating temperature with the free water mostly removed on heating to 150°C. For Na-silicates, NBO contribution from the network modifiers (Na and H) shows that both silanols and solvating water are present even at high temperature, suggesting an equilibrium between the two structural units for protons. The amount of initial water in the silicate and molar ratio Na_2O/SiO_2 directly influence the amount of silanols in the network. Higher overall water retained for the molar ratio Na_2O/SiO_2=0.5 suggests the network to possess more H as NBOs when compared to Na_2O/SiO_2=0.29 leading to extensive volumetric expansion in terms of foaming.

In contrast, slightly different structural changes are observed on thermal evolution of pre-dried K and Li-silicate powders. Multiple activation energies for both silicates are seen mainly due to the formation of different crystalline phases confirmed by the deconvoluted solid-state ^{29}Si NMR as well as XRD data. Na-silicate solutions do not crystallize on heating up to 450°C. K_2O/SiO_2=0.29 is crystallized even at 150°C with a DOC of 60% when dried for 17 h. Orthorhombic and monoclinic $KHSi_2O_5$ crystalline phases are formed that tend to evolve with temperature (DOC increases to ~80% at 400°C) until partial melting is observed at 450°C. Both Li-silicate molar ratios, on the other hand, are amorphous at 150°C while crystallization appears at 275°C with the formation of orthorhombic Li_2SiO_3 and $Li_2Si_2O_5$ phases. DOC increases as a function of temperature with the gradual conversion of Li_2SiO_3 into $Li_2Si_2O_5$. This crystallization behavior in K and Li-silicates is suggested to have a direct impact on the macroscopic evolution of the silicates. Rietveld refinement of XRD diffractograms has helped in the deconvolution of the data that has aided in establishing a quantitative measure of the evolution of alkali ions and proton-related species.

Pre-dried Na-silicates have a gradual and continuous evolution of amorphous network silanols and solvating water molecules leading to extensive foaming stemming from the fact that the network is relatively mobile as well as water can leave the system easily. K_2O/SiO_2=0.5 behaves in a similar manner as that observed for Na-silicates, however, phase diagram suggests the system to contain thermodynamically more stable water content indicating the system to be mobile while being extremely hygroscopic at the same time.

Amorphous silanols in the network are lost altogether at 275°C for both K_2O/SiO_2=0.29 and Li-silicates while those linked to $KHSi_2O_5$ phase stay intact until 400°C. The network in K_2O/SiO_2=0.29 retains somewhat its mobility due to leftover K ions in the amorphous phase even after crystallization as well as the possibility of some solvating water molecules to be intact, however, crystallization is expected to reduce quite a bit the foaming capacity when compared to Na-silicates. The network in Li-silicates is less mobile due to the existence of strong cross-links between Li ions and polysilicate particles. Furthermore, the studied compositions lie in the phase separation regime indicating the formation of a SiO_2 rich matrix phase that is reasonably brittle and prevents the structure from being mobile. Crystallization at temperatures approaching 250°C leads to the removal of Li ions from the amorphous phase whereby all Li ions move into the crystalline counterpart at 350°C reducing further the already low mobility in Li-silicate systems, thus, supposedly limiting the volumetric expansion.

3.5. Appendix

Liquid-state ^{29}Si NMR repetition delay measurements on Na-silicate solution

Figure A 3.1 shows the impact of liquid-state ^{29}Si NMR spectra on changing the repetition delay (r_d) for measurements acquired on Na_2O/SiO_2=0.29 solution. A total of 5000 scans were run for each r_d of 0.5, 1, 5, 10 and 20 s. A reduction in the noise intensity can be seen on increasing r_d and 5 s (using 5000 scans) was chosen as the optimum value for all the liquid-state ^{29}Si NMR spectra shown in **section 3.1** in the main text.

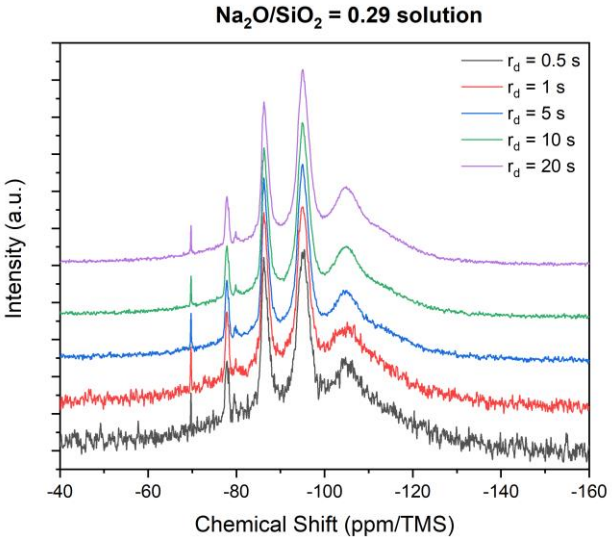

Figure A 3.1: Liquid-state ^{29}Si NMR for Na_2O/SiO_2=0.29 solution at repetition delay of 0.5 s, 1 s, 5 s, 10 s and 20 s and 5000 scans each.

Isothermal TGA mass loss evolution of Na-silicate solution at 150°C

Isothermal TGA mass loss plot at 150°C for Na_2O/SiO_2=0.29 solution is shown in **Figure A 3.2**. On heating at 10°C/min to 150°C for 4 h, the system does not seem to lose any more water after 2 hours of drying.

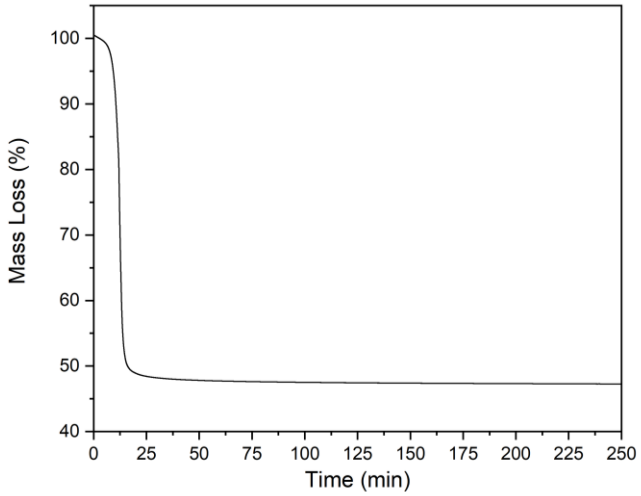

Figure A 3.2: Isothermal TGA mass loss of Na_2O/SiO_2=0.29 solution at 150°C for 4 h.

Solid-state ^{29}Si NMR repetition delay measurements on Na and Li-silicate

The impact of changing r_d on the response of Na and Li-silicate powders is shown in **Figure A 3.3**. Solid-state ^{29}Si NMR spectra were acquired for Na_2O/SiO_2=0.29 powder pre-dried at 150°C at 20, 100, 200, 300 and 1500 s for 789 scans. An increase in signal intensity is observed on going from 20 to 1500 s as shown in **Figure A 3.3**(a), however, the response is the same.

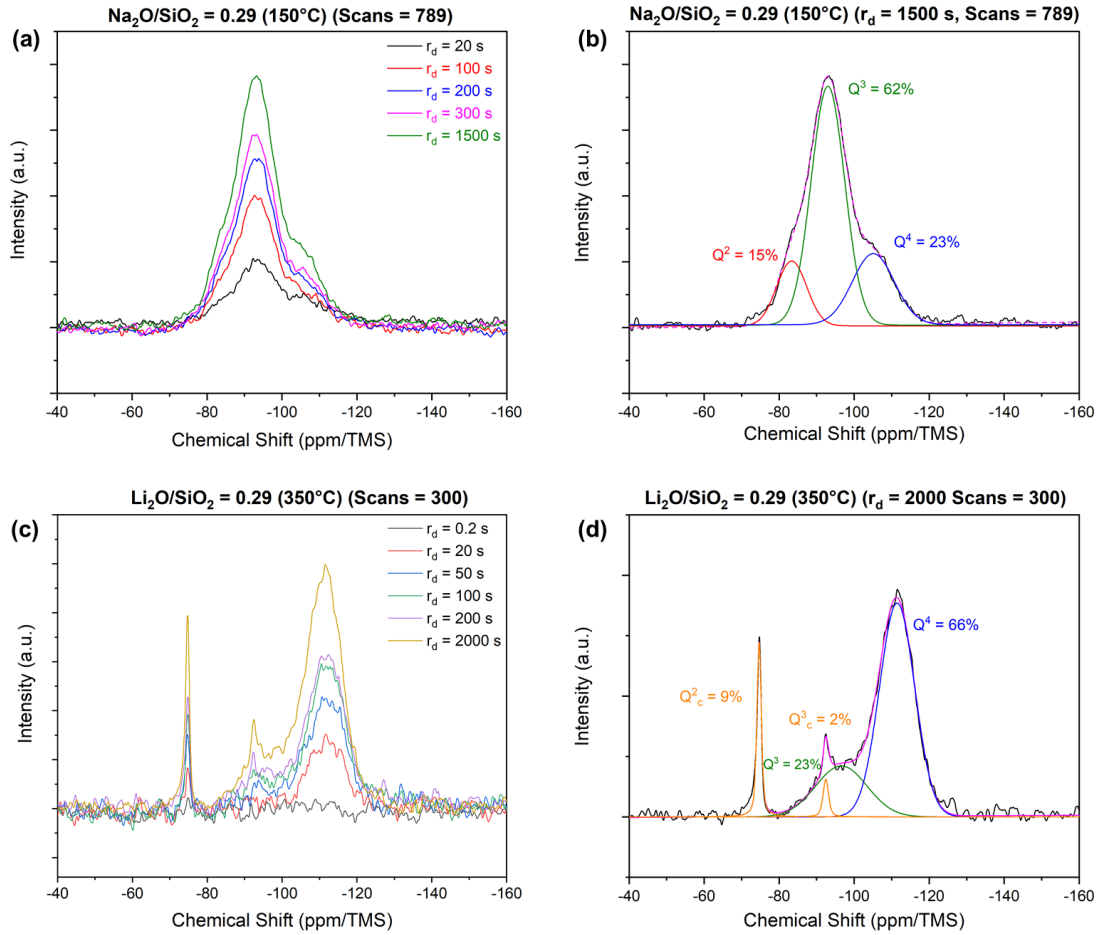

Figure A 3.3: Repetition delay experiments for fixing parameters for solid-state ^{29}Si NMR at 8.4 T: (a) Na_2O/SiO_2=0.29 powder obtained by pre-drying at 150°C with 789 spectra acquired at 20 s, 100 s, 200 s, 300 s & 1500 s, (b) deconvoluted Na_2O/SiO_2=0.29 spectrum acquired at 1500 s, (c) Li_2O/SiO_2=0.29 powder obtained by pre-drying at 350°C with 300 spectra acquired at 0.2 s, 20 s, 50 s, 100 s, 200 s & 2000 s and (d) deconvoluted Li_2O/SiO_2=0.29 spectrum acquired at 2000 s.

Similarly, spectra were also acquired for Li_2O/SiO_2=0.29 powder pre-dried at 350°C (since it's a combination of both crystalline and amorphous character) to check for the impact of changing the alkali type on the NMR response. **Figure A 3.3**(c) indicates only an increase in the intensity of the signal on going through the r_d values 0.2, 20, 50, 100, 200 and 2000 s for 300 scans each with the relative proportion of different Q^n units remaining the same.

Deconvolution of the spectrum at a r_d of 1500 s for Na_2O/SiO_2=0.29 (**Figure A 3.3**(b)) and 2000 s for Li_2O/SiO_2=0.29 (**Figure A 3.3**(d)) corresponds well with that observed for Na_2O/SiO_2=0.29 150°C (**Figure 3.12**(a)) and Li_2O/SiO_2=0.29 350°C (**Figure 3.20**(a)), respectively, in the main text.

Impact of pre-drying time on the thermal evolution of Na-silicate

Figure A 3.4 shows the thermal behavior of powders obtained by pre-drying Na_2O/SiO_2=0.5 solution at 120°C and 150°C for 17 h to see the impact of the retained water content on global water evolution. Both the powders behave the same way in terms of mass loss evolution, the only difference being the amount of retained water that happens to be higher for the powder pre-dried at 120°C thus suggesting (along with **Figure 3.7**(a) in the main text) that the kinetics of mass loss evolution in Na-silicates is dependent mainly on temperature.

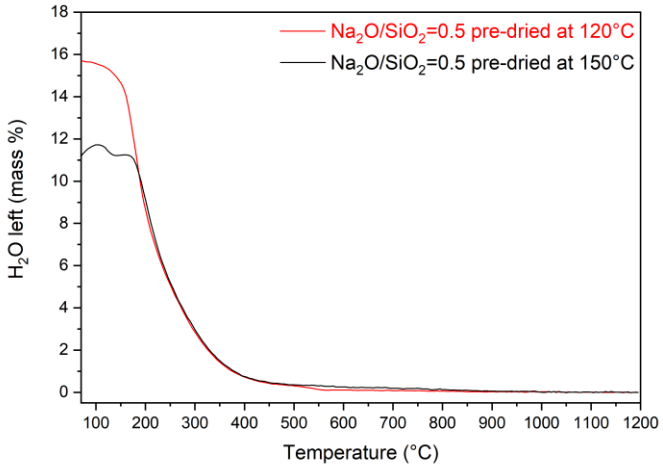

Figure A 3.4: Impact of pre-drying temperature on the thermal evolution of Na_2O/SiO_2=0.5 powders observed through TGA mass loss measurement.

Binary phase diagrams for crystallization in K-silicates

The crystallization binary phase diagrams for K-silicates are shown in **Figure A 3.5**. The different crystalline phases possible are denoted by the relevant chemical formulas. 'gas_real' corresponds to the water molecules that are released on thermal treatment while 'Aqueous_DD' is representative of free water in the system. Note that we observed hydrated crystalline phases ($KHSi_2O_5$ or $KHSiO_3$) and as a function of drying time thus making it difficult to relate our systems directly with these phase diagrams.

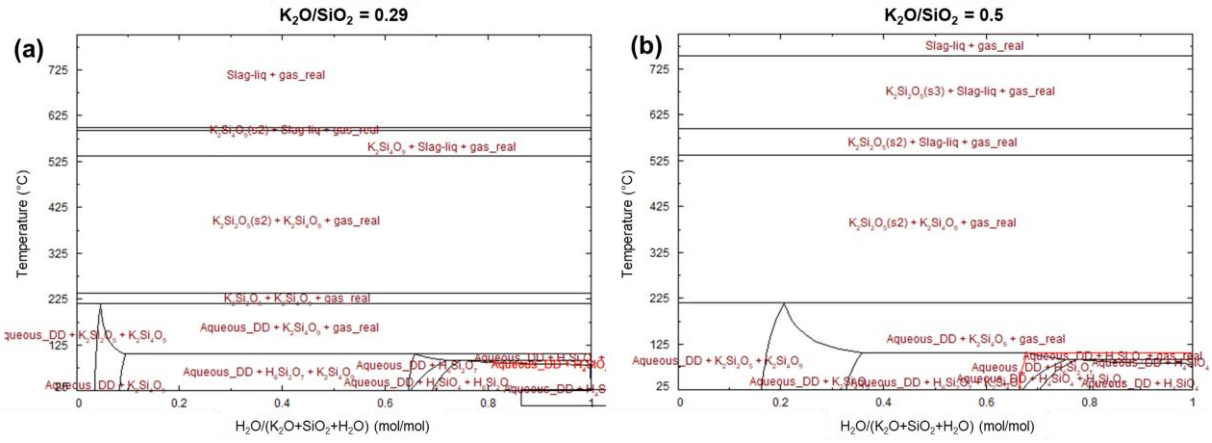

Figure A 3.5: Binary crystallization phase diagram for (a) K_2O/SiO_2=0.29 and (b) K_2O/SiO_2=0.5 calculated from FactSage software.

Solid-state ^{29}Si NMR deconvolution parameters

Table A 3.1: Fitting parameters used for deconvolution of solid-state ^{29}Si NMR spectra obtained at 8.4 T.

Na-silicate	T (°C)	Q^1 (ppm)		Q^2 (ppm)		Q^3 (ppm)		Q^4 (ppm)	
		Pos.	Wid.	Pos.	Wid.	Pos.	Wid.	Pos.	Wid.
Na_2O/SiO_2 = 0.29	150	-	-	-82.9	10.1	-92.7	10.6	-104.9	13.6
	275	-	-	-81.6	9.4	-91.7	10.8	-105.6	14.5
	350	-	-	-78.8	7.1	-91.5	10.7	-105.9	13.9
	400	-	-	-	-	-92.0	10.7	-105.5	12.9
	450	-	-	-	-	-91.5	10.8	-105.9	13.3
23% Na_2O Glass	RT	-	-	-	-	-92.1	10.4	-105.2	12.5
Na_2O/SiO_2 = 0.5	150	-70.0	11.7	-81.6	9.6	-90.1	10.8	-	-
	275	-	-	-80.9	11.3	-89.1	10.0	-	-
	350	-	-	-78.8	10.3	-88.3	9.8	-	-
	400	-	-	-78.9	9.0	-88.8	9.4	-98.7	12.0
	450	-	-	-78.9	9.0	-88.8	9.3	-98.7	13.5
33% Na_2O Glass	RT	-	-	-78.1	5.9	-89.4	9.8	-100.9	13.5

K-silicate	T (°C)	Q^1 (ppm)		Q^2 (ppm)		Q^3 (ppm)		Q^3_c (ppm)				Q^4 (ppm)	
								Orthorhombic		Monoclinic			
		Pos.	Wid.	Pos.	Wid.	Pos.	Wid.	Pos.	Wid.	Pos.	Wid.	Pos.	Wid.
K_2O/SiO_2 = 0.29	150	-	-	-	-	-89.2	12.6	-91.7	2.6	-99.3	3.8	-101.7	8.3
	275	-	-	-	-	-90.6	10.6	-91.4	1.8	-98.8	4.7	-101.8	10.3
	350	-	-	-	-	-91.9	8.5	-91.4	1.6	-98.8	4.9	-102.0	10.9
	400	-	-	-	-	-92.8	8.8	-91.6	1.8	-98.8	4.1	-102.1	11.0
	450	-	-	-	-	-93.2	9.1	-	-	-	-	-103.9	12.1
K_2O/SiO_2 = 0.5	150	-74.6	4.6	-82.3	9.4	-91.8	10.2	-87.4	3.2	-94.9	1.6	-	-
	275	-	-	-82.1	9.9	-95.2	12.1	-	-	-	-	-	-
	350	-	-	-81.9	10.4	-91.6	11.0	-	-	-	-	-	-
	400	-	-	-79.9	7.4	-91.4	10.7	-	-	-	-	-	-
	450	-	-	-78.2	6.6	-91.7	11.2	-	-	-	-	-102.7	12.6

Li-silicate	T (°C)	Q^2 (ppm)		Q^2_c (ppm)		Q^3 (ppm)		Q^3_c (ppm)		Q^4 (ppm)	
		Pos.	Wid.	Pos.	Wid.	Pos.	Wid.	Pos.	Wid.	Pos.	Wid.
Li_2O/SiO_2 = 0.29	150	-81.4	14.0	-	-	-93.5	14.4	-	-	-107.9	10.7
	275	-	-	-74.8	2.3	-95.2	15.5	-	-	-111.4	10.6
	350	-	-	-74.8	1.4	-95.0	15.4	-92.5	1.5	-111.9	11.1
	400	-	-	-74.8	1.6	-94.5	15.3	-92.6	1.6	-112.2	11.6
	450	-	-	-74.7	1.5	-92.4	14.1	-92.4	1.9	-111.4	11.3
Li_2O/SiO_2 = 0.4	150	-81.6	11.4	-	-	-91.1	11.4	-	-	-107.1	11.8
	275	-	-	-75.3	1.4	-96.7	16.9	-93.4	1.3	-112.2	9.7
	350	-	-	-75.1	1.5	-94.5	16.4	-92.6	1.7	-111.6	9.9
	400	-	-	-75.0	1.4	-94.1	14.2	-92.7	1.4	-111.7	11.1
	450	-79.5	5.9	-74.7	1.9	-91.6	15.6	-92.8	2.3	-109.1	12.5

Hygroscopic nature of K_2O/SiO_2=0.5 and the possibility of crystallization

The extremely hygroscopic nature of K_2O/SiO_2=0.5 makes it difficult to acquire the exact solid-state ^{29}Si NMR spectrum at a pre-drying step of 150°C as the resulting spectrum shows the existence of all the Q^n species as shown in **Figure A 3.6**(a) that is more like the structure observed in solutions. It could also be because the powder after the pre-drying step at 150°C is not exactly a xerogel. Therefore, the pre-drying at 150°C was done over a week, that shows the appearance of orthorhombic $KHSiO_3$ crystalline phase as given in **Figure A 3.6**(b) corresponding to the solid-state NMR spectrum shown in **Figure 3.19**(b) in the main text.

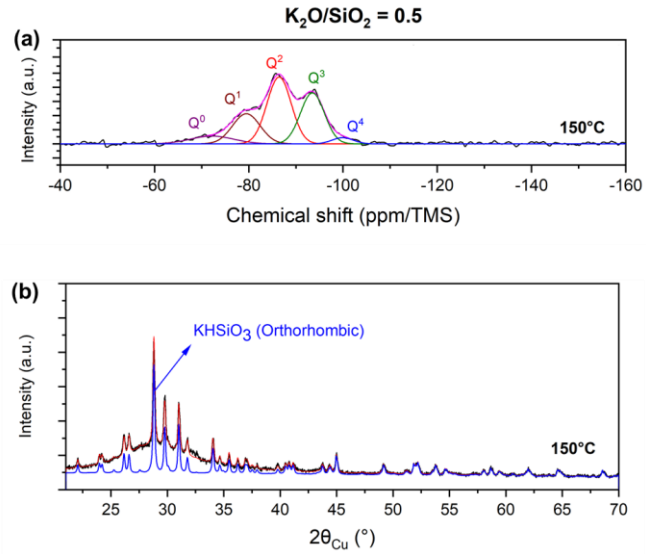

Figure A 3.6: (a) Solid-state ^{29}Si NMR spectrum at 8.4 T for K_2O/SiO_2=0.5 pre-dried at 150°C for 17 h showing the existence of all the Q^n units due to extremely hygroscopic nature and issues with spinning of sample in the rotor and (b) XRD diffractogram suggesting the formation of orthorhombic $KHSiO_3$ crystalline phase on pre-drying K_2O/SiO_2=0.5 solution at 150° for 1 week.

Fitting parameters for the deconvolution of K and Li-silicate XRD spectra

Table A 3.2 and **Table A 3.3** show all the unit cell fitting parameters used for the deconvolution of XRD diffractograms (**Figure 3.21** in the main text) and the corresponding outputs in terms of degree of crystallinity (DOC) for K and Li-silicates, respectively. The different phases observed in each system, the relevant space group and reference numbers for crystallographic information files are all mentioned discreetly.

Table A 3.2: Fitting parameters and the corresponding output for degree of crystallinity (DOC) for K-silicate obtained by Rietveld refinement approach using TOPAS.

K-silicate	Temp. (°C)	Amorp. (wt%)	DOC (wt%)	$KHSi_2O_5$ Orthorhombic (Pcmn) JCPDS 01-083-2393, ICSD 200612				$KHSi_2O_5$ Monoclinic (C2/m) JCPDS 00-045-0020, mp-1201235				Rp	GOF
				wt%	a (Å)	b (Å)	c (Å)	wt%	a (Å)	b (Å)	c (Å)		
K_2O/SiO_2=0.29	150	37.21	62.79	10.22	4.7591	8.1301	12.5671	89.78	14.5680	8.4129	9.4527	7.48	4.96
	275	41.15	58.85	79.54	4.7588	8.1302	12.5416	20.46	14.5783	8.4181	9.4534	4.21	2.69
	350	18.21	81.79	87.85	4.7576	8.1308	12.5280	12.15	14.4354	8.4006	9.4656	7.33	4.36
	400	20.66	79.34	86.45	4.7629	8.1385	12.5310	13.55	14.4613	8.4135	9.4657	5.59	3.18
K_2O/SiO_2=0.5				$KHSiO_3$ Orthorhombic (Bmab) JCPDS 01-072-1643, COD 2310604									
				wt%		a (Å)		b (Å)		c (Å)			
	150	62.4	37.6	100		11.5355		11.2672		9.7035		4.00	1.35

Table A 3.3: Fitting parameters and the corresponding output for degree of crystallinity (DOC) for Li-silicates obtained by Rietveld refinement approach using TOPAS.

Li-silicate	Temp. (°C)	Amorp. (wt%)	DOC (wt%)	Li_2SiO_3 Orthorhombic (Cmc21) JCPDS 01-083-1517, COD 2003027				$Li_2Si_2O_5$ Orthorhombic (Ccc2) JCPDS 01-072-0102, ICSD 15414				Rp	GOF
				wt%	a (Å)	b (Å)	c (Å)	wt%	a (Å)	b (Å)	c (Å)		
Li_2O/SiO_2=0.29	275	91.57	8.43	94.64	9.3749	5.4017	4.6757	5.36	5.8171	14.6106	4.7956	1.93	1.68
	350	52.89	47.11	75.70	9.3664	5.4178	4.6662	24.30	5.8195	14.6172	4.7880	3.26	2.58
	400	51.35	49.65	76.19	9.3725	5.4206	4.6666	23.81	5.8249	14.6341	4.7851	3.46	2.67
	450	49.93	50.07	74.80	9.3756	5.4205	4.6649	25.20	5.8239	14.6358	4.7823	3.59	2.74
Li_2O/SiO_2=0.4	275	84.28	15.72	93.78	9.3736	5.4029	4.6747	6.22	5.8175	14.6083	4.7946	2.20	1.91
	350	53.76	46.24	75.79	9.3699	5.4186	4.6682	24.21	5.8238	14.6246	4.7891	3.29	2.48
	400	52.23	47.77	75.20	9.3708	5.4187	4.6655	24.80	5.8219	14.6271	4.7839	3.37	2.52
	450	80.45	19.55	58.83	9.3877	5.4119	4.6645	41.17	5.8222	14.6397	4.7808	1.79	1.30

Chapter 4.

Intumescent properties

Thermally treating aqueous alkali silicates leads to macroscopic and microscopic structural changes. A detailed fundamental analysis, at the microscopic scale, on the evolution of two different molar ratios of Na, K and Li-silicate is given in **Chapter 3.** The combination of various characterization tools has suggested the temperature evolution below 500°C to be linked to the type and concentration of alkali ion in the silicate network as well as the quantity of proton-related species. Structural changes at the microscopic scale directly influence the macroscopic evolution of alkali silicates in terms of intumescence/foaming. Thus, it is essential to investigate the behavior of these systems from a more macroscopic or visual standpoint due to its industrial relevance. This chapter on the mechanism of foaming is dedicated to the analysis of aqueous alkali silicates in solutions, pre-dried powders and thick coatings in terms of their foaming/intumescent behavior by linking with the discussion in **Chapter 3**.

4.1. Foaming behavior

4.1.1. Solutions

Macroscopic structural changes in terms of volumetric expansion are observed when some alkali silicates undergo thermal treatments.[53,59,157,158] For instance, on heating a droplet of Na-silicate solution with a heating gun, evolution from liquid to solid occurs as shown in **Figure 4.1**(a) for Na_2O/SiO_2=0.29 and is explained schematically in **Figure 4.1**(b). As a result of solvent evaporation, a viscous membrane-like layer appears at the top at lower temperatures which is linked to the formation of strains at the surface due to condensation of the gel,[159] slowing down the removal of free water from the inside of the material. Therefore, compared to the mg-sized samples we studied with thermogravimetric analysis (TGA) as discussed in **Chapter 3**, the droplet is further from equilibrium due to the small quantity of material used. At 130-150°C, the 'skin' membrane becomes very viscous, preventing bubbles of boiling water from escaping. Increasing the temperature further allows the membrane-like layer to cross the glass transition (T_g) (as in **Figure 4.1**(b)) and, hence, results in the removal of the trapped free water. Most of the free water is removed around 150-200°C leaving behind a solid that is hard. Increasing temperature further causes transition from a hard to soft phase (as also observed during grinding of the xerogel) with an abrupt structural expansion of the solid mass due to the pressure imposed by water bubbles. This occurs at the 'softening point' or 'foaming temperature' which represents the apparent T_g of the silicate responsible for an actual softening of the structure resulting in the formation of a viscous phase. The temperature referred here as the softening point is different from the formal temperature defined as the viscosity of 10^6 Pas. It does not correspond to one single value but rather a more general process i.e. significant mobility of the network which means that once this

particular temperature value is crossed, the system keeps on losing water continuously as a consequence of condensation due to the fact that the network is mobile enough to let that happen. Note that the existence and the value of a softening temperature or glass transition for materials heated from a solution needs to be further investigated in future work, since we only measured it on materials pre-dried at 150°C due to foaming-related experimental challenges. This may be achieved by following the thermal evolution of room temperature dried solution under a Hot-stage Microscope to observe the shape changes associated with the underlying transitions.[61]

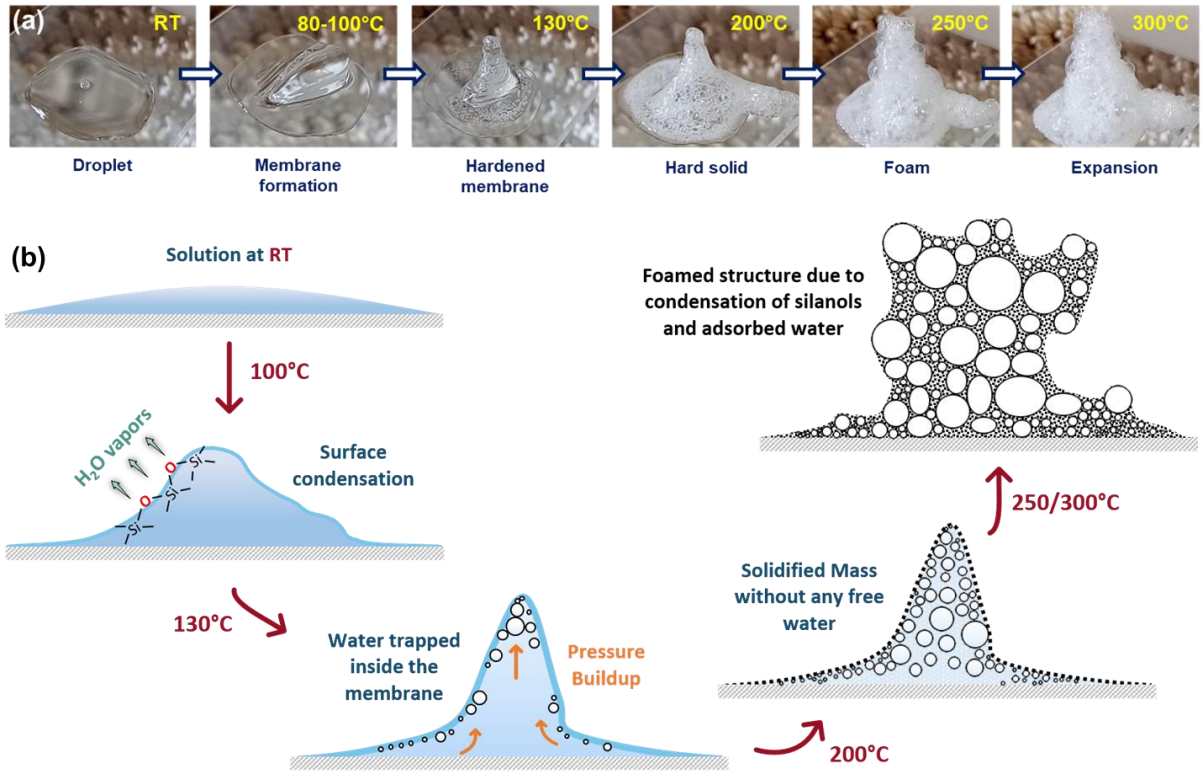

Figure 4.1: Foaming mechanism of molar ratio Na_2O/SiO_2=0.29 (a) solution under a heating gun, (b) schematic illustration of foaming mechanism of liquid.

Such a low value of softening temperature in Na-silicates is due to the presence of water and has already been reported in the literature for glasses in terms of T_g.[87,148] Foaming phenomenon itself indicates that we have a soft glass once we cross the softening point, with the structure becoming more and more condensed on increasing temperature. Heating further to temperatures above 250°C tends to cause further foaming but the extent of expansion is reduced due to a reduction in the amount of available silanols. Similar trend is observed on heating silicate with higher Na content (Na_2O/SiO_2=0.5) resulting in an increased swelling (**Figure 4.2**) due to the presence of higher amount of retained water in the structure. Thus, the lower softening temperature of 175°C observed for Na_2O/SiO_2=0.5 as compared to 210°C for Na_2O/SiO_2=0.29 in **Figure 3.7**(a) and (b) is mainly a consequence of higher amount of silanols in the silicate network. Qualitatively, we explain the foaming mechanism by an out-of-equilibrium build-up of water vapor pressure inside the material after the xerogel transition, when the material becomes too viscous (especially in a dried skin) for water to diffuse out of the material.

Extensive volumetric expansion observed for Na-silicates is, thus, a consequence of the release of proton-related species from the system present as silanols and solvating water molecules with the concentration of Na ion in the network also playing a role in increasing network mobility. The impact of changing the alkali type was also investigated in order to draw a comparison in the thermal behavior of each system. 2 ml solutions (in 5 cm long glass vials) of Na, K and Li-silicates were heated to 250°C, maximum achievable temperature, in a rate-controlled oven to compare the different molar ratios and the corresponding impact of heating rate on their foaming behavior. **Figure 4.2**(a) shows all the solutions before thermal treatment where the height of each solution is 5 mm. Na-silicates show extensive foaming with more expansion observed for Na_2O/SiO_2=0.5 as discussed above, irrespective of the heating rate, and shown in **Figure 4.2**(b), (c) and (d). However, reducing the heating rate tends to reduce the extent of expansion in both cases i.e. going from a heating rate of 10°C/min (**Figure 4.2**(b)) to 1°C/min (**Figure 4.2**(d)) reduces the expansion from 450% to 280%, respectively, owing to a reduction in the abruptness of water release form the system.

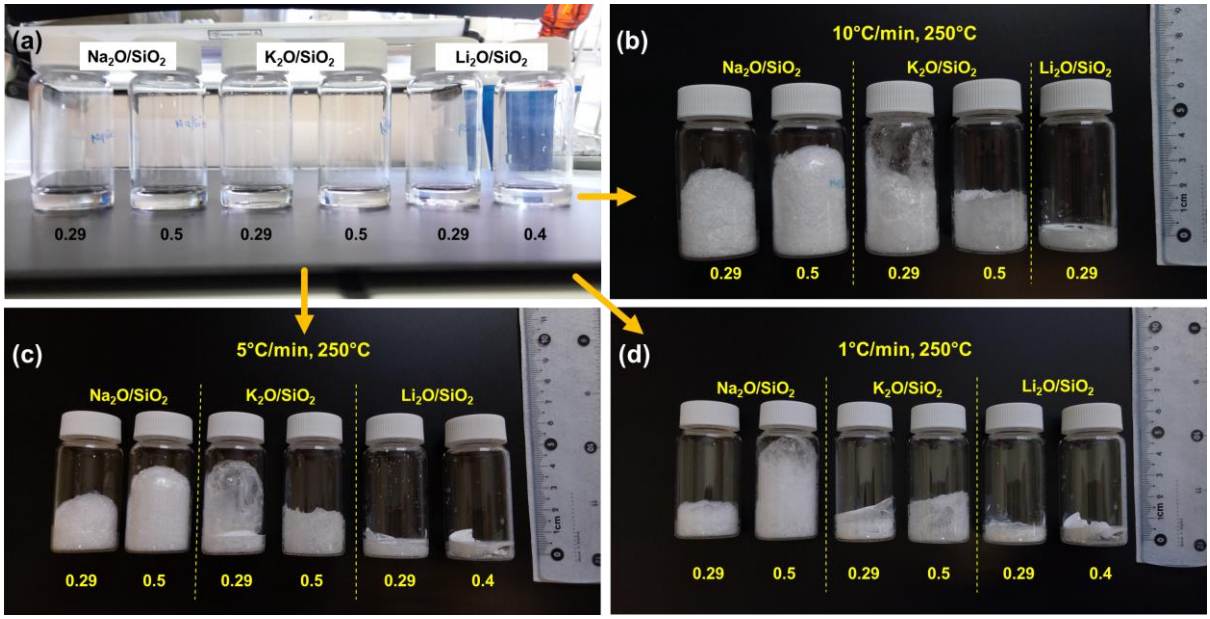

Figure 4.2: Aqueous alkali silicates of two different compositions each in glass vials (a) before and (b, d, f) after heat treatment to 250°C. 2 ml initial solution was used in each case with an initial height equivalent to 5 mm in the measurement scale shown in (b, d, f). (b) 10°C/min, (c) 5°C/min and (d) 1°C/min heating ramps were used for the rate-controlled oven set at 250°C.

K-silicates foam as well[53] with extensive foaming (more than Na_2O/SiO_2=0.29) at 10°C/min observed especially in the case of K_2O/SiO_2=0.29 shown in **Figure 4.2**(b) suggesting a behavior similar to that observed for Na-silicates. K_2O/SiO_2=0.5 does not expand as much due to the fact that the composition has, up to 300°C, a water content that is relatively more thermodynamically stable as compared to K_2O/SiO_2=0.29 (refer to phase diagrams in **Chapter 3**) and Na-silicates discussed in the phase diagrams shown in **Figure 3.10** with the resulting foam being relatively hollow (and hygroscopic) when viewed from the top. Reducing the heating rate tends to impact quite a bit the way K-silicates behave, in particular for K_2O/SiO_2=0.29. The behavior of K_2O/SiO_2=0.5 is not influenced much on going from 10°C/min to 1°C/min with a minor reduction in the extent of the foam. However, foaming seems to have been suppressed for K_2O/SiO_2=0.29 with 470%

expansion observed at 10°C/min to a roughly non-foamed state at 1°C/min as shown in **Figure 4.2**(d). This suppression of foaming is in fact a consequence of crystallization (formation of $KHSi_2O_5$) as discussed extensively in **Chapter 3** that tends to render the network of the material relatively less mobile (and more viscous) with K ions and silanol protons leaving the amorphous matrix to participate in crystallization. Even at a rate of 5°C/min (**Figure 4.2**(c)), the system does not expand as extensively as that observed at 10°C/min, and foaming seems to have been suppressed due to crystallization. Note that the apparent foam type shape for K_2O/SiO_2=0.29 in **Figure 4.2**(c) is in actual a small portion of the silicate that expanded, but it is completely hollow from inside like a bubble with the major mass of the material limited to roughly 70% expansion from initial volume of the liquid.

No apparent foaming seems to occur in Li-silicates but rather a dried powder is obtained, irrespective of the composition and heating rate as shown in **Figure 4.2**. This stems from the fact that our starting compositions are in the phase separation regime[93] where the very viscous SiO_2 matrix phase, that is supposedly independent of any silanols or Li ions, is much less mobile (discussed in details in **Chapter 3**). A further heating to temperatures approaching 400°C might have an influence on the expansion as network silanols and all the Li ions leave the system (with Li participating in crystallization) at temperatures approaching 350°C (**Figure 3.23**(e) and (f)) but a drastic change is not expected.

Briefly, Na-silicate solutions foam extensively without any limitations posed by crystallization or phase separation for the composition range studied, while crystallization tends to suppress foaming in K-silicates. Li-silicates don't show any foaming on thermal treatments up to 250°C, a consequence of the studied compositions being in the phase separation regime. Ideally, microscopic structural investigation starting directly from the solutions would have provided with a more real-time evaluation of the systems. However, due to the foaming-related limitations (i.e. powder falling out of the crucible on heating) posed by the experimental techniques like TGA, solutions could not be directly used for the measurements shown in **Chapter 3**, so a pre-drying step was necessary.

4.1.2. Pre-dried powders

Pre-dried powders were prepared by drying the solutions at 150°C (below the foaming temperature) for 17 h to remove all the free water. In order to investigate the effect of this pre-drying step on the foaming behavior, powder pellets were prepared to follow their thermal evolution under a Hot-stage Microscope as shown in **Figure 4.3**. Na_2O/SiO_2=0.29 pre-dried powder pellet, when heated to 400°C at 10°C/min, shows extensive foaming[61] (**Figure 4.3**(a)) similar to how solution evolves above 200°C suggesting that foaming is indeed a consequence of the condensation and removal of solvating water molecules and is not influenced much by the quantity of free water in the system.

Heating a pre-dried K_2O/SiO_2=0.29 pellet does not show any expansion as the system is crystallized (**Figure 4.3**(b)) i.e. longer drying times seem to favor the formation of crystallites[21] that in turn suppress any expected structural expansion. **Figure A 4.1** shows the impact of drying time

at 150°C on foaming of K_2O/SiO_2=0.29. A 15 min drying time is not enough for the system to crystallize and thus on further thermal treatment to 300°C, extensive foaming is observed as the network is mobile enough to expand. Drying for 3 h results in crystallization (that seems to be saturated) with the formation of $KHSi_2O_5$ phase suppressing foaming altogether. So, a pre-drying step of 17 h induces enough crystallization in the K_2O/SiO_2=0.29 powder to prevent any foaming.

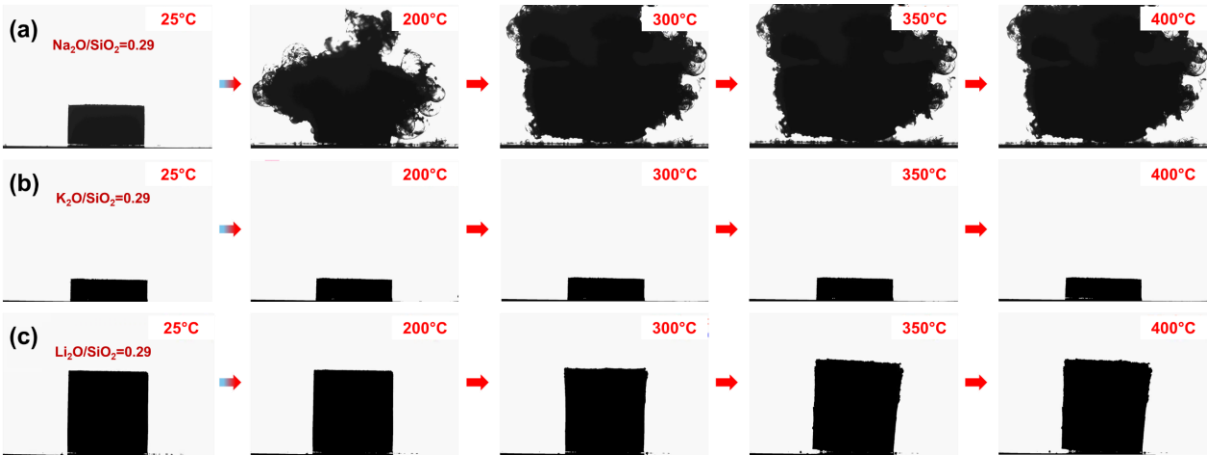

Figure 4.3: Thermal behavior up to 400°C, under a 10X Objective Hot-stage Microscope, of (a) Na_2O/SiO_2=0.29 (at 10°C/min), (b) K_2O/SiO_2=0.29 at (10°C/min) and (c) Li_2O/SiO_2=0.29 (at 5°C/min) pre-dried powder pellets prepared by drying solutions at 150°C (for 17 h) using a 5 mm die and a load of 1 ton.

No foaming is observed for Li_2O/SiO_2=0.29 pre-dried pellet either, but up to 250°C above which a very slight expansion is observed on going all the way to 400°C as shown in **Figure 4.3**(c). This arises from the fact that even though the starting composition is in the phase separation regime and the matrix phase is pure SiO_2 that should prevent any foaming from occurring, the release of leftover silanols from the amorphous Li-silicate network (that is still mobile) at 275°C (discussed in **Figure 3.23**(e)) is enough to cause this expansion visible under a microscope. Furthermore, crystallization seems to happen within the same temperature range starting at 275°C with all Li ions leaving the amorphous phase at 350°C leading to the formation of $Li_2Si_2O_5$ and Li_2SiO_3 crystalline phases. Crystallite formation might also be a reason for the slight expansion observed up to 350°C above which no further expansion is observed.

Thus, the volumetric expansion observed in pre-dried alkali silicate powders is dependent on whether the system crystallizes or phase separation takes place. Pre-dried Na-silicates foam extensively, K-silicates don't due to crystallization while Li-silicates also don't foam due to phase separation and crystallization. Hence, a global fundamental understanding has been established for the thermal evolution of these aqueous alkali silicates in terms of their foaming properties by creating a link between macroscopic and microscopic structural variations that is expected to help in providing some solutions to application-related challenges. These include utilization or tuning of foaming for fire-resistant applications or others where foaming may not be required. The understanding of the influence of heating rate and composition (amount of water, alkali content) is expected to open up possibilities of developing targeted systems for catering industrial needs.

Employment of such systems especially as thick coatings (>50 µm) for industrial applications is important but limited and demands an investigation into the thermal behavior as rheological

issues related to inhomogeneous and cracked coatings have been reported. Prior studies were mostly concerned with properties of thin films[11,50] that were homogeneous but do not inform about thick coatings and their corresponding thermal properties. Therefore, it is important to investigate the possibilities of developing homogeneous, thick and high-quality coatings to follow their thermal evolution as a starting approach towards achieving industrially viable systems.

4.1.3. Deposition as coatings

4.1.3.1. Thin films

Deposition of homogeneous thin films (200-250 nm) is possible by spin coating the aqueous solutions onto a silicon wafer or glass substrate. **Figure 4.4**(a) shows a 250 nm Na_2O/SiO_2=0.29 thin film spin coated at 2000 rpm for 60 s that happens to be homogeneous and without cracks. Thermal treatment (450°C) leads to a reduction in thickness (around 60%) as a consequence of condensation as shown in **Figure 4.4**(b). Further analysis suggests the formation of surface carbonates[11] (**Figure 4.4**(c) and (d)) due to a supposed diffusion of Na ions towards the surface where a reaction with atmospheric CO_2 results in the formation of Na_2CO_3.

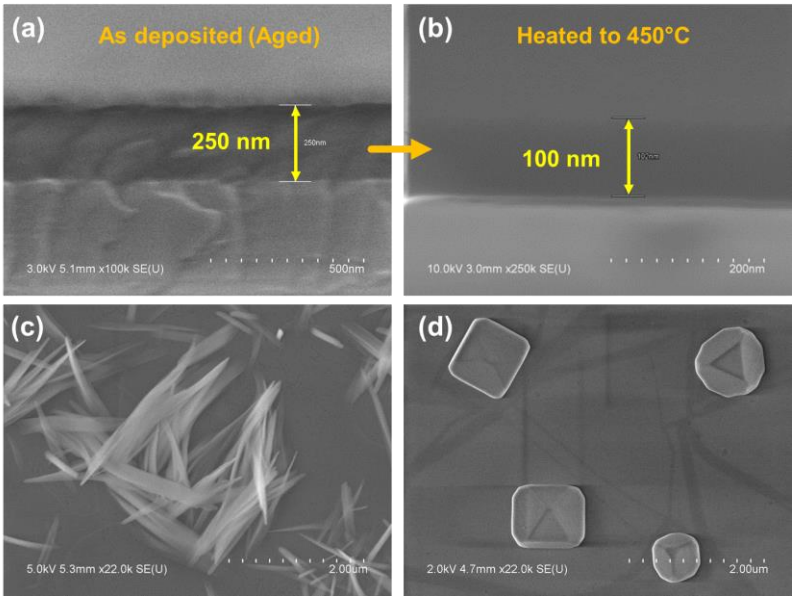

Figure 4.4: SEM image of Na_2O/SiO_2=0.29 thin film spin-coated on a silicon wafer at 2000 rpm for 60 s (a) before and (b) after thermal treatment to 450°C indicating a reduction in thickness due to condensation while surface carbonates in the form of (c) petals and (d) crystals appear on the surface on ageing.

Fourier-Transform Infra-Red (FT-IR) spectra of the corresponding as-deposited film is shown in **Figure 4.5**(a). On ageing the film for a few days, carbonation peaks tend to appear at 860 cm^{-1} and 1440 cm^{-1}. These peaks keep on increasing in intensity due to the continuous diffusion of ions. After 2 weeks of ageing under ambient conditions, these surface carbonates start converting into HCO_3^- as a result of prolonged exposure to moisture in the atmosphere. Carbonation is detrimental to overall mechanical properties of the system as the structure tends to become brittle due to the continuous loss of Na ions, leaving the network more polymerized and relatively less flexible.

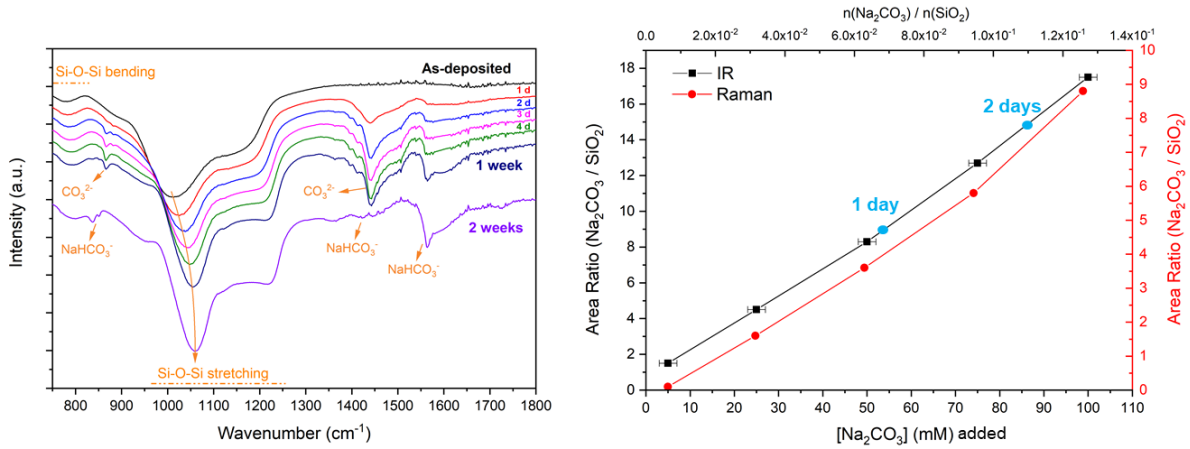

Figure 4.5: (a) FT-IR spectra of Na_2O/SiO_2=0.29 thin film and (b) amount of carbonates inside the starting Na_2O/SiO_2=0.29 solution and thin film upon ageing (the initial solution corresponds to the molar ratio Na_2CO_3/SiO_2=0.28). The two blue points in (b) represent the amount of surface carbonates that have been formed on ageing a thin film obtained from a non-carbonated commercial Na_2O/SiO_2=0.29 solution.

For investigating the stability of starting solutions regarding carbonation and to be sure that carbonates on the surface were formed after deposition of the film, a study was performed to check for the amount of dissolved carbonates in the commercial Na_2O/SiO_2=0.29 solution. A known concentration of Na_2CO_3 was added into the original solution followed by the deposition of corresponding solution to form a thin film. FT-IR spectra were obtained and the relative area of the carbonate peak was plotted against the initial concentration of dissolved carbonates in the solution as shown by the black curve in **Figure 4.5**(b). A maximum concentration of 4 mM corresponding to dissolved carbonates was obtained which is negligible as compared to the initial total amount of Na ions (3.6 M) in the commercial solution, thus, indicating that the initial solutions were not carbonated. This plot has also been utilized to study the kinetics of carbonation in thin films as shown by the blue dots in **Figure 4.5**(b) indicating 10% Na ions to have been converted into carbonates after 2 days.

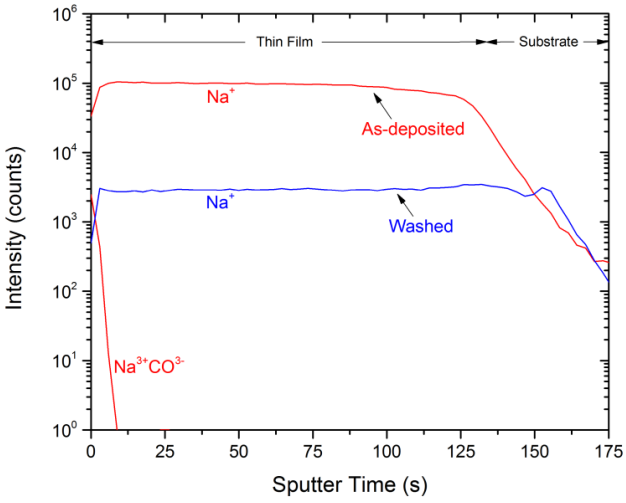

Figure 4.6: Na^+ ion diffusion profiles for Na_2O/SiO_2=0.29 thin film using the O_2 cluster source in TOF-SIMS at -100°C.

Mass diffusion of ions is not only towards the surface that results in the formation of surface carbonates, but also towards the interface if the substrate is glass that can further impact the overall properties of the film. A detailed analysis on the diffusion-related aspects of alkali ions is also necessary to fully understand the microscopic structural details and the relevance with thermal treatments. Thus, this two-way mobility needs to be characterized thoroughly to be able to control or limit the movement of Na ions but that is out of the scope of the work reported here. However, to aid in possible future studies, extensive calibration of parameters was done on secondary ion mass spectroscopy (SIMS) with profiles shown in **Figure 4.6** and **Figure A 4.2**. To obtain the distribution of ions, diffusion profiles of Na were acquired throughout the Na_2O/SiO_2=0.29 spin coated thin film on silicon wafer substrate. Different sputter sources were used for SIMS analysis, including O_2^+ ion source, Cs^+ ion source and O_2 cluster source at room temperature and low temperature (-100°C), to calibrate the diffusion profiles of Na^+. O_2 cluster source at low temperature gave the best profiles as shown in **Figure 4.6** suggesting a homogeneous distribution of ions within the depth of the film. On washing the deposited film with water, surface carbonates as well as Na^+ ions in the film are removed resulting in films that rarely carbonate any further but at the expense of mechanical properties.[11]

Spin coating route generally allows to deposit thinner films (few 100s of nm) that are quite homogeneous and without any cracks. From a more industrial point of view, the requirement is to deposit thicker coatings with thickness in the order of 10s of microns. Furthermore, thin films are not easy to characterize in terms of structural properties using Raman spectroscopy where the resolution is not enough and thickness values >5 µm are generally preferred to reduce substrate contribution. The upcoming section discusses the possibilities of depositing thicker coatings using various methods, along with the impact of thermal treatment in terms of the foaming-related evolution to draw comparisons with solutions and powder systems studied earlier.

4.1.3.2. Thick coatings

Coatings that are thick are expected to be cracked as a consequence of the accumulation of strains due to composition and rheological issues related to viscosity and water release. Na_2O/SiO_2=0.5, having a lower viscosity than Na_2O/SiO_2=0.29, is expected to result in relatively crack-free coatings and, thus, was chosen for some initial experiments in the process of determining the possibility of achieving thicker coatings from other alkali silicate compositions and the corresponding impact of thermal treatments.

4.1.3.2.1. Spin coating

Thicker coatings can be deposited by spin coating. **Figure 4.7** shows the SEM images of coatings obtained by changing the starting concentration of Na_2O/SiO_2=0.5 solution used for deposition at 2000 rpm and 60 s. An 800 nm thick coating condenses (instead of foaming as observed for solutions and powders) on heating to 400°C (**Figure 4.7**(a) and (b)). Depositing raw commercial solution without any dilution leads to a coating with thickness approaching 4 µm that is homogeneous and crack-free as shown in **Figure 4.7**(c). A further increase in thickness values approaching 9 µm (**Figure 4.7**(d)) is possible, without inducing inhomogeneities or cracks before thermal treatment, by depositing multiple layers of the same solution one above the other once

the initial coating is pre-dried at 60°C for 5 min. Thus, thicker coatings have been developed through spin coating. However, the process is time consuming and is limited to a few 10s of micron thickness values along with posing limitations of substrate size, making it is less relevant for industrial scale tests.

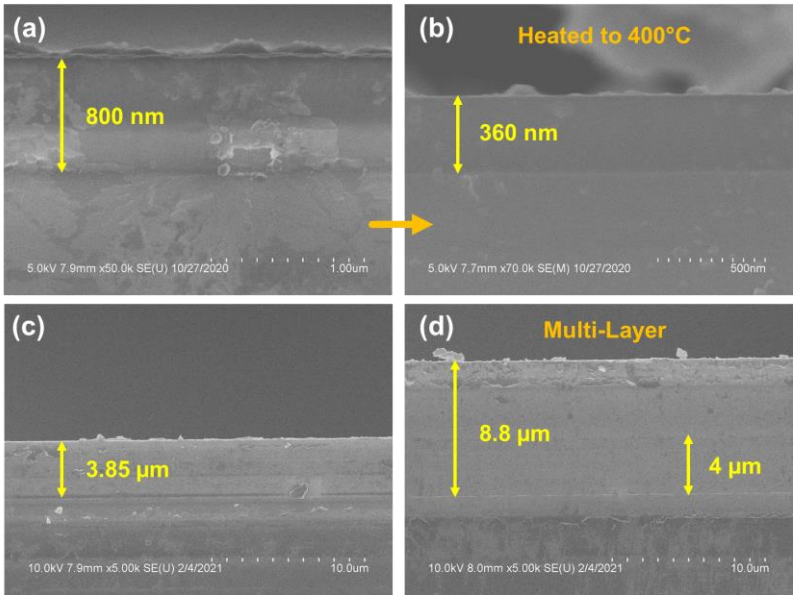

Figure 4.7: SEM image of thicker coatings obtained from the spin coating route at 2000 rpm, 60 s for Na_2O/SiO_2=0.5 by changing the concentration of the starting solution with 3 M solution (in terms of c[SiO_2]) film (a) before & (b) after heating to 400°C while (c) single and (d) multiple thick layers obtained from raw as deposited 5.7 M (in terms of c[SiO_2]) commercial solution.

4.1.3.2.2. Blade/Pool coating

A homogeneous 30 µm thick Na_2O/SiO_2=0.5 coating, as shown by the SEM image in **Figure 4.8**(a), can be developed by creating a pool for the solution to dry in. Note that the surface roughness on the cross-section is due to the cutting procedure and not the actual aspect of the coating itself. **Figure 4.8**(b) shows a 1 mm thick coating on glass substrate deposited using the same method. Heat treating thicker coatings of the order of 10s of microns leads to extensively foaming[1,21,47] as evident from the heat treatment at 300°C in **Figure 4.8**(b).

The striking contrast in the behavior of thin films condensing while thicker films foaming on thermal treatment suggests the existence of a critical thickness for foaming to occur. To probe the existence of this behavior, raw Na_2O/SiO_2=0.5 solution was spin coated to obtain single and multiple layer samples as shown in **Figure 4.8**(c). A single layer of 4 µm thickness does not foam on heating to 400°C while 2, 3 and 4 layered samples show extensive foaming with an increase in the size of foam with thickness of the coating giving a clear indication of a critical thickness for foaming.

4.1.3.2.3. Gradient coating

Na-silicates

A homogeneous gradient in thickness coating was deposited on a glass plate using a thickness adjustable bar coater with values set to 10-100 µm. The critical thickness value of around 6 µm (after drying and before thermal treatment) is observed for Na_2O/SiO_2=0.5 on heating to 300°C

above which a gradual increase in foam bubbles is observed as shown in **Figure 4.8**(d), (e) and (f). The existence of such a behavior is linked to the release of water from the system.

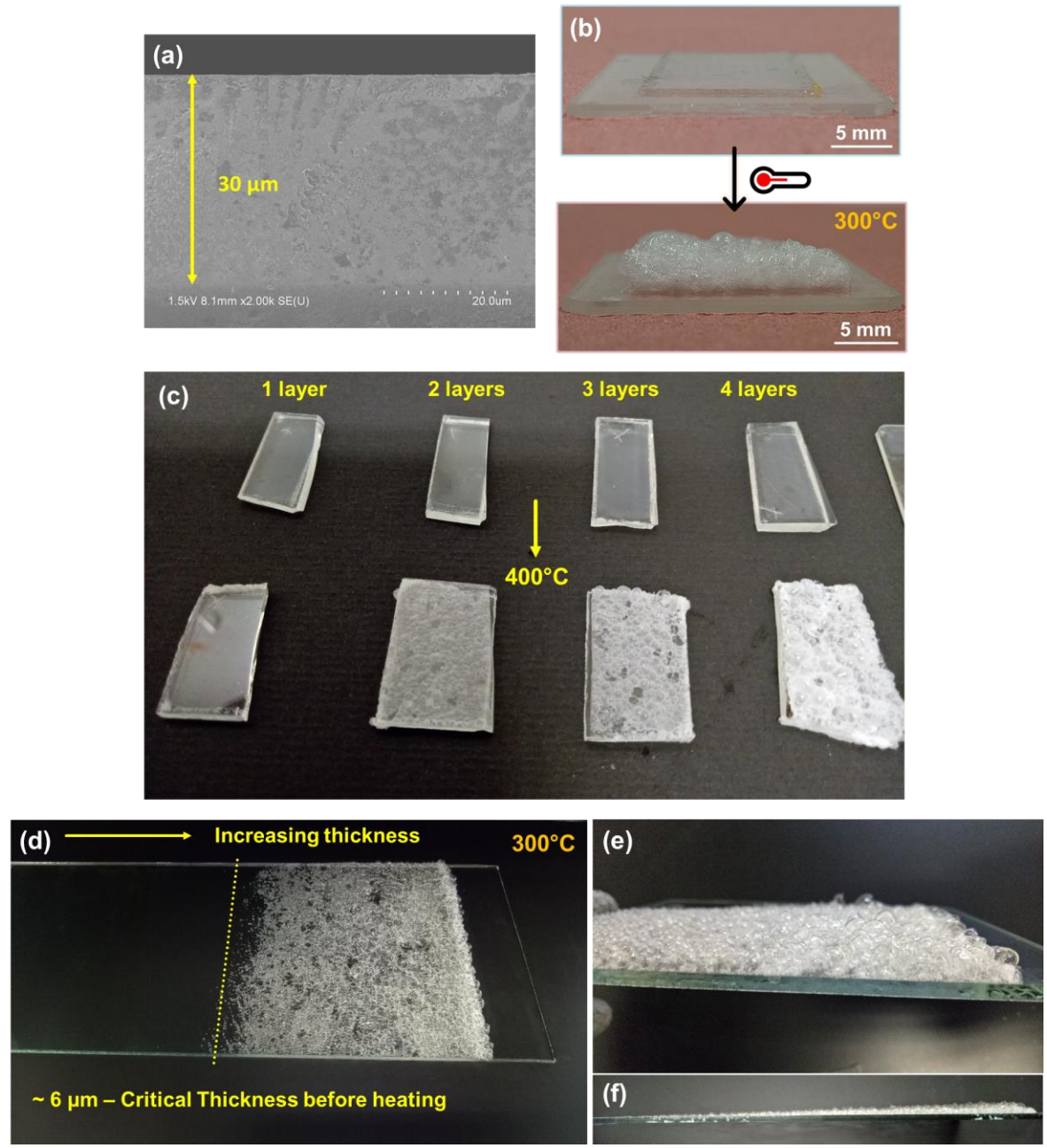

Figure 4.8: Thick Na_2O/SiO_2=0.5 coatings: (a) SEM image of a 30 µm, (b) 1 mm thick coating (before and after heating to 300°C) obtained from blade/pool coating route, (c) single and multi-layer coatings (before and after heating to 300°C) obtained from the spin coating route at 2000 rpm for 60 s, (d) gradient coating (after heating to 300°C) obtained by depositing raw solution using a bar coater (note that the bar was set to the range 10-100 µm) showing the existence of a critical thickness for foaming and (e, f) close-up images of the foam showing a gradual increase in bubble size as a function of thickness.

Figure 4.9 shows the schematic illustration of the proposed mechanism for the existence of critical thickness for foaming. On heating a gradient in thickness coating, surface condensation takes place due to the release of water molecules closer to the surface resulting in a condensed layer of a particular thickness value depending upon the starting composition. The thickness of this condensed layer is proposed to be related to the diffusion length of evaporating water

molecules. Below the critical thickness, the coating is a fully surface condensed membrane as that observed on heating the solutions (**Figure 4.1**) preventing any extensive condensation leading to foaming. Above the critical thickness, water is available under this surface condense layer that escapes on increasing temperatures and provides the necessary driving force for expansion.

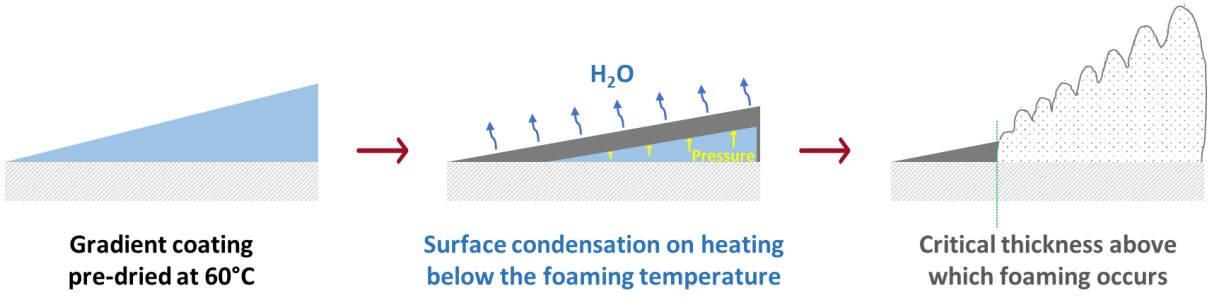

Figure 4.9: Schematic illustration of the existence of critical thickness for foaming in gradient coatings.

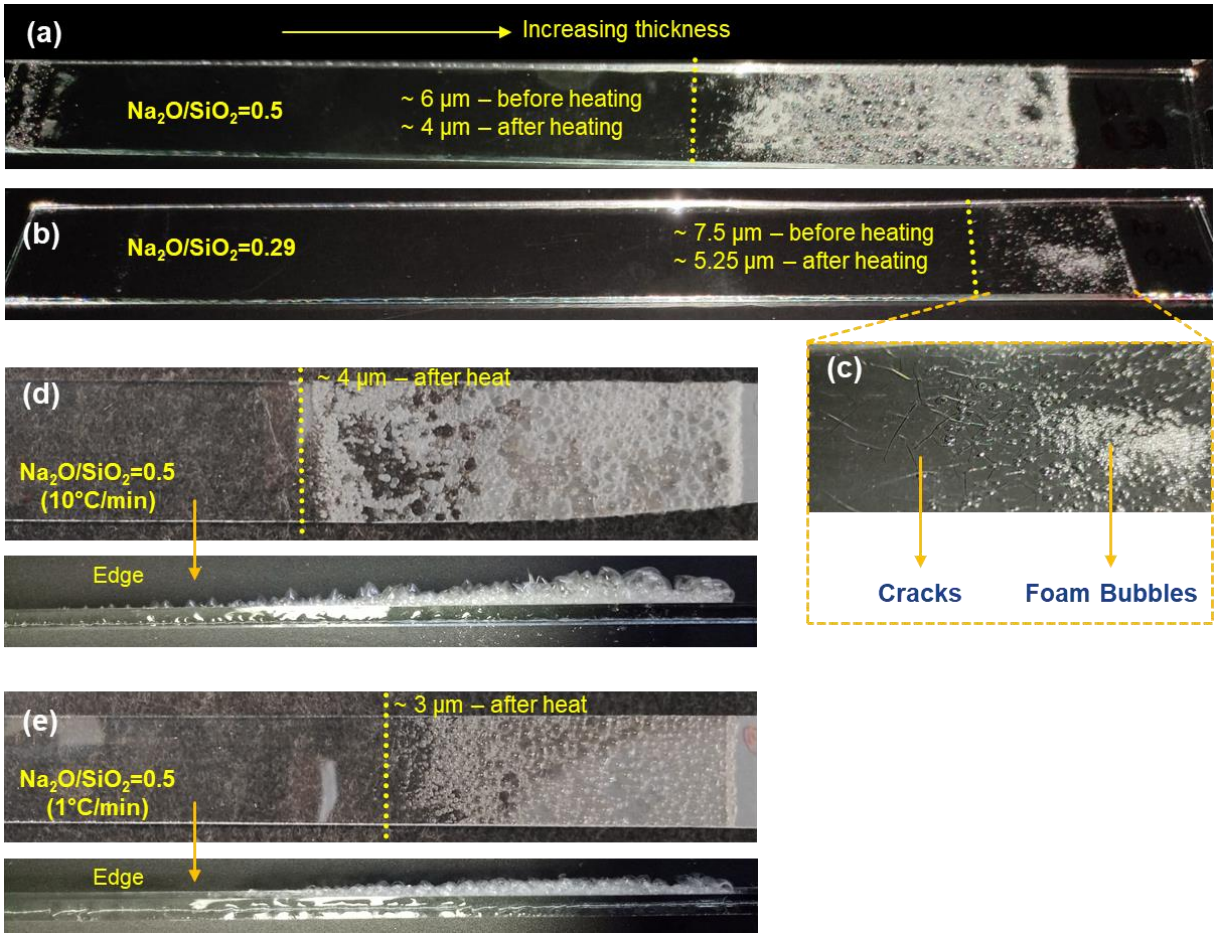

Figure 4.10: Na-silicate gradient coatings (obtained from bar coating method with bar values set to 10-100 µm) after heating to 250°C: (a) Na_2O/SiO_2=0.5 at 5°C/min, (b) Na_2O/SiO_2=0.29 at 5°C/min, (c) close-up image of Na_2O/SiO_2=0.29 coating above the critical thickness showing the presence of both cracks and foam bubbles and Na_2O/SiO_2=0.5 gradient coating at a heating rate of (d) 10°C/min & (e) 1°C/min.

Figure 4.10 shows the impact of changing the Na-silicate concentration on the corresponding thermal behavior. Na_2O/SiO_2=0.29 also shows a critical thickness for foaming (**Figure 4.10**(b)) but

a higher value of 7.5 µm (before heating) is observed in contrast to 6 µm seen for Na_2O/SiO_2=0.5 system mainly due to a reduced mobility and amount of silanols in the system as that seen for pre-dried powder samples.

The difference in the critical thickness region values before and after heating are given in **Figure A 4.4**. which show a condensation of the coating below the critical thickness. Furthermore, the Na_2O/SiO_2=0.29 coating tends to crack on heating to 250°C at 5°C/min as shown in **Figure 4.10**(c) due to the release of strains generated in the structure linked, again, to the increased viscosity, reduced mobility and lower amount of network silanols as predicted from the discussion in **Chapter 3**.

The impact of heating rate was also investigated in order to analyze the variations in critical thickness of foaming and is shown for Na_2O/SiO_2=0.5 in **Figure 4.10**(d) and (e) where the coating was heated to 250°C at 10°C/min and 1°C/min, respectively. A difference of 1 µm is observed on going from 10°C/min to 1°C/min suggesting not a drastic impact of the heating rate. Furthermore, the extent of expansion of bubbles is higher for the high heating rate due to the abruptness of the water release. Thus, the critical thickness and extent of foaming seems to be mainly dependent upon the composition of Na-silicates similar to what is observed in solutions and pre-dried powders which also show extensive foaming.

K-silicates

Foaming behavior of K-silicate solutions and pre-dried powders is dependent upon the composition as well as kinetics of thermal treatment in the sense that crystallization plays a role in suppressing volumetric expansion. Impact of thermal treatment on gradient coatings (bar value set at 10-250 µm) for the two K-silicate molar ratios deposited from the aqueous solutions is given in **Figure 4.11**. K_2O/SiO_2=0.5 gradient coating on heating to 250°C at 5°C/min shows a behavior similar to that observed for Na_2O/SiO_2=0.5 with the existence of a critical thickness for foaming (**Figure 4.11**(a)), however, the exact value could not be determined due to difficulties in acquiring SEM images as the sample was very hygroscopic.

K_2O/SiO_2=0.29, on the other hand, seems to have two critical thicknesses: for (1) crystallization (light scattering by crystals) which approaches 4.4 µm (before heating) and (2) foaming, for which the value could not be ascertained, as shown in **Figure 4.11**(b). The corresponding SEM images showing cross-section of the coating are given in **Figure A 4.5**. Above the critical thickness (2), crystallization and foaming seem to co-exist (synonymous to the behavior of solution at 5°C/min as shown in **Figure 4.2**(c)) suggesting that the heating rate might have an influence on the thickness for foaming. A lower heating ramp would thus be expected to either fully suppress foaming or shift the corresponding critical thickness to values larger than the experimental limits of the bar. Orthorhombic and monoclinic $KHSi_2O_5$ crystallites are formed (as in pre-dried powders) up to 250°C as shown in **Figure 4.11**(d) and (e) along with the appearance of $KHCO_3^-$ corresponding to the formation of some surface carbonates due to diffusion of ions. Appearance of crystallites is a consequence of the network releasing protons and some K ions.

Heating the K_2O/SiO_2=0.29 sample to 450°C leads to the melting of these crystallites, a behavior similar to pre-dried powders of the same composition, with SEM image in **Figure 4.11**(e) showing the respective grain boundaries of melted crystallites and XRD diffractogram in **Figure 4.11**(f) indicating the disappearance of $KHSi_2O_5$ phase. Furthermore, the coating becomes transparent on heating to 450°C as shown in **Figure 4.11**(c) once the whitish aspect due to crystallization is gone.

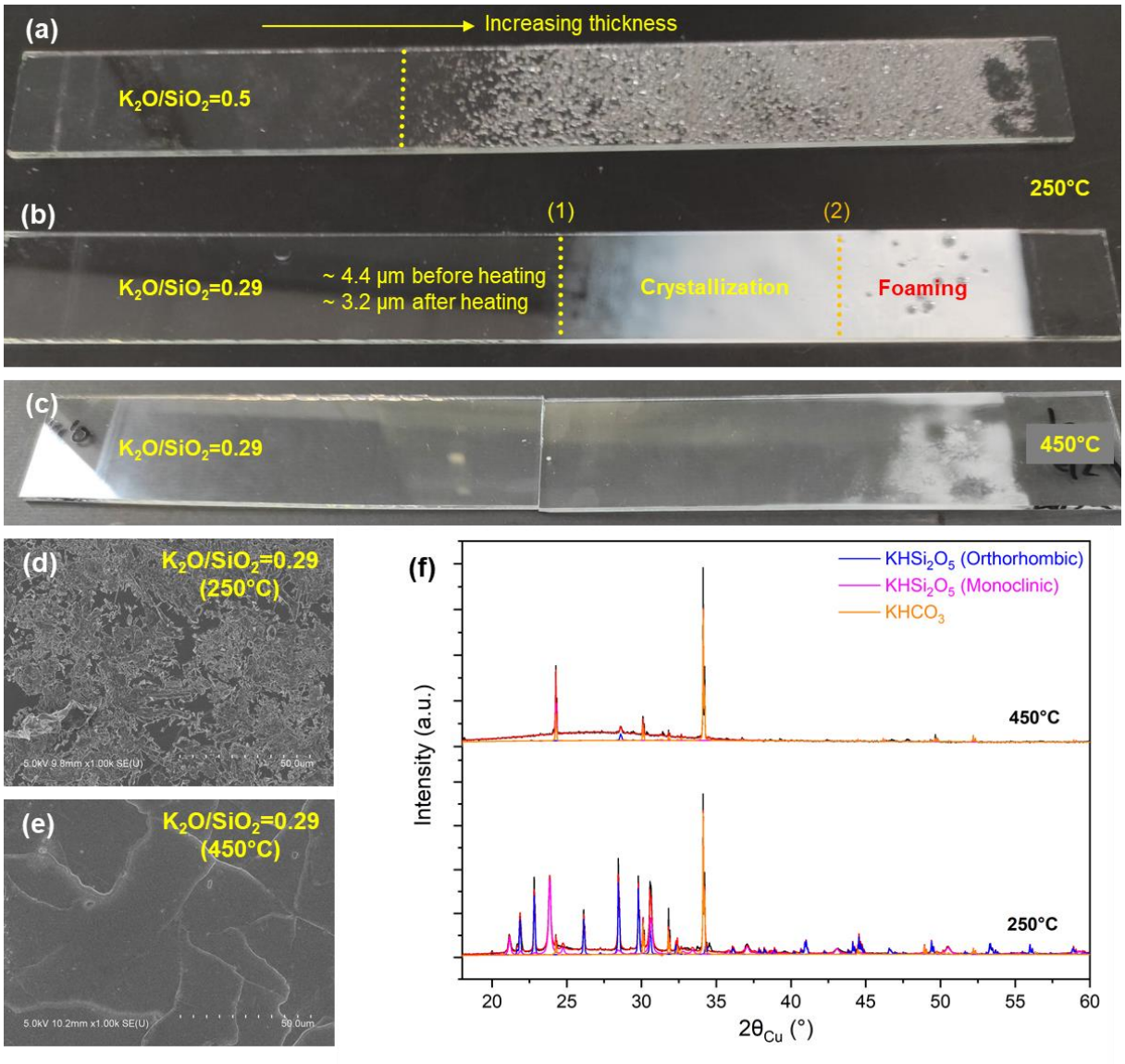

Figure 4.11: K-silicate gradient coatings heated at 5°C/min: (a) K_2O/SiO_2=0.5 (bar was set to 10-100 µm) to 250°C, K_2O/SiO_2=0.29 (bar was set to 10-250 µm) to (b) 250°C & (c) 450°C with the respective SEM images in (d) & (e) and (f) XRD confirming the presence of $KHSi_2O_5$ (Monoclinic-C2/m: JCPDS 00-045-0020, mp-1201235; Orthorhombic-Pcmn: JCPDS 01-083-2393, ICSD 200612) as well as $KHCO_3$ (Monoclinic-P21/a: JCPDS 01-070-0995, ICSD 002074).

K-silicates, thus, show a critical thickness irrespective of composition with K_2O/SiO_2=0.5 showing a critical thickness for foaming while K_2O/SiO_2=0.29 exhibiting a critical thickness for crystallization as well as foaming at 5°C/min.

Li-silicates

Li-silicate gradient coatings obtained by setting bar values to 10-100 µm and thermally treated to 250°C at 5°C/min show the existence of critical thickness of cracking rather than crystallization or foaming as shown in **Figure 4.12**(a) and (b). This stems from the fact that the starting Li-silicate compositions are relatively concentrated in the quantity of SiO_2 because not all the Li ions are a part of the network. Li ions are also present as LiOH that leaves the network more brittle and strained. Since the compositions are in the phase separation regime, heat treatment leads to cracking rather than foaming consistent with the results obtained for solutions or pre-dried powders. A higher critical thickness value is observed for Li_2O/SiO_2=0.4 than Li_2O/SiO_2=0.29, a behavior similar in all the alkali silicates investigated. A homogeneous aspect of the coating is observed for Li_2O/SiO_2=0.4 while Li_2O/SiO_2=0.29 presents micro-cracking even below the global critical thickness as evident from the SEM images in **Figure 4.12**(e) and (f), respectively.

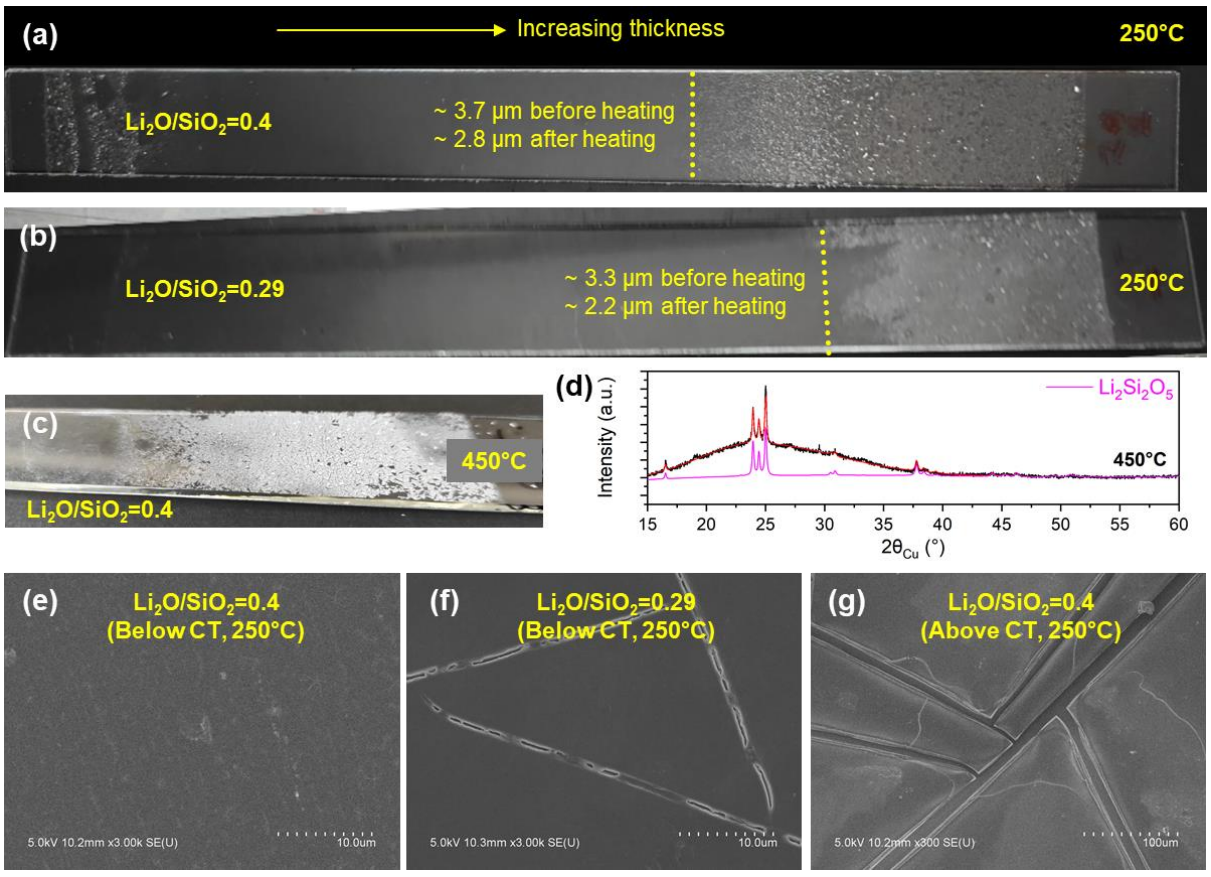

Figure 4.12: Li-silicate gradient coatings heated at 5°C/min (bar was set to 10-100 µm): (a) Li_2O/SiO_2=0.4 to 250°C, (b) Li_2O/SiO_2=0.29 to 250°C, (c) Li_2O/SiO_2=0.4 to 450°C, (d) XRD confirming the presence of $Li_2Si_2O_5$ (Orthorhombic-Ccc2: JCPDS 01-072-0102, ICSD 15414)) at 450°C and (e, f, g) SEM images below and above the critical thickness.

Heat treating the systems to 450°C leads to crystallization mainly in the region above critical thickness, as shown in **Figure 4.12**(c) and confirmed by XRD in **Figure 4.12**(d), suggesting the coexistence of cracks and crystallites with the formation of orthorhombic $Li_2Si_2O_5$ phase, seen also in pre-dried Li-silicates above 275°C as discussed in the quantitative analysis in **Chapter 3**. Thus, Li-silicates present a single critical thickness for cracking and crystallization (depending upon the temperature) for both molar ratios. Note that crystallization measurements couldn't be carried

out for Li_2O/SiO_2=0.29 as the coating delaminated due to extensive cracking resulting from the rigidity of the network.

The analysis of flat thick coatings and gradient in thickness coatings discussed above suggests that it is indeed possible to deposit homogeneous, thick and high-quality alkali silicate coatings but that is dependent upon the starting composition and the hydration level. Thermal treatment leads to macroscopic structural changes in terms of the existence of a critical thickness of foaming for Na-silicates and K_2O/SiO_2=0.5, crystallization and foaming for K_2O/SiO_2=0.29 whereas cracking and crystallization for Li-silicates. The existence of the different phenomenon, apart from critical thickness, is consistent with the macroscopic evolution observed for solutions and pre-dried silicates. However, limitations on the possibilities of characterization using tools like ex-situ and in-situ Raman spectroscopy, mainly for the distribution and evolution of proton-related species, has restricted an in-depth analysis synonymous to the one discussed in **Chapter 3** for pre-dried powders. Hence, conclusive discussion has not been provided in terms of the questions related to the existence of various critical thicknesses depending upon the alkali type and, thus, further investigation is required in the category of perspective work.

4.2. Foaming control

Aqueous alkali silicates present a thermal behavior strongly dependent upon the type of alkali ion with Na-silicates showing extensive foaming in solution, pre-dried powder and thick coatings. This intumescent behavior is of industrial interest for applications involving fire-resistant properties e.g. fire-resistant glasses. Tuning their foaming behavior by manipulating the composition can improve the existing systems as well as open new avenues of their potential utilization. Hence, some trials were made to control/limit the extent of this foaming observed by adding some foreign entities in Na-silicates solutions.

4.2.1. Addition of ethylene glycol

Ethylene glycol (EG), an organic compound and a well-known anti-foaming agent[160] with a chemical formula $(CH_2OH)_2$, was mixed with the commercial Na-silicate solutions to be able to limit/control the extent of foaming. **Figure 4.13**(a) shows the foaming behavior of a Na_2O/SiO_2=0.29 solution droplet on heating to 300°C, the detailed description of which has been provided in section **4.1.1**. Adding known quantity of EG into this solution appears to change the thermal behavior i.e. the extent of foaming seems to have been reduced on going up to 300°C as shown in **Figure 4.13**(b). This appears to be a consequence of the release of large amount of solvent before the membrane-like layer is formed as the boiling point of EG is around 200°C reducing considerably the extent of expansion. Furthermore, it may be possible that EG molecules tend to replace the silanols in the Na-silicate network (further investigation required), causing a change in density, and limiting the possibilities of condensation that has been linked to the expansive nature.

The impact of thermal treatment was also investigated on the coatings developed from a mixture (in vol%) of Na_2O/SiO_2=0.5 and EG. **Figure 4.13**(c) shows double-layer spin coated samples (roughly 8 µm thick) of pure Na_2O/SiO_2=0.5 solution with a coating above the critical thickness

value (6 µm). Heating the sample to 250°C causes foaming to occur. On addition of 20 vol% EG in Na_2O/SiO_2=0.5 commercial solution, the extent of foaming is reduced to a large extent. Similarly, very thick coatings (>30 µm in thickness) using the blade/pool coating approach were also obtained from the mixture of the solutions. A similar behavior of reduction in the extent of foaming is observed on increasing the concentration of EG in the silicate from 5 vol% to 20 vol% where the foaming seems to have been suppressed as shown in **Figure 4.13**(d). Thus, EG acts as a reasonable anti-foaming agent by replacing the network silanols to reduce the driving force for structural expansion. However, this anti-foaming property of EG is limited to temperatures below 400°C whereas decomposition of the species at ≥ 500°C leads to structural expansion. The density of the system is expected to be different that could potentially have an impact on the fire-resistant properties at temperatures approaching 500/600°C.

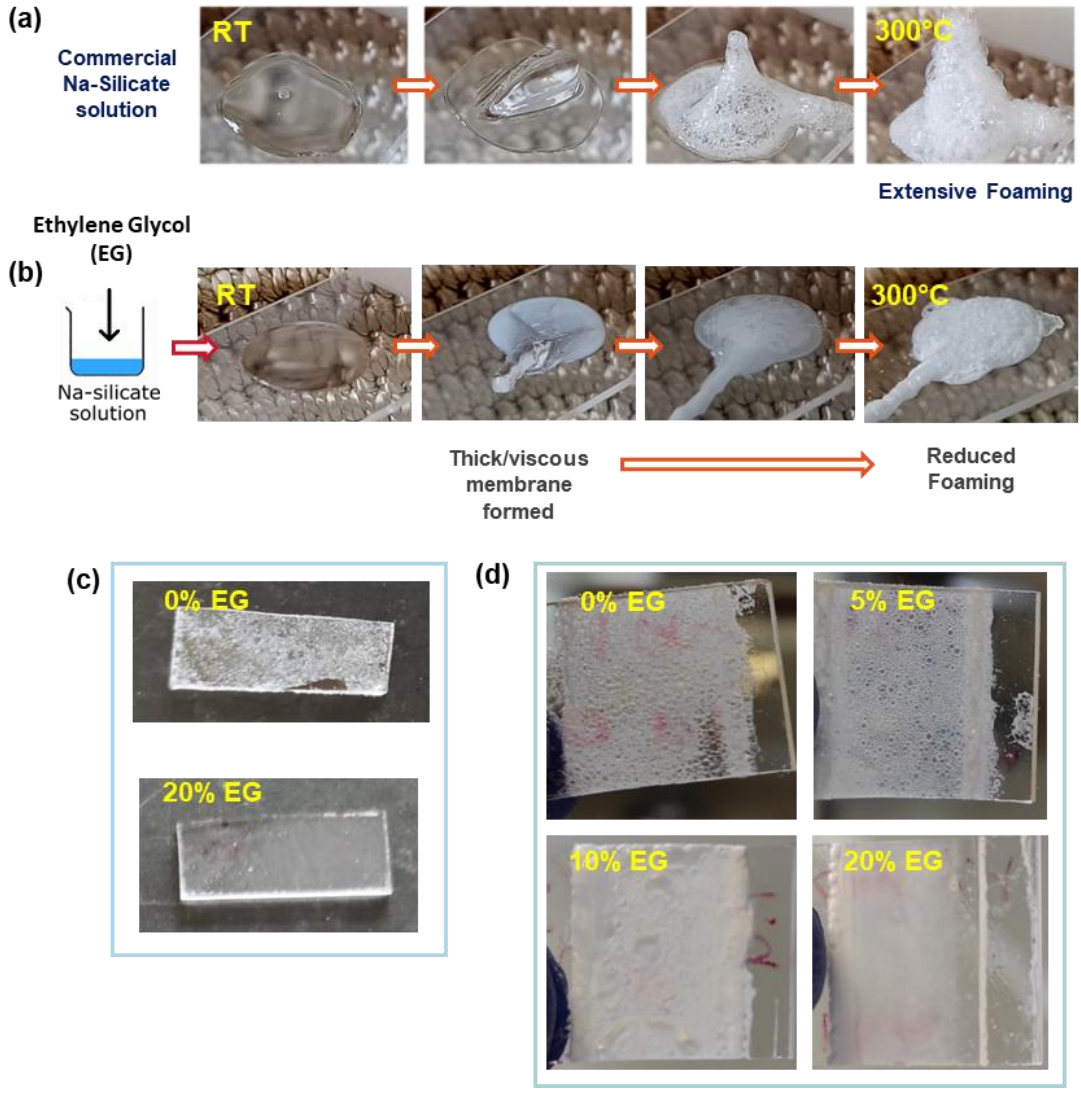

Figure 4.13: Foaming behavior of (a) commercial Na_2O/SiO_2=0.29 & (b) commercial Na_2O/SiO_2=0.29 + Ethylene Glycol (EG) solution droplet, and EG mixed Na_2O/SiO_2=0.5 (c) spin coated (double layer with 8 µm thickness) & (d) blade/pool coated samples (single tape used with thickness=170 µm) heat treated to 250°C. Note that EG was mixed in terms of the vol% indicated.

4.2.2. Addition of tetramethylammonium silicate

Tetramethylammonium silicate (TMAS), with a linear formula $(CH_3)_4N(OH).2SiO_2$, has a structure quite similar to alkali silicates, the main difference being the replacement of alkali ion in the network with organic TMA^+ ion. Thermally treating a thick coating (>30 µm) of TMAS solution to 300°C results in no structural expansion as shown in **Figure 4.14**(a) with the appearance of a whitish aspect all over the coating attributed to the presence of micro-cracks. Thick coatings (>60 µm) obtained from a mixture of TMAS solution in commercial Na_2O/SiO_2=0.5 are shown in **Figure 4.14**(b) suggesting a reduction in the extent of foaming observed in pure Na_2O/SiO_2=0.5 coating on increasing the concentration (in vol%) of TMAS. Even at 10 vol% TMAS, the coating tends to have a different aspect for foaming with the system appearing to be more viscous in terms of its rheological properties. At 50 vol% TMAS, the suppression of foaming seems to appear especially in the middle region while the edges are too thick to show any plausible reduction in foaming. This suggests that the reduction in foaming may well be thickness dependent with very thick TMAS-based coatings offering a lower degree of foaming suppression.

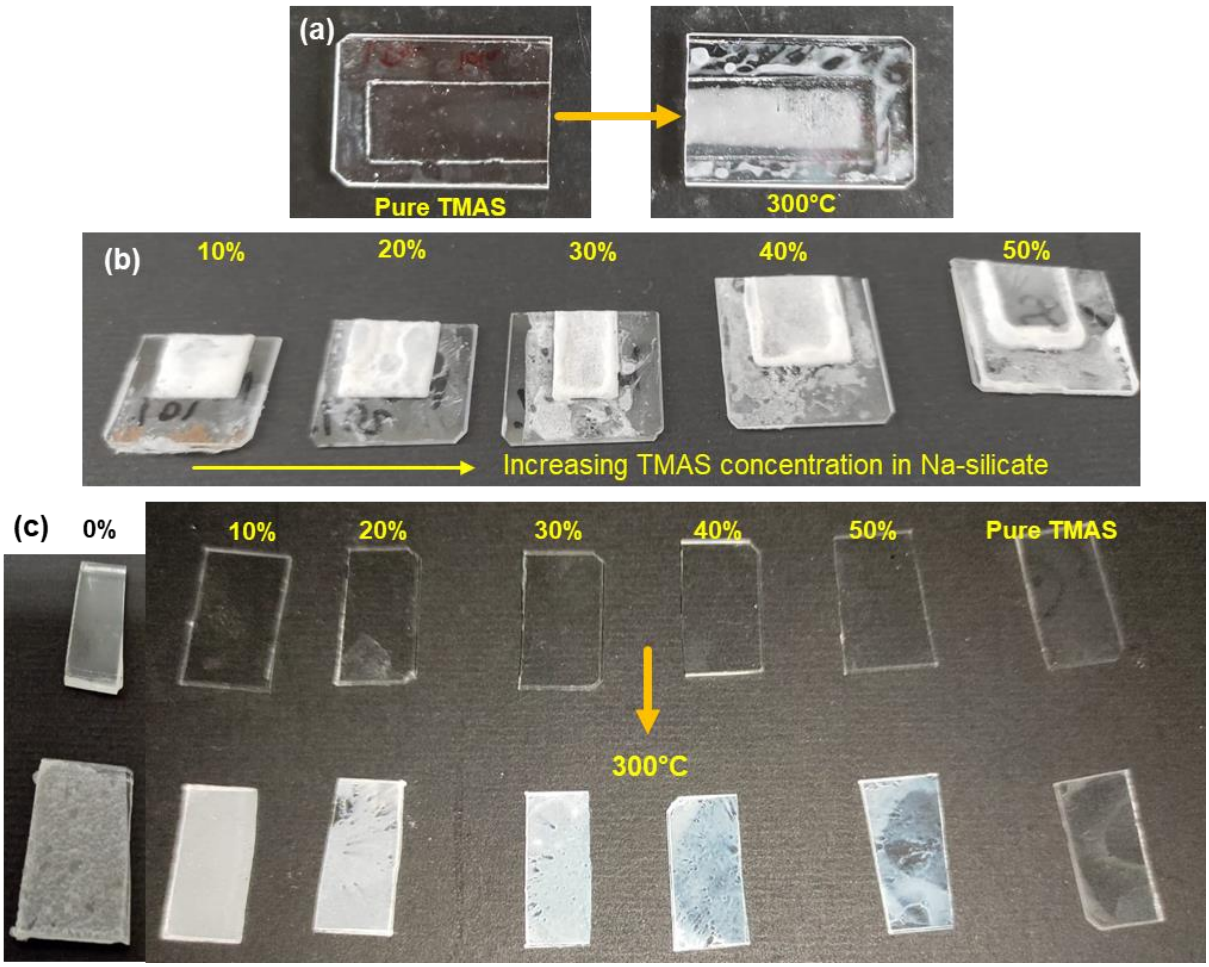

Figure 4.14: Thermal behavior (on heating to 300°C) of (a) pure tetramethylammonium silicate (TMAS) thick coating (single tape used with thickness=170 µm), (b) TMAS mixed Na_2O/SiO_2=0.5 thick coating obtained from blade/pool coating route (two tape layers used with total tape thickness=340 µm) and (c) TMAS mixed Na_2O/SiO_2=0.5 double-layer coating (≥8 µm) obtained from spin coating route. Note that TMAS was mixed in terms of the vol% indicated.

Double-layer spin coated systems (≥ 8 µm thick) offer a similar behavior, in terms of reduction in foaming extent, as that observed for thicker coatings as shown in **Figure 4.14**(c). Pure Na_2O/SiO_2=0.5 coating shows extensive foaming while the addition of TMAS reduces the extent on increasing the concentration with 50 vol% TMAS concentration moving closer to transparency. Note that the whitish aspect in TMAS added coatings **Figure 4.14**(c) corresponds to small-sized foam bubbles (and possibly some by product on thermal treatment that vanishes after a week with coatings appearing relatively transparent). The reason for the suppression of foaming on the addition of TMAS may be attributed to a mechanism similar to that observed with the addition of EG with TMA^+ ions replacing the silanol sites or forming a cross-link with a nearby silanol hindering in a way the condensation reaction. However, further analysis is needed to explore in detail the exact structural changes associated with the addition of TMAS into commercial Na-silicate solution.

Thus, it is indeed possible to reduce the extent of foaming observed in Na-silicates, mainly by the addition of foreign elements that tend to change the viscosity of the system by replacing the silanols in the alkali silicate network. EG and TMAS are two reasonable candidates but an in-depth study needs to be carried out for ascertaining their efficiency keeping in view the industrial priorities as both of these solutions appear to be incompatible with optical transparency.

4.3. Conclusions

Thermally treating aqueous alkali silicates leads to macroscopic structural changes depending upon the type of alkali ion and the corresponding composition of the system. Foaming is observed in some cases that is linked to the removal of water from the systems present as solvating water and silanols. Na-silicate solutions show extensive foaming with the formation of a viscous condensed membrane on the droplet followed by the gradual release of water from the system on increasing temperature. Na_2O/SiO_2=0.5 solution foams more as compared to Na_2O/SiO_2=0.29 due to a higher amount of network silanols. Reducing the heating rate reduces the extent of foaming in Na-silicates. K-silicate solutions foam at 10°C/min with extensive foaming, comparable to Na-silicates, observed in K_2O/SiO_2=0.29. Reducing the heating rate to 5°C/min or 1°C/min results in the suppression of volumetric expansion due to crystallization ($KHSi_2O_5$). Li-silicate solutions don't show any foaming when heated to 250°C irrespective of the heating rate mainly because of the compositions being in the phase separation regime.

Pre-dried powder pellets obtained by drying solutions for 17 h at 150°C show the existence of extensive foaming in Na-silicates suggesting the foaming behavior to be a consequence of condensation of silanols and the corresponding removal of solvating water molecules. No foaming is seen in pre-dried K_2O/SiO_2=0.29 due to crystallization while Li_2O/SiO_2=0.29 does not foam until 250°C but a slight expansion in the pellet size is observed around 300°C linked to the removal of leftover silanols in the network as well as crystallization since all Li is lost around 350°C above which no further expansion is observed.

Thick and homogeneous coatings can be deposited through multi-layer spin coating approach (less efficient), blade/pool coating method (results in coatings of 100s of microns in thickness) and

bar coating route (for gradient coatings). Furthermore, the quality of the coatings is dependent highly on the type of alkali ion and the composition of the alkali silicates including the hydration level. A critical thickness is observed on thermal treatment of gradient coatings obtained from all the studied compositions and is linked to the way water is released from the system. Na-silicates show a critical thickness of foaming below which the coating is relatively stable and homogenous with condensation observed on thermal treatment to 250°C. K_2O/SiO_2=0.5 shows a critical thickness of foaming similar to Na-silicates while K_2O/SiO_2=0.29 exhibits two critical thicknesses, one for crystallization (with the formation of $KHSi_2O_5$, which tends to disappear on heating to 450°C) and the second where foaming seems to appear along with crystallization. Li-silicates also show a critical thickness on thermal treatment of gradient coatings with extensive cracking observed above it for both the molar ratios linked to the higher SiO_2 percentage as compared to Na or K-silicates. Crystallization ($Li_2Si_2O_5$) is also observed on thermally treating Li-silicate coatings to 450°C.

Finally, addition of foreign entities e.g. ethylene glycol and tetramethylammonium silicate tends to impact the foaming behavior of Na-silicates with an increasing concentration of these solutions resulting in the suppression of foaming in thicker coatings, that may be a consequence of the replacement of Na-silicate network silanols.

4.4. Appendix

Impact of drying time on foaming behavior of K_2O/SiO_2=0.29

Figure A 4.1 shows the impact of drying time on foaming properties of K_2O/SiO_2=0.29 solution. Drying the solution for 15 min followed by thermal treatment to 300°C results in extensive foaming due to the release of water. A 3 or 15 h drying step at 150°C tens to suppress the volumetric expansion on further heating to 300°C due the formation of orthorhombic and monoclinic $KHSi_2O_5$ crystalline phase as confirmed by powder XRD diffractograms shown in **Figure A 4.1**(c). Furthermore, drying at 200°C for 15 min or 2 h leads to foaming, but no further expansion is observed on heating to 300°C.

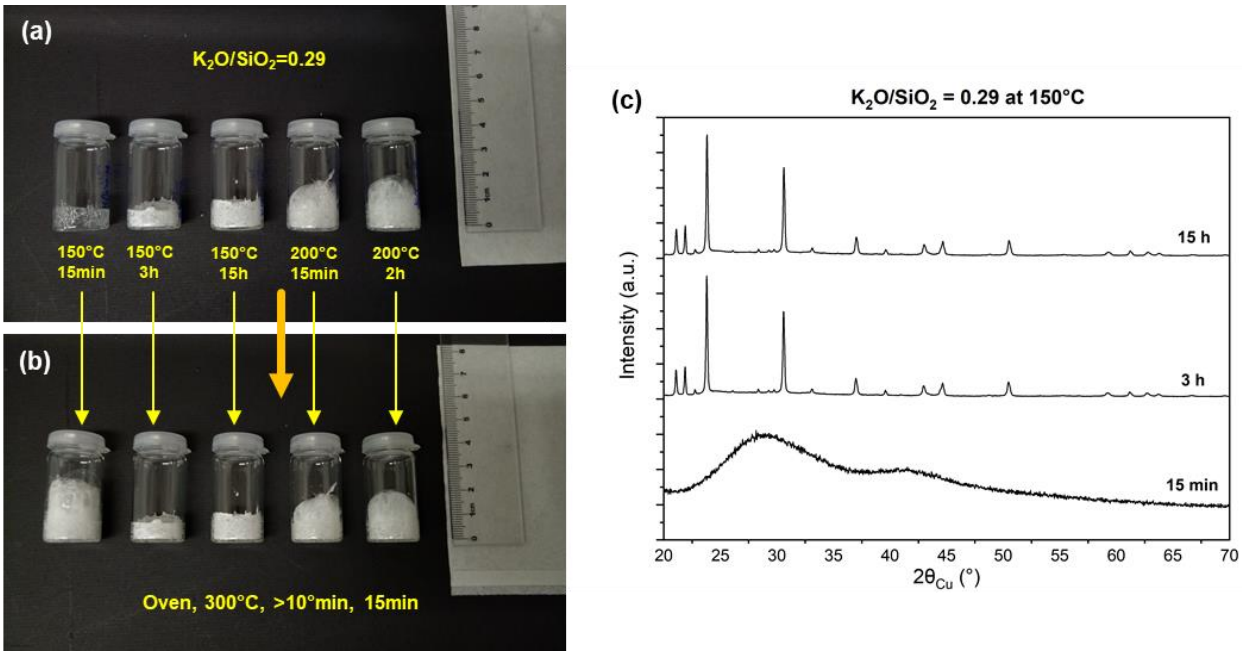

Figure A 4.1: Impact of drying time on the foaming behavior of K_2O/SiO_2=0.29 on heating at (a) 150°C & 200°C followed by thermal treatment to (b) 300°C. Crystallization appears within 3h of dehydration at 300°C as shown in (c) with the formation of $KHSi_2O_5$ phase limiting foaming.

Calibration of SIMS diffusion profiles for Na_2O/SiO_2=0.29 thin film

The SIMS diffusion profiles of 250 nm spin coated Na_2O/SiO_2=0.29 film are shown in **Figure A 4.2**. Different sputtering sources were used for acquiring the Na^+ and Si^+ profiles. O_2^+ ion source results in inhomogeneous Na^+ diffusion profile as shown in **Figure A 4.2**(a) for the as-deposited sample. This is caused by the 'charging effect' of incoming ions suggesting Na^+ ions to be highly sensitive. A 'shadowing effect' due to the formation of surface carbonates could also lead to these inhomogeneities but that seems to be less likely due to the relatively fresh nature of the sample. Changing the ion source to Cs^+ results in slightly better profile, shown in **Figure A 4.2**(b), due to relatively larger size of the incoming ions, but the charging effect still happens to impact the distribution of Na^+ ions in the coating. Using and O_2 cluster source at ambient conditions leads to reasonable diffusion profiles for the as-deposited sample (**Figure A 4.2**(c)) while the impact of charging is still observed in washed sample (**Figure A 4.2**(d)) where the amount of Na^+ ions is reduced quite a bit. Using the O_2 cluster source at -100°C, finally, results in linear profiles as shown in **Figure 4.6** (in the main text) representative of the actual distribution of ions throughout the coating.

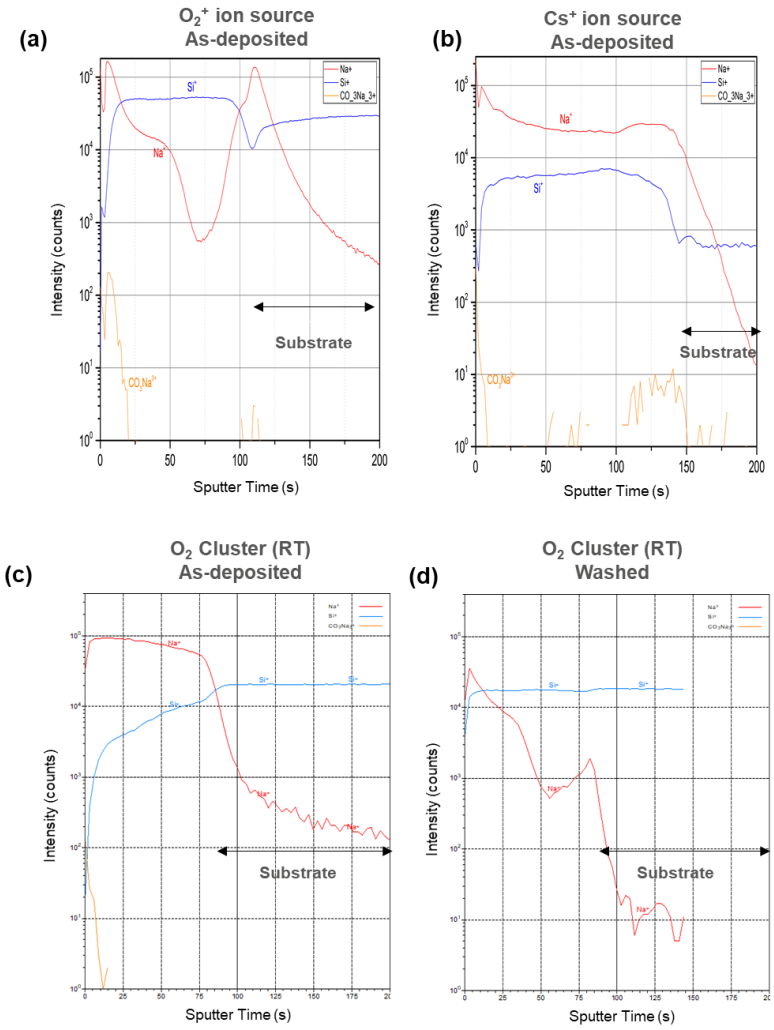

Figure A 4.2: SIMS profiles obtained on the as-deposited Na_2O/SiO_2=0.29 thin film using (a) O_2^+ ion source, (b) Cs^+ ion source & (c) O_2 cluster source at room temperature, and on the washed sample using (d) O_2 cluster source at room temperature.

Thickness measurements thick alkali silicate coatings

Figure A 4.3 shows the cross-section of a thick coating (single and double-layer) obtained by spin coating raw concentrated Na_2O/SiO_2=0.29 commercial solution. The coting is relatively homogeneous with the crack-like appearance of the cross0-section resulting from the cutting procedure and is not representative of the actual aspect of the coating.

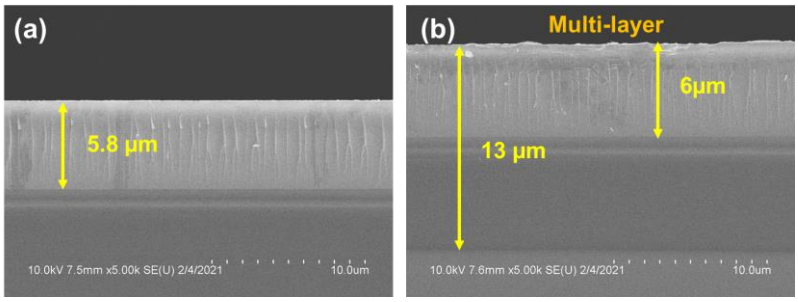

Figure A 4.3: SEM image showing the cross-section of Na_2O/SiO_2=0.29 raw solution (a) single-layer and (b) multi-layer thick coating obtained by spin coating at 2000 rpm for 60 s.

Figure A 4.4, **Figure A 4.5** and **Figure A 4.6** show the cross-sectional SEM images of Na, K and Li-silicate gradient coatings, respectively, before and after thermal treatments. A reduction in thickness is observed in the regions below the critical thickness due to condensation.

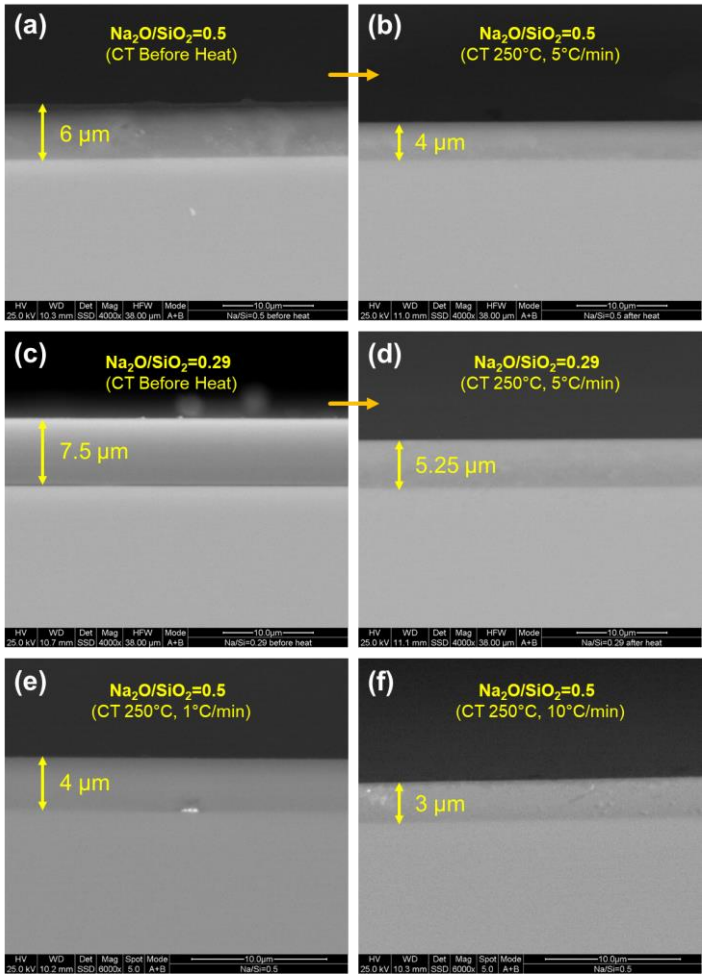

Figure A 4.4: Cross-sectional SEM images of the critical thickness (CT) region in Na-silicate gradient coatings (a, c) before and (b, d, e, f) after heating to 250°C.

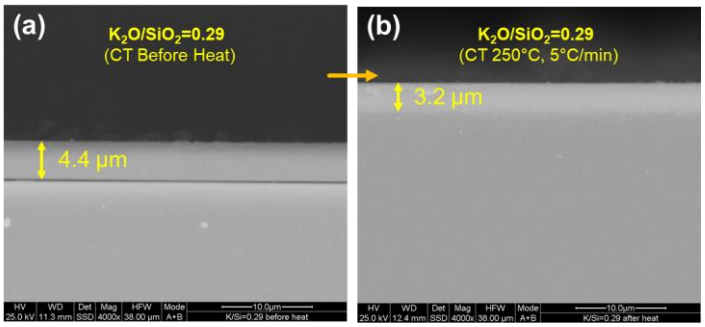

Figure A 4.5: Cross-sectional SEM images of the critical thickness (CT) region in K_2O/SiO_2=0.29 gradient coating (a) before and (b) after heating to 250°C at 5°C/min.

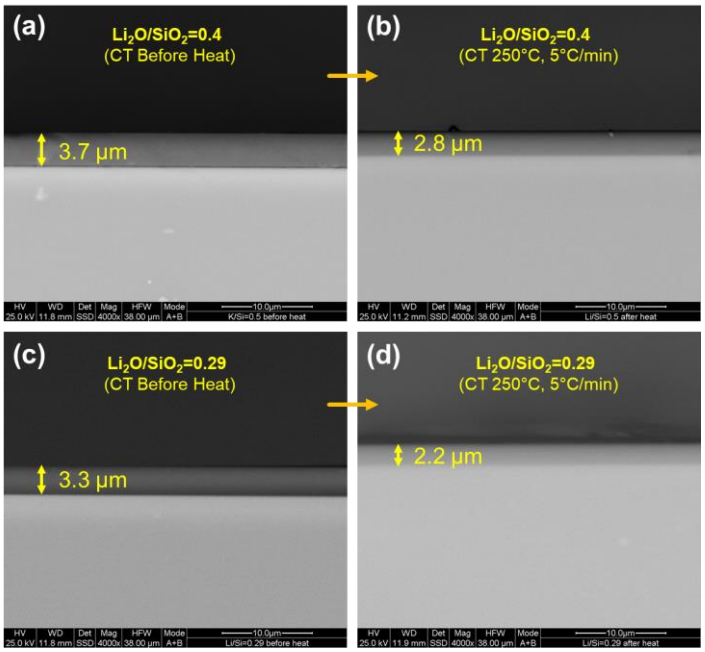

Figure A 4.6: Cross-sectional SEM images of the critical thickness (CT) region in Li-silicate gradient coatings before and after heating to 250°C at 5°C/min.

Chapter 5.

Outcomes & perspectives

5.1. Global conclusions

Structural properties of aqueous alkali silicates based on sodium (Na), potassium (K) and lithium (Li) have been investigated to probe the macroscopic and microscopic state of the materials for establishing an in-depth fundamental understanding of their thermal behavior. An experimental strategy involving the utilization of a combination of characterization tools has been developed in the process to monitor the systems. Analysis has been performed visually in terms of foaming/intumescent behavior of aqueous alkali silicates followed by the prediction of structural changes at the network scale. Hence, a link created between macroscopic changes and the corresponding microscopic thermal evolution has allowed to gain insights interesting from an industrial standpoint.

5.1.1. Macroscopic behavior

Aqueous alkali silicates of two different molar ratios (M_2O/SiO_2=0.29 and 0.5 for Na and K while 0.29 and 0.4 for Li-silicate) were investigated in this work. Thermal treatment of these solutions leads to structural changes associated with the removal of proton-related species from the system available as free water, network silanols and solvating water (molecules H-bonded to network silanols or alkali ions). Macroscopically speaking, foaming or intumescence is observed in some cases whereby the silicate structure expands volumetrically as shown in **Figure 5.1**. Na-silicate solutions show extensive foaming with, initially at lower temperatures, the formation of a viscous surface condensed membrane followed by an out-of-equilibrium build-up of water vapor pressure inside the material as the temperature increases. Na_2O/SiO_2=0.5 solution foams more as compared to Na_2O/SiO_2=0.29 due to a higher amount of network silanols confirmed from microscopic measurements. Reducing the heating rate from 10°C/min to 1°C/min reduces the extent of foaming in Na-silicates due to a less abrupt water release.

K-silicate solutions foam at 10°C/min with extensive foaming, comparable to Na-silicates, observed in K_2O/SiO_2=0.29. Reducing the heating rate to 5°C/min or 1°C/min results in the suppression of volumetric expansion due to crystallization (monoclinic or orthorhombic $KHSi_2O_5$). K_2O/SiO_2=0.5 foams, irrespective of the heating rate, but not extensively as the system is highly hygroscopic due to water being in a relatively stable state up to 300°C. Li-silicate solutions don't show any foaming when heated to 250°C irrespective of the compositions and heating rate mainly because of the starting compositions being in the phase separation regime. In general, at a rate of 5°C/min that has been used as the standard way for drying of solutions at different temperatures for quantitative analysis, Na-silicate solutions foam extensively, Li-silicates don't foam while an intermediate behavior is observed for K-silicates.

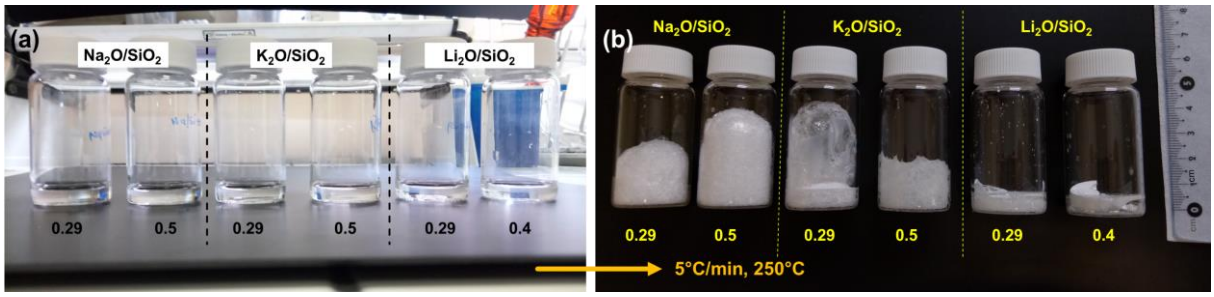

Figure 5.1: Aqueous alkali silicates of two different compositions each in glass vials (a) before and (b) after heat treatment to 250°C at 5°C/min.

Pre-dried powder (necessary due to experimental limitations associated with various techniques) pellets obtained by drying solutions for 17 h at 150°C (to remove all the free water) show the existence of extensive foaming in Na-silicates on heating to 400°C suggesting the foaming behavior to be a consequence of condensation of silanols and the corresponding removal of solvating water molecules. Foaming seems to be suppressed in pre-dried K_2O/SiO_2=0.29 due to crystallization while Li_2O/SiO_2=0.29 does not foam until 250°C. A slight expansion in the pellet size is observed around 300°C linked to the removal of leftover silanols in the network as well as crystallization since all Li is lost around 350°C above which no further expansion is observed.

Mass loss evolution, obtained from TGA, is dependent upon temperature (independent of kinetics in Na-silicates), the pre-drying time (for K-silicates) and alkali content in the silicate. Thermally treating pre-dried powders suggests the existence of an offset of mass loss with higher alkali content systems showing a lower initial dehydration temperature. For Na-silicates, increasing the Na content tends to reduce the softening temperature (175°C for Na_2O/SiO_2=0.5 and 210°C for Na_2O/SiO_2=0.29) along with a higher amount of overall water retention after the initial pre-drying step at 150°C. Such low values of an apparent T_g are consistent with the T_g values reported in the literature for water-containing glasses of similar composition. A same order of magnitude for mass loss evolution is observed for both the Na-silicate molar ratios with an activation energy of 29.4 $kJ.mol^{-1}$ for Na_2O/SiO_2=0.5 as compared to 34.1 $kJ.mol^{-1}$ for Na_2O/SiO_2=0.29. In contrast, multiple activation energies are observed for K and Li-silicates mainly due to the formation of different crystalline phases, confirmed by XRD, suggesting the structure to be behaving differently than Na-silicates, as observed macroscopically.

5.1.2. Microscopic thermal evolution

Heating pre-dried Na-silicate powders tends to increase the degree of network polymerization apart from the macroscopic volumetric expansion observed on foaming. The system moves towards a state with more Q^4 at the expense of lower Q^n units. A xerogel-to-glass evolution in terms of Q^n units at around 400°C is observed for Na-silicates when compared with reference glasses. Complementary information provided by Raman spectroscopy also indicates that the structure condenses and the Raman spectra at 400°C become similar to that of the corresponding glasses (especially in terms of Q^n units) for both the Na-silicate molar ratios with ring-type structure being more dominant in glasses.

Further structural investigation indicates that Na ions are connected to both Q^2 and Q^3 silicon sites for Na_2O/SiO_2=0.29 suggesting a completely random distribution, while all protons are connected to Q^3 (both Q^2 and Q^3 connectivity is observed in the case of Na_2O/SiO_2=0.5) i.e. no free water is present at 150°C. For Na-silicates, NBO contribution from the network modifiers (Na and H) shows that both silanols and solvating water molecules are present even at high temperature, suggesting an equilibrium between the two structural units for protons as shown in **Figure 5.2** (obtained by combining TGA mass loss curves and solid-state ^{29}Si NMR data). Thus, the extensive foaming observed in pre-dried systems confirms the actual cause of this phenomenon to be the release of water molecules as a consequence of condensation of silanols. Condensation of silanols leads to solvating water molecules that in turn leave the system indicating the existence of a single activation energy approaching 30 $kJ.mol^{-1}$ in Na-silicate systems. The amount of initial water in the silicate and molar ratio Na_2O/SiO_2 directly influence the amount of these condensing silanols in the network. Higher overall water is retained after the pre-drying step for the molar ratio Na_2O/SiO_2=0.5 suggesting the network to possess more H as NBOs when compared to Na_2O/SiO_2=0.29 leading to more volumetric expansion in terms of foaming as observed in **Figure 5.1**(b).

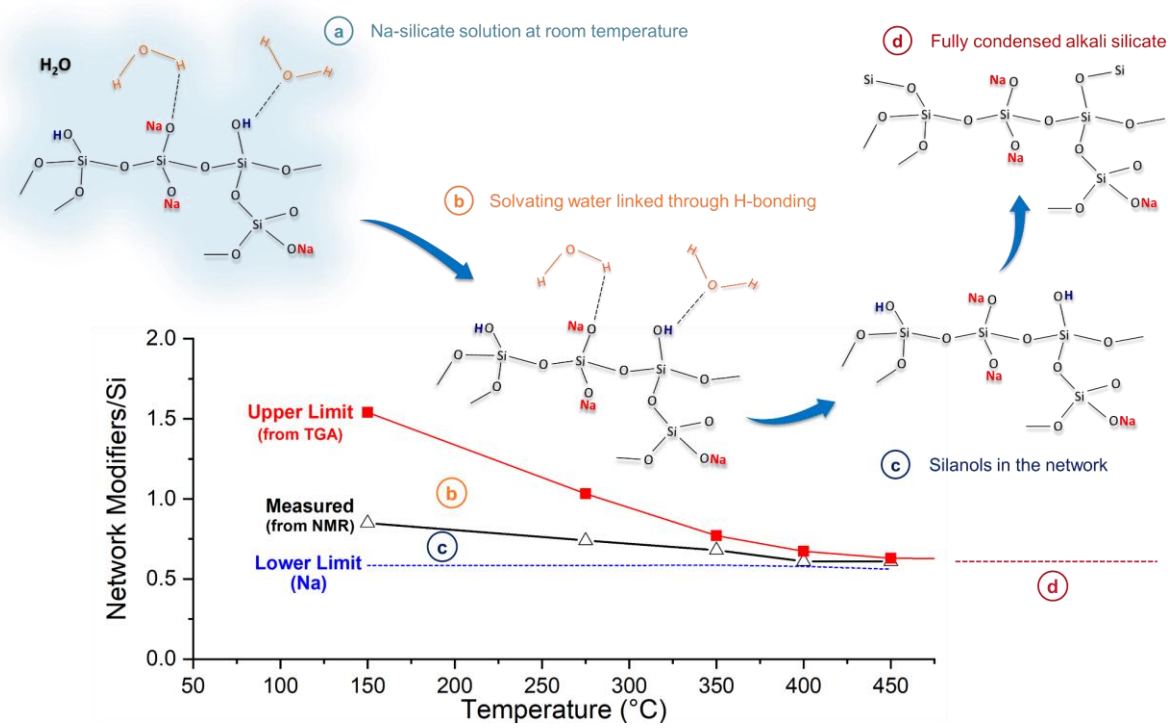

Figure 5.2. Total Network Modifiers/Si from both (■) TGA and (△) solid-state ^{29}Si NMR spectra of Na-silicate (Na_2O/SiO_2=0.29) powder with region 'b' corresponding to the amount of adsorbed/solvating water linked to the network, 'c' corresponding to the relative proportion of OH as NBO and 'd' referring to a completely condensed state at temperatures well above 800°C.

Na-silicate solutions or pre-dried powders do not crystallize on heating up to 450°C. A direct heating of K_2O/SiO_2=0.29 solution to 450°C at heating rates ≥ 10°C/min would show a behavior similar to Na-silicates in terms of foaming with the possibility to quantify the amount of silanols in the amorphous network and the corresponding solvating water molecules. However, K_2O/SiO_2=0.29 tends to crystallize even at 150°C (depending upon the time of drying, 1 h and 30

min is enough) with a degree of crystallinity (DOC) of 60% when dried for 17 h. Orthorhombic and monoclinic $KHSi_2O_5$ crystalline phases are formed that tend to evolve with temperature (DOC increases to ~80% at 400°C) until partial melting is observed at 450°C. Both Li-silicate molar ratios, on the other hand, are amorphous at 150°C while crystallization appears at 275°C with the formation of orthorhombic Li_2SiO_3 and $Li_2Si_2O_5$ phases. DOC increases as a function of temperature with the gradual conversion of Li_2SiO_3 into $Li_2Si_2O_5$. This crystallization behavior in K and Li-silicates is suggested to have a direct impact on the macroscopic evolution of the silicates. Rietveld refinement of XRD diffractograms has helped in the deconvolution of the data that has aided in establishing a quantitative measure of the evolution of alkali ions and proton-related species in crystallized systems.

Pre-dried Na-silicates have a gradual and continuous evolution of amorphous network silanols and solvating water molecules (**Figure 5.3**(a)) leading to extensive foaming stemming from the fact that the network is relatively mobile as well as water can leave the system easily. K_2O/SiO_2=0.5 behaves in a similar manner as that observed for Na-silicates, however, phase diagram suggests the system to contain thermodynamically more stable water content indicating the system to be mobile while being extremely hygroscopic at the same time.

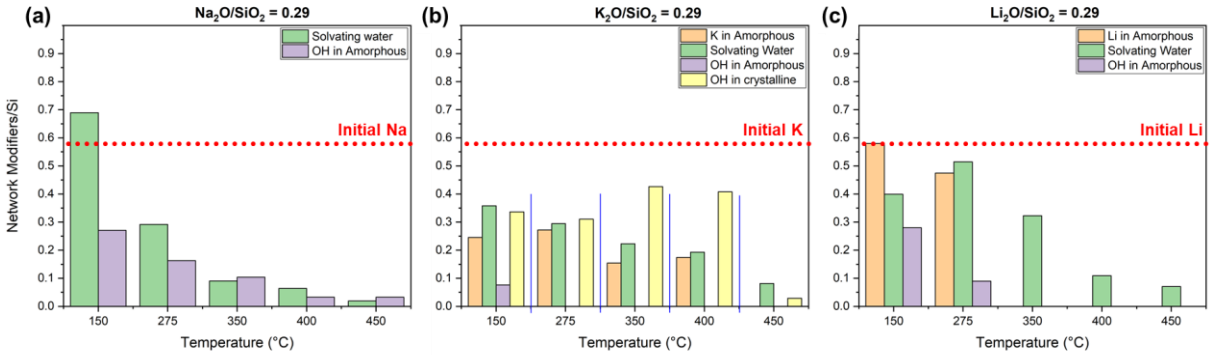

Figure 5.3: Quantitative thermal evolution of different species i.e solvating water, silanols (in amorphous or crystalline phase) and alkali ions for (a) Na_2O/SiO_2=0.29, (b) K_2O/SiO_2=0.29 and (c) Li_2O/SiO_2=0.29.

Amorphous silanols in the network (for pre-dried powders) are lost altogether at 275°C for both K_2O/SiO_2=0.29 and Li-silicates (**Figure 5.3**(b) and (c), respectively) while the protons linked to $KHSi_2O_5$ phase stay intact until 400°C. The network in K_2O/SiO_2=0.29 retains somewhat its mobility due to leftover K ions in the amorphous phase even after crystallization as well as the possibility of some solvating water molecules to be intact. However, crystallization is expected to reduce quite a bit the foaming capacity when compared to Na-silicates as the amorphous network mobility is reduced along with the absence of any silanols above 150°C. The network in Li-silicates is less mobile due to the existence of strong cross-links between Li ions and polysilicate particles. Furthermore, the studied compositions lie in the phase separation regime indicating the formation of a SiO_2 rich matrix phase that is reasonably brittle and prevents the structure from being mobile. Crystallization at temperatures approaching 275°C leads to the removal of Li ions from the amorphous phase whereby all Li ions move into the crystalline counterpart at 350°C reducing further the already low mobility in Li-silicate systems, thus, supposedly limiting the volumetric expansion.

The xerogel-to-glass evolution in Na-silicates at 400/450°C suggests a high temperature evolution (>450°C) of the pre-foamed Na-silicate powder pellets to have the same macroscopic behavior as the reference (dry) glasses. An exponentially decreasing trend of viscosity is observed for both the molar ratios consistent with the reference glasses and literature models suggesting glass-like properties to indeed have been achieved. A behavior similar to Na-silicates is observed for pre-dried K_2O/SiO_2=0.29 pellet while Li_2O/SiO_2=0.29 doesn't evolve much up to 1200°C apart from being sintered. Further investigation is required where an extrapolation of the current data is expected to aid in the investigation of rheological properties in the foaming regime in terms of variations in viscosity.

5.1.3. Foaming in coatings

Thick and homogeneous coatings are possible to deposit through multi-layer spin coating approach (less efficient), blade/pool coating method (results in coatings of 100s of microns in thickness) and bar coating route (for gradient coatings). The quality of the developed coatings is dependent highly on the type of alkali ion and the composition of the alkali silicates including the hydration level. In general, compositions with higher alkali content tend to reduce cracking that may otherwise be the case. A critical thickness is observed on thermal treatment of gradient coatings obtained from all the studied compositions and is linked to the way water is released from the system.

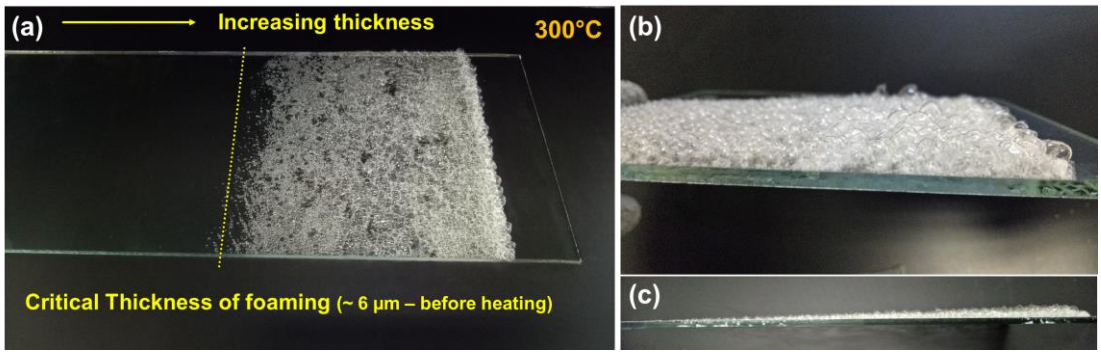

Figure 5.4: Na_2O/SiO_2=0.5 gradient coating (after heating to 300°C) showing the existence of a critical thickness for foaming (a), and the close-up images of the foamed region from (b) top and (c) edge.

Na-silicates show a critical thickness of foaming (**Figure 5.4**) below which the coating is relatively stable and homogenous with condensation observed on thermal treatment to 250°C. The existence of this critical thickness is linked to the release of water from the system. Below the critical thickness value, the coating corresponds to a viscous condensed surface layer similar to that observed in solutions with limited possibilities for water molecules to form bubbles due to limitations of diffusion path length. Above the critical thickness value, surface condensed layer has the same thickness as that observed below, with a gradual increase in the amount of water molecules resulting in the structural expansion. K_2O/SiO_2=0.5 gradient coating shows a critical thickness of foaming similar to Na-silicates while K_2O/SiO_2=0.29 exhibits two critical thicknesses, one for crystallization (with the formation of $KHSi_2O_5$, which tends to disappear on heating to 450°C) and the second where foaming seems to appear along with crystallization. Li-silicates also show a critical thickness on thermal treatment of gradient coatings with extensive cracking

observed above it for both the molar ratios linked to the higher SiO_2 percentage as compared to Na or K-silicates. Crystallization ($Li_2Si_2O_5$) is also observed on thermally treating Li-silicate coatings to 450°C.

Finally, it is possible to alter the foaming behavior of alkali silicates by manipulating the composition. Addition of foreign entities e.g. ethylene glycol (EG) and tetramethylammonium silicate (TMAS) tends to impact the foaming behavior of Na-silicates with an increasing concentration of these solutions resulting in the suppression of foaming in thicker coatings, a consequence of the replacement of Na-silicate network silanols.

The in-depth fundamental understanding of the macroscopic and microscopic thermal behavior of aqueous alkali silicates has brought about a meaningful advancement to the subject. The structural changes associated with and responsible for foaming-related aspects of these materials have been analyzed qualitatively along with a more quantitative approach for being able to predict accurately the differences among Na, K and Li-silicates. However, further exploration of these systems is still required for a comprehensive know-how of their structural properties in, especially, coatings for providing a more close-to-industrial R&D solution.

5.2. Perspectives

For further advancement in the understanding of aqueous alkali silicate-based systems, various directions are possible to be explored.

5.2.1. Quantitative analysis of coatings

5.2.1.1. Q^n units

NMR data discussed in this work gives a quantitative information on the structural organization of alkali silicates, however, the technique is limited to mainly solutions and pre-dried powder samples. For thick coatings-related understanding of thermal evolution, Raman spectroscopy may provide with a plausible information but the corresponding measurements obtained add more to the qualitative understanding. Deconvolution of the Raman spectra into individual Q^n units is thus required, but it is not directly quantitative due to the existence of this intensity factor associated to the various structural units ($Q_{Raman}=I_{Raman} \times Q_{quantity}$) with lower Q^n units being more visible. **Figure 5.5** shows the deconvoluted Raman spectra (in terms of area under each peak) of Na-silicate powders in the range 825-1250 cm^{-1}. A decreasing trend for Q^2 and increasing for Q^3 and Q^4 is observed suggesting the network to be moving towards a more polymerized state until glass-like values are obtained.

For making the values quantitative, a correlation can be established by plotting the NMR Q^n units vs the %Area of these species from Raman spectroscopy as shown for Q^2 and Q^3 in **Figure 5.5**(d). This indicates that in the absence of tabulated cross-section values, we have made a calibration to get quantitative data out of Raman spectroscopy as it not only allows for faster measurements but also enables to acquire data for other samples including thin films or thicker coatings which may not be so convenient with NMR spectroscopy. However, issues related to the exact way of

deconvoluting these Raman bands associated with Q^n units (and whether absolute or relative values should be used) needs further probing.[131]

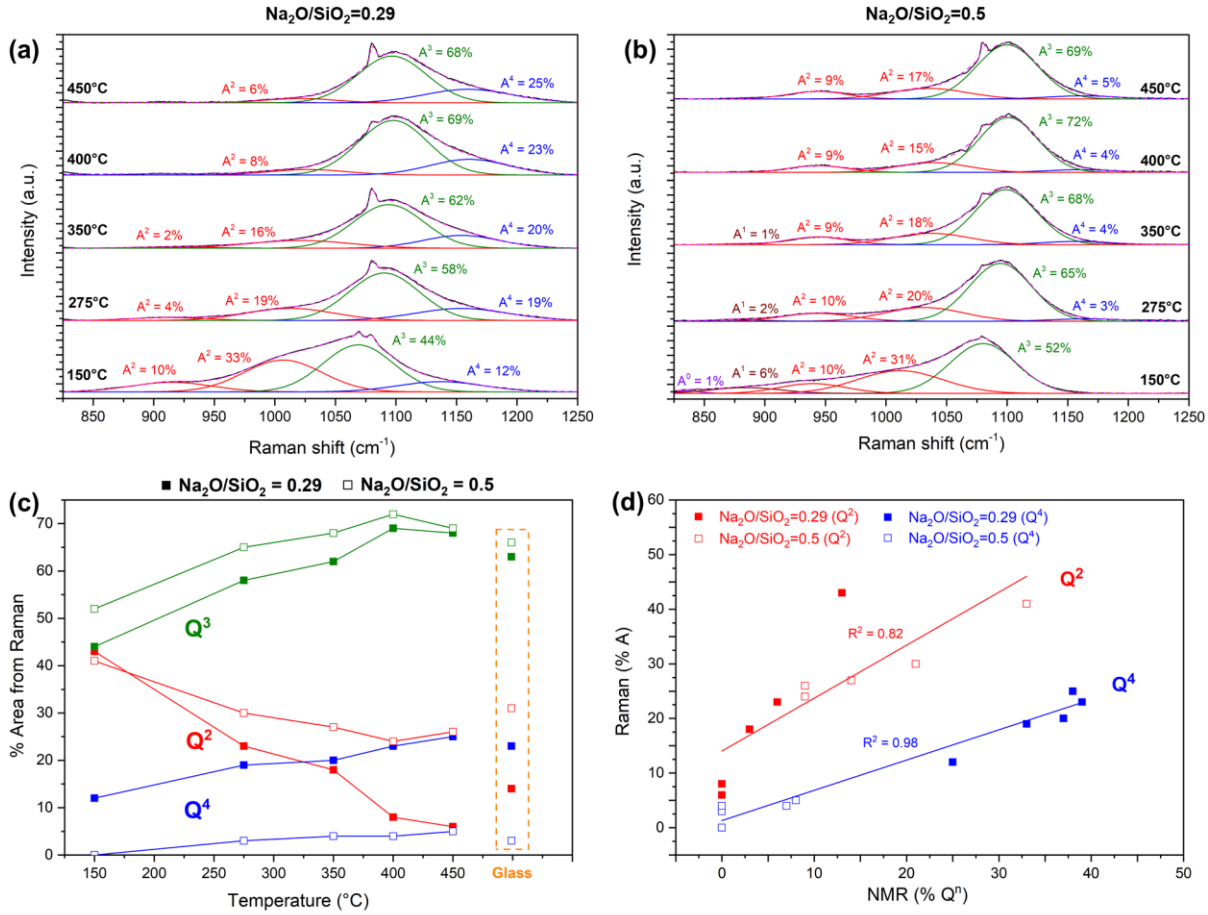

Figure 5.5: (a), (b) Deconvoluted experimental Raman spectra (825-1250 cm^{-1}) of Na-silicate powders, together with fitted curves, individual components (in terms of %Area, not the actual quantity) and their relative fractions, (c) variation of %Area of Q^n with temperature for the two molar ratios (■ for Na_2O/SiO_2=0.29 and □ for Na_2O/SiO_2=0.5) and points for the corresponding glasses (■ for 77% SiO_2 – 23% Na_2O and □ for 67% SiO_2 – 33% Na_2O), and (d) correlation between Raman and NMR data (extracted from **Figure 3.11**) for Q^2 and Q^4 (■ for Na/Si=0.29 and □ for Na/Si=0.5) in order to make Raman quantitative.

Raman spectra were successfully obtained on Na-silicate thin films (a few 100s of nm) deposited on tantalum (Ta)-coated glass (to remove signal from the substrate) shown in **Figure 5.6**(a) and (b) suggesting that the network indeed tends to polymerize on thermal treatment in a manner similar to that observed for pre-dried powders. Note that thicker coatings could not be used for these measurements due to problems arising from foaming. So, the coating thicknesses should be below the critical thickness values observed from gradient coating samples. Further analysis is required for quantifying the distribution of these Q^n units by utilizing the 'to be obtained precise' NMR-Raman correlation plot in a manner similar to the one shown in **Figure 5.5**(d).

5.2.1.2. Evolution of proton-related species

Apart from the network changes in terms of the Q^n units, evolution of proton-related species has to be investigated to establish an understanding similar to that achieved for pre-dried powders. One way of following the evolution of water is to use in-situ Raman spectroscopy on Ta-coated substrates. Some initial trials and adjustments were made to the home-built in-situ Raman

spectroscopy setup but the measurements could not be properly realized due to the formation of bubbles in some regions as well as the fact that the water band signal (in the range 2400-3400 cm^{-1}) was not intense enough at temperatures approaching 200-250°C to draw some solid conclusions, suggesting further improvements to be made. Another way of following the evolution of proton-related species is to use FT-IR on thicker coatings (≤ 5 µm) as shown for Na_2O/SiO_2=0.29 in **Figure 5.6**(c). It is, thus, possible to extract a more precise information for free water, solvating water and silanols on deconvoluting the broad water band observed in FT-IR spectra.

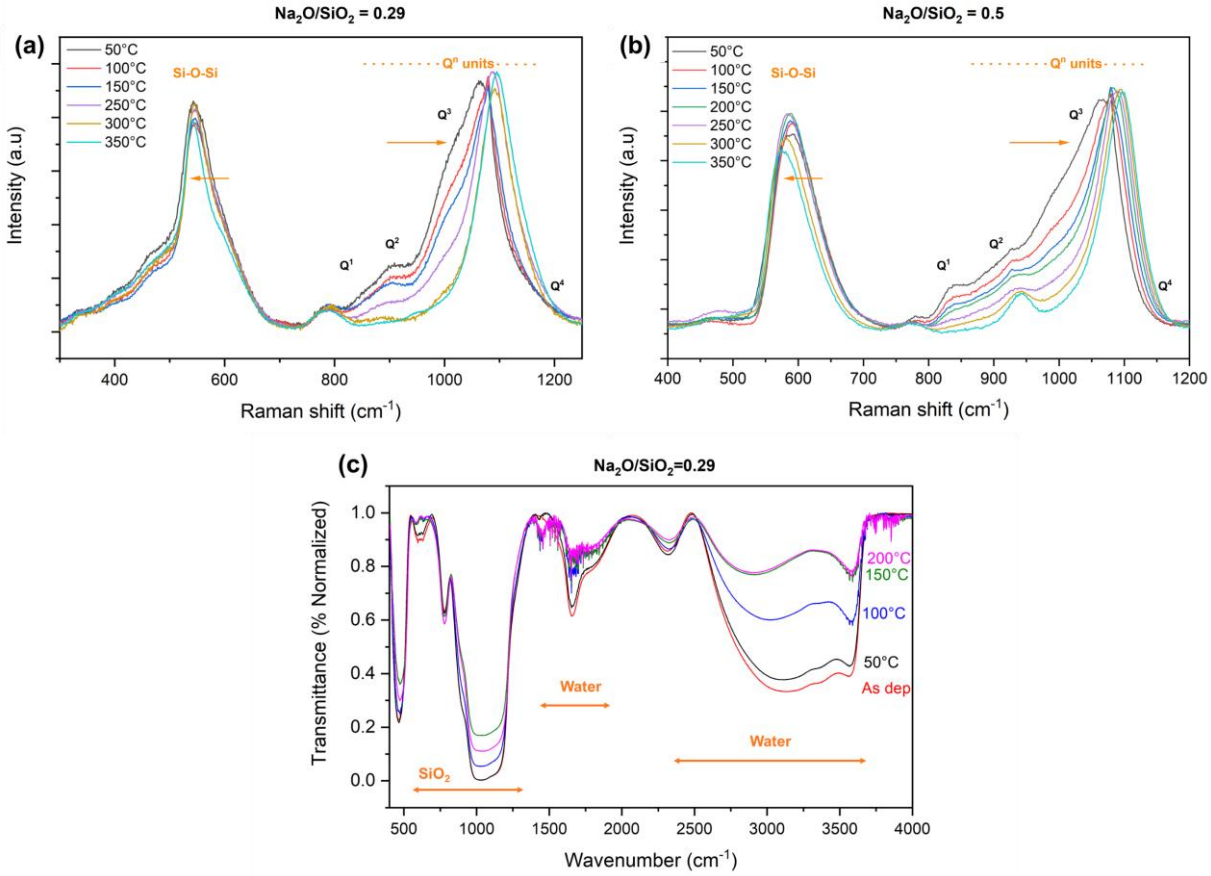

Figure 5.6: Raman spectra thermal evolution on tantalum (Ta)-coated glass for (a) Na_2O/SiO_2=0.29 and (b) Na_2O/SiO_2=0.5 spin coated samples, and (c) the evolution of water peaks obtained from FTIR spectroscopy measurements on Na_2O/SiO_2=0.29 spin-coated on double-side polished Si wafer.

5.2.1.3. Better understanding of critical thickness

Understanding of the foaming behavior and existence of critical thickness in gradient coatings is also necessary. Critical thickness has been suggested to be related to the amount of water and the corresponding diffusion length for which a more quantitative analysis is required. Surface and depth mapping of the water band through Raman spectroscopy could give an indication of the distribution of water below and above critical thickness regions mainly for the as-deposited coating and the one heated to temperatures just below the values where foaming starts. Some initial trials have already been made on such systems but the current results are, for the moment, not so easy to interpret to provide conclusive evidence.

5.2.2. Controlling foaming

Being able to control the foaming behavior or extent in Na and K-silicate solutions, pre-dried powders and coatings by manipulating the starting composition could be a step forward in terms of the industrial significance of these alkali silicates. Addition of foreign entities into the aqueous silicates or mixing of the silicates needs further investigation in this regard. The general goal, in coatings, would be to shift the critical thickness to very high thickness values by somehow controlling the hydration level of these systems.

5.2.2.1. Addition of foreign elements

Initial trials made by mixing ethylene glycol and tetramethylammonium silicate solutions show promising results in the reduction of foaming in Na-silicates. However, further exploration is required for an in-depth analysis in terms of the changes induced at the structural scale using TGA, NMR & Raman spectroscopy and XRD.

5.2.2.2. Mixing of silicates

Mixing different alkali silicates could impact the way they behave thermally. For instance, **Figure 5.7** shows the impact of mixing Na_2O/SiO_2=0.29 and Li_2O/SiO_2=0.2 on thermal treatment to 300°C. Pure Na-silicate solution droplet foams while Li-silicate does not due to the solution composition being in the phase separation regime. Adding 5% Na_2O/SiO_2=0.29 doesn't lead to any foaming while some expansion is observed on increasing the concentration to 50%. This might suggest that the addition of Na tends to move the Li-silicate composition out of the phase separation regime, giving an indication of the ability to control the thermal behavior of the two silicates as required.

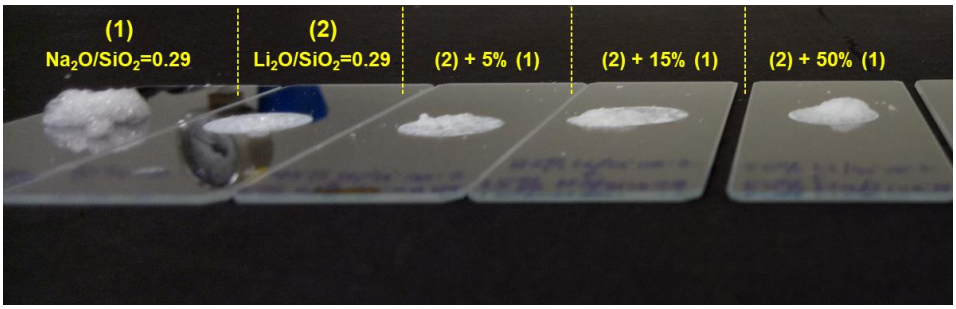

Figure 5.7: Impact of mixing Na_2O/SiO_2=0.29 and Li_2O/SiO_2=0.2 on thermal treatment to 300°C.

5.2.3. High temperature properties

Thermal properties at higher temperatures (≥ 500°C) are required to understand the behavior of K and Li-silicates. Na-silicates behave in a manner similar to the reference glasses while similar viscosity models are to be predicted for other alkali silicate compositions by comparing with the respective glasses. Furthermore, high temperature evolution of pre-foamed Na and K-silicates suggests the shrinkage of these materials, a property interesting to be exploited for applications requiring sintering of glass. This property could also be used for acting as a binder in coatings, e.g. mixing pigments with pre-foamed Na-silicates could allow to have pigmented glass coatings.

Moreover, the interest could also lie in understanding the thermal evolution of compositions other than those studied here in order to predict, through the quantitative methods developed, what controls the quantity of water up to 400°C. Different molar ratio values or even mixture of

alkali silicates could potentially have interesting thermal evolution and several intrinsic phenomena.

5.2.4. Diffusion studies

Lastly, diffusion-related properties of coatings obtained from aqueous alkali silicates need to be investigated further. A SIMS protocol is already in place for investigation of the diffusion behavior for different systems. Ageing of these systems, especially, Na-silicates, leads to surface carbonation as shown in **Figure 5.8** resulting in not only reduced aesthetics but also impacting the mechanical stability of the coating network i.e. rendering it more brittle and as a consequence prone to cracking.

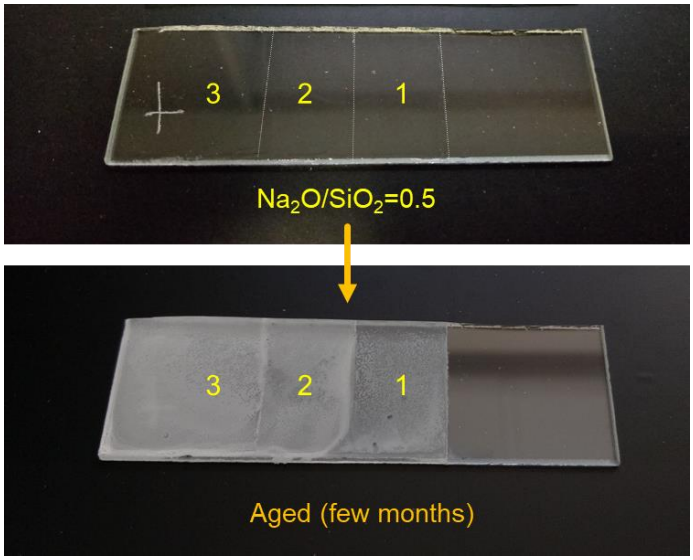

Figure 5.8: Impact of ageing on Na_2O/SiO_2=0.5 spin coated glass slide with a step coating containing 1, 2 and 3 layers.

Addition of foreign elements e.g. Al ions/Al_2O_3 nanoparticles, divalent ions (Ca^{2+}, Mg^{2+}) to the solutions could allow to limit or completely control surface carbonation in coatings by limiting the diffusion of alkalis. Al has the ability to act as a charge center for, let's say, Na ions and can thus pin them preventing their diffusion.

References

(1) Bulewicz, E. M.; Pelc, A.; Kozjowski, R.; Miciukiewicz, A. Intumescent Silicate-Based Materials: Mechanism of Swelling in Contact with Fire. *Fire Mater.* **1985**, *9* (4), 171–175.

(2) Weil, E. D. Fire-Protective and Flame-Retardant Coatings - A State-of-the-Art Review. *J. Fire Sci.* **2011**, *29* (3), 259–296.

(3) Prud'Homme, E.; Michaud, P.; Joussein, E.; Clacens, J. M.; Arii-Clacens, S.; Sobrados, I.; Peyratout, C.; Smith, A.; Sanz, J.; Rossignol, S. Structural Characterization of Geomaterial Foams - Thermal Behavior. *J. Non. Cryst. Solids* **2011**, *357*, 3637–3647.

(4) Delair, S.; Prud'homme, É.; Peyratout, C.; Smith, A.; Michaud, P.; Eloy, L.; Joussein, E.; Rossignol, S. Durability of Inorganic Foam in Solution: The Role of Alkali Elements in the Geopolymer Network. *Corros. Sci.* **2012**, *59*, 213–221.

(5) Strozi Cilla, M.; Colombo, P.; Raymundo Morelli, M. Geopolymer Foams by Gelcasting. *Ceram. Int.* **2014**, *40*, 5723–5730.

(6) Dimas, D.; Giannopoulou, I.; Panias, D. Polymerization in Sodium Silicate Solutions: A Fundamental Process in Geopolymerization Technology. *J. Mater. Sci.* **2009**, *44* (14), 3719–3730.

(7) Gettwert, G.; Rieber, W.; Bonarius, J. One-Component Silicate Binder Systems for Coatings. *Surf. Coatings Int.* **1998**, *81* (12), 596–603.

(8) Weldes, H. H.; Lange, R. K. Properties of Soluble Silicates. *Ind. Eng. Chem.* **1969**, *61* (4), 29–44.

(9) Petersen, R. R.; Christensen, J. F. S.; Jørgensen, N. T.; Gustafson, S.; Lindbjerg, L. A.; Yue, Y. Preparation and Thermal Properties of Commercial Vermiculite Bonded with Potassium Silicate. *Thermochim. Acta* **2021**, *699*, 178926-.

(10) Veinot, D. E.; Langille, K. B.; Nguyen, D. T.; Bernt, J. O. Efflorescence of Soluble Silicate Coatings. *J. Non. Cryst. Solids* **1991**, *127*, 221–226.

(11) Jaffrès, A.; Boudot, M.; Chevalier, S.; Mohammedi, R.; Maron, S.; Devys, L.; Gacoin, T. Revisiting Aqueous Alkaline Silicates as Precursors for Sol-Gel Optical Coatings. *J. Am. Ceram. Soc.* **2019**, *102* (7), 3887–3896.

(12) Zachariasen, W. H. The Atomic Arrangement in Glasses. *J. Am. Chem. Soc.* **1932**, 3841–3851.

(13) Lamkin, M. A.; Riley, F. L.; Fordham, R. J. Oxygen Mobility in Silicon Dioxide and Silicate Glasses: A Review. *J. Eur. Ceram. Soc.* **1992**, *10*, 347–367.

(14) Matson, D. W.; Sharma, S. K.; Philpotts, J. A. The Structure of High-Silica Alkali-Silicate Glasses. A Raman Spectroscopic Investigation. *J. Non. Cryst. Solids* **1983**, *58* (2–3), 323–352.

(15) Shelby, J. E. Property/Morphology Relations in Alkali Silicate Glasses. *J. Am. Ceram. Soc.*

1983, *66* (11), 754–757.

(16) Day, D. E. Mixed Alkali Glasses-Their Properties and Uses. *J. Non. Cryst. Solids* **1976**, *21*, 343–372.

(17) Vidal, L.; Joussein, E.; Colas, M.; Cornette, J.; Sanz, J.; Sobrados, I.; Gelet, J. L.; Absi, J.; Rossignol, S. Controlling the Reactivity of Silicate Solutions: A FTIR, Raman and NMR Study. *Colloids Surfaces A Physicochem. Eng. Asp.* **2016**, *503*, 101–109.

(18) Svensson, I. L.; Sjöberg, S.; Öhman, L.-O. Polysilicate Equilibria in Concentrated Sodium Silicate Solutions. *J. Chem. Soc., Faraday Trans. I* **1986**, *82*, 3635–3646.

(19) Tognonvi, M. T.; Massiot, D.; Lecomte, A.; Rossignol, S.; Bonnet, J. P. Identification of Solvated Species Present in Concentrated and Dilute Sodium Silicate Solutions by Combined ^{29}Si NMR and SAXS Studies. *J. Colloid Interface Sci.* **2010**, *352* (2), 309–315.

(20) Ray, N. H.; Plaisted, R. J. The Constitution of Aqueous Silicate Solutions. *J. Chem. Soc. Dalt. Trans* **1983**, 475–481.

(21) Langille, K. B.; Nguyen, D.; Bernt, J. O.; Veinot, D. E.; Murthy, M. K. Mechanism of Dehydration and Intumescence of Soluble Silicates Part I Effect of Silica to Metal Oxide Molar Ratio. *J. Mater. Sci.* **1991**, *26*, 695–703.

(22) Iler, R. K. Water-Soluble Silicates. In *The Chemistry of Silica*; Wiley-Interscience, John Wiley & Sons, 1979; pp 116–171.

(23) Fraci, A. T. Waterborne Silicates in Coatings and Construction Chemicals. In *48th Annual Surface Coatings Association Australia Conference*; 2008.

(24) Gettwert, G.; Rieber, W.; Bonarius, J. One-Component Silicate Binder Systems for Coatings. *JOCCA - Surf. Coatings Int.* **1998**, *81* (12), 596–603.

(25) Leute, M.; Lind, J. Basics of alkali silicates https://geopolymer.org/fichiers/gpcamp-2013/Lauter - Basics alkali silicates - Wöllner.pdf (accessed 2021 -09 -30).

(26) PQ Europe. Sodium and Potassium Silicates https://www.pqcorp.com/docs/default-source/recommended-literature/pq/lithium-silicate/sodium-and-potassium-silicates-brochure-eng-oct-2004.pdf?sfvrsn=d22426fb_3 (accessed 2021 -09 -30).

(27) Otterstedt, J.-E. A.; Ghuzel, M.; Sterte, J. P. Colloidal Components in Solutions of Alkali Silicates. *J. Colloid Interface Sci.* **1987**, *115* (1), 95–103.

(28) Brykov, A. S.; Danilov, V. V.; Aleshunina, E. Y. State of Silicon in Silicate and Silica-Containing Solutions and Their Binding Properties. *Russ. J. Appl. Chem.* **2008**, *81* (10), 1717–1721.

(29) Hunt, J. D.; Kavner, A.; Schauble, E. A.; Snyder, D.; Manning, C. E. Polymerization of Aqueous Silica in H_2O-K_2O Solutions at 25-200°C and 1bar to 20kbar. *Chem. Geol.* **2011**, *283* (3–4), 161–170.

(30) Beard, W. C. Infrared Studies of Aqueous Silicate Solutions. In *Molecular Sieves*; Meier, W. M., Uytterhoeven, J. B., Eds.; American Chemical Society: Washington DC, 1973; pp 162–168.

(31) McCormick, A. V; Bell, A. T.; Radke, C. J. Quantitative Determination of Siliceous Species

in Sodium Silicate Solutions by ^{29}Si n.m.r. Spectroscopy. *Zeolites* **1987**, *7* (3), 183–190.

(32) Kinrade, S. D.; Pole, D. L. Effect of Alkali-Metal Cations on the Chemistry of Aqueous Silicate Solutions. *Inorg. Chem.* **1992**, *31*, 4558–4563.

(33) Kinrade, S. D.; Swaddle, T. W. Silicon-29 NMR Studies of Aqueous Silicate Solutions. 1. Chemical Shifts and Equilibria. *Inorg. Chem.* **1988**, *27*, 4253–4259.

(34) Harris, R. K.; Bahlmann, E. K. F.; Metcalfe, K.; Smith, E. G. Quantitative Silicon-29 NMR Investigations of Highly Concentrated High-Ratio Sodium Silicate Solutions. *Magn. Reson. Chem.* **1993**, *31*, 743–747.

(35) Autef, A.; Joussein, E.; Gasgnier, G.; Rossignol, S. Role of the Silica Source on the Geopolymerization Rate. *J. Non. Cryst. Solids* **2012**, *358* (21), 2886–2893.

(36) Gharzouni, A.; Joussein, E.; Samet, B.; Baklouti, S.; Pronier, S.; Sobrados, I.; Sanz, J.; Rossignol, S. The Effect of an Activation Solution with Siliceous Species on the Chemical Reactivity and Mechanical Properties of Geopolymers. *J. Sol-Gel Sci. Technol.* **2015**, *73* (1), 250–259.

(37) Vail, J. G. *Soluble Silicates*; Reinhold Publishing Corporation: New York, 1952.

(38) Yang, X.; Zhang, S. Characterizing and Modeling the Rheological Performances of Potassium Silicate Solutions. *J. Solution Chem.* **2016**, *45*, 1890–1901.

(39) Nordström, J.; Sundblom, A.; Jensen, G. V.; Pedersen, J. S.; Palmqvist, A.; Matic, A. Silica/Alkali Ratio Dependence of the Microscopic Structure of Sodium Silicate Solutions. *J. Colloid Interface Sci.* **2013**, *397*, 9–17.

(40) Nordström, J.; Nilsson, E.; Jarvol, P.; Nayeri, M.; Palmqvist, A.; Bergenholtz, J.; Matic, A. Concentration- and PH-Dependence of Highly Alkaline Sodium Silicate Solutions. *J. Colloid Interface Sci.* **2011**, *356* (1), 37–45.

(41) Tognonvi, M. T.; Rossignol, S.; Bonnet, J. P. Effect of Alkali Cation on Irreversible Gel Formation in Basic Medium. *J. Non. Cryst. Solids* **2011**, *357* (1), 43–49.

(42) Bass, J. L.; Turner, G. L. Anion Distributions in Sodium Silicate Solutions. Characterization by ^{29}Si NMR and Infrared Spectroscopies, and Vapor Phase Osmometry. *J. Phys. Chem. B* **1997**, *101*, 10638–10644.

(43) Harris, R. K.; Knight, C. T. G. Silicon-29 Nuclear Magnetic Resonance Studies of Aqueous Silicate Solutions. *J. Chem. Soc., Faraday Trans. 2* **1983**, *79*, 1539–1561.

(44) Engelhardt, G.; Michel, D. ^{29}Si NMR of Silicate Solutions. In *High-Resolution solid-state NMR of silicates and zeolites*; John Wiley & Sons Ltd., 1987; pp 75–105.

(45) Halasz, I.; Agarwal, M.; Li, R.; Miller, N. Molecular Spectroscopy of Alkaline Silicate Solutions. *Stud. Surf. Sci. Catal.* **2008**, *174* (B), 787–792.

(46) Vidal, L.; Gharzouni, A.; Joussein, E.; Colas, M.; Cornette, J.; Absi, J.; Rossignol, S. Determination of the Polymerization Degree of Various Alkaline Solutions: Raman Investigation. *J. Sol-Gel Sci. Technol.* **2017**, *83* (1), 1–11.

(47) Langille, K. B.; Nguyen, D.; Bernt, J. O.; Veinot, D. E.; Murthy, M. K. Mechanism of Dehydration and Intumescence of Soluble Silicates Part II Effect of the Cation. *J. Mater.*

Sci. **1991**, *26*, 704–710.

(48) Langille, K.; Nguyen, D.; Veinot, D. E. Inorganic Intumescent Coatings for Improved Fire Protection of GRP. *Fire Technol.* **1999**, *35* (2), 99–110.

(49) Essaidi, N.; Laou, L.; Yotte, S.; Ulmet, L.; Rossignol, S. Comparative Study of the Various Methods of Preparation of Silicate Solution and Its Effect on the Geopolymerization Reaction. *Results Phys.* **2016**, *6*, 280–287.

(50) Boudot, M.; Boissière, C.; Burov, E.; Gacoin, T. Engineering of Silica Thin-Film Nanoporosity via Alkali-Ion-Assisted Reconstruction. *Chem. Mater.* **2019**, *31* (7), 2390–2400.

(51) Dent Glasser, L. S.; Lee, C. K. Drying of Sodium Silicate Solutions. *J. Appl. Chem. Biotechnol.* **1971**, *21*, 127–133.

(52) Roggendorf, H.; Böschel, D.; Trempler, J. Structural Evolution of Sodium Silicate Solutions Dried to Amorphous Solids. *J. Non. Cryst. Solids* **2001**, *293–295* (1), 752–757.

(53) Xu, L.; Hu, Y.; Mu, Y.; Zhang, F.; Wang, J.; Chen, W.; Li, Y.; Zu, C. Kinetics of Foaming Process of Potassium Silicate Gel at High Temperature. *Mater. Lett.* **2020**, *281*, 128614.

(54) Iler, R. K. Polymerization of Silica. In *The Chemistry of Silica*; Wiley-Interscience, John Wiley & Sons, 1979; pp 172–311.

(55) Brinker, C. J.; Scherer, G. W. *Sol-Gel Science: The Physics and Chemistry of Sol-Gel Processing*; Academic Press Limited: London, 1990.

(56) Roggendorf, H. Structural Characterization of Concentrated Alkaline Silicate Solutions by ^{29}Si-NMR Spectroscopy, FT-IR Spectroscopy, Light Scattering, and Electron Microscopy-Molecules, Colloid. *Glas. Ber. Glas. Sci. Technol.* **1996**, *69*, 216–231.

(57) Roggendorf, H.; Fischer, M.; Roth, R.; Godehardt, R. Influence of Temperature and Water Vapour Pressure on Drying Kinetics and Colloidal Microstructure of Dried Sodium Water Glass. *Adv. Chem. Eng. Sci.* **2015**, *05* (01), 72–82.

(58) Knudsen, M. Die Gesetze Der Molekularströmung Und Der Inneren Reibungsströmung Der Gase Durch Röhren. *Ann. Phys.* **1909**, *333* (1), 75–130.

(59) Roggendorf, H.; Böschel, D.; Rödicker, B. Differential Scanning Calorimetry at Hydrothermal Conditions of Amorphous Materials Prepared by Drying Sodium Silicate Solutions. *J. Therm. Anal. Calorim.* **2001**, *63* (3), 641–652.

(60) Roggendorf, H.; Böschel, D. Hydrous Sodium Silicate Glasses Obtained by Drying Sodium Silicate Solutions. *Glas. Sci. Technol. Glas. Berichte* **2002**, *75* (2), 103–111.

(61) Hesky, D.; Aneziris, C. G.; Groß, U.; Horn, A. Water and Waterglass Mixtures for Foam Glass Production. *Ceram. Int.* **2015**, *41* (10), 12604–12613.

(62) Widmann, G.; Riesen, R. The Glass Transition of Water and Aqueous Systems. *J. Therm. Anal.* **1998**, *52*, 109–113.

(63) Greaves, G. N.; Sen, S. Inorganic Glasses, Glass-Forming Liquids and Amorphizing Solids. *Advances in Physics*. January 2007, pp 1–166.

(64) Moynihan, C. T.; Easteal, A. J.; Wilder, J.; Tucker, J. Dependence of the Glass Transition Temperature on Heating and Cooling Rate. *J. Phys. Chem.* **1974**, *78* (26), 2673–2677.

(65) Greaves, G. N. EXAFS and the Structure of Glass. *J. Non. Cryst. Solids* **1985**, *71* (1–3), 203–217.

(66) Phalippou, J. From Gel to Glass. *C. R. Chim.* **2002**, *5*, 855–863.

(67) Tan, J.; Zhao, S.; Wang, W.; Davies, G.; Mo, X. The Effect of Cooling Rate on the Structure of Sodium Silicate Glass. *Mater. Sci. Eng. B Solid-State Mater. Adv. Technol.* **2004**, *106* (3), 295–299.

(68) Husung, R. D.; Doremus, R. H. The Infrared Transmission Spectra of Four Silicate Glasses before and after Exposure to Water. *J. Mater. Res.* **1990**, *5* (10), 2209–2217.

(69) Maekawa, H.; Maekawa, T.; Kawamura, K.; Yokokawa, T. The Structural Groups of Alkali Silicate Glasses Determined from ^{29}Si MAS-NMR. *J. Non. Cryst. Solids* **1991**, *127*, 53–64.

(70) Emerson, J. F.; Stallworth, P. E.; Bray, P. J. High-Field ^{29}Si NMR Studies of Alkali Silicate Glasses. *J. Non. Cryst. Solids* **1989**, *113* (2–3), 253–259.

(71) Doremus, R. H. *Glass Science*, Second.; Wiley-Interscience, John Wiley & Sons: New York, 1994.

(72) Yasumori, A.; Inoue, S.; Yamane, M. Preparation of Na_2O-SiO_2 Glasses in the Metastable Immiscibility Region. *J. Non. Cryst. Solids* **1986**, *82*, 177–182.

(73) Prassas, M.; Phalippou, J.; Hench, L. L. Preparation of XNa_2O-$(1-x)SiO_2$ Gels for the Gel-Glass Process II. The Gel-Glass Conversion. *J. Non. Cryst. Solids* **1984**, *63* (3), 375–389.

(74) Hench, L. L.; Prassas, M.; Phalippou, J. Preparation of 33 Mol% Na_2O-67 Mol% SiO_2 Glass by Gel-Glass Transformation. *J. Non. Cryst. Solids* **1982**, *53*, 183–193.

(75) Puyané, R.; James, P. F.; Rawson, H. Preparation of Silica and Soda-Silica Glasses by the Sol-Gel Process. *J. Non. Cryst. Solids* **1980**, *41*, 105–115.

(76) Kim, S. S.; Sanders, T. H. Thermodynamic Modeling of Phase Diagrams in Binary Alkali Silicate Systems. *J. Am. Ceram. Soc* **1991**, *74* (8), 1833–1840.

(77) Brawer, S. A.; White, W. B. Raman Spectroscopic Investigation of the Structure of Silicate Glasses. I. The Binary Alkali Silicates. *J. Chem. Phys.* **1975**, *63* (6), 2421–2432.

(78) Malfait, W. J.; Zakaznova-Herzog, V. P.; Halter, W. E. Quantitative Raman Spectroscopy: High-Temperature Speciation of Potassium Silicate Melts. *J. Non. Cryst. Solids* **2007**, *353* (44–46), 4029–4042.

(79) Hass, M. Raman Spectra of Vitreous Silica, Germania and Sodium Silicate Glasses. *J. Phys. Chem. Solids* **1970**, *3* (1), 41–422.

(80) McMillan, P. F.; Wolf, G. H.; Poe, B. T. Vibrational Spectroscopy of Silicate Liquids and Glasses. *Chem. Geol.* **1992**, *96* (3–4), 351–366.

(81) Malfait, W. J.; Zakaznova-Herzog, V. P.; Halter, W. E. Quantitative Raman Spectroscopy: Speciation of Na-Silicate Glasses and Melts. *Am. Mineral.* **2008**, *93* (10), 1505–1518.

(82) Nesbitt, H. W.; Bancroft, G. M.; Henderson, G. S.; Ho, R.; Dalby, K. N.; Huang, Y.; Yan, Z. Bridging, Non-Bridging and Free (O_2^-) Oxygen in Na_2O-SiO_2 Glasses: An X-Ray Photoelectron Spectroscopic (XPS) and Nuclear Magnetic Resonance (NMR) Study. *J. Non. Cryst. Solids* **2011**, *357* (1), 170–180.

(83) Malfait, W. J.; Halter, W. E.; Morizet, Y.; Meier, B. H.; Verel, R. Structural Control on Bulk Melt Properties: Single and Double Quantum ^{29}Si NMR Spectroscopy on Alkali-Silicate Glasses. *Geochim. Cosmochim. Acta* **2007**, *71*, 6002–6018.

(84) Uchino, T.; Sakka, T.; Lwasaki, M. Interpretation of Hydrated States of Sodium Silicate Glasses by Infrared and Raman Analysis. *J. Am. Ceram. Soc.* **1991**, *74* (2), 306–313.

(85) Bartholomew, R. F. High-Water Containing Glasses. *J. Non. Cryst. Solids* **1983**, *56*, 331–342.

(86) Cody, G. D.; Mysen, B. O.; Lee, S. K. Structure vs. Composition: A Solid-State ^{1}H and ^{29}Si NMR Study of Quenched Glasses along the Na_2O-SiO_2-H_2O Join. *Geochim. Cosmochim. Acta* **2005**, *69* (9), 2373–2384.

(87) Zietka, S.; Deubener, J.; Behrens, H.; Müller, R. Glass Transition and Viscosity of Hydrated Silica Glasses. *Phys. Chem. Glas. Eur. J. Glas. Sci. Technol. Part B* **2007**, *48* (6), 380–387.

(88) Yamashita, S.; Behrens, H.; Schmidt, B. C.; Dupree, R. Water Speciation in Sodium Silicate Glasses Based on NIR and NMR Spectroscopy. *Chem. Geol.* **2008**, *256* (3–4), 231–241.

(89) Tomozawa, M.; Takata, M.; Acocella, J.; Bruce Watson, E.; Takamori, T. Thermal Properties of $Na_2O{\cdot}3SiO_2$ Glasses with High Water Content. *J. Non. Cryst. Solids* **1983**, *56* (1–3), 343–348.

(90) Pandya, N.; Muenow, D. W.; Sharma, S. K.; Sherriff, B. L. The Speciation of Water in Hydrated Alkali Silicate Glasses. *J. Non. Cryst. Solids* **1994**, *176*, 140–146.

(91) Zotov, N.; Keppler, H. The Influence of Water on the Structure of Hydrous Sodium Tetrasilicate Glasses. *Am. Mineral.* **1998**, *83*, 823–834.

(92) Stebbins, J. F.; Sen, S. Oxide Ion Speciation in Potassium Silicate Glasses: New Limits from ^{17}O NMR. *J. Non. Cryst. Solids* **2013**, *368*, 17–22.

(93) Soares, P. .; Zanotto, E. .; Fokin, V. .; Jain, H. TEM and XRD Study of Early Crystallization of Lithium Disilicate Glasses. *J. Non. Cryst. Solids* **2003**, *331* (1–3), 217–227.

(94) Bischoff, C.; Eckert, H.; Apel, E.; Rheinberger, V. M.; Höland, W. Phase Evolution in Lithium Disilicate Glass-Ceramics Based on Non-Stoichiometric Compositions of a Multi-Component System: Structural Studies by ^{29}Si Single and Double Resonance Solid State NMR. *Phys. Chem. Chem. Phys.* **2011**, *13* (10), 4540–4551.

(95) Soares, R. S.; Monteiro, R. C. C.; Lima, M. M. R. A.; Silva, R. J. C. Crystallization of Lithium Disilicate-Based Multicomponent Glasses - Effect of Silica/Lithia Ratio. *Ceram. Int.* **2015**, *41*, 317–324.

(96) Fernandes, H. R.; Tulyaganov, D. U.; Pascual, M. J.; Ferreira, J. M. F. Structure-Property Relationships and Densification-Crystallization Behaviours of Simplified Lithium

Disilicate Glass Compositions. *Ceram. Int.* **2014**, *40*, 129–140.

(97) Zhang, P.; Li, X.; Yang, J.; Xu, S. The Crystallization and Microstructure Evolution of Lithium Disilicate-Based Glass-Ceramic. *J. Non. Cryst. Solids* **2014**, *392–393*, 26–30.

(98) Sycheva, G. A. Phase Separation and Crystallization in Glasses of the Lithium Silicate System $XLi_2O \cdot (100 - X)SiO_2$ (x = 23.4, 26.0, 33.5). *Glas. Phys. Chem.* **2011**, *37* (2), 135–149.

(99) Zanotto, E. D. Effect of Liquid Phase Separation on Crystal Nucleation in Glass-Formers. Case Closed. *Ceram. Int.* **2020**, *46* (16), 24779–24791.

(100) Sycheva, G. A. Determination of the Size of the Critical Nucleus of Crystals in Lithium and Sodium Silicate Glass. *Glas. Phys. Chem.* **2015**, *41* (3), 302–306.

(101) Prassas, M.; Hench, L. L. *Ultrastructure Processing of Ceramics, Glasses and Composites*; Hench, L. L., Ulrich, D. R., Eds.; Wiley: New York, 1984.

(102) Lu, G.; Klein, L. C. Unidirectional Crystallization of Potassium Disilicate II. Experimental Study. *J. Cryst. Growth* **1983**, *64* (3), 479–484.

(103) Masoudi Alavi, A.; Sax, A.; Quirmbach, P. Interaction of Aluminum Metaphosphates in the Setting of Potassium Silicate Solutions in Terms of the Crystalline Phase Composition. *ChemistryOpen* **2020**, *9* (5), 631–636.

(104) Sycheva, G. A. Evalution of the Surface Energy at the Crystal-Glass Interface in Sodium Silicate Glass $46Na_2O{\cdot}54\ SiO_2$. *Glas. Phys. Chem.* **1998**, *24* (1), 47–53.

(105) Stebbins, J. F.; Sen, S. Silicate Species Exchange, Viscosity, and Crystallization in a Low-Silica Melt: In Situ High-Temperature MAS NMR Spectroscopy. *Am. Mineral.* **1995**, *80*, 861–864.

(106) Zhang T, B.; Easteal, A. J.; Edmonds, N. R.; Bhattacharyya, D. Sol-Gel Preparation and Characterization of Lithium Disilicate Glass-Ceramic. *J. Am. Ceram. Soc.* **2007**, *90* (5), 1592–1596.

(107) Li, P.; Ferguson, B. A.; Francis, L. F. Sol-Gel Processing of Lithium Disilicate Part I Crystalline Phase Development of Gel-Derived Powders. *J. Mater. Sci.* **1995**, *30*, 4076–4086.

(108) Sycheva, G. A.; Kostyreva, T. G. Nucleation and Morphology of Crystals in Simple and Complex Silicate Glasses $R'_2O\text{-}SiO_2$, $R'_2O\text{-}R''O\text{-}SiO_2$, (R' = Li, Na, K; R" = Ca, Mg) Synthesized by the Sol-Gel Method. *Glas. Phys. Chem.* **2014**, *40* (5), 513–520.

(109) Subasri, R.; Näfe, H. Phase Evolution on Heat Treatment of Sodium Silicate Water Glass. *J. Non. Cryst. Solids* **2008**, *354* (10–11), 896–900.

(110) Elcometer Web Page: https://www.elcometer.com/fr/inspection-revetements/materiel-dessai-physique-et-de-laboratoire/application-de-film/bar-coaters-applicateurs-de-film/applicateurs-de-film-baker-rglables-elcometer-3525-3530.html (accessed 2021 -09 -04).

(111) Massiot, D.; Fayon, F.; Capron, M.; King, I.; Le Calvé, S.; Alonso, B.; Durand, J. O.; Bujoli, B.; Gan, Z.; Hoatson, G. Modelling One- and Two-Dimensional Solid-State NMR Spectra.

Magn. Reson. Chem. **2002**, *40* (1), 70–76.

(112) Vaitkus, A.; Merkys, A.; Grazulis, S. Validation of the Crystallography Open Database Using the Crystallographic Information Framework. *J. Appl. Crystallogr.* **2021**, *54*, 661–672.

(113) Jain, A.; Ong, S. P.; Hautier, G.; Chen, W.; Richards, W. D.; Dacek, S.; Cholia, S.; Gunter, D.; Skinner, D.; Ceder, G.; Persson, K. A. Commentary: The Materials Project: A Materials Genome Approach to Accelerating Materials Innovation. *APL Mater.* **2013**, *1*, 011002-1-011002–011011.

(114) Knoche, R.; Dingwell, D. B.; Seifert, F. A.; Webb, S. L. Non-Linear Properties of Supercooled Liquids in the System Na_2O-SiO_2. *Chem. Geol.* **1994**, *116*, 1–16.

(115) Lara, C.; Pascual, M. J.; Prado, M. O.; Durán, A. Sintering of Glasses in the System RO-Al_2O_3-BaO- SiO_2 (R=Ca, Mg, Zn) Studied by Hot-Stage Microscopy. *Solid State Ionics* **2004**, *170* (3–4), 201–208.

(116) Harris, R. K.; Newman, R. H. ^{29}Si N.M.R. Studies of Aqueous Silicate Solutions. *J. Chem. Soc. Faraday Trans. 2* **1977**, *73*, 1204–1215.

(117) Mohsin, H.; Maron, S.; Maurin, I.; Burov, E.; Tricot, G.; Devys, L.; Gouillart, E.; Gacoin, T. Thermal Behavior of Waterglass: Foaming and Xerogel-to-Glass Evolution. *J. Non. Cryst. Solids* **2021**, *566*, 120872-undefined.

(118) Shen, A.; Keppler, H. Infrared Spectroscopy of Hydrous Silicate Melts to 1000 °C and 10 Kbar: Direct Observation of H_2O Speciation in a Diamond-Anvil Cell. *Am. Mineral.* **1995**, *80* (11–12), 1335–1338.

(119) Nowak, M.; Behrens, H. The Speciation of Water in Haplogranitic Glasses and Melts Determined by in Situ Near-Infrared Spectroscopy. *Geochim. Cosmochim. Acta* **1995**, *59* (16), 3445–3450.

(120) Stolper, E. Contributions to Mineralogy and Petrology Water in Silicate Glasses: An Infrared Spectroscopic Study. *Contrib. to Mineral. Petrol.* **1982**, *81*, 1–17.

(121) Bale, C. W.; Chartrand, P.; Degterov, S. A.; Eriksson, G.; Hack, K.; Mahfoud, R. Ben; Melanqon, J.; Pelton, A. D.; Petersen, S. FactSage Thermochemical Software and Databases. *Calphad* **2002**, *26* (2), 189–228.

(122) Huang, S.; Zhang, B.; Huang, Z.; Gao, W.; Cao, P. Crystalline Phase Formation, Microstructure and Mechanical Properties of a Lithium Disilicate Glass-Ceramic. *J. Mater. Sci.* **2013**, *48*, 251–257.

(123) Huang, S.; Zujovic, Z.; Huang, Z.; Gao, W.; Cao, P. Crystallization of a High-Strength Lithium Disilicate Glass-Ceramic: An XRD and Solid-State NMR Investigation. *J. Non. Cryst. Solids* **2017**, *457*, 65–72.

(124) Shelby, J. E. Property/Morphology Relations in Alkali Silicate Glasses. *J. Am. Ceram. Soc.* **1983**, *66* (11), 754–757.

(125) Furukawa, T.; Fox, K. E.; White, W. B. Raman Spectroscopic Investigation of the Structure of Silicate Glasses. III. Raman Intensities and Structural Units in Sodium Silicate Glasses. *J. Chem. Phys.* **1981**, *75* (7), 3226–3237.

(126) McMillan, P. Structural Studies of Silicate Glasses and Melts-Applications and Limitations of Raman Spectroscopy. *Am. Mineral.* **1984**, *69*, 622–644.

(127) Matson, D. W.; Sharma, S. K.; Philpotts, J. A. The Structure of High-Silica Alkali-Silicate Glasses. A Raman Spectroscopic Investigation. *J. Non. Cryst. Solids* **1983**, *58* (2–3), 323–352.

(128) Mysen, B. O.; Frantz, J. D.; Mysen, B. O.; Frantz, J. D. Silicate Melts at Magmatic Temperatures: In-Situ Structure Determination to 1651°C and Effect of Temperature and Bulk Composition on the Mixing Behavior of Structural Units. *Contrib Miner. Pet.* **1994**, *117*, 1–14.

(129) Sharma, S. K.; Mammone, J. F.; Nicol, M. F. Raman Investigation of Ring Configurations in Vitreous Silica. *Nature* **1981**, *292*, 140–141.

(130) Galeener, F. L. Planar Rings in Vitreous Silica. *J. Non. Cryst. Solids* **1982**, *49*, 53–62.

(131) Kilymis, D.; Ispas, S.; Hehlen, B.; Peuget, S.; Delaye, J. M. Vibrational Properties of Sodosilicate Glasses from First-Principles Calculations. *Phys. Rev. B* **2019**, *99*, 054209.

(132) Colomban, P.; Paulsen, O. Non-Destructive Determination of the Structure and Composition of Glazes by Raman Spectroscopy. *J. Am. Ceram. Soc.* **2005**, *88* (2), 390–395.

(133) Vega, A. J.; Scherer, G. W. Study of Structural Evolution of Silica Gel Using ^{1}H and ^{29}Si NMR. *J. Non. Cryst. Solids* **1989**, *111*, 153–166.

(134) Kinney, D. R.; Chuang, I.-S.; Maciel, G. E. Water and the Silica Surface As Studied by Variable-Temperature High-Resolution NMR. *J. Am. Chem. Soc* **1993**, *115*, 6786–6794.

(135) Brus, J.; Dybal, J. Hydrogen-Bond Interactions in Organically-Modified Polysiloxane Networks Studied by 1D and 2D CRAMPS and Double-Quantum ^{1}H MAS NMR. *Macromolecules* **2002**, *35* (27), 10038–10047.

(136) D'Espinose de la Caillerie, J.-B.; Aimeur, M. R.; Kortobi, Y. El; Legrand, A. P. Water Adsorption on Pyrogenic Silica Followed by ^{1}H MAS NMR. *J. Colloid Interface Sci.* **1997**, *194*, 434–439.

(137) Leboda, R.; Turov, V. V.; Marciniak, M.; Malygin, A. A.; Malkov, A. A. Characteristics of the Hydration Layer Structure in Porous Titania-Silica Obtained by the Chemical Vapor Deposition Method. *Langmuir* **1999**, *15* (24), 8441–8446.

(138) Kümmerlen, J.; Merwin, L. H.; Sebald, A.; Hans, K. Structural Role of H_2O in Sodium Silicate Glasses: Results from ^{29}Si and ^{1}H NMR Spectroscopy. *J. Phys. Chem.* **1992**, *96*, 6405–6410.

(139) Robert, E.; Whittington, A.; Fayon, F.; Pichavant, M.; Massiot, D. Structural Characterization of Water-Bearing Silicate and Aluminosilicate Glasses by High-Resolution Solid-State NMR. *Chem. Geol.* **2001**, *174*, 291–305.

(140) Schaller, T.; Sebald, A. One-and Two-Dimensional ^{1}H Magic-Angle Spinning Experiments on Hydrous Silicate Glasses. *Solid State Nucl. Magn. Reson.* **1995**, *5*, 89–102.

(141) Simakin, A. G.; Salova, T. P.; Zavelsky, V. O. Mechanism of Water Dissolution in Sodium-

Silicate Melts and Glasses: Structural Interpretation of Spectroscopic Data. *Geochemistry Int.* **2008**, *46* (2), 107–115.

(142) Hayashi, S. Solid-State NMR Study of Locations and Dynamics of Interlayer Cations and Water in Kanemite. *J. Mater. Chem* **1997**, *7* (6), 1043–1048.

(143) Beerkens, R. G. C. Modeling the Kinetics of Volatilization from Glass Melts. *J. Am. Ceram. Soc.* **2004**, *84* (9), 1952–1960.

(144) Brandriss, M. E.; Stebbins, J. F. Effects of Temperature on the Structures of Silicate Liquids: ^{29}Si NMR Results. *Geochim. Cosmochim. Acta* **1988**, *52*, 2659–2669.

(145) Dupree, R.; Holland, D.; Mortuza, M. G. A MAS-NMR Investigation of Lithium Silicate Glasses and Glass Ceramics. *J. Non. Cryst. Solids* **1990**, *116*, 148–160.

(146) Koroleva, O. N.; Bychinskii, V. A.; Tupitsyn, A. A.; Shtenberg, M. V.; Krenev, V. A.; Fomichev, S. V. Physicochemical Model as a Method for Calculating and Making Consistent Thermodynamic Properties of Structural Units in Alkali Silicate Melts. *Russ. J. Inorg. Chem.* **2015**, *60* (9), 1104–1109.

(147) Zhang, P.; Dunlap, C.; Grandinetti, P.; Farnan, I.; Stebbins, J. Silicon Site Distributions in an Alkali Silicate Glass Derived by Two-Dimensional ^{29}Si Nuclear Magnetic Resonance. *J. Non. Cryst. Solids* **1996**, *204*, 294–300.

(148) Deubener, J.; Müller, R.; Behrens, H.; Heide, G. Water and the Glass Transition Temperature of Silicate Melts. *J. Non. Cryst. Solids* **2003**, *330* (1–3), 268–273.

(149) Mysen, B. O.; Frantz, J. D. Structure and Properties of Alkali Silicate Melts at Magmatic Temperatures. *Eur. J. Mineral.* **1993**, *5* (3), 393–407.

(150) Madsen, I. C.; Scarlett, N. V. Y.; Kern, A. Description and Survey of Methodologies for the Determination of Amorphous Content via X-Ray Powder Diffraction. *Zeitschrift fur Krist.* **2011**, *226* (12), 944–955.

(151) Scherer, G. W. Editorial Comments on a Paper by Gordon S. Fulcher. *J. Am. Ceram. Soc.* **1992**, *75* (5), 1060–1062.

(152) Fulcher, G. S. Analysis of Recent Measurements of Viscosity of Glasses. *J. Am. Ceram. Soc.* **1925**, *8* (6), 339–355.

(153) Montanari, F.; Miselli, P.; Leonelli, C.; Boschetti, C.; Henderson, J.; Baraldi, P. Calibration and Use of the Heating Microscope for Indirect Evaluation of the Viscosity and Meltability of Archeological Glasses. *Int. J. Appl. Glas. Sci.* **2014**, *5* (2), 161–177.

(154) Pascual, M. J.; Durán, A.; Prado, M. O. A New Method for Determining Fixed Viscosity Points of Glasses. *Phys. Chem. Glas.* **2005**, *46* (5), 512–520.

(155) Panna, W.; Wyszomirski, P.; Kohut, P. Application of Hot-Stage Microscopy to Evaluating Sample Morphology Changes on Heating. *J. Therm. Anal. Calorim.* **2016**, *125* (3), 1053–1059.

(156) Pascual, M. J.; Pascual, L.; Durán, A. *Determination of the Viscosity-Temperature Curve for Glasses on the Basis of Fixed Viscosity Points Determined by Hot Stage Microscopy*; 2001; Vol. 42.

(157) Zhang, S.; Lee, Y. R.; Ahn, J. W.; Ahn, W. S. Sodium Silicate Insulating Foam Reinforced with Acid-Treated Fly Ash. *Mater. Lett.* **2018**, *218*, 56–59.

(158) Li, Y.; Cheng, X.; Cao, W.; Gong, L.; Zhang, R.; Zhang, H. Fabrication of Adiabatic Foam at Low Temperature with Sodium Silicate as Raw Material. *Mater. Des.* **2015**, *88*, 1008–1014.

(159) Pauchard, L.; Allain, C. Buckling Instability Induced by Polymer Solution Drying. *Europhys. Lett.* **2003**, *62* (6), 897–903.

(160) Kekevi, B.; Berber, H.; Yıldırım, H. Synthesis and Characterization of Silicone-Based Surfactants as Anti-Foaming Agents. *J. Surfactants Deterg.* **2012**, *15* (1), 73–81.

Publications

1. **H. Mohsin et al**, Intumescent behavior of alkali silicate thick coatings obtained from solution route (*in submission phase*)
2. **H. Mohsin et al**, Crystallization induced suppression of intumescence in aqueous alkali silicates (*in submission phase*)
3. **H. Mohsin et al**, Thermal behavior of waterglass: foaming and xerogel-to-glass evolution, *Journal of Non-Crystalline Solids*, 2021, 566, 120872

Conferences/Seminars/Workshops

- GOMD '21 Virtual Conference – Oral (Dec 2021)
- PhD seminar, Saint-Gobain Research Paris – Oral (Jun 2021)
- SiO_2 2021 Virtual Conference – Oral (Jun 2021)
- GERM Virtual Conference – Poster (Apr 2021)
- RFL Group, Saint-Gobain Research Paris – Oral (Dec 2020)
- PhD seminar, Saint-Gobain Research Paris – Oral (Nov 2020)
- PhD seminar, Saint-Gobain Research Paris – Oral (Nov 2019)
- ED Interface Day, UniversitéParis-Saclay – Poster (Nov 2019)
- 11^{th} ICG Montpellier Summer School, France (Jul 2019)
- Gay-Lussac Day, Saint-Gobain Research Paris – Poster (July 2019)
- DGG-USTV Joint Conference, Germany – Poster (May 2019)
- PhD seminar, Saint-Gobain Research Paris – Oral (Feb 2019)

Journal of Non-Crystalline Solids 566 (2021) 120872

Contents lists available at ScienceDirect

Journal of Non-Crystalline Solids

journal homepage: www.elsevier.com/locate/jnoncrysol

Thermal behavior of waterglass: foaming and xerogel-to-glass evolution

Hamza Mohsin [a,b], Sébastien Maron [a], Isabelle Maurin [a], Ekaterina Burov [b], Grégory Tricot [c], Lucie Devys [d], Emmanuelle Gouillart [b,*], Thierry Gacoin [a]

[a] Laboratoire de Physique de la Matière Condensée, Ecole Polytechnique, CNRS, IP Paris, 91128 Palaiseau, France
[b] Laboratoire Surface du Verre et Interfaces (SVI), UMR 125 CNRS/Saint-Gobain Recherche, 93303 Aubervilliers, France
[c] Université de Lille, CNRS, UMR 8516-LASIR-Laboratoire de Spectrochimie Infrarouge et Raman, F-59000 Lille, France
[d] Département Couches Minces, Saint-Gobain Recherche, 93303 Aubervilliers, France

ARTICLE INFO

Keywords:
Sodium silicate solutions
Hydrated silicates
Foaming
Q^n structural units
Xerogel
Glass transition

ABSTRACT

Structural properties of aqueous Na-silicates at both room and high temperature (below 500°C) have been investigated to better understand the microscopic evolution of structure and the macroscopic phenomenon of foaming. NMR spectroscopy has provided a direct quantification of structural units defined as Q^n. Solid-state NMR along with Raman spectroscopy has indicated the extent of local structural reorganization on heating the silicates. Heating an aqueous Na-silicate leads to structural changes due to the removal of water, where the quantity of leftover water in the system obeys an Arrhenian evolution with an activation energy of 30 $kJ.mol^{-1}$. TGA, NMR and Raman measurements suggest that the structure becomes similar to the one of hydrated silicate glasses studied in geochemistry. Increasing the Na concentration results in a larger quantity of water retained after a pre-drying treatment, which correlates with a lower softening temperature of the material and is, macroscopically, related to foaming of the silicate.

1. Introduction

Aqueous sodium silicates represent a cheap and green class of alkali silicates that find potential in several industrial applications such as binders,[1,2] coatings[3–5] and fire-retardant materials[6–8] to name a few. Fire-resistant properties of these silicates are of particular interest due to growing urban demand in the construction sector. Their intumescent behavior is a consequence of endothermic removal of water on contacting fire, resulting in a rigid foam (see Figure S1) that is thermally insulating. This motivates a thorough structural investigation at both the microscopic and macroscopic levels for a better understanding of their evolution with temperature and the underlying foaming phenomenon.

Sodium silicate solutions, which are a mixture of sodium oxide (Na_2O) and silicon dioxide (SiO_2) dissolved in water, are in general characterized by the Na_2O/SiO_2 molar ratio and the silicon concentration, that determine the structure of the polymeric silicate network. Microscopic structure of these silicate solutions at room temperature has been widely reported with particular emphasis on the effect of changing the initial concentration of Na on the distribution of Q^n (where 'n=0 to 4' represents structural units that correspond to the number of bridging oxygens (BOs) in the SiO_4 tetrahedrons).[9–12] Several techniques including Raman,[11,13] infra-red (IR)[2,11,14] and ^{29}Si nuclear magnetic resonance (NMR)[11,14] spectroscopy as well as small angle X-ray scattering (SAXS)[15] have suggested an increased degree of polymerization of the network with decreasing Na content in aqueous Na-silicates due to a reduction in their occupancy of non-bridging oxygens (NBOs). On the other hand, widely conducted studies have also been reported at both room[16–21] and elevated temperatures[17,22–25] for binary Na-silicate glasses prepared by conventional melt and quench process using the aforementioned characterization tools.

A majority of the studies on Na-silicates have focused on the solution properties at ambient conditions and therefore do not inform about the temperature stability of dried silicate and its behavior in the temperature range relevant for fire-retardant applications. Above 100°C, a limited number of studies have been reported on the microscopic evolution during drying of Na-silicate solutions with temperature, mainly suggesting the condensation of silanols associated to water evaporation.[26] Macroscopic changes including structural expansion corresponding to foaming at and above 150°C have been observed on drying Na-silicate solution,[27–30] and the extent of this expansion decreases on increasing the SiO_2 concentration while keeping Na content constant.[6] Heating further to temperatures as high as 800°C leads to a progressive

* Corresponding Author
E-mail address: emmanuelle.gouillart@saint-gobain.com (E. Gouillart).

https://doi.org/10.1016/j.jnoncrysol.2021.120872
Received 20 January 2021; Received in revised form 12 April 2021; Accepted 13 April 2021
Available online 8 May 2021

transition between a dried gel i.e. a xerogel, and a compound with glass-like properties. Similar to glasses obtained from the melt and quench technique, crystallization[31] may also be observed, especially when considering compositions with high sodium content.

However, a lack of in-depth studies on microscopic structural evolution with temperature above 100°C and below 500°C (i.e. before any crystallization occurs) using quantification techniques like NMR and Raman spectroscopy has limited the thorough understanding of properties that might influence the behavior at macroscopic scale (e.g. foaming). Furthermore, this temperature range crosses the frontier between soft chemistry and conventional glass chemistry, and a clear gap exists in linking the structural properties of Na-silicate solutions and sol-gel derivatives to the corresponding binary glasses prepared by the industrial melt and quench process.

An important motivation to fill this gap is the understanding of the structural evolution occurring while heating a silicate xerogel, starting from a sol-gel condensed siloxane network to a glass-like network exhibiting a typical glass transition temperature (T_g). Over which temperature range does this transition occur? How does the progressive elimination of water from condensation lead to foaming? What is the effect of water on the rheology of the network and how does it impact the T_g? Only little is known on these queries while it is evident that water drastically impacts the glass properties. As an example, glass transition values as low as 180°C have been reported for glasses with a direct dependency on the amount of water in the silicate[32] and the concentration of Na_2O in the network.[33] Therefore, it is also interesting to compare the evolution of alkali silicate solutions at high temperatures with the large body of research on the structure of hydrated alkali silicate glasses and melts in geochemistry and glass science.[32,34–38]

In this work, we report on the investigation of temperature evolution of commercially available aqueous Na-silicates starting from solutions to 450°C for creating a link between the microscopic properties of these solutions and the corresponding Na_2O-SiO_2 glasses prepared by melt and quench process. The effect of changing the Na_2O/SiO_2 molar ratio has also been investigated. Thermogravimetric analysis (TGA) has been performed to measure the mass loss of hydrated silicate powders while NMR spectroscopy has allowed to have a quantitative as well as qualitative information on the polymerization and connectivity of the silicate network. Raman spectroscopy has been utilized as a complementary tool to NMR for qualitative comparison of different Na_2O/SiO_2 molar ratios. From the combination of these techniques, we estimate the amount of water remaining in the material under its different forms (free water, solvating water and silanols)[39] as a function of temperature. This provides structural information allowing to explain macroscopic evolution of the silicate upon thermal treatment, such as rheological behavior and foaming.

2. Materials and Methods

2.1. Raw materials and sample preparation

Commercially available Na-silicate solutions were used as the starting materials. They have been defined in terms of their molar ratio as **$X=nNa_2O/nSiO_2$**. Na-silicate extra pure solution (27.75 wt% SiO_2 – 8.25 wt% Na_2O – 64 wt% H_2O) corresponding to the molar ratio X=0.29 was purchased from Sigma-Aldrich while Na-silicate crystal 0095 solution (27.25 wt% SiO_2 – 13.75 wt% Na_2O – 59 wt% H_2O) corresponding to the molar ratio X=0.5 was purchased from PQ Corporation. Both solutions were used as received. Reference bulk glasses of the composition 77% SiO_2 – 23% Na_2O (corresponding to X=0.29 silicate solution) and 67% SiO_2 – 33% Na_2O (corresponding to X=0.5 solution) were prepared by melt and quench process.

Na-silicate dried powders were prepared by heating the initial solutions in an oven at 150°C for 15 h to remove maximum amount of free water and limit the extent of foaming while performing further analyses. For our investigations, further thermal treatments were achieved on these powders at 275°C, 350°C, 400°C and 450°C at a heating rate of 5°C/min for 2 h each. Obtained powders or reference glasses were grinded and stored in sealed glass vials. 500 mg powder pellets were prepared by a Specac Manually Operated 15-ton Hydraulic Press using a 13 mm diameter die at a load of 2 tons for 60 s.

2.2. Characterization tools

2.2.1. Thermal analysis

Thermogravimetric analysis (TGA) was performed using a NETZSCH STA 409 Thermal Analyzer for obtaining mass loss curves up to 1200°C to monitor the evolution of leftover water or silanols with temperature in Na-silicate powders pre-dried at 150°C. An alumina crucible was used as the container and a moisture-free atmosphere was provided by continuously flowing N_2/O_2 gases in nearly equal volume. The measurement was repeated twice. Temperature calibration was performed at heating rates of 5, 10 and 20°C/min from the DTA signal using metal standards with different melting temperatures. Note that the calibration is not accurate at low temperature sweeps when the DTA signal is significantly broadened. Only small quantities of samples could be analyzed, typically 15 mg of the powder pre-dried at 150°C, because of foaming. This led to improper correction of the buoyancy effects in the RT-150°C temperature range.

Differential scanning calorimetry (DSC) was utilized for measuring the heat capacity of these silicates on a NETZSCH DSC 404 C under continuous N_2 flow. Typically, 10 mg of pre-dried powders prepared at 150°C were used as the starting materials and loaded as-received into a platinum-rhodium crucible without compressing. A heating rate of 10°C/min was employed. For heat capacity measurements, calibration was done by recording a baseline (without the sample) and a reference measurement with Sapphire which gives an energy calibration allowing subsequent calculations to be made using the processing software.

2.2.2. Nuclear Magnetic Resonance Spectroscopy

Liquid-state ^{29}Si NMR: The structure of Na-silicate solutions in terms of Q^n units was analyzed using liquid-state ^{29}Si NMR. Spectra were recorded at 59.63 MHz on a 300 MHz AVANCE II Bruker spectrometer with a BBO probe. A $\pi/2$ pulse was used with a repetition delay optimized at 5 s. 30 vol% heavy water (D_2O) was added to the samples for locking. All ^{29}Si chemical shifts were referenced to tetraethoxysilane (TEOS) as external reference [Chemical shift (Si)=-82 ppm vs TMS]. The contribution of the glass tube was corrected by subtracting the spectrum of empty tube from the final spectrum of silicate solutions. The relative proportion of Q^n units was determined by integrating the area under the curve of each peak for an exact quantification of the various species.

Solid-state MAS NMR: The samples treated at different temperatures and the prepared glasses were analyzed with solid-state magic angle spinning (MAS) NMR experiments. The 1D ^{29}Si NMR spectra were acquired at 71.53 MHz on a Tecmag Apollo360 spectrometer equipped with a 4 mm Bruker probe head operating at a spinning frequency (ν_{rot}) of 15 kHz. The acquisitions were performed with a 3.55 μs pulse length (corresponding to a $\pi/2$ flip angle), 3072 transients and a repetition delay of 20 s. The repetition delay was optimized by going up to 1500 s but that does not provide higher signal intensity. ^{23}Na and ^{1}H MAS-NMR experiments were recorded at 211.6 and 800 MHz, respectively, on an 18.8 T Bruker spectrometer. All the experiments were performed with a 3.2 mm probe head operating at ν_{rot} of 20 kHz. ^{23}Na MAS-NMR experiments were obtained with a 1 μs pulse length (corresponding to a $\pi/8$ flip angle), 256 transients and an optimized repetition delay of 0.5 s. ^{1}H MAS-NMR spectra were obtained with a 2.7 μs pulse length (corresponding to $\pi/2$ flip angle), 64 transients and an optimized repetition delay of 5 s. The NMR spectra were corrected from the signal coming from the probe. ^{29}Si, ^{23}Na and ^{1}H chemical shifts were referred to TEOS, NaCl and TMS solutions at -82, 0 and 0 ppm, respectively. Deconvolution of the ^{29}Si NMR spectra was performed using the Dmfit software[40]

with Gaussian fitting function because of the chemical shift distribution of amorphous structures. In order to analyze the $^{1}H/^{29}Si$ and $^{23}Na/^{29}Si$ interactions, correlation NMR was also applied at 9.4 T with an HXY-4 mm probe head operating at ν_{rot} of 8 kHz. 1D ^{29}Si (^{23}Na) Cross Polarization (CP) NMR technique was used to determine the distribution of Na ions within the silicate network. The experiment was performed with optimized low radio-frequency fields (around 5-6 kHz for both channels) allowing for an efficient transfer, a contact time of 6 ms and 400 k transients separated by a repetition delay of 0.2 s. 2D ^{29}Si (^{1}H) CP spectra were acquired to trace the Si-OH linkages. The 2k x 10 acquisition points were recorded under rotor-synchronized conditions with ^{1}H and ^{29}Si radiofrequency fields of 50 and 34 kHz and a contact time of 6 ms. Each direct slice was recorded with 512 transients and a repetition delay of 4 s.

2.2.3. Raman spectroscopy

Structural changes in terms of densification and polymerization of the silicate network with temperature were studied qualitatively using Raman spectroscopy. The data was acquired on Na-silicate powder pellets using a Renishaw Qontor Raman Spectrometer equipped with a 532 nm green laser and 50 mW power. A 50X objective lens was utilized for acquiring 992 spectra in the range 300-1300 cm^{-1} with a 90 μm step-size and an exposure time of 20 s. These spectra were averaged using principle component analysis (PCA) for denoising and homogenizing the composition variations from grain to grain over the pellet surface.

2.2.4. Visual monitoring of foaming process

The foaming behavior of a liquid droplet was visually inspected by recording a video of the droplet using a smartphone during heating under a temperature adjustable Steinel HL 220 E heat gun. Images at different temperatures were extracted from the video to show the corresponding thermal evolution of the droplet (details are given in section 3.2.4). The schematic illustration and description of the setup used is given in SI 2.

Images of a powder pellet (500 mg; diameter=13 mm; load=2 tons for 60 s) discussed in section 3.2.4 were captured using a smartphone at different temperatures during heating in a box furnace. This was achieved by manually opening the furnace door at set temperature points during the 5°C/min ramp. For a precise in-situ monitoring of thermal evolution of a powder pellet, a hot-stage microscope equipped with a 10X objective was utilized to record a video by capturing several images on ramping up to 400°C. Further details of the experimental parameters and the setup can be found in SI 2.

3. Results and discussion

3.1. Macroscopic evolution: global water content

Dried Na-silicate powders prepared from the two commercial solutions (X=0.29 and 0.5) by heating overnight at 150°C were subjected to further heating for investigation of properties at both macroscopic (global water evolution) and microscopic (structural) scale. These powders, dried but still hydrated will be referred to as “pre-dried” silicates. In this section, we describe the macroscopic evolution of these silicate powders and the effect of initial Na content.

Thermal evolution of the pre-dried Na-silicates was derived from

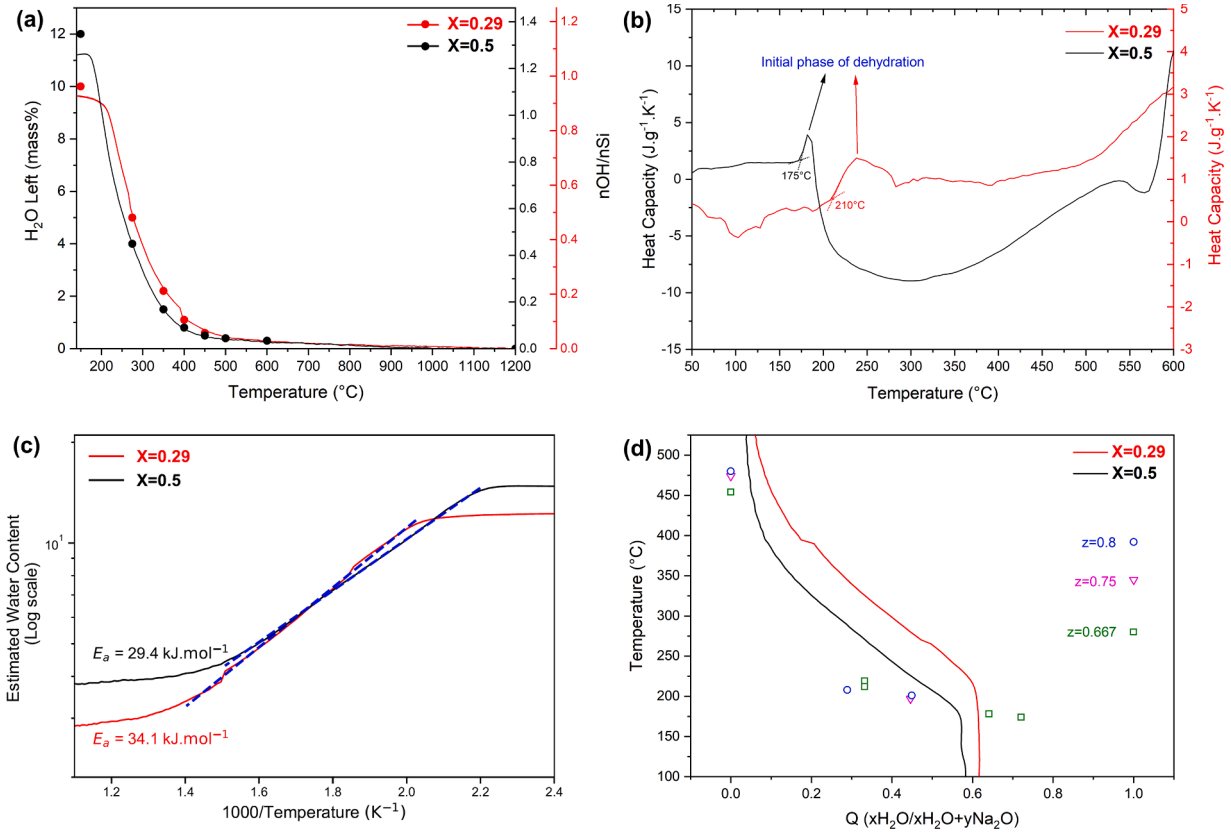

Figure 1. (a) Evolution of total water left in the network for the two molar ratios (TGA measurement performed at 10°C/min); note that both y-axes on the right, red corresponding to X=0.29 and black to X=0.5, represent nOH/nSi, (b) DSC measurements for heat capacity at 10°C/min also performed on pre-dried powder (the onset of the peaks are identified as a glass transition and match well with the macroscopic foaming temperature), (c) Arrhenian plot of TGA mass loss curves (the fitting temperature range is 220-450°C for X=0.29 and 180-400°C for X=0.5, respectively) and (d) comparison of our TGA curves (represented by solid lines) with glass transition temperature reported for hydrated glasses[32,35,36] (Q represents the mole fraction of water whereas the molar content of SiO_2 (at 150-500°C), represented by z, is in the range 0.56-0.77 moles for X=0.29 and 0.46-0.66 moles for X=0.5, respectively, while constant for literature points).

TGA measurements as shown in Figure 1. X=0.29 silicate powder was subjected to mass loss measurements at heating ramps of 5, 10 and 20°C/min to determine if the evolution was controlled by kinetic effects (see Figure S3(a)). A heating rate of 10°C/min was chosen for further studies as the mass loss seemed to be only temperature dependent, at least for the range of heating rates tested.

The mass loss curves for the two molar ratios at a heating rate of 10°C/min are shown in Figure S3(b) while the percentage of leftover water (calculated by subtracting percentage mass loss at 275, 350, 400, 450, 500, 600 and 1200°C from the overall mass lost in TGA measurements) is plotted as a function of temperature in Figure 1(a). Note that the step around 400°C for X=0.29 in Figure 1(a) is a consequence of splashing or bubble bursting from the powder and corresponds to a mass loss of 0.4% which is not significant and is, thus, a part of the calculations made here. Dehydration occurs very quickly after heating at temperatures higher than 150°C (pre-drying temperature). Interestingly, DSC curves shown in Figure 1(b) suggest that the silicates experience a T_g around 210°C for X=0.29 and 175°C for X=0.5, in the same range of temperature where dehydration starts. Note that there is an interplay between glass transition and water removal which means that decreasing the water content changes the (supposed) T_g and when the DSC-determined glass transition is reached, water removal increases since the silica network is more mobile and water diffusion is enhanced within the material.

More overall mass is lost for the silicate with higher Na content in the network indicating a slightly more retention of leftover water in the starting powder prepared at 150°C. Assuming that all water is lost at 1200°C, total water retention is 12% in X=0.5 and 10% in X=0.29 starting powder as shown in Table 1. This slight difference in the amount of water may explain the offset of temperature observed by DSC suggesting a connection between the water content and softening (more mobile network) of the material. Near 150°C, the presence of more retained water when there is higher Na content in the silicate can be attributed to solvating water (linked to silanols or ionic hydration)[39] and a higher number of silanols.

The global evolution behavior of TGA mass loss is almost the same for the two molar ratios although the two curves are just shifted. For a better comparison of the two molar ratios, we plot the leftover water content versus inverse temperature in an Arrhenian diagram in Figure 1(c). Since TGA data is independent of the ramping speed, we can consider that the Arrhenius law may describe temperature dependence of reaction rates. Considering that all free water has been removed by the pre-drying step at 150°C, the following possible reactions leading to water release are considered:

$$2SiOH \rightleftharpoons Si-O-Si + H_2O_{atm} \quad (1)$$

$$SiO^-H^+/H_2O_{solv} (or SiO^- - H_3O^+) \rightleftharpoons SiOH + H_2O_{atm} \quad (2)$$

$$SiO^-Na^+/H_2O_{solv} \rightleftharpoons SiONa + H_2O_{atm} \quad (3)$$

where the left-hand side of eq. 1, 2 and (3) represent proton-related species i.e. isolated silanols as well as silanols and Na-linked NBOs solvated by water molecules in the silicate, while the right-hand side indicates water evaporating into the atmosphere on thermal treatment.

As a rough approximation, we consider that reaction 1 prevails in the Arrhenius plot since its activation energy is expected to be much higher than the two other reactions associated to the removal of solvated water. The reaction constant (k) of reaction 1 can, therefore, be expressed as:

$$k = \frac{p[H_2O]}{c[SiOH]^2} = A exp\left(\frac{-E_a}{RT}\right) \quad (4)$$

where 'p' is the partial pressure, 'c' the concentration, 'A' the pre-exponential factor, 'E_a' the activation energy, 'R' the gas constant (8.3145 J.mol^{-1}.K^{-1}) and 'T' the temperature in K. Considering that the partial pressure of water is fixed by a large atmospheric reservoir, therefore, making it constant, the E_a is linked to protons as:

$$[SiOH] \sim \exp\left(\frac{E_a}{2RT}\right) \quad (5)$$

The calculated E_a values in the low temperature range (below 450°C) are 34.1 kJ.mol^{-1} and 29.4 kJ.mol^{-1} for the molar ratio X=0.29 and X=0.5, respectively, suggesting same order of magnitude for the two Na-silicates. Such low values of E_a are consistent with literature studies on Na-based silicate glass melts with values approaching 30 kJ.mol^{-1}.[37,38] Therefore, this suggests that the removal of water is controlled by two simultaneous mechanisms: the removal of solvated water, and the transformation of some hydroxyl groups into solvated water to maintain a ratio corresponding to the equilibrium speciation of water at a given temperature. The latter mechanism also implies that the proton-involving network is relatively mobile.

Regarding the mobility of the network, literature data were obtained from geochemistry studies[32,35,36] on the T_g (corresponding to a viscosity of 10^{12} Pa.s) of hydrated sodium silicate glasses obtained by dissolving water into the melts at high pressure. These values are reported in Figure 1(d) for different molar ratios along the pure sodium oxide to pure water line. We have also included in this figure the TGA curves corresponding to specific water over sodium content at particular temperature points. Interestingly, the onset of the mass loss corresponds to a temperature just above the literature data for the glass transition, suggesting that water removal is possible only after the network becomes mobile. As the temperature increases, the water content of the material remains high enough so that the glass transition for the obtained composition is lower than the actual temperature, meaning that the network always keeps some mobility. Nevertheless, the difference between the temperature (for a given composition resulting from water loss) and the corresponding T_g is small, suggesting that the system loses water until the viscosity of the system becomes too high. It is possible that in the temperature range of our observations, the composition versus temperature evolution corresponds to an iso-viscosity line.

These measurements give us a global picture of how water evolves in Na-silicate powders with temperature once the free water has been mostly removed. For a microscopic view of the structure of the material, and in particular the distribution of water between solvated water and silanols, it is important to investigate structural evolution using spectroscopic measurements.

Table 1
Comparison of the composition (in wt%) of Na-silicates before and after pre-drying at 150°C.

X=nNa_2O/nSiO_2	Pre-drying	SiO_2 (%)	Na_2O (%)	H_2O (%)
0.29	None	27.75	8.25	64
	150°C	69.3	20.7	10
0.5	None	27.25	13.75	59
	150°C	58.7	29.3	12

3.2. Structural properties

The structure of Na-silicate solutions (X=0.29 and X=0.5) has been investigated quantitatively by liquid-state NMR. Their spectra exhibit multiple peaks indicative of the coexistence of different Q^n species, where n represents the number of bridging or bonded oxygens (BOs) in the silicate network while the other oxygens are referred to as non-bridging or non-bonding oxygens (NBOs) as shown in Figure S4. The relative proportion of each Q^n was determined by taking the integral under each peak and is shown in the corresponding NMR spectrum in Figure S4(a) and (b).

3.2.1. Evolution of structure with temperature

Heating Na-silicate solutions leads to microscopic structural changes along with changes at the macroscopic scale. Evolution of structural

properties with temperature was studied on powders by solid-state ^{29}Si MAS-NMR in terms of the evolution of Q^n units. Broad peaks are observed due to the glassy character of the silicates i.e. broad distribution of chemical shifts due to various chemical environments in the structure. These broad bands were deconvoluted into individual Q^n units as shown in Figure 2(a), (b) and (c). The deconvolution error is estimated to be a few percent for the different units.

Q^2, Q^3 and Q^4 are the only species observed for X=0.29 powders with a variation in the relative proportion of each on increasing temperature. Network polymerization occurs on heating as indicated by the increase of Q^4 along with the decrease of Q^2 as shown in Figure 2(a). Q^2 vanishes at 400°C while the amount of Q^4 increases from 25% at 150°C to 39% at 400°C indicating an increase in the network connectivity. A similar trend is observed in the system with higher Na content (X=0.5) as shown in Figure 2(b). Higher Q^2 fraction is measured for higher Na content in the initial solution due to an already depolymerized network. Q^1, Q^2 and Q^3 units represent the majority species up to 350°C, whereas a small Q^4 contribution (7%) appears at 400°C. Q^1 vanishes at 275°C while a decrease from 33% at 150°C to 9% at 450°C is observed for Q^2 indicating network polymerization. Q^3 is observed to increase until 350°C while the appearance of Q^4 is observed at 400°C. This polymerization of the network is a result of the condensation reaction of silanols present in the network as NBOs. A detailed analysis on the role of free water, solvating water and silanols is given later in section 3.2.3 and 3.2.4.

The structure in terms of the relative fraction of Q^n units of these xerogels after heating to 400°C indicates a structural arrangement very similar to that found in the corresponding glasses prepared by melt and quench process as shown in Figure 2(c) and (d). The evolution of Q^n fractions with temperature for the two molar ratios and corresponding fraction of Q^n units for glasses is compared in Figure 2(d). Q^2 and Q^4 follow a similar trend for the two molar ratios while a relatively different behavior is observed for Q^3. The fraction of Q^3 does not change much for X=0.29 on increasing temperature suggesting it to be relatively independent of the polymerization reaction. For X=0.5, Q^2 converts into Q^3 until 350°C followed by the formation of Q^4 at 400°C where the fraction of structural units roughly equates to that of the corresponding glasses for both the molar ratios. Interestingly, for a molar ratio of 0.5, the additional structural disorder associated to the Q^3 dismutation reaction (in our case, $2Q^3 \leftrightarrow Q^2+Q^4$, representing the average structure corresponding exactly to Q^3), is the same for the materials prepared from the solution and from the melt and quench protocol. The fact that the structure of the material is close to the one of the melt is another hint that the material crosses a glass transition and its silicate network is able to rearrange in order to reach equilibrium.

The local structural reorganization of the silicate network can also be determined by Raman spectroscopy which, although being not quantitative, is sensitive to mid-range structural units (e.g. rings) and allows to have a qualitative assessment of the silica network modifications with temperature. Figure 3 shows the Raman response of Na-silicate pellets at different temperatures along with the spectrum of glasses corresponding to each molar ratio.

Each spectrum shows two major bands usually observed in sodo-silicates,[17,18,41,42] one corresponding to the bending vibrational mode of Si-O-Si network (centered between 535-550 cm^{-1} for X=0.29 and

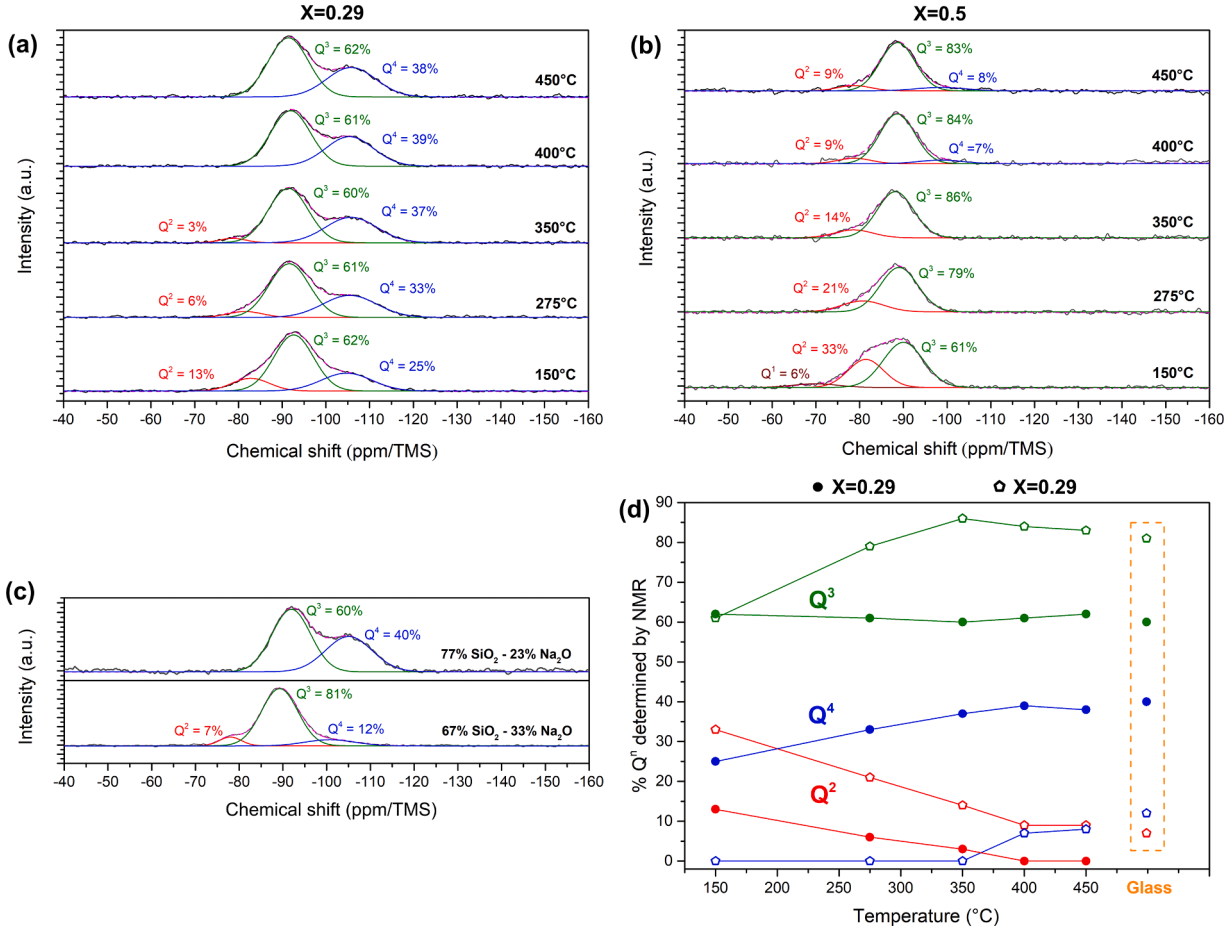

Figure 2. Deconvoluted experimental solid-state ^{29}Si MAS-NMR spectra of Na-silicate powders with a molar ratio (a) X=0.29 & (b) X=0.5 and (c) Na-silicate glasses (77% SiO_2 – 23% Na_2O and 67% SiO_2 – 33% Na_2O), together with fitted curves, individual components and their relative fractions, and (d) variation of Q^n fractions with temperature for the two molar ratios (for X=0.29 and for X=0.5) and points for the corresponding glasses (for 77% SiO_2 – 23% Na_2O and for 67% SiO_2 – 33% Na_2O) showing the same fraction of Q^n units at 400/450°C.

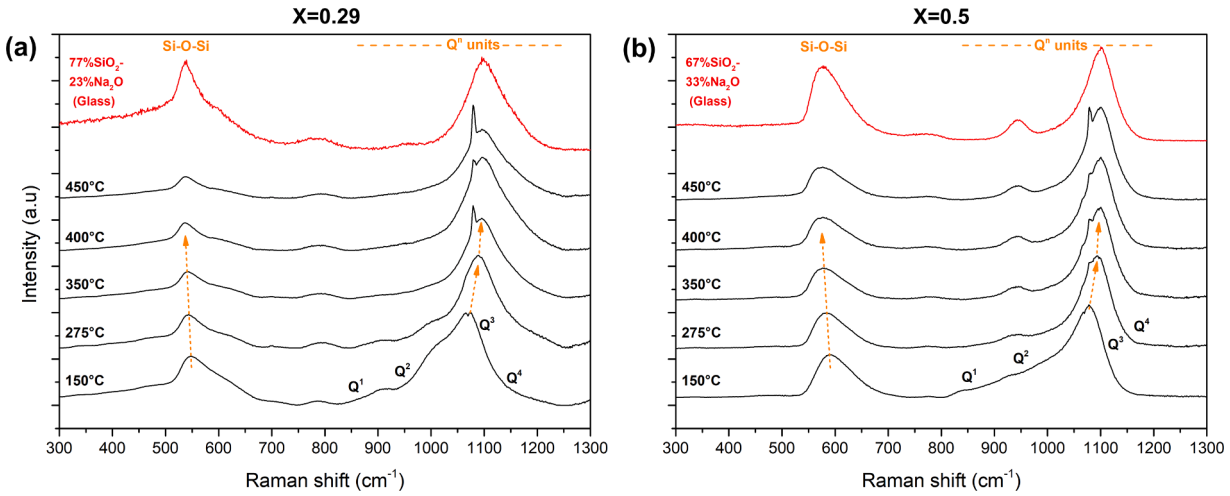

Figure 3. Evolution of Raman spectrum (in black) of Na-silicate pellets with temperature for (a) X=0.29 and (b) X=0.5. Raman spectra of the corresponding glasses (77% SiO_2 – 23% Na_2O and 67% SiO_2 – 33% Na_2O) are shown by red curves for both the molar ratios. The peak centered at 1080 cm^{-1} (or slight shoulder at 1078 cm^{-1}) is indicative of the presence of carbonates/hydrogen carbonates which are expected to be formed due to the mobility of Na ions and a subsequent reaction with atmospheric CO_2.

575-590 cm^{-1} for X=0.5) while the other in the range 825-1250 cm^{-1} is representing the symmetrical stretching vibration of Si-O bonds related to the Q^n units. The small localized contribution centered around 1080 cm^{-1} corresponds to the presence of carbonates that are formed due to high reactivity of Na ions at the surface of the sample. From literature,[17,22,43] the different Q^n configurations have specific vibrational fingerprints inside the stretching envelope with the contribution of Q^1, Q^2, Q^3 and Q^4 near 850, 920, 1080 and 1140 cm^{-1}, respectively (see Figure 3). The increase in lower wave number contribution (Q^1, Q^2) with increasing Na content shows the proportion of lower Q^n species to be higher, as observed from the spectra at 150°C and the reference glasses in Figure 3, due to silica network depolymerization.

The general trend in terms of network polymerization with increasing temperature is the same as observed from ^{29}Si NMR data. A change in the shape of the broad band representing Q^n units is observed for both the molar ratios on going from 150°C to 400°C resulting from the reduction in contribution of lower Q species (Q^1, Q^2) and an increase in the signal from Q^4 indicating a tendency towards more network connectivity on increasing temperature. A slight peak shift is also observed i.e. Q^n band moves from a Raman shift of 1070 cm^{-1} at 150°C to 1097 cm^{-1} at 400°C for X=0.29 while a shift in position from 1079 cm^{-1} at 150°C to 1100 cm^{-1} at 400°C is observed for X=0.5, as shown in Figure 3(a) and (b) respectively.

The intensity of the band centered at lower Raman shift values, attributed to the different Si-O-Si angles or other local configurational variations, is observed to change on changing Na content in the silicate. The different contributions at this band could be due to the existence of different types of bridging oxygens (Q^3-O-Q^3, Q^4-O-Q^4, Q^2-O-Q^3 etc.) or ring configurations.[44,45] Furthermore, network consolidation increases on going from 150°C to 400°C as evident from the left shift in the peak position of Si-O-Si vibration, representative of the variation of Si-O-Si bond angles with temperature. These constraints on bond angles have been reported for Na-silicate glasses[46] where ab-initio calculations showed a variation in the distribution of bond angles on changing Na content. The spectrum at 400°C for both the molar ratios is very similar to the one obtained for corresponding melt and quench glasses suggesting glass-like structural properties (especially in terms of Q^n units) to have been achieved. Taking the area ratio of the peak at lower Raman shift value to that at higher frequency shows a decreasing trend on increasing temperature indicative of network condensation[47] as shown in Figure S5. Furthermore, the ratio of peaks is very high for the corresponding reference glasses suggesting the silicate structure for our Na-silicates to be more chain-like than the ring-type observed in glasses. Thus, Raman spectroscopy has provided a complementary understanding of the structural evolution of Na-silicates. At 400°C, the short-range structure (Q^n units) of the xerogel is very close to the one of a melt and quench glass, but at a longer range (at the scale of silica rings), the structure is different, in particular it is less dense.

Structural changes at the microscopic scale are linked to and influenced by the existence and distribution of Na ions and protons in the structure as well as the presence of solvating water. Therefore, it is important to understand the interaction and evolution of these species with the silicate network. Further details of each of these species are discussed in the upcoming sub-sections.

3.2.2. *Na distribution within the silicate network*

The nature, distribution and specific connectivity of Na in the network was determined by performing ^{23}Na and $^{23}Na/^{29}Si$ NMR on X=0.29 powders and 77% SiO_2 – 23% Na_2O reference glass. The corresponding spectra are shown in Figure 4(a). A peak centered at a chemical shift of -2.5 ppm is observed in the ^{23}Na MAS-NMR experiments for the silicate powders at each temperature and glass indicating the environment of Na to be the same in all the cases. Furthermore, a slight shoulder centered at 10 ppm can also be seen for each temperature and this corresponds to the presence of carbonates. Also, we did not find a signature of NaOH, meaning that all sodium ions belong to the silicate network. Information about the distribution was given by the 1D ^{29}Si (^{23}Na) CP NMR spectrum (Figure 4(b)). This spectrum shows only the signature of silicate species experiencing a very close spatial proximity to Na ions. In other words, the spectrum in Figure 4(b) shows the silicate units involved in $Si\text{-}O^{-}\ ^{+}Na$ linkages. Therefore, the presence of Q^3, Q^2 and Q^1 signals in the CP spectrum indicates that Na ions are homogeneously distributed within the silicate network. This suggests that Na is connected to both Q^2 and Q^3 for X=0.29 and Q^1, Q^2 and Q^3 for X=0.5, respectively.

3.2.3. *Evolution of water/silanols*

Apart from the structural/network changes in terms of Q^n units, another important aspect to be considered is the evolution of solvating water and silanols. After the removal of free water around the boiling temperature, the network is mainly composed of solvating water (water molecules H-bonded to the network or due to some dipole-dipole interactions) and silanols. Figure 5(a) shows the ^{1}H NMR spectra for X=0.29 powders and 77% SiO_2 – 23% Na_2O reference glass. Multiple

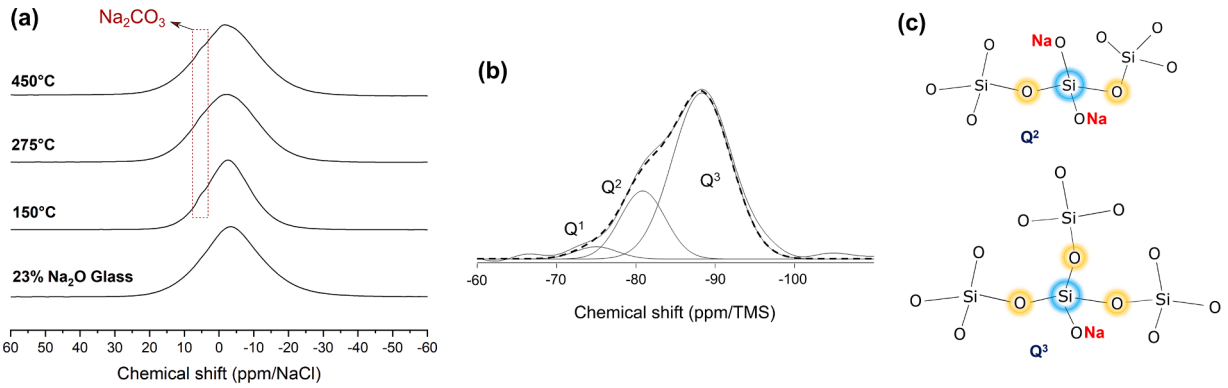

Figure 4. Solid-state (a) ^{23}Na NMR spectra of Na-silicate powder with X=0.29 and the corresponding glass, (b) ^{29}Si (^{23}Na) CP NMR spectrum for the powder with X=0.5 at 150°C and (c) the corresponding connectivity of Na in the network for X=0.29.

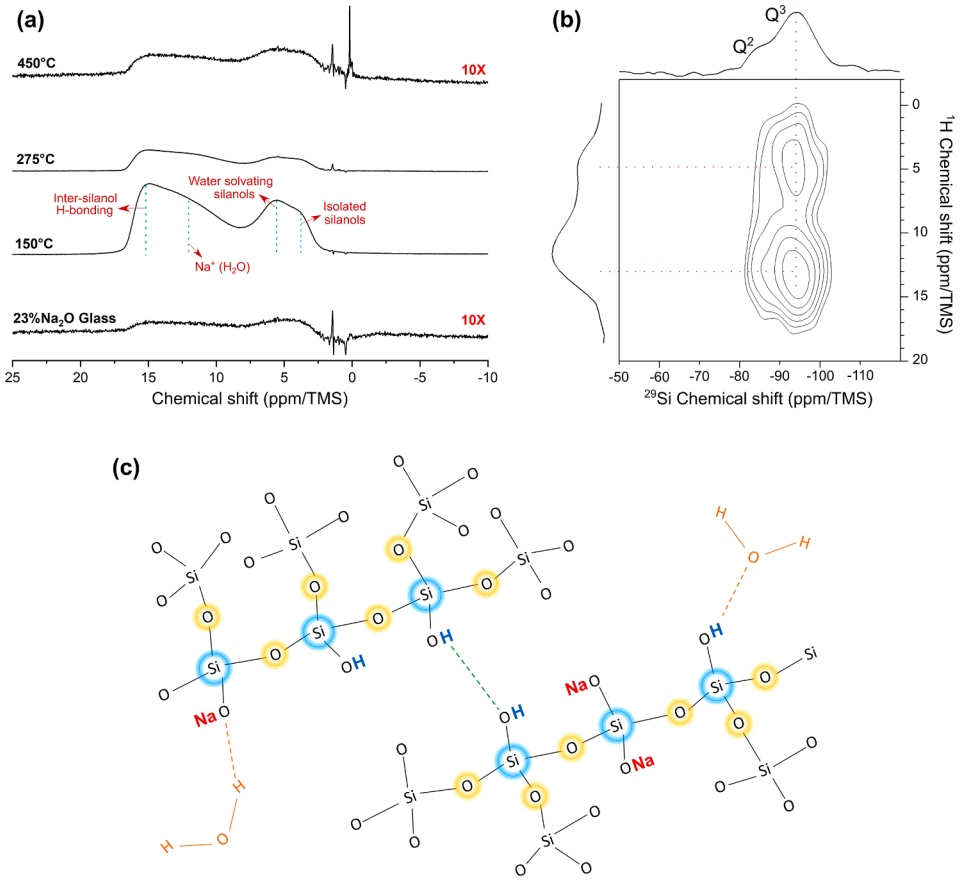

Figure 5. Solid-state (a) ^{1}H NMR spectra of Na-silicate (X=0.29) powder and the corresponding reference glass (band assignment according to literature[54–56]), (b) 2D ^{29}Si (^{1}H) CP-HETCOR NMR spectrum for the powder with X=0.29 at 150°C and (c) connectivity of H in the network. The peaks between 0-2 ppm in (a) correspond to signal of the probe.

bands can be seen in all the spectra, especially for the Na-silicate powder at 150°C and 275°C indicating the presence of multiple proton-related species. The band in the range of chemical shift 3-8 ppm, in case of silica, corresponds to silanols[48–50] with possible multiple configurations as well as adsorbed or solvating water molecules.[49,51,52] Hydrous Na-silicate glasses have been reported to have a characteristic connectivity of proton-related species in the network[53–56] very similar to the one shown in Figure 5(a). Isolated silanols and those solvated by water molecules appear to be centered at ~3.9 ppm and ~5.7 ppm, respectively. The origin of the band from 8-17 ppm is representative of water molecules solvating Na ions (or NaOH) and long-range SiOH-O$^-$ H-bonding. Long range H-bonding has been proposed to be a consequence of inter-lamellar interaction, especially in the case of Kanemite ($NaHSi_2O_5.3H_2O$) where the structure is composed of consecutive sheets of SiO_2 tetrahedra arranged in the form of rings.[57,58] This might be representative of inter-silanol interaction in our case as we do not expect our Na-silicates to be composed of a lamellar arrangement.

The detected species in our case are linked mainly to Q^3 as shown by the 2D ^{29}Si (^{1}H) CP-HETCOR NMR spectrum for X=0.29 (see Figure S6 for X=0.5) in Figure 5(b) suggesting the structure to be composed of silanols and solvating water, with some inter-silanol H-bonding (see Figure 5(c)). The fraction of each proton-related specie is reduced on

thermal evolution until a proportion quite similar to the reference glass is obtained. Thus, the initial hypothesis that the silicate is converting into hydrated metastable melt (in terms of structural properties) seems to be further cemented with the removal of solvating water and silanols, and the connectivity of protons to the network.

Figure 6 shows the overall schematic illustration of the existence of solvating water and silanols in terms of the variation of NBOs with temperature for X=0.29. The red curve represents potentially available network modifiers from the same TGA data shown in Figure 1(a) and calculated from eq. (6) as:

$$\frac{Network\ Modifiers}{Si} = \frac{nNa}{nSi} + \frac{nOH}{nSi} \tag{6}$$

where '*n*' represents the number of moles. The black curve in Figure 6 represents NBOs calculated from the NMR data shown in Figure 2(a) using the eq. (7) given as:

$$\frac{NBOs}{Tetrahedra} = 4Q^0 + 3Q^1 + 2Q^2 + Q^3 \tag{7}$$

where Q^0 is multiplied by a factor of 4 because it has four NBOs per tetrahedron and so on. The relative amount of Na as NBOs is shown in blue and remains constant with temperature (assuming that all Na ions are acting as network modifiers). For X=0.29, using the NMR results that all the protons in silanol units are linked to Q^3, eq. (7) implies that 45% of Na ions are connected to Q^2 and 55% to Q^3 (i.e. 52% Q^3 sites are occupied by protons and the remaining 48% by Na).

Initial silicate solution at room temperature is composed of free water, solvating water and silanols that act as NBOs as shown by the region 'a' in Figure 6. Region 'b' represents the difference between TGA and NMR NBOs and corresponds to solvating water that is still present (though in very small amount) at 400°C. Silanols in the network are represented by the region 'c' which is the difference in NMR and Na as NBOs. Their amount is less than half of the solvating water at 150°C but the ratio between silanols and solvating water increases with temperature, consistent with results on the speciation of water obtained in the geochemistry community.[37,38] Fully condensed state is shown by the region 'd' where there are no more solvating water molecules or silanols in the network and all the NBOs correspond to the presence of Na linked only to Q^3 structural unit.

Interestingly, there seems to be some kind of a proportionality between Si-OH and solvating water molecules suggesting a possible existence of an equilibrium between the two species that is proposed to be a consequence of the following reaction:

$$2SiOH \rightleftharpoons SiOSi + H_2O_{solv/ads} \rightleftharpoons Si - O - Si + H_2O_{atm} \tag{8}$$

The existence of such an equilibrium indicates that silanols, after all, may not be resulting in the direct evaporation of water on condensation rather they seem to be converting into water molecules that tend to behave as solvating species followed by their release into the atmosphere. Thus, the existence of a single E_a (as discussed in section 3.1) appears to be a consequence of this equilibrium.

The comparison of the two molar ratios in terms of NBOs from TGA and NMR data is shown in Figure S7. The trend is the same for both molar ratios with the existence of all the regions mentioned in Figure 6, the only major difference being the amount of Na in the initial silicate. Na and H ions acting as network modifiers or NBOs are influencing the overall structural properties. The amount of calculated NBOs is less for the X=0.29 silicate due to the structure being in a more condensed state than X=0.5.

The molar ratio X is expected to directly influence the amount of silanols in the network. Higher Na concentration in the network has been found to result in higher amount of silanols as NBOs[34] (evident also from the comparison of Figure 5 and Figure S6). This suggests the network to possess more H as NBOs for X=0.5 as also evident from Figure S7. The correlation between the concentration of sodium ions and silanol units suggests an equilibrium between sodium and protons at network-modifier sites of the silicate network.

The removal of solvating water and silanols has a direct influence not only on the degree of densification or polymerization but also the extent of volumetric expansion of Na-silicates observed visually. Though the

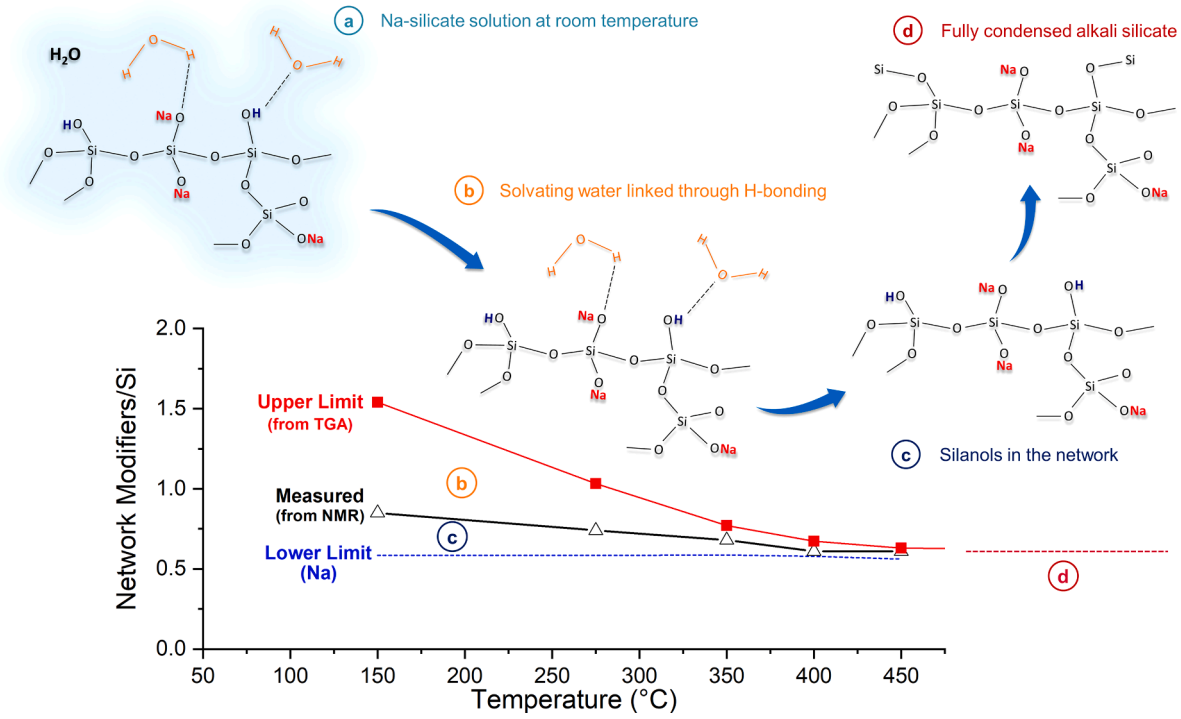

Figure 6. Total Network Modifiers/Si from both (■) TGA and (△) solid-state ^{29}Si NMR spectra of Na-silicate (X=0.29) powder with region 'b' corresponding to the amount of adsorbed/solvating water linked to the network, 'c' corresponding to the relative proportion of OH as NBO and 'd' referring to a completely condensed state at temperatures well above 800°C.

structural properties start corresponding to glasses at around 400°C where most of the solvating water and silanols have been removed, experimental evaluation suggests the existence of a much softer material as compared to glass, probably because of the presence of water as compared to the dry glass. Apart from the evolution of Q^n units and NBOs, revisiting the macroscopic evolution of Na-silicates from a visual perspective is, therefore, also necessary to understand how the material might behave in different industrial applications especially those related to fire retardance. Hence, the next section is devoted to a qualitative description of what happens upon heating a liquid droplet.

3.2.4. Foaming

On heating a droplet of Na-silicate solution with a heating gun, evolution from liquid to solid occurs as shown in Figure 7(a) for X=0.29 and is explained schematically in Figure 7(c). A viscous membrane-like layer appears at the top at lower temperatures which is linked to the formation of strains at the surface due to condensation of the gel,[59] slowing down the removal of the free water from the inside of the material. Therefore, compared to the mg-sized samples we studied with TGA, the droplet is further from equilibrium. At 130-150°C, the "skin" membrane becomes very viscous, preventing bubbles of boiling water from escaping. Increasing the temperature further allows the membrane-like layer to cross the T_g (as in Figure 7(c)) and, hence, results in the removal of the trapped free water. Most of the free water is removed around 150-200°C leaving behind a solid that is hard. Increasing temperature further causes transition from a hard to soft phase (as also observed during grinding) with an abrupt structural expansion of the solid mass due to the pressure imposed by water bubbles. This occurs at the 'softening point' or 'foaming temperature' which represents the apparent T_g of the silicate responsible for an actual softening of the structure resulting in the formation of a viscous solid. The temperature referred here as the softening point is different from the formal temperature defined as the viscosity of 10^6 Pas. It does not correspond to one single value but rather a more general process i.e. significant mobility of the network which means that once this particular temperature value is crossed, the system keeps on losing water continuously due to the fact that the network is mobile enough to let that happen. Note that the existence and the value of a softening temperature or glass transition for materials heated from a solution needs to be further investigated in future work, since we only measured it on pre-dried materials due to foaming-related experimental challenges.

Such a low value of softening temperature is due to the presence of water and has already been reported in the literature for glasses in terms of T_g.[32,34] Foaming phenomenon itself indicates that we have a soft glass once we cross the softening point, with the structure becoming more and more condensed on increasing temperature. Heating further to temperatures above 250°C tends to cause further foaming but the extent of expansion is reduced due to a reduction in the amount of available silanols. Similar trend is observed on heating silicate with higher Na content (X=0.5) resulting in an increased swelling due to the presence of

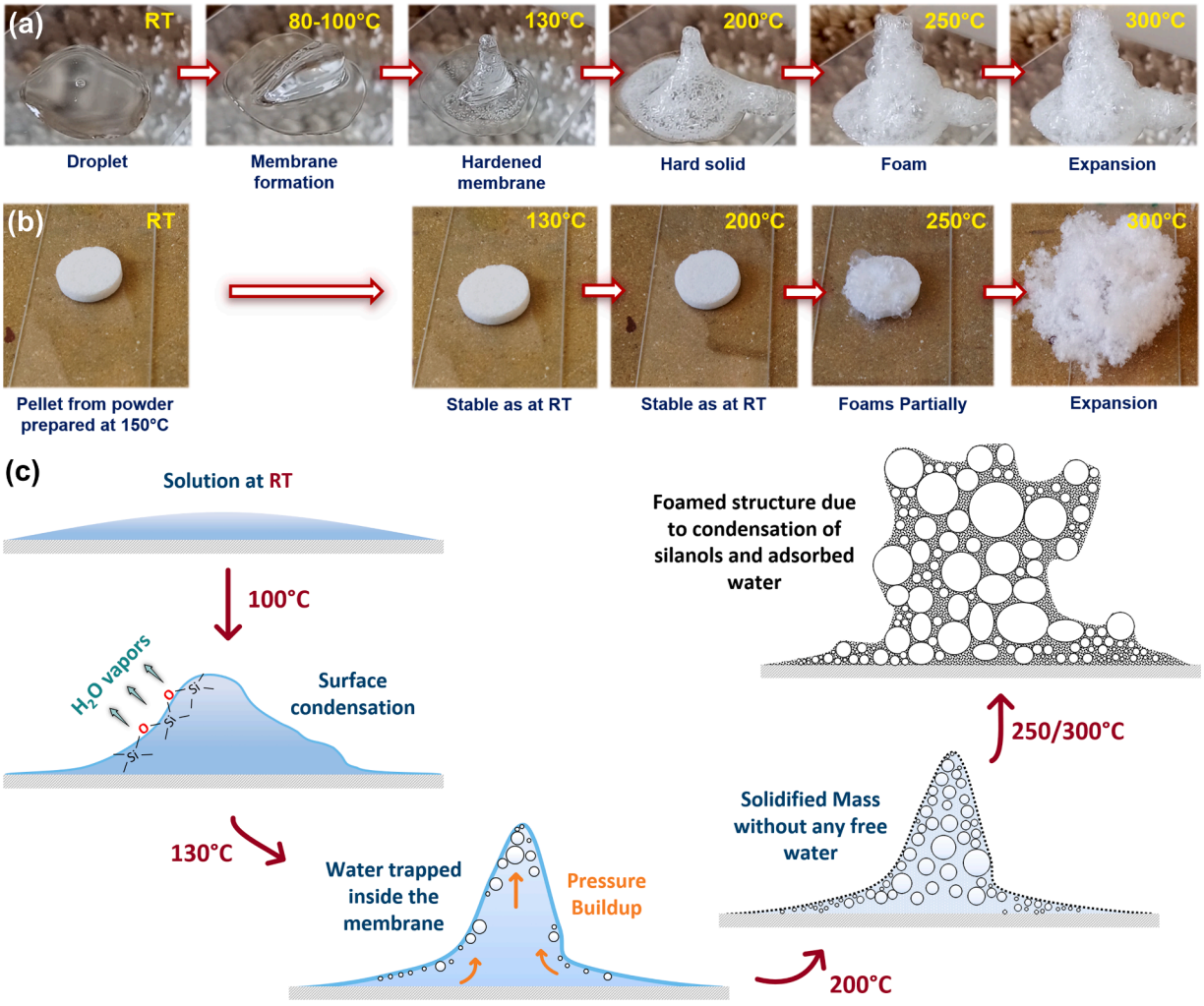

Figure 7. Foaming mechanism of molar ratio X=0.29 (a) solution under a heating gun (video in SI, schematic illustration of the experimental setup in Figure S2(a)), (b) pellet pre-dried at 150°C followed by heat treatment in a furnace and (c) schematic illustration of foaming mechanism of liquid.

higher amount of retained water in the structure. Thus, the lower softening temperature of 175°C observed for X=0.5 as compared to 210°C for X=0.29 in Figure 1(a) and (b) is mainly a consequence of higher amount of silanols in the silicate network.

Figure 7(b) shows the corresponding foaming behavior of a pre-dried X=0.29 powder pellet. The pellet remains unchanged until 200°C and tends to foam partially on reaching 250°C due to the powder being in a compressed state. Major swelling occurs on going up to 300°C as the pressure tends to buildup due to mainly the condensation of remaining silanols and solvating water.

Qualitatively, we explain the foaming by an out-of-equilibrium build-up of water vapor pressure inside the material after the xerogel transition, when the material becomes too viscous (especially in a dried skin) for water to diffuse out of the material. Change in viscosity is therefore expected to be one of the driving forces behind this structural expansion but the role of silanols and solvating water on rheological properties and the exact conditions for the existence of this foaming phenomenon need further research evidence. The rheological properties of the silicate network need to be addressed in this regard along with the influence of boiling water bubbles as a viscous liquid maybe formed at some point that may not be completely permeable to let these bubbles escape. Investigations using hot-stage microscopy (video of preliminary test in SI and corresponding details of the experimental parameters and setup in Figure S2(b)) and in-situ Raman spectroscopy are expected to aid in better understanding of the foaming behavior.

4. Conclusions

Structural properties of Na-silicates of two different molar ratios (X=0.29 and X=0.5) investigated at both the macroscopic and microscopic scale have allowed to have a better understanding of structural evolution with temperature. Mass loss evolution is dependent on temperature and Na content in the silicate. Increasing the Na content tends to reduce the softening temperature along with a higher amount of overall water retention after the initial pre-drying step. A same order of magnitude for mass loss evolution is observed for both molar ratios with an E_a of 29.4 kJ.mol^{-1} for X=0.5 as compared to 34.1 kJ.mol^{-1} for X=0.29. Furthermore, the higher the amount of Na in the network, the more depolymerized the Q^n structural units tend to be with no Q^4 observed by liquid-state ^{29}Si NMR for the molar ratio X=0.5.

Heating pre-dried Na-silicate powders tends to increase the degree of polymerization until the xerogel shows glass-like structural properties in terms of Q^n units at around 400°C when compared with reference Na-silicate glasses. Complementary information provided by Raman spectroscopy also indicates that the structure condenses and the Raman spectra at 400°C become similar to that of the corresponding glasses (especially in terms of Q^n units) for both the molar ratios with ring-type structure being more dominant in glasses.

Further structural investigation indicates that Na ions are connected to both Q^2 and Q^3 silicon sites for X=0.29 suggesting a completely random distribution, while all the protons are connected to Q^3 (both Q^2 and Q^3 connectivity is observed in case of X=0.5) i.e. no free water is present at 150°C.

Initial solutions are composed of free water, solvating water and silanols which tend to evolve depending upon the heating temperature with the free water mostly removed on heating to 150°C. NBO contribution from the network modifiers (Na and H) shows that both silanols and solvating water molecules are present even at high temperature, suggesting an equilibrium between the two structural units for protons. The amount of initial water in the silicate and molar ratio X directly influence the amount of silanols in the network. Higher overall water retained for the molar ratio X=0.5 suggests the network to possess more H as NBOs when compared to X=0.29. From a macroscopic point of view, heating a silicate solution tends to induce structural changes due to the removal of water. Structural expansion is observed once the softening temperature threshold is crossed due to the expulsion/condensation of water resulting from the buildup of bubbles inside. The existence of volumetric expansion is linked to the foaming phenomenon, a better understanding of which is required at this stage to aid in further exploration of the potential of silicate coatings in fire-retardant industrial applications.

CRediT authorship contribution statement

Hamza Mohsin: Formal analysis, Investigation, Writing - original draft, Writing - review & editing. **Sébastien Maron:** Formal analysis, Investigation. **Isabelle Maurin:** Formal analysis, Investigation. **Ekaterina Burov:** Conceptualization, Formal analysis, Supervision, Writing - review & editing. **Grégory Tricot:** Formal analysis, Investigation. **Lucie Devys:** Conceptualization. **Emmanuelle Gouillart:** Conceptualization, Formal analysis, Supervision, Writing - review & editing. **Thierry Gacoin:** Conceptualization, Formal analysis, Supervision, Writing - review & editing.

Declaration of Competing Interest

The authors declare that they have no known competing financial interests or personal relationships that could have appeared to influence the work reported in this paper.

Acknowledgments

Financial support from the IR-RMN-THC Fr3050 CNRS for conducting ^{1}H and ^{23}Na NMR experiments is gratefully acknowledged. The authors would also like to thank Johnny Vallon for the preparation of the melt and quench sodium silicate glasses at Saint-Gobain Research Paris. This work benefits from the extremely helpful discussions with Cédric Boissière (Laboratoire de Chimie de la Matière Condensée de Paris-LCMCP, Sorbonne Université, France) and Michael Toplis (L'Institut de Recherche en Astrophysique et Planétologie-IRAP, Université de Toulouse, France).

Supplementary materials

Supplementary material associated with this article can be found, in the online version, at doi:10.1016/j.jnoncrysol.2021.120872.

References

[1] N. Essaidi, L. Laou, S. Yotte, L. Ulmet, S. Rossignol, Comparative Study of the Various Methods of Preparation of Silicate Solution and Its Effect on the Geopolymerization Reaction, Results Phys 6 (2016) 280–287.
[2] D. Dimas, I. Giannopoulou, D. Panias, Polymerization in Sodium Silicate Solutions: A Fundamental Process in Geopolymerization Technology, J. Mater. Sci. 44 (14) (2009) 3719–3730.
[3] A. Jaffrès, M. Boudot, S. Chevalier, R. Mohammedi, S. Maron, L. Devys, T. Gacoin, Revisiting Aqueous Alkaline Silicates as Precursors for Sol-Gel Optical Coatings, J. Am. Ceram. Soc. 102 (7) (2019) 3887–3896.
[4] M. Boudot, C. Boissière, E. Burov, T. Gacoin, Engineering of Silica Thin-Film Nanoporosity via Alkali-Ion-Assisted Reconstruction, Chem. Mater. 31 (7) (2019) 2390–2400.
[5] Q.Z. Huang, J.F. Shi, L.L. Wang, Y.J. Li, L.W. Zhong, G. Xu, Study on Sodium Water Glass-Based Anti-Reflective Film and Its Application in Dye-Sensitized Solar Cells, Thin Solid Films 610 (2016) 19–25.
[6] E.M. Bulewicz, A. Pelc, R. Kozjowski, A. Miciukiewicz, Intumescent Silicate-Based Materials: Mechanism of Swelling in Contact with Fire, Fire Mater 9 (4) (1985) 171–175.
[7] E.D. Weil, Fire-Protective and Flame-Retardant Coatings - A State-of-the-Art Review, J. Fire Sci. 29 (3) (2011) 259–296.
[8] R.G. Puri, A.S. Khanna, Intumescent Coatings: A Review on Recent Progress, J. Coatings Technol. Res. (1) (2017) 14.
[9] I.L. Svensson, S. Sjöberg, L.-O. Öhman, Polysilicate Equilibria in Concentrated Sodium Silicate Solutions, J. Chem. Soc., Faraday Trans. I 82 (1986) 3635–3646.
[10] J. Nordström, A. Sundblom, G.V. Jensen, J.S. Pedersen, A. Palmqvist, A. Matic, Silica/Alkali Ratio Dependence of the Microscopic Structure of Sodium Silicate Solutions, J. Colloid Interface Sci. 397 (2013) 9–17.
[11] L. Vidal, E. Joussein, M. Colas, J. Cornette, J. Sanz, I. Sobrados, J.L. Gelet, J. Absi, S. Rossignol, Controlling the Reactivity of Silicate Solutions: A FTIR, Raman and NMR Study, Colloids Surfaces A Physicochem. Eng. Asp. 503 (2016) 101–109.

[12] N.H. Ray, R.J. Plaisted, The Constitution of Aqueous Silicate Solutions, J. Chem. Soc. Dalt. Trans (1983) 475–481.
[13] L. Vidal, A. Gharzouni, E. Joussein, M. Colas, J. Cornette, J. Absi, S. Rossignol, Determination of the Polymerization Degree of Various Alkaline Solutions: Raman Investigation, J. Sol-Gel Sci. Technol. 83 (1) (2017) 1–11.
[14] J.L. Bass, G.L. Turner, Anion Distributions in Sodium Silicate Solutions. Characterization by ^{29}Si NMR and Infrared Spectroscopies, and Vapor Phase Osmometry, J. Phys. Chem. B 101 (1997) 10638–10644.
[15] M.T. Tognonvi, D. Massiot, A. Lecomte, S. Rossignol, J.P. Bonnet, Identification of Solvated Species Present in Concentrated and Dilute Sodium Silicate Solutions by Combined ^{29}Si NMR and SAXS Studies, J. Colloid Interface Sci. 352 (2) (2010) 309–315.
[16] P. Zhang, C. Dunlap, P. Grandinetti, I. Farnan, J. Stebbins, Silicon Site Distributions in an Alkali Silicate Glass Derived by Two-Dimensional ^{29}Si Nuclear Magnetic Resonance, J. Non. Cryst. Solids 204 (1996) 294–300.
[17] P. McMillan, Structural Studies of Silicate Glasses and Melts-Applications and Limitations of Raman Spectroscopy, Am. Mineral. 69 (1984) 622–644.
[18] D.W. Matson, S.K. Sharma, J.A. Philpotts, The Structure of High-Silica Alkali-Silicate Glasses. A Raman Spectroscopic Investigation, J. Non. Cryst. Solids 58 (2–3) (1983) 323–352.
[19] P. McMillan, B. Piriou, Raman Spectroscopic Studies of Silicate and Related Glass Structure: A Review, Bull. Mineral. 106 (1983) 57–75.
[20] H.W. Nesbitt, G.M. Bancroft, G.S. Henderson, R. Ho, K.N. Dalby, Y. Huang, Z. Yan, Bridging, Non-Bridging and Free (O_2^-) Oxygen in Na_2O-SiO_2 Glasses: An X-Ray Photoelectron Spectroscopic (XPS) and Nuclear Magnetic Resonance (NMR) Study, J. Non. Cryst. Solids 357 (1) (2011) 170–180.
[21] H. Maekawa, T. Maekawa, K. Kawamura, T. Yokokawa, The Structural Groups of Alkali Silicate Glasses Determined from 29Si MAS-NMR, J. Non. Cryst. Solids 127 (1991) 53–64.
[22] B.O. Mysen, J.D. Frantz, B.O. Mysen, J.D. Frantz, Silicate Melts at Magmatic Temperatures: In-Situ Structure Determination to 1651°C and Effect of Temperature and Bulk Composition on the Mixing Behavior of Structural Units, Contrib Miner. Pet. 117 (1994) 1–14.
[23] H. Maekawa, T. Yokokawa, Effects of Temperature on Silicate Melt Structure: A High Temperature ^{29}Si NMR Study of $Na_2Si_2O_5$, Geochim. Cosmochim. Acta 61 (13) (1997) 2569–2575.
[24] M.E. Brandriss, J.F. Stebbins, Effects of Temperature on the Structures of Silicate Liquids: ^{29}Si NMR Results, Geochim. Cosmochim. Acta 52 (1988) 2659–2669.
[25] J.F. Stebbins, I. Farnan, X. Xue, The Structure and Dynamics of Alkali Silicate Liquids: A View from NMR Spectroscopy, Chem. Geol. 96 (1992) 371–385.
[26] L.S. Dent Glasser, C.K. Lee, Drying of Sodium Silicate Solutions, J. Appl. Chem. Biotechnol. 21 (1971) 127–133.
[27] H. Roggendorf, D. Böschel, J. Trempler, Structural Evolution of Sodium Silicate Solutions Dried to Amorphous Solids, J. Non. Cryst. Solids 293–295 (1) (2001) 752–757.
[28] T. Otaka, Y. Asako, Thermal Intumescent Characteristics of Heated Sodium Silicate, Trans. Japan Soc. Mech. Eng. Ser. B 69 (688) (2003) 2733–2739.
[29] H. Roggendorf, D. Böschel, B. Rödicker, Differential Scanning Calorimetry at Hydrothermal Conditions of Amorphous Materials Prepared by Drying Sodium Silicate Solutions, J. Therm. Anal. Calorim. 63 (3) (2001) 641–652.
[30] H. Roggendorf, D. Böschel, Hydrous Sodium Silicate Glasses Obtained by Drying Sodium Silicate Solutions, Glas. Sci. Technol. Glas. Berichte 75 (2) (2002) 103–111.
[31] R. Subasri, H. Näfe, Phase Evolution on Heat Treatment of Sodium Silicate Water Glass, J. Non. Cryst. Solids 354 (10–11) (2008) 896–900.
[32] S. Zietka, J. Deubener, H. Behrens, R. Müller, Glass Transition and Viscosity of Hydrated Silica Glasses, Phys. Chem. Glas. Eur. J. Glas. Sci. Technol. Part B 48 (6) (2007) 380–387.
[33] J.E. Shelby, Property/Morphology Relations in Alkali Silicate Glasses, J. Am. Ceram. Soc. 66 (11) (1983) 754–757.
[34] J. Deubener, R. Müller, H. Behrens, G. Heide, Water and the Glass Transition Temperature of Silicate Melts, J. Non. Cryst. Solids 330 (1–3) (2003) 268–273.
[35] M. Tomozawa, M. Takata, J. Acocella, E. Bruce Watson, T. Takamori, Thermal Properties of $Na_2O{\bullet}3SiO_2$ Glasses with High Water Content, J. Non. Cryst. Solids 56 (1–3) (1983) 343–348.
[36] R.F. Bartholomew, High-Water Containing Glasses, J. Non. Cryst. Solids 56 (1983) 331–342.
[37] A. Shen, H. Keppler, Infrared Spectroscopy of Hydrous Silicate Melts to 1000°C and 10 Kbar: Direct Observation of H_2O Speciation in a Diamond-Anvil Cell, Am. Mineral. 80 (11–12) (1995) 1335–1338.
[38] M. Nowak, H. Behrens, The Speciation of Water in Haplogranitic Glasses and Melts Determined by in Situ Near-Infrared Spectroscopy, Geochim. Cosmochim. Acta 59 (16) (1995) 3445–3450.
[39] K.B. Langille, D. Nguyen, J.O. Bernt, D.E. Veinot, M.K. Murthy, Mechanism of Dehydration and Intumescence of Soluble Silicates Part I Effect of Silica to Metal Oxide Molar Ratio, J. Mater. Sci. 26 (1991) 695–703.
[40] D. Massiot, F. Fayon, M. Capron, I. King, S. Le Calvé, B. Alonso, J.O. Durand, B. Bujoli, Z. Gan, G. Hoatson, Modelling One- and Two-Dimensional Solid-State NMR Spectra, Magn. Reson. Chem. 40 (1) (2002) 70–76.
[41] T. Furukawa, K.E. Fox, W.B. White, Raman Spectroscopic Investigation of the Structure of Silicate Glasses. III. Raman Intensities and Structural Units in Sodium Silicate Glasses, J. Chem. Phys. 75 (7) (1981) 3226–3237.
[42] W.J. Malfait, V.P. Zakaznova-Herzog, W.E. Halter, Quantitative Raman Spectroscopy: Speciation of Na-Silicate Glasses and Melts, Am. Mineral. 93 (10) (2008) 1505–1518.
[43] D.W. Matson, S.K. Sharma, J.A. Philpotts, The Structure of High-Silica Alkali-Silicate Glasses. A Raman Spectroscopic Investigation, J. Non. Cryst. Solids 58 (2–3) (1983) 323–352.
[44] S.K. Sharma, J.F. Mammone, M.F.Raman Nicol, Investigation of Ring Configurations in Vitreous Silica, Nature 292 (1981) 140–141.
[45] F.L. Galeener, Planar Rings in Vitreous Silica, J. Non. Cryst. Solids 49 (1982) 53–62.
[46] D. Kilymis, S. Ispas, B. Hehlen, S. Peuget, J.M. Delaye, Vibrational Properties of Sodosilicate Glasses from First-Principles Calculations, Phys. Rev. B 99 (2019), 054209.
[47] P. Colomban, O. Paulsen, Non-Destructive Determination of the Structure and Composition of Glazes by Raman Spectroscopy, J. Am. Ceram. Soc. 88 (2) (2005) 390–395.
[48] A.J. Vega, G.W. Scherer, Study of Structural Evolution of Silica Gel Using ^{1}H and ^{29}Si NMR, J. Non. Cryst. Solids 111 (1989) 153–166.
[49] D.R. Kinney, I.-S. Chuang, G.E. Maciel, Water and the Silica Surface As Studied by Variable-Temperature High-Resolution NMR, J. Am. Chem. Soc 115 (1993) 6786–6794.
[50] J. Brus, J. Dybal, Hydrogen-Bond Interactions in Organically-Modified Polysiloxane Networks Studied by 1D and 2D CRAMPS and Double-Quantum ^{1}H MAS NMR, Macromolecules 35 (27) (2002) 10038–10047.
[51] J.-B. D'Espinose de la Caillerie, M.R. Aimeur, Y. Kortobi, A.P. El; Legrand, Water Adsorption on Pyrogenic Silica Followed by ^{1}H MAS NMR, J. Colloid Interface Sci. 194 (1997) 434–439.
[52] R. Leboda, V.V. Turov, M. Marciniak, A.A. Malygin, A.A. Malkov, Characteristics of the Hydration Layer Structure in Porous Titania-Silica Obtained by the Chemical Vapor Deposition Method, Langmuir 15 (24) (1999) 8441–8446.
[53] J. Kümmerlen, L.H. Merwin, A. Sebald, K. Hans, Structural Role of H_2O in Sodium Silicate Glasses: Results from ^{29}Si and ^{1}H NMR Spectroscopy, J. Phys. Chem. 96 (1992) 6405–6410.
[54] E. Robert, A. Whittington, F. Fayon, M. Pichavant, D. Massiot, Structural Characterization of Water-Bearing Silicate and Aluminosilicate Glasses by High-Resolution Solid-State NMR, Chem. Geol. 174 (2001) 291–305.
[55] T. Schaller, A. Sebald, One-and Two-Dimensional ^{1}H Magic-Angle Spinning Experiments on Hydrous Silicate Glasses, Solid State Nucl. Magn. Reson. 5 (1995) 89–102.
[56] G.D. Cody, B.O. Mysen, S.K. Lee, Composition: A Solid-State ^{1}H and ^{29}Si NMR Study of Quenched Glasses along the Na_2O-SiO_2-H_2O Join, Geochim. Cosmochim. Acta 69 (9) (2005) 2373–2384.
[57] A.G. Simakin, T.P. Salova, V.O. Zavelsky, Mechanism of Water Dissolution in Sodium-Silicate Melts and Glasses: Structural Interpretation of Spectroscopic Data, Geochemistry Int 46 (2) (2008) 107–115.
[58] S. Hayashi, Solid-State NMR Study of Locations and Dynamics of Interlayer Cations and Water in Kanemite, J. Mater. Chem 7 (6) (1997) 1043–1048.
[59] L. Pauchard, C. Allain, Buckling Instability Induced by Polymer Solution Drying, Europhys. Lett. 62 (6) (2003) 897–903.

ECOLE DOCTORALE

Titre : Évolution thermique des silicates alcalins binaires en solution aqueuse : propriétés des solutions, des xérogels et des revêtements

Mots clés : Silicates aqueux, xérogel, moussant/intumescence, transition vitreuse, cristallisation, revêtements épais

Résumé : Le comportement thermique des silicates alcalins aqueux pour l'industrie est d'un intérêt particulier en particulier dans les applications résistantes au feu en raison de leur nature intumescente. Ils ont été étudiés pour les silicates de Na, K et Li de deux rapports molaires différents afin de mieux comprendre l'évolution structurelle macroscopique et microscopique en termes de moussage et de condensation du réseau. Une stratégie expérimentale quantitative impliquant une combinaison d'outils (ATG, spectroscopie RMN du ^{29}Si, DRX) a été utilisée pour sonder l'évolution thermique de l'état du réseau en partant essentiellement de « xérogels ». Le chauffage des silicates alcalins entraîne des modifications structurelles dues à l'évolution de l'eau où la quantité d'eau restante (des silanols de réseau ou d'eau de solvatation) dans le xérogel, lorsqu'elle est observée à partir d'ATG, suit une loi d'Arrhénius pour les silicates de sodium avec une énergie d'activation de 30 kJ.mol^{-1} en dessous de 400 °C, conforme à la littérature géochimique. En revanche, de multiples énergies d'activation sont présentes pour les silicates de potassium et de lithium en raison de leur cristallisation.

Un moussage est observé à des températures supérieures à 150 °C dans les silicates de Na et de K, principalement en raison de la condensation des silanols et de l'élimination subséquente des molécules d'eau de solvatation en fonction de la composition et de la vitesse de chauffage. L'augmentation de la concentration en alcalin, par exemple en Na, entraîne une plus grande quantité d'eau retenue dans le xérogel, ce qui est corrélé à une température de ramollissement inférieure du matériau et est, macroscopiquement, lié à un moussage plus élevé du silicate. Les solutions de silicate de potassium moussent abondamment à une vitesse de chauffage de 10 °C/min ; cependant, la suppression du moussage est une conséquence de la cristallisation lors du chauffage soit à une vitesse plus faible (en particulier pour une teneur en K plus faible) soit lors du pré-séchage à 150°C. Un effet combiné de séparation de phases et de cristallisation est responsable de l'absence de mousse observée dans les solutions de silicate de Li et les xérogels, quelle que soit la vitesse de chauffage, résultant d'une nature relativement moins mobile du réseau en raison de la quantité limitée de silanols et d'ions alcalins. Des mesures à haute température dans le cas des silicates de sodium suggèrent que les systèmes présentent une évolution xérogel-verre à 400 °C au-dessus de laquelle un comportement similaire aux verres conventionnels est observé jusqu'à 1100 °C sous un microscope à platine chauffante. Enfin, des revêtements homogènes et épais à gradient de silicate (de l'ordre du micron) développés à partir de ces solutions présentent une épaisseur critique pour : le moussage dans les silicates de Na, la cristallisation et le moussage dans les silicates de K selon la composition, ou le craquage dans les silicates de Li. De plus, l'ajout d'entités étrangères comme l'éthylène glycol et le silicate de tétraméthylammonium limite le moussage dans le cas des silicates de sodium. Une telle étude a permis d'avoir une meilleure compréhension du comportement thermique des silicates alcalins pour répondre aux problématiques rencontrées dans le secteur industriel.

Title: Thermal evolution of binary aqueous alkali silicates: Properties of solutions, xerogels and coatings

Keywords: Soluble silicates, xerogels, foaming/intumescence, glass transition, crystallization, thick coatings

Abstract: The thermal behavior of industrially valuable aqueous alkali silicates is of particular interest especially in fire-resistant applications owing to their intumescent nature, and has been investigated for Na, K and Li-silicates of two different molar ratios to better understand the macro and microscopic structural evolution in terms of foaming and network condensation. A quantitative experimental strategy involving a combination of tools (TGA, ^{29}Si NMR spectroscopy, XRD) has been utilized to probe the state of the network on thermal evolution starting mainly from 'xerogels'. Heating alkali silicates leads to structural changes due to the evolution of water where the quantity of leftover water (network silanols or solvating water) in the xerogel, when observed from TGA, obeys an Arrhenius evolution for Na-silicates with an activation energy of 30 kJ.mol^{-1} below 400°C, consistent with the geochemistry literature. In contrast, multiple activation energies are displayed by K and Li-silicates due to crystallization.

Foaming is observed at temperatures above 150°C in Na and K-silicates due to mainly the condensation of silanols and subsequent removal of solvating water molecules with dependence upon the composition and heating rate. Increasing the alkali concentration, for instance Na, results in a larger quantity of water retained in the xerogel, which correlates with a lower softening temperature of the material and is, macroscopically, related to a higher foaming of the silicate. K-silicate solutions foam extensively at a heating rate of 10°C/min, however, suppression of foaming is a consequence of crystallization on heating at either lower rate (especially for lower K content) or pre-drying at 150°C. A combined effect of phase separation and crystallization is responsible for no foaming observed in Li-silicate solutions and xerogels, irrespective of the heating rate, resulting from a relatively less mobile nature of the network due to limited quantity of silanols and alkali ions. High temperature measurements in the case of Na-silicates suggest the systems to exhibit a xerogel-to-glass evolution at 400°C above which a behavior similar to conventional glasses is observed when seen under a Hot-stage Microscope. Finally, homogeneous and thick silicate gradient coatings (in the order of microns) developed from these solutions show a critical thickness for: foaming in Na-silicates, crystallization and foaming in K-silicates depending upon the composition, or cracking in Li-silicates. Furthermore, the addition of foreign entities like ethylene glycol and tetramethylammonium silicate limit foaming in the case of Na-silicates. Such a study has allowed us to have a better understanding of the thermal behavior of alkali silicates for addressing the issues being faced in the industrial sector.

Institut Polytechnique de Paris
91120 Palaiseau, France